NOTTINGHAM TRENT UNIVERSITY

Spatial considerations in the resolution of inflammation

Anahita Bayani

A thesis submitted in partial fulfilment of the requirements of Nottingham Trent University for the degree of Doctor of Philosophy.

March 2020

Copyright statement

Abstract

Understanding the mechanisms that control the body's response to inflammation is of key importance, due to its involvement in myriad medical conditions, including cancer, arthritis, Alzheimer's disease and asthma. While resolving inflammation has historically been considered a passive process, since the turn of the century the hunt for novel therapeutic interventions has begun to focus upon active manipulation of constituent mechanisms, particularly involving interactions between immune cells and pro- and anti-inflammatory mediators. We here address the specific question of how inflammatory damage can spread spatially due to the motility of these cells and mediators using mathematical and agent-based modelling.

We firstly extend the existing homogeneous models of Dunster *et al.* (2014) to incorporate spatial behaviours. Through bifurcation analysis and numerical simulation of the resulting partial differential equation (PDE) models, we show that spatially-inhomogeneous outcomes can present close to the switch from bistability to guaranteed resolution in the corresponding homogeneous models, but that this behaviour is tightly controlled by the dynamics of anti-inflammatory mediators. We then move to a hybrid PDE-Agent Based Model (ABM) approach, capable of simulating individual cells and a more diverse range of cell behaviours. In particular, we address the questions of whether initially localised damage can invade neighbouring healthy tissue, and the extent to which sub-optimal directed cell motility (such as that associated inflammatory conditions such as chronic obstructive pulmonary

disease) can impact upon the long-term outcome. We illustrate that changes to the values of physiologically-relevant parameters can act as a switch between healthy and pathological scenarios; with careful parameterisation, our approach exhibits scope for elucidating how these key mechanisms could be actively manipulated to potentially identify new therapeutic interventions.

Acknowledgements

I would like to thank my supervisors: Martin Nelson, Jonathan Crofts, Nadia Chuzhanova and Joanne Dunster. The guidance which they have provided throughout this project is greatly appreciated. I am also thankful to Nottingham Trent University, for providing funding for this project.

Declaration

I declare that the thesis has been composed by myself and that the work has not be submitted for any other degree or professional qualification. I confirm that the work submitted is my own, except where work which has formed part of jointly-authored publications has been included.

Parts of the work presented in this thesis have be submitted for publication as follows:

Paper 1 Bayani A., Dunster, J.L., Crofts, J.J., Nelson M.R. Mechanisms and points of control in the spread of inflammation: a mathematical investigation. *Bulletin of Mathematical Biology.* 2020; 82(4):45. DOI: 10.1007/s11538-020-00709-y.

Paper 2 Bayani A., Dunster, J.L., Crofts, J.J., Nelson M.R. Spatial considerations in the resolution of inflammation: elucidating leukocyte interactions via an experimentally-calibrated agent-based model. *PLoS Computational Biology.* 2020; 16(11):e1008413. DOI: 10.1371/journal.pcbi.1008413

Paper 1 encompasses the work of Chapter 3. Paper 2 encompasses the work of Chapter 5.

Contents

Chapter 1

Introduction

Inflammation (and its resolution) is central to the progression of many diseases and health conditions. Therefore, a thorough understanding of the process involved in the inflammatory response is central to the ongoing hunt for new treatments and therapies. The over-arching aim of this thesis is to investigate, through mathematical models, the implications of the spatial spread of inflammation on the long-term global outcome, examining whether spatially-dependent aspects of the inflammatory response, such as cell motility, can allow localised damage to invade neighbouring healthy tissue or can present a switch between restoration of health and chronic outcomes. This is motivated by current gaps in the existing literature, in which theoretical models of inflammation overwhelmingly focus on its temporal dynamics, often neglecting the spatial domain in which biological variables of interest operate.

In this study, we aim at addressing these gaps by developing spatial models of inflammation, focusing on interactions between groups of cells prompted by the immune response upon tissue injury. We first extend an existing homogeneous model that captures interactions between inflammatory mediators, neutrophils and macrophages to incorporate spatial behaviour. Through bifurcation analysis and numerical simulation, we show that spatially inhomogeneous outcomes can present close to the switch

from bistability to guaranteed resolution in the corresponding homogeneous model. Finally, we show how aberrant spatial mechanisms can play a role in the failure of inflammation to resolve and discuss our results within the broader context of seeking novel inflammatory treatments. We then proceed to describe the assembly of a hybrid mathematical model in which the spatial spread of inflammatory mediators is described through partial differential equations, and immune cells (neutrophils and macrophages) are described individually via an agent-based modelling approach. We pay close attention to how immune cells chemotax toward pro-inflammatory mediators, presenting a model for cell chemotaxis that is calibrated against experimentally observed cell trajectories in healthy and Chronic Obstructive Pulmonary Disease (COPD)-affected scenarios. We illustrate how variations in key model parameters can drive the switch from resolution of inflammation to chronic outcomes, and show that aberrant neutrophil chemotaxis can move an otherwise healthy outcome to one of chronicity. Finally, we reflect on our results in the context of the on-going hunt for new therapeutic interventions.

This chapter presents an overview of the main topics of interest for this work, by providing a theoretical introduction to a number of subjects that will be further developed in the following chapters. Firstly, a brief summary of the conditions that involve inflammation is provided in Section 1.1; a detailed biological description of the inflammatory process follows in Section 1.2; a review of the relevant literature in the modelling of inflammation is also presented in Section 1.3, followed by the definition and significance of patterns in biology and mathematics in Section 1.4; finally an overview of the whole thesis is provided, by outlining each chapter's content in Section 1.5.

1.1 The prominence of inflammation in health and disease

Inflammation has a central role in a large variety of pathophysiological processes and has long been recognised as a crucial step in the development of many diseases and chronic conditions. Although the range of pathologies that feature or arise from inflammation varies greatly (from cancer, to diabetes, to arthritis just to name a few), the cellular and chemical pathways that characterise the acute inflammatory response remain the same, making it important to specify and clarify these generic underlying mechanisms that control and lead these processes. As the common denominator in response to both tissue injuries and infectious agents, inflammation has long been associated to many diseases, thus suggesting a new approach in investigating complex pathologies such as cancer or Alzheimer, amongst others, by tackling those inflammatory mechanisms that have been shown to play a role in the development of such serious conditions. In this sense, inflammation can be regarded as key to a variety of diseases, many of which are still poorly understood; studying inflammation thus provides scope for new perspectives in the development of drugs and treatments (Hunter, 2012). While acute inflammation in itself is a physiological process aimed at promoting the release and action of specific cells and chemicals in order to restore a healthy state that has been disrupted by either injury or external pathogens, impairments and disorders affecting the delicate network of interactions that tightly regulate the inflammatory response can lead to chronic damage. Most diseases associated with inflammation arise from its degeneration into chronic state (Libby, 2007), with perpetual or recurring inflammations recognised as symptoms and features of such conditions.

Diabetes, a metabolic disease affecting an ever increasing number of people world-

wide, has long been associated with inflammation, with researchers identifying the role of the immune system in its pathogenesis (Pollack *et al.*, 2016). While this connection has already been characterised in type 1 diabetes, the links suggesting the exact mechanisms of inflammation's action on pancreatic cells and insulin resistance are still poorly understood, but nevertheless remain key in type 2 diabetes as well, as illustrated by Donath & Shoelson (2011). While traditional treatment for type 2 diabetes focuses on reducing hyperglycemia, completely neglecting the role of inflammation in this disease, in recent years a great interest has been posed in targeting this debilitating and costly long term condition with anti-inflammatory therapies. However, it still remains challenging to fully appreciate the inflammatory pathways that feature in diabetes and how best to address them in terms of development of new drugs and treatments (Deans & Sattar, 2006). Furthermore, the link between inflammation and diabetes has much wider implications, by directly involving or triggering other pathologies such as obesity, which has also been associated to low levels of chronic inflammation, as exposed by Wellen & Hotamisligil (2005).

A number of heart conditions have also been shown to arise in response to inflammatory mechanisms. Given the impact of these diseases and their strong correlation to type 2 diabetes and obesity, the centrality of inflammation and in particular of pro-inflammatory cytokines as markers of cardiac disorders motivate the interest of researchers in further investigating the links between these often complementary and overlapping conditions (Yudkin *et al.*, 2000). Following this pattern, Koenig (2001) and Yudkin *et al.* (2000) have individuated specific inflammatory mediators that are key in the development of coronary heart disease. More generally, as illustrated by Hansson (2005), atherosclerosis, which eventually leads to coronary heart disease, is in itself an inflammatory disease that still remains challenging to tackle in spite of its high incidence in mortality rates worldwide (Barquera *et al.*, 2015; Roquer & Ois, 2010). As explained by Libby (2006), the focus of researchers in this area is to better

clarify the inflammatory mechanisms that underlie cardiovascular diseases, in order to help targeting and prevent their development at much earlier stages.

Among the pathologies directly arising as a result of systemic chronic inflammation, rheumatoid arthritis is of particular importance. This disease is characterised by recurring inflammation of joints, eventually leading to their irreversible deterioration and triggering in turn the activation of additional inflammatory pathways (Sweeney & Firestein, 2004; Chimenti *et al.*, 2015). The systemic spread of inflammatory processes initiated by articular inflammation further worsens the risks of cardiovascular morbidity and constitutes a precursor of ventricular arrhythmias (Lazzerini *et al.*, 2017).

Pulmonary diseases also figure amongst the many chronic conditions associated with inflammatory mechanisms. As highlighted by Gan *et al.* (2004), inflammatory markers are expressed in correspondence to impaired lung functionality, typical of chronic obstructive pulmonary disease. This disease is itself a leading factor towards a number of conditions like cardiovascular disorders and osteoporosis. Again, a fundamental link between these diseases is systemic inflammation, as exposed by Sevenoaks & Stockley (2006), with early detection of the pro-inflammatory activity and targeted therapeutics currently being crucial points of focus within the research community.

As it is well established that many cancers arise from chronic states of inflammation (Moss & Blaser, 2005; Itzkowitz & Xianyang, 2004), much of the research related to tumourigenesis as well as its proliferation and metastatisation involves the study and analysis of the inflammatory pathways from which neoplasias may arise. While it is clear that inflammation does not necessarily degenerate into cancer development, the understanding of the mechanisms that regulate its chronicisation remains one of the key issues researchers are interested in. Inflammation is known to be a risk factor for many cancers (Shanthini & Balkwill, 2015), while also playing a critical role in further stages of tumour progression (Grivennikov *et al.*, 2010; Coussens & Werb, 2002).

As such, the new approaches in both the diagnosis of early tumour formation and the development of anti-tumoural drugs point towards the benefits of targeting inflammation as a promising alternative to more traditional and aggressive treatments. In particular, the expression of inflammatory cytokines within the neoplastic microenvironment suggests to further investigate the impact of anti-inflammatory therapies in the treatment of cancer. While tumour related therapies already include a number of anti-inflammatory drugs and treatments, the clarification of the role of inflammation in tumour growth and spread remains a promising leading aspect of cancer research (Rayburn *et al.*, 2009; Balkwill *et al.*, 2005).

Inflammation has been shown to be critical and possibly decisive also in the broader spectrum of Central Nervous System (CNS) injuries and diseases as well as modulating the progression of neurodegenerative disorders. The implications of such a link are multiple and fundamental in suggesting new investigative and therapeutic approaches to a variety of serious conditions (strokes, Alzheimer's and Parkinson's diseases, ...) that are still incurable and affect a growing number of people worldwide. In particular, inflammatory activity within the CNS is now recognised as a leading factor in the development of neurodegenerative diseases (Perry, 2004). On the other hand, the expression of different cytokines and their varied effects at different stages of the inflammatory response highlights the difficulties in determining the exact mechanisms that regulate the progression of CNS diseases. The highly dynamical nature of inflammation as a tightly balanced and controlled response of both beneficial and disruptive cascades of interactions explains the more recent interest of researchers in investigating the impact of the promotion of specific inflammatory pathways as a therapeutic tool, rather than suppressing inflammation altogether (Wyss-Coray & Mucke, 2002). Lucas *et al.* (2006) expose the promising but still partial results that this approach has provided for various CNS diseases, by targeting specific inflammatory mediators in the development of new therapies. While the potential benefits of

this approach for acute CNS injuries (traumatic brain injuries, stroke, cerebral ischaemia, epilepsy, ...) are already clear, this paper also highlights the criticality and challenges in the characterisation of chronic CNS diseases, where the exact role and effect of inflammatory mediators on the progression of neurodegenerative disorders are still poorly understood, with experimental trials and animal models providing mixed results. In particular, as shown by Gao & Hong (2008), is the degeneration of neuroinflammation into an uncontrolled process that characterises the progression of irreversible neurodegenerative diseases such as Alzheimer's, Parkinson's and Huntington's diseases and multiple and amyotrophic lateral scleroses. The understanding and regulation of inflammation is thus seen as key in the progression of neurodegenerative disorders, whose development and outcome can be modulated by the same inflammatory mechanisms that trigger them. This principle has since shifted the focus of researchers in treating and analysing Alzeheimer's as an inflammatory disease (Strohmeyer & Rogers, 2001; Heppner *et al.*, 2015; Holmes & Butchart, 2011), with Wyss-Coray & Rogers (2012) identifying inflammation as a possible tuning tool in the prevention and treatment of Alzheimer's. Similarly, the research of other prominent neurodegenerative disorders has also seen significant progress in this direction (Hald & Lotharius, 2005; Perez-Cerda *et al.*, 2016; Rocha *et al.*, 2016).

Below, we examine in greater detail the key cellular and molecular events that contribute to the inflammatory response in the myriad conditions described above.

1.2 A biological introduction to inflammation

Inflammation is a physiological process that involves a complex and intricate chain of reactions, at both cellular and molecular levels, as well as on a macroscopic scale, that has long been investigated and studied. The understanding of acute inflammation can be easily traced back to antiquity, with the four cardinal signs of the

inflammatory event being identified, more than two millennia ago, by the Roman physician Cornelius Celsus as *rubor et tumor cum calore et dolore*, that is redness and swelling with heat and pain (Woolf, 1986; Plytycz & Seljelid, 2003). By taking into account also a fifth key feature, that is *functio laesa* or loss of function, a minimal but accurate description of what inflammation is already emerges. In the following centuries and up to now, many more in-depth mechanisms have been identified and clarified, outlining how inflammation consists of a number of many complex, different and overlapping events, with the main aim of restoring the perturbed equilibrium of a previous healthy state. This perturbation can come in a variety of forms, most commonly by either injury or pathogenic infection, with any of such disruptive events eventually damaging the tissue and thus immediately triggering acute inflammation, expressly a series of localised and cellular changes that typically resolve within hours to days.

In this context, upon damage, the inflammatory response is set up by specific immune cells which are locally recruited and serve as sentinels of the insulted tissue (Diegelmann & Chalfant, 2016). Sentinel cells are a group of various cells that are involved, with different roles, in the first line of defence to develop an appropriate line of action against the occurring injury. More specifically, this consists in identifying the damage (either traumatic or pathogenic) through special surface receptors that recognise molecular patterns typical of wounded tissue or infectious agents. The swift sensing of sentinel cells is the main trigger to a larger scale of cellular interactions and prompts the further release of pro-inflammatory mediators which in turn contribute to and actively promote the inflammatory response. The chain of cellular interactions that spur from the prolonged pro-inflammatory activity eventually leads to a quick and efficient clearance of the damaged site, paving the way for tissue repair and full recovery, by a strong decrease in concentration of both pro-inflammatory mediators and acute inflammatory cells while enhancing the production of anti-inflammatory

mediators which actively counteract inflammation's spread and development, thus ensuring that a healthy condition is restored (Serhan *et al.*, 2010).

1.2.1 Cellular events in acute inflammation

The tight network of events that regulate acute inflammation, upon tissue damage, provide the injured site with a quick and continuous release of inflammatory mediators that differentiate in nature, specific function and timespan effectiveness but overall help to coordinate, promote and eventually resolve inflammation. In particular, two large groups of chemicals serving as pro- and anti-inflammatory mediators are active and high in concentration, the former at early and progressing stages of inflammation and the latter in its final stages. Pro-inflammatory mediators comprise a wide range of molecules, with a subset already present and stored as preformed in the healthy tissue and immediately released by specific cells (mast cells, Diegelmann & Chalfant, 2016). From the variety of chemicals released by these cellular granular stores, (namely serine proteases, vasoactive amines, cytokines and growth factors), the vasoactive amine histamine is responsible for vasodilation and increase in capillary permeability. This is a key feature to allow circulating immune cells and proteins to enter the injured area that results in local edema. Activated mast cells are also responsible for synthesising a variety of inflammatory cytokines and lipid molecules, while more mediators are the resulting product of plasma protein pathways (regulated by complement and coagulation systems, Phillips *et al.*, 2006).

Similarly to the onset of acute inflammation, as most recent research studies have underlined, resolution of inflammation is also an active process, with anti-inflammatory mediators modulating cellular interactions and prompting restoration of the healthy pre-inflammatory condition (Lawrence *et al.*, 2002). A high number of anti-inflammatory mediators have been identified in the form of endogenous molecules

that either restore vascular permeability (such as adrenaline and noradrenaline) or inhibit leukocytes activation (through the second messenger signalling molecule cAMP). Another group of hormones, glucocorticoids, provide the main feedback responsible for the reduction of inflammation by antagonising the production of pro-inflammatory mediators on one hand and enhancing the synthesis of more anti-inflammatory mediators on the other (Lawrence *et al.*, 2002). Similarly, lipid mediators also contribute to the anti-inflammatory activity by actively promoting resolution of inflammation and tightly regulating cellular concentration levels at the injury site (Lawrence *et al.*, 2002).

Much of the inflammatory activity initiated by chemical mediators is carried out by leucocytes or white blood cells, characteristic of the immune system and comprising a varied group of cells with different features and functions. In general, upon tissue damage, the initial release of pro-inflammatory mediators causes enhanced vasodilation and reduces capillary blood flow, thus resulting in locally increased recruitment of leucocytes directly interacting with vascular endothelium and finally entering the injured site through molecule-bound adhesion mechanisms. Different types of leucocytes are recruited at different times and with varied functions. Neutrophils, the most numerous white blood cells in humans, making up to 75% of the total circulating, are the first cell population to rapidly intervene in the earlier stages of acute inflammation with varied tasks in tackling the local tissue disruption. Neutrophils are produced in the bone marrow and released into the blood stream in an already active form (Kolaczkowska & Kubes, 2013). The main feature of neutrophilic activity is the ability to rapidly and efficiently migrate to the injury site to engulf or neutralise the sources causing tissue damage. While most neutrophils are recruited to the injured site, a smaller number of other leukocytes can already be present in the area of interest (Woolf, 1986). The efficient recruitment of neutrophils is crucial to inflammation development and its eventual resolution, with these white blood cells typically en-

tering the insulted site within minutes of the occurred injury. The emigration from the blood stream to the local damaged tissue is prompted by specific signalling interactions between neutrophils and endothelial cells that, upon activation, attract the flowing neutrophils to the endothelium through adhesion mechanisms. The consequent cell-to-cell recognition and interaction between the endothelial structure and adhering neutrophils allows the latter to pass the cellular endothelium gaps and finally enter the extravascular space (Woolf, 1986; Diegelmann & Chalfant, 2016). This whole process, while being particularly complicated and presenting some interactive mechanisms that are not completely clarified yet, is quite rapid and usually requires from two to fifteen minutes to complete (Kolaczkowska & Kubes, 2013).

The articulate signalling activity that attracts neutrophils to the injury site and coordinates their phagocytic and neutralising action is known as *chemotaxis*. This consists of a chain of signal transmission and transduction events that results in a highly organised and ordered vectorial motion of neutrophils to the inflammation site, together with a selective action on those pathogens or harming particles responsible for the ongoing inflammation (Woolf, 1986). Once at the injury site, the specificity of neutrophil activity is ensured by a precise recognition of the insulting object that is thus phagocytosed through engulfment of the intrusive particles to the membrane and their inclusion in internal vesicles in which they are finally digested and neutralised. Alternatively, neutrophils can also externally trap pathogens or damaging debris through a network of extracellular fibres, known as Neutrophil Extracellular Traps (NET), primarily composed of neutrophilic DNA and granular proteins that effectively clear the selected targets (Kaplan & Radic, 2012; Zawrotniak & Rapala-Kozik, 2013). Furthermore, essential to the inflammation progress and eventual resolution, neutrophils release internal granular contents to the extracellular environment in the form of mediators, mainly comprising Reactive Oxygen Species (ROS) and proteases, that further promote inflammation and recruitment of new neutrophils. On

the other hand, upon phagocytosis, the internal disposal of the phagocytic activity heavily relies on enzymatic and oxygen-dependant mechanisms also involving ROS. The typical toxicity of both these enzymatic particles and highly reactive molecules already suggests a further critical feature of the inflammatory process, that is the adequate removal and clearance of neutrophils that have completed their activity and phagocytosis. These neutrophils thus undergo apoptosis, a physiological process of programmed cellular death that prepares for their clearance and removal, biologically designed to prevent neutrophilic release of toxic contents (Fox *et al.*, 2010). It is important to highlight that apoptosis is fundamentally different from necrosis, in which the cellular death is triggered by irreversible cell damage involving the pouring out of intracellular particles, that are potentially disruptive and provide a further source of inflammation (Quinn *et al.*, 2007). On the other hand, neutrophils become apoptotic upon a regulated change in both their receptivity to specific signalling and membrane proteins, as well as an impairment in adhesion mechanisms (Greenlee-Wacker, 2016). The morphological and chemical alterations that appear to characterise the transition from active to apoptotic neutrophils are fundamental in initiating a further cascade of cellular events crucially leading to the resolution of inflammation. In fact, apoptotic neutrophils induce an increase in anti-inflammatory mediators, while their presence in apoptotic form is actually limited as a result of a highly effective clearance mechanism. This typically happens through the intervention of another group of phagocytic white blood cells, called macrophages whose manifold activity includes, but is not limited to, phagocytising apoptotic neutrophils.

Similarly to neutrophils, macrophages are also produced in the bone marrow but are released in the blood stream in the immature form of monocytes. Instead, mature cells are typically within the tissue and prompted into action by a variety of stimuli characteristic of the earlier stages of inflammation. Depending on the residing tissue, mature macrophages present different morphologies and functionalities and have

distinct nomenclature to reflect their localisation. However, overall they share the same distinctive feature of countering intruding agents and further coordinating the inflammatory response. While classic literature (as suggested by Mosser & Edwards, 2008 and Diegelmann & Chalfant, 2016) considered a well established distinction between two types of macrophages, namely M1 and M2 phenotypes, differentiating in specific functions, with M1 macrophages traditionally designated to promote pro-inflammatory activity and M2 macrophages later releasing anti-inflammatory mediators, it has more recently emerged that such subsets are quite limited in their biological description of the inflammatory events (Lawrence *et al.*, 2002). Rather, macrophages are believed to express a wide range of phenotypes in between the M1 and M2 ones, with particular specificities but also overlapping functions. More importantly, it is now well established that macrophages play a key role in the resolution of inflammation, highlighting how the positive outcome of the inflammatory event is an active process (Serhan *et al.*, 2007; Ortega-Gomez *et al.*, 2013; Freire & Van Dyke, 2013). In this regard, when exposed to the early inflammatory response led by neutrophils' rapid recruitment and release of pro-inflammatory mediators, macrophages are induced to further reinforce the phagocytic activity, with similar mechanisms to that of neutrophils. Furthermore, at this stage the interaction of macrophages with endothelial cells results in chemotactic recruitment of additional pro-inflammatory mediators that in turn enhance neutrophil activity. With the sequential and coordinated efforts of leukocytes to phagocytose and neutralise the damaging particles and pathogens, macrophages gradually expose more anti-inflammatory phenotypes that lead to the eventual resolution of inflammation. The wound healing process lead by macrophages inhibits the pro-inflammatory response by releasing a variety of chemicals as anti-inflammatory mediators and growth factors that induce and promote tissue repair. Furthermore, an important step towards resolution of inflammation relies on an efficient clearance by macrophages of the apoptotic neutrophils at the in-

flammation site. This process involves multiple interactions between the two groups of cells, with macrophages firstly attracted by apoptotic neutrophils (Hochreiter-Hufford & Ravichandran, 2013) and consequently ingesting them through a process named efferocytosis. Efferocytosis ensures a rapid clearance of apoptotic neutrophils, whose otherwise prolonged presence and spilling of toxic contents would result in damage of the local tissue, thus ensuring a correct healing process. This also further clarifies how in healthy development and resolution of inflammation, levels of apoptotic neutrophils are relatively low, since their clearance is physiologically rapid and effective. On the other hand, impaired macrophagic activity would prolong inflammation, possibly preventing correct tissue restoration and eventual resolution.

1.2.2 Unresolved outcomes: chronic inflammation

While the physiological response to any tissue damage is immediate and tightly regulated by specific cellular signalling, acute inflammation is not always naturally or fully resolved and can degenerate into a pathological state, giving way to inflammatory diseases and chronic inflammations (Phillips *et al.*, 2006). In this regard, it is still challenging to understand fully the mechanisms that prevent a healthy and physiological recovery and lead instead to a critical and potentially disruptive condition. At the same time, a variety of faulty events have been recognised and described that are known to impair or prevent a correct resolution of inflammation, while further research into this topic is key to suggesting new therapeutic targets to address the current shortcomings of the understanding of chronic inflammation. Chronic inflammation can result from a wide range of disfunctions of the inflammatory reactions, as well as repetitive tissue injuries, that interfere with the physiological course of inflammation and cause its proliferation by prolonging it and further damaging neighbouring tissues. Preventing the pathological spread of inflammation or appropriately

and efficiently treating its chronic condition would ensure fundamental advance in possible therapies of many numerous diseases that invariably present typical chronic inflammatory patterns in their development and manifestation, such as cancer, diabetes, cardiovascular and autoimmune diseases, neurodegenerative disorders (Hunter, 2012). At the cellular level, chronic inflammation is characterised by high concentrations of macrophages that in turn provoke an overproduction of pro-inflammatory mediators, eventually resulting in inflammation spread. In this context, endothelial cells also undergo pathological changes that lead to an overexpression of adhesive molecules, thus attracting even more leukocytes to enter the site. Endothelial repair is also affected with common formation of fibrous scar tissue, possibly preventing function recovery (Phillips *et al.*, 2006). The mechanisms here described characterising the disfunctions leading to chronic inflammation will be discussed in greater detail throughout the thesis.

1.3 Previous mathematical models of inflammation

With inflammation being such a prominent and complex event that, if uncontrolled, might eventually lead to a variety of pathologies and unhealthy outcomes (chronic inflammation, atherosclerosis, diabetes, cancer, etc.), it has long been a primary interest of biologists and physicians to better understand inflammatory mechanisms and exactly characterise the different pathways that are featured. The lack of knowledge of specific interactions at both cellular and molecular levels regulating the cascades of reactions that determine the inflammation spread and outcome has so far prevented the development of effective and appropriate therapeutic strategies, considerably increasing health costs and resources while also dramatically affecting patients (Pfizer,

2017). As such, mathematical models are a particularly advantageous tool to further deal with and investigate in this field. In general, mathematically modelling biological processes is of great utility for multiple reasons, especially by enabling us to predict outcomes of interest, with state of the art models practically providing reliable simulations that considerably cut both economic and time costs. The study and development of mathematical models for a wide range of biological applications has thus been of great interest among the scientific community, involving researchers from different backgrounds and relying on both a deep knowledge of the relevant biology and its realistic mathematical representation, with the ultimate aim of biologically analysing and interpreting the mathematical results with regard to insights and predictions (Murray, 2001).

Many researchers have already developed and investigated valuable mathematical models of inflammation, with particular focus on its dynamics and progression lead by infective sources. While, in parallel, animal models are widely investigated (Webb, 2014), the important disadvantages given by this approach, being considerably more expensive and time-consuming than *in silico* alternatives, coupled with the ethical limitations of both animal experimentation and human trials, have further encouraged computational modelling research and development (Seoka *et al.*, 2013). The surge in mathematical models of inflammation comes in response to the inadequacy of inflammation suppression as a valid and effective therapeutic tool. Meanwhile, the variety of mathematical approaches that can be applied to the modelling task (Vodovotz & An, 2013), such as equation-based models, hybrid models (combining computational model comprising multiple scales), and *in silico* trials (computational simulations of clinical trials), provide the opportunity to investigate and clarify those inflammatory mechanisms that are still poorly understood, possibly suggesting how to target and regulate therapeutic strategies (Dunster & Dransfield, 2016).

Earlier studies of inflammatory mechanisms at the tissue level, particularly focus-

ing on the effectiveness of the immune response arising from bacterial infection, are presented in a series of papers developing mathematical models that investigate the interactions between inoculated bacteria and resident phagocytosing cells (Lauffenburger & Keller, 1979; Lauffenburger & Kennedy, 1981, 1983). In their papers, these researchers highlight the crucial role of localised accumulation of leukocytes at sites of infection. Overall, the analysis posed in Lauffenburger & Keller (1979); Lauffenburger & Kennedy (1983) is however more focused on the mathematical parametrisation of these features rather than studying the impact different spatial distributions might have in terms of infection spread and eventual outcome. In particular, Lauffenburger & Keller (1979) develop a one dimensional model comprising of a group of bacteria acting as a chemoattractant source to leukocytes that in turn neutralise infectious agents in order analyse how immune cells' chemotaxis is affected upon bacterial infection. A detailed bifurcation analysis determines two possible spatially homogeneous outcomes of a uniformly healthy or damaged tissue, with chemotaxis proving to be crucial in effectively overcoming bacterial infection. Furthermore, conditions for the potential existence of spatially heterogeneous steady states are also individuated, suggesting the need to extend the model for further confirmation. This is achieved in Lauffenburger & Kennedy (1983) in which a more refined model of the interactions between bacteria and phagocytosing cells exhibits spatially inhomogeneous results in response to threshold values of the parametrised chemotaxis. In particular, the non-homogeneous states are shown to arise from the rapidity of cells' motility with respect to bacterial motility, with chemotaxis becoming less effective in driving spatially inhomogeneous steady states upon an increased random motility of bacteria. The related bifurcation analysis provides parametric conditions to predict the homogeneity of steady states, with spatial heterogeneity viewed as undesirable in terms of tissue health. This is further confirmed by numerical results that successfully predict the spatial nature of the steady states, upon varying values of chemotaxis, by also

providing a biological interpretation of the severity of infection with respect to bacterial concentrations. On the other hand, the authors point to a lack of experimental data on cells chemotaxis preventing a more accurate analysis of results in terms of phagocytes spatial behaviour. Values for motility parameters are also adjusted in order to overcome the limitations introduced by the oversimplification of the model as well as to try to adapt the available in vitro experimental data to in vivo scenarios.

An interesting inflammatory model was developed by Kumar *et al.* (2004) by investigating the mass-action kinetics of two groups of early and late pro-inflammatory mediators triggered by pathogenic action. The late pro-inflammatory mediator effectiveness is bound to a saturating kinetics. The model's analysis shows a set of results consistent with typical acute inflammatory outcomes. In particular, through careful manipulation of parameters, the model determines the links between pathogen's virulence and inflammatory response to inform on possible treatment approaches for sever sepsis. Conversely, a major limitation of this model comes from overlooking possible varied outcomes that may result from the same setting of clinical symptoms. To tackle this, a more structured model that includes more biologically significant variables and handles overlapping symptoms is required. In this regard, it is of particular importance to take into account the active role of anti-inflammatory mediators in the resolution of inflammation (Serhan *et al.*, 2008) and appropriately model it. Brady *et al.* (2016) propose a mathematical model investigating the pro- and anti-inflammatory interactions spurting from bacterial infection. The model is calibrated to experimental measurements, with the mediators' dynamics providing patient-customised prediction of levels of specific groups of chemicals acting as both pro- and anti-inflammatory mediators. Since cytokines of interest are modelled and accounted for separately, the model lacks the analysis of inflammatory pathways arising from other mediators that have not been included.

A detailed model of inflammation studying the dynamics of anti-inflammatory

processes has been proposed by Reynolds *et al.* (2006). This model studies the inflammatory components at cellular level, analysing measures of pathogens, active phagocytes, tissue damage and anti-inflammatory mediators in time. The many parameters featuring in the resulting system of ordinary differential equations (ODEs) are partly inferred from previous literature and partly assessed through bifurcation analysis of the system's steady states. As expected and widely supported by previous research, anti-inflammatory mechanisms are shown to be key to a healthy outcome. On the other hand, in this work, the acute inflammation is modelled as a response to pathogenic action, thus excluding those instances of inflammation arising from tissue damage and without any pathogens involved. Furthermore, as is intrinsic to any model representation of complex processes, the simplifications introduced fail to capture some biological mechanisms that may be determinant to the overall outcome, while not all the quantities analysed have a straightforward biological correspondent. Nonetheless, this model has been further expanded and analysed also by other researchers, with interesting applications. One such application is the work of Day *et al.* (2010) that proposes a predictive model to suggest therapeutic indications for severe sepsis emerging from pathogenic infection, highlighting the potential benefits introduced by feedback control methods. In response to the crucial need of recognising early the different inflammatory stages and delivering effective therapeutic strategies accordingly, Radosavljevic *et al.* (2013) develop a prediction model that assesses past states and past drugs' doses in order to predict new levels of pathogen, pro-inflammatory mediators, markers of tissue damage, and anti-inflammatory mediators. This approach showed higher accuracy in the results, while also confirming that a patient's response to acute inflammation and specific therapies is complex and varied. A further study focusing on the inflammatory response triggered by infection proposes a mathematical model that captures the interactive dynamics between inflammatory mediators and pathogens (Roy *et al.*, 2007). The prominence of inflam-

mation in a variety of medical conditions has prompted more researchers to investigate the potential benefits of computational models to wider and more specific scenarios that inevitably involve inflammatory events (Russo *et al.*, 2010; Day *et al.*, 2015).

In more recent works, Torres *et al.* (2019) develop a mathematical model investigating the dynamics of the influx of immune cells upon inflammation driven by peritonitis. A system of ODEs representing the interactions between different groups of leukocytes is studied with respect to the polarised behaviour of macrophages between the inflammatory and anti-inflammatory phenotypes. The model is further fitted to *in vivo* experimental data providing an extended framework to test intervention hypotheses to best assess targets and outcomes of therapeutic actions on macrophage phenotypes. A further investigation in the role of macrophages is presented by Jansen *et al.* (2019) with a particular focus on human inflammatory bowel disease. This work illustrates the scope for effectively combining *in silico* modelling and analysis of data extrapolated from laboratory experimentations. In particular the authors examine the impact of including rich datasets inferred from relevant biopsies into mechanistic models, suggesting improved parametrisation and higher spatio-temporal resolution, which in turn broaden the applicability of such models. An in-depth study of variations in neutrophil recruitment and death pathway in the inflammatory response is presented by Presbitero *et al.* (2019). In their work, Presbitero *et al.* (2019) investigate the effects of neutrophil apoptosis and necrosis in terms of evolutionary game theory. Within this framework, apoptosis and necrosis are presented as diverging strategies and driving mechanisms regulating the inflammatory outcome. The integration of this model with data inferred from inflammatory markers further provides analyses of benefits and costs of each pathway and the prediction of percentages of occurrence of both apoptotic and necrotic events with respect to the original insult triggering the inflammatory response.

While the mathematical models reviewed so far consider inflammation at a mi-

croscopic level, with system variables accounting for group of cells and chemicals, other researchers have also proposed different approaches by modelling inflammatory mechanisms at body level. Sullivan & Yotov (2006) develop a spatial model of inflammation (later also included in the paper of Upperman *et al.* (2007)) investigating organs' walls and structures, with leukocyte and cytokine interactions being framed within lumen, epithelium, tissue and blood vessels, with a larger focus on pathogenic action (with the bacteria's anatomy affecting the cells migration). In their work, the main interest is to investigate the response of organ walls to the specific pathological events that commonly arise within premature infants (necrotizing enterocolitis). The key results show that, when in presence of damaged epithelial membranes, otherwise harmless bacteria can penetrate the tissue and cause infection. This, in turn, affects the final outcome of the body's inflammatory response, with full healthy recovery in simulations with membranes damaged only partially, while on the other hand, upon a complete lack of membrane walls, the results highlight persisting inflammation and spread of damage. While it provides valuable evidence in terms of spatial modelling, the specificity of the pathological implications investigated in this work, render this model quite different from the main objective of our project, thus further motivating our interest in clarifying the spatial characterisation of the non-pathogenic inflammatory response and individuation of possible therapeutic targets, with this latter aspect missing in the work of Sullivan & Yotov (2006).

An effort in addressing part of these open issues is offered by Penner *et al.* (2012), with a mathematical model of skin inflammation to study spatial patterns typical of rash formations. In this model, the biological relation and interactions of macrophages, chemoattractant chemicals and anti-inflammatory cytokines are simplified such that phagocytosing cells appear as a fixed quantity, and anti-inflammatory mediators inhibiting both themselves and chemoattractants and acting on slower timescales. This inhibitory and delayed action is proven to further push the model's

spatial behaviour, as highlighted by the study of the system's stability and numerical simulations, with particular emphasis on the classification of patterns at varying values of key parameters. While valuable for including spatial considerations in the study of acute inflammation, this model still lacks fundamental biological features (namely, the characterisation of macrophage dynamics in terms of phagocytosis and turnover, the pro-inflammatory activity of both leukocytes and chemicals), as well as not providing any link up with experimental data in terms of both parameter values and simulations assessment.

Of particular significance to this work is the work of Dunster *et al.* (2014), since this work will form the basis of the novel models presented throughout this thesis. Analogously to the model of Day *et al.* (2010), Dunster *et al.* (2014) also propose a mathematical representation of inflammation at cellular level in the form of an ODE system, monitoring the dynamics of cellular components (active and apoptotic neutrophils, macrophages) and chemicals (pro- and anti-inflammatory mediators). The acute inflammation is considered to be in response to generic tissue damage, and is thus in the absence of pathogens. In particular, three different models are constructed and analysed in which individual populations of white blood cells are accounted for separately, namely comprising active neutrophils, apoptotic neutrophils and macrophages. Such differentiation allows for an accurate description of the immune cells behaviour, with neutrophils promoting inflammation and macrophages actively initiating its resolution. The first of the three models presented is deliberately simple in its functions, omitting any anti-inflammatory mediators and characterising cellular interactions in response to pro-inflammatory mediators only, which trigger the acute inflammation. The numerical analysis of this initial ODE model provides two sets of results, corresponding to either a healthy (zero) steady state or unhealthy (chronic, non-zero) steady state. Manipulation of key parameters, namely the number of cycles of damage and rate at which macrophages phagocytose apoptotic

neutrophils, are also shown to affect the systems results. Increases in the former promote unresolved outcomes while enhancing the rate of phagocytosis enables previously chronic outcomes to fully resolve. The bistability of the model is further investigated through bifurcation diagrams, exposing the role of other key parameters acting as a switch between chronic and resolved inflammation. In particular, manipulation of the parameters controlling the rate at which macrophages leave the tissue and the concentration of neutrophils required for half-maximal release of pro-inflammatory mediators can result in a change of the systems stability. In particular, the increase of the level at which neutrophils saturate in the presence of pro-inflammatory mediators prompts the gradual weakening of the inflammatory response. Such behaviour ceases for larger values of this saturation parameter when surpassing a bifurcation point, after which only the healthy steady state is viable. Conversely, the system is bistable for large values of the rate at which macrophages leave the tissue, while only healthy outcomes are permissible for smaller values.

In order to model neutrophils behaviour more accurately, to account for them actively promoting inflammation by releasing toxic granules meant to counter infection, regardless of the actual presence of pathological agents, the authors then present a revised model that accounts for this added feature in the form of a positive feedback for active neutrophils. Numerical and bifurcation analyses of this second model confirm the results inferred from the first model while also additionally exposing the key role of the parameter controlling the rate of neutrophils apoptosis. In particular, an increased rate of apoptosis favours healthy outcomes.

Finally, in order to include the anti-inflammatory role of macrophages, the authors further extend the model by adding a separate variable accounting for anti-inflammatory mediators, whose behaviour contrasts that of pro-inflammatory chemicals. Crucially, this extended model exhibits, in addition to the healthy and unhealthy steady states, a sustained oscillatory regime, which is more closely associ-

ated with chronic inflammation. This third model retrieves the results highlighted by the previous models and additionally suggests, through bifurcation analysis, the key role of the parameter controlling the production of anti-inflammatory mediators by macrophages. In particular, an increase in the production of anti-inflammatory mediators, reduces the rate of phagocytosis needed to prompt the resolution of inflammation.

While the results of Dunster *et al.* (2014) further confirm the critical and active role of anti-inflammatory mechanisms in the resolution of inflammation, a key limitation of this work is that spatial behaviours are omitted, with all three models focusing on spatially-averaged, temporal dynamics. Simulating inflammatory interactions between leukocytes and cytokines and analysing their spatial development and spread is crucial in understanding those mechanisms that still remain unclear and that could potentially open the way to new effective therapeutic strategies. We take the homogeneous model of Dunster *et al.* (2014) as the starting point for our theoretical studies; hence, we revisit the corresponding models in Chapters 2 and 3. In particular, we present more detailed reviews of the governing equations of the first and third models from this paper in Sections 2.1 and 3.2 respectively.

As the relevant literature (cited above) in the context of mathematical models of inflammation shows, existing gaps emerge between the robust implementation of mathematically complex models and their direct applicability in clinical contexts. This is part of a more general gap investigating a variety of biological topics and not specific of inflammation. The high interest in researching and developing effective models of biological processes is further motivated by the need to overcome important limitations of both *in vivo* and *in vitro* approaches. Along with the most immediate advantages in significantly optimising both costs and time and replicability of results, mathematical models offer the possibility to assess quantities that cannot be measured directly and to tailor patient-customised approaches by careful

manipulation of parameters, which studies of inflammation cannot otherwise directly address.

Narrowing our aims to contribute to the research of mathematical models of inflammation, we individuate the lack of studies in the spatial spread of damage and how this affects the acute inflammatory response as an important limitation in the current state of the art. As such, our main objective within this thesis is to address, through mathematical models, how localised damage can spread and invade into surrounding healthy tissues.

1.4 Pattern formation

Highly structured and regular patterns feature prominently in a variety of physical and biological phenomena; it is thus of primary interest to understand the mechanisms that lead to spontaneous patterning. Natural patterns arise from a wide range of systems and, while the environmental contexts that frame spatial patterning can vary greatly, specific features and characteristics in shape are easily encountered in developed patterns that would otherwise have very little in common. Several straightforward examples can be given in this regard, by observing the striped nature of zebra skin, sandy crests and meteorological convective rolls all exhibiting the same stripe structure, including the characteristic merging of two stripes into one (Hoyle, 2006). This strongly suggests that, in order to understand and analyse these phenomena, it is important to focus on the symmetries, rather than the environmental surroundings, and the mathematical theory that underlies these. Most spatiotemporal patterns that are observed empirically can be described and reproduced mathematically, but while the current state of the art in pattern formation modelling does not yet provide exhaustive details of these complex processes (Maini & Othmer, 2001), patterning and structured forms emerge both from physical laws and in living systems (Chuong &

Richardson, 2009) and can thus be mathematically analysed in depth.

The criticality of fully understanding the mechanisms that lead to structural morphogenesis on, one hand, and that could potentially prevent or counter the development of pathological and disruptive events on the other hand motivates the interest in analysing pattern formation when mathematically modelling biological processes (Maini & Othmer, 2001). A variety of mathematical structures are effective in describing and characterising patterns that arise naturally in different biological scenarios. Among others, reaction-diffusion systems are particularly suited to describing different patterning phenomena and have been deeply investigated to this purpose, starting from the seminal work of Turing (1952). In particular, in its simplest form, the interaction between the ligand and the morphogen of a reaction-diffusion systems represent the patterning mechanism upon which the system generates spatial patterns autonomously (Kondo & Miura, 2010). The Turing instability is defined as the destabilisation of a stable homogeneous steady state by diffusion, resulting in stable inhomogeneous static configurations. Turing instabilities are of significant relevance in theoretical biology by providing an explanatory model for the formation of varied patterns independent of their initial spatial configuration. The specific conditions for Turing patterns to arise are detailed in appendix A.

More generally, the existence of spatially-inhomogeneous solutions to reaction-diffusion (PDE) models is often associated with changes in the stability of steady states in the corresponding homogeneous (ODE) models, as can be exposed by classical bifurcation analysis. In particular, the nature of those critical points marking a change in the stability of fixed points informs on the possible existence of spatially inhomogeneous solutions, thus providing an effective tool to explore the dependence of the system on its parameters and a map of the solutions to be expected accordingly. In particular, Hopf bifurcation points, that is bifurcation points where the stability of fixed points changes and periodic orbits are created, are relevant in the character-

isation of many systems' spatial behaviour. This field of investigation is particularly prominent in a number of classic dynamical systems that are extended to include more complex scenarios. Shi *et al.* (2019) study patterns arising from Hopf bifurcation in a delayed diffusive logistic model, while also diffusive extensions of the predator-prey system are widely studied. In this regard, Lin *et al.* (2019) investigate the ecological mechanisms that drive the formation of patterns within the predator-prey model, determining how both spatially homogeneous and inhomogeneous periodic solutions originate from Hopf bifurcations. Turing and Hopf instabilities are not mutually exclusive, with a prominent example being the reaction-diffusion Gray-Scott model. Mazin *et al.* (1996) detail the conditions under which the spatial patterning of this model originates, while McGough & Riley (2004) particularly focus on the bifurcation analysis supporting the nature of the patterns that the solutions exhibit. A detailed investigation of pattern formation in inflammatory models is provided by Penner *et al.* (2012), where the authors examine the conditions triggering spatial inhomogeneity when chemotactic motion of a fixed population of immune cells is involved. In particular, with the aim of studying skin rash developments, Penner *et al.* (2012) model the interactions between a group of cells, releasing both chemokines which serve as chemoattractant and inhibitors which act on a slower time scale. In their study, a combination of Hopf and Turing bifurcations prompt the development of varied spatial configurations, with the instabilities arising upon low levels of the inhibitor. In particular, the authors focus on defining the conditions on parameter values in obtaining the different spatial configurations.

Finally, another broad modelling framework that can emit spatially inhomogeneous outcomes and particularly relevant to this work is Agent Based Model (ABM) modelling. This modelling approach, which will be introduced and discussed in detail in the dedicated chapters, is used in many multidisciplinary studies including theoretical biology, effectively capturing a wide range of mechanisms prominent in evolving

cellular systems, from morphogenesis to cancer growth and wound healing (Deutsch & Dormann, 2016). In their book, Adamatzky & Martinez (2016) present a variety of patterns arising from ABM models and the different implementing approaches that give rise to them. In addition to the biologically relevant capability of these models to generate spatially inhomogeneous structures, ABM frameworks are also used in the detection of patterns, which serves as a key role in many biomedical applications (Ahangaran & Beigy, 2009; Miranda *et al.*, 2016).

1.5 Thesis overview and objectives

The aims of this study are to develop spatial models of inflammation and assess the impact of its spatial spread through manipulation of related parameters. In particular, we examine the scope for the formation of spatial patterns, and the extent to which localised damage can spread into neighbouring healthy tissue. In this work, two different approaches for modelling the acute inflammatory response at the tissue level are deployed and compared; in Chapters 2 and 3, we take a PDE-based approach, and in Chapters 4 and 5 we take an agent-based approach, and examine the extent to which key conclusions are sensitive to the modelling approach used.

Firstly, in Chapter 2, we present a simple model of inflammation with the main objective being to investigate pattern formation from an analytical point of view. In particular, in Chapter 2, a basic model of inflammation is presented, where the first ordinary differential equation (ODE) model of Dunster *et al.* (2014), describing the mechanisms at play between immune cells and pro-inflammatory mediators, is extended to include relevant interactions within a spatial domain. In this chapter, we construct a partial differential equation (PDE) model in which cells and mediators move diffusively. In order to facilitate analytical progress, we keep the model deliberately simple, including only a minimal set of biological interactions. We examine

the extent to which the resulting reaction-diffusion equations exhibit spatial patterns, including those potentially arising via Turing instabilities and Hopf bifurcations.

In Chapter 3, we build upon the model of Chapter 2 to include biological features previously neglected, namely cellular chemotaxis, the presence of anti-inflammatory mediators and the enhanced feedback of neutrophils in the production of pro-inflammatory mediators. In doing so, we develop a model that we believe incorporates a full repertoire of biological feedbacks, and constitutes an extension of Model 3 of Dunster *et al.* (2014) to a spatial domain. The primary objective in this chapter is to understand the impact of these additional behaviours within a spatial setting, with particular emphasis on investigating the model's capability of admitting spatially inhomogeneous results and individuating possible therapeutic targets.

In Chapter 4, by moving to an agent-based modelling approach, we address the objective of evaluating whether our conclusions are sensitive to the modelling approach used. To this end, a novel model of inflammation is built in Chapter 4, by using the ABM framework, thus providing us the opportunity to further refine specific cellular mechanisms that are not captured in our PDE descriptions of the inflammatory response, while also overcoming the shortcomings of purely deterministic approaches. We present simulations of our agent-based model, demonstrate how variations in key parameters can switch the inflammatory outcome from health to chronicity, or *vice versa*, and show a comparison between the two models of inflammation developed in Chapters 3 and 4. To further quantify the dependence upon model's parameters, we perform a local parameter sensitivity analysis, to provide insight into which mechanisms could potentially be manipulated in new therapeutic strategies.

The objectives of Chapter 5 are to focus specifically upon the role efficient chemotaxis of leukocytes has in resolving inflammation and to construct an accurate chemotaxis model that can be calibrated against experimental data. We construct a refined model of chemotaxis (within our ABM framework) that integrates both sensitivity to

the chemotactic gradient and persistence in cells directions of motion, and examine how weaker chemotactic sensitivity or stronger directional persistence (such as is observed in some inflammatory conditions or in ageing) can drive a switch from health to chronicity. The model is calibrated against previously published experimental data related to healthy patients and patients with the highly impacting chronic inflammatory disease Chronic Obstructive Pulmonary Disease (COPD) (Sapey *et al.*, 2011), in order to effectively reproduce both healthy and pathological cellular directed motion. We integrate this improved model of chemotaxis into our larger agent-based inflammatory model, assess the results and compare them to those yielded by the model in Chapter 4.

Finally, Chapter 6 will present the main conclusions arising from this work, discussing all relevant results, summarising the key observations emerging from our investigation into the spatial modelling of inflammation, and also addressing possible directions for future works.

Chapter 2

Immune cell interactions with pro-inflammatory mediators

In this chapter we aim to extend Model 1 of Dunster *et al.* (2014) to include a spatial domain. Our primary objective is to analytically assess the models capability of admitting spatially inhomogeneous results, for example via Turing instabilities or via bifurcations in the dynamics of the underlying ODE model. To facilitate this, we favour the simplicity of using the model of Dunster *et al.* (2014) as a starting point, since it includes only a minimal set of basic biological interactions and thus allows the greatest scope for analytical investigation. In this regard, a preliminary version of an inflammation model is provided and analysed, focussing on the interactions between immune cells and pro-inflammatory mediators. Firstly, a spatially-independent model presented by Dunster *et al.* (2014) is reviewed in detail, before being later extended by including terms representing spatial movement of the groups of cells and chemicals featuring in the model. These interactions are studied at cellular level, by not only focusing on the impact of inflammation in time but also on its spatial spread, by deriving the conditions that lead to possible spatial patterning and highlighting its relevance in biological terms. A key assumption that will hold throughout this

chapter is the absence of pathogens. This allows us to focus on the progression of the inflammatory response, with generic tissue damage considered as the physiological trigger to the acute inflammation.

2.1 ODE model review

A first version of an inflammation model is presented in Dunster *et al.* (2014), in which no pathogens are included, while interactions between three groups of generic cells and mediators evolving in time (t^*) are considered (with stars denoting dimensional variables), namely: active neutrophils $n^*(t^*)$; apoptotic neutrophils $a^*(t^*)$, which are inactive, *unable to move*, have little phagocytic ability and release toxic chemicals when undergoing necrosis; macrophages $m^*(t^*)$, activating to clear apoptotic neutrophils; and pro-inflammatory mediators $c^*(t^*)$, attracting both neutrophils and macrophages.

The biological description of the chain of events leading to interactions of pro- and anti-inflammatory nature in response to damage allows us to derive useful modelling parameters. Following a generic trauma, a complex variety of chemical species is released within the damaged tissue, comprising cytokines, chemokines and complementary proteins, triggering proteolytic cascades resulting in the production of effective pro-inflammatory mediators, as well as activating relevant cellular signalling (Dunkelberger & Song, 2010; Aziz *et al.*, 2013). In this sense, the overall release and decay rates of any generic pro-inflammatory mediator (c^*) are defined as α^* and γ_c^* respectively. Furthermore, upon a prolonged inflammatory state or new damage, new concentrations of c^* are released, with k_a^* being the concentration of mediators released on lysis of apoptotic neutrophils. This prompts the migration of neutrophils to the damaged site, with a maximal incoming influx rate represented by χ_n^*. Active neutrophils (n^*) undergo a rapid apoptotic process while circulating in the blood

stream (Cross *et al.*, 2008), with apoptotic neutrophils a^* appearing with rate ν^*, *i.e.* the rate at which active neutrophils become apoptotic. These in turn undergo secondary necrosis with rate γ_a^*, spilling their internal toxic chemicals. This new pro-inflammatory action presents a saturation level denoted by β_a^* and is counteracted by the action of macrophages, appearing at a maximal rate of χ_m^*, engulfing the apoptotic neutrophils at a constant rate ϕ^* and finally leaving the tissue at rate γ_m^*. Finally, as part of our modelling assumptions for this initial model (and its following extensions), a sterile environment is considered for both neutrophils and macrophages; that is, there is no direct pathogenic action affecting the physiological leukocytes' behaviour.

The dynamics between active and apoptotic neutrophils, macrophages and pro-inflammatory mediators are described by the following *spatially averaged* ODE model:

$$\frac{\mathrm{d}n^*}{\mathrm{d}t^*} = \chi_n^* c^* - \nu^* n^*, \tag{2.1}$$

$$\frac{\mathrm{d}a^*}{\mathrm{d}t^*} = \nu^* n^* - \gamma_a^* a^* - \phi^* m^* a^*, \tag{2.2}$$

$$\frac{\mathrm{d}m^*}{\mathrm{d}t^*} = \chi_m^* c^* - \gamma_m^* m^*, \tag{2.3}$$

$$\frac{\mathrm{d}c^*}{\mathrm{d}t^*} = \alpha^* f(t^*) + k_a^* \gamma_a^* \left(\frac{a^{*2}}{\beta_a^{*2} + a^{*2}} \right) - \gamma_c^* c^* \quad , \tag{2.4}$$

with f being the model stimulus, describing physical damage to the tissue, as defined by Dunster *et al.* (2014), with

$$f(t^*) = H(t^*) \sin^2(t^*) \,, \tag{2.5}$$

and

$$H(t^*) = \begin{cases} 1 & \text{if } t^* < A^* \pi \\ 0 & \text{if } t^* > A^* \pi \,, \end{cases} \tag{2.6}$$

in which A^* represents the number of cycles of damage, approximating days of infection. The parameters involved are presented in Table 2.1, while initial conditions are

set at zero, that is:

$$n^*(0) = a^*(0) = m^*(0) = c^*(0) = 0. \tag{2.7}$$

While not all the above mentioned parameters are known and available in absolute values, a few assumptions can be made and useful estimations can be derived from the existing literature and experimental data. We review these parameter values in detail in Section 2.2.1.

Figure 2.1 provides a schematic representation of model (2.1)–(2.4) in which all the interactions between the system's variables are shown by highlighting all non-spatial parameters.

The initial analysis of this model focuses on assessing its qualitative behaviour under different inputs in order to evaluate it in terms of the inflammatory response, with the key results of the ODE model presented in Section 2.4.1. Our primary aim is to investigate the effects of spatial dependency in the development and eventual outcome of inflammation. In particular, two different outcomes, corresponding to two different stable states, are expected: the first being the complete resolution of the inflammation and the second being a chronic inflammatory state. To this end, the dynamical analysis will be combined with the study of spatial patterning, by modelling key biological features that directly affect the inflammation progression and final outcome.

2.2 Adding spatial information

We now extend the model of Dunster *et al.* (2014), above, to incorporate spatial movement of cells and mediators. For simplicity, we consider a 1D spatial domain and assume that cells and mediators move diffusively. This assumption does not hold for apoptotic neutrophils which instead do not move, being dying cells eventually

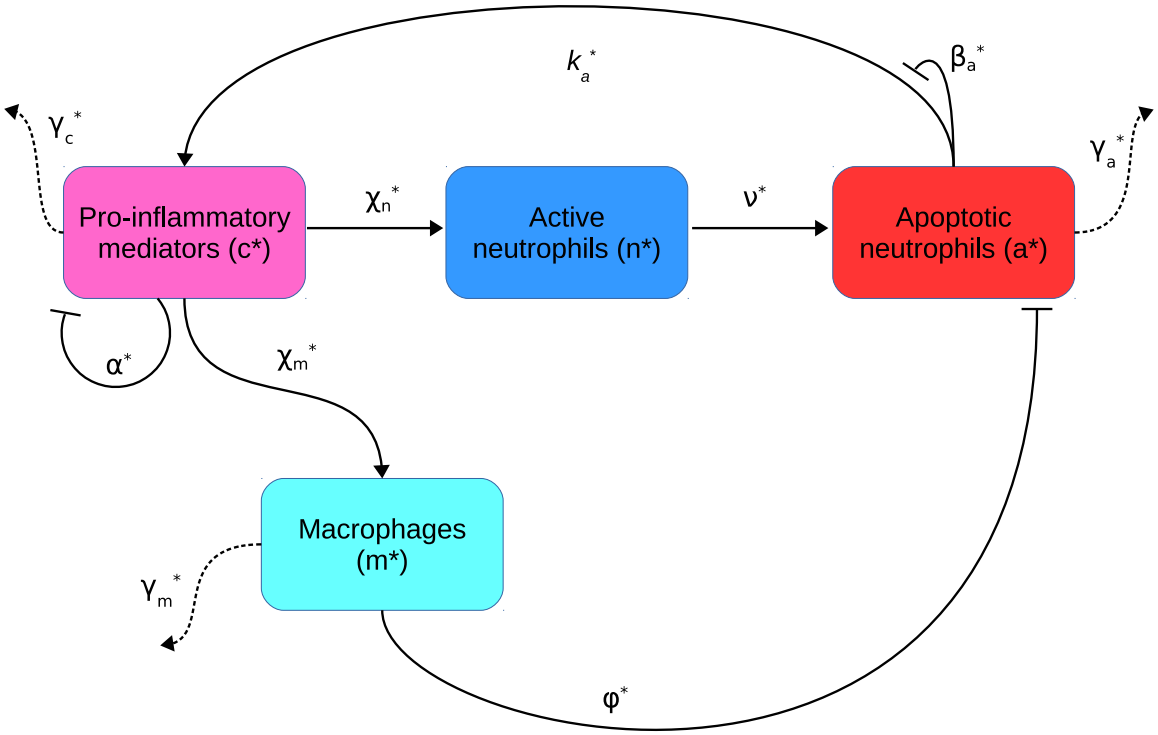

Figure 2.1: Schematic diagram representing model (2.1)–(2.4) and illustrating the constituent interactions between populations of healthy neutrophils (n^*), apoptotic neutrophils (a^*) and macrophages (m^*) in response to pro-inflammatory mediators (c^*), with associated parameters. Dashed lines indicate decay rates.

cleared out by macrophages.. In fact, while diffusion of all inanimate depends to an extent on their size, the temperature and their local environment, it is negligibly small compared to that of macrophages and active neutrophils. Addition of diffusion into the model in this spatial context provides a mechanism via which motility of cells and mediators can act to smooth out strong inhomogeneities in the spatial distributions of the model components. This has the potential to allow localised damage to spread to neighbouring healthy tissue, and also to destabilise the homogeneous steady states identified in the ODE model of Dunster via e.g. Turing instability (as discussed in Section 1.4). In general, there is scope for cell diffusivities (in particular) to vary temporally or in function of mediator concentrations; however, since we are primarily interested in ascertaining whether addition of diffusion can yield inhomogeneous steady states (patterns) in this model, we restrict attention to the case of constant diffusivities for all model components here. Since the inflammatory response in the model of Dunster, and our extension below, is driven by an initial stimulus f that vanishes in the longer term, we anticipate that the addition of time-dependent diffusion would affect only early-time solutions, with long-term steady states being unaffected. Denoting the diffusivities of active neutrophils, macrophages and mediators by D_n^*, D_m^* and D_c^* respectively, the ODE model of (2.1)–(2.4) is then transformed into the following system of PDEs:

$$\frac{\partial n^*}{\partial t^*} = \chi_n^* c^* - \nu n^* + D_n^* \nabla^2 n^* \,, \tag{2.8}$$

$$\frac{\partial a^*}{\partial t^*} = \nu^* n^* - \gamma_a^* a^* - \phi^* m^* a^* \,, \tag{2.9}$$

$$\frac{\partial m^*}{\partial t^*} = \chi_m^* c^* - \gamma_m^* m^* + D_m^* \nabla^2 m^* \,, \tag{2.10}$$

$$\frac{\partial c^*}{\partial t^*} = \alpha^* f(x^*, t^*) + k_a^* \gamma_a^* \left(\frac{a^{*2}}{\beta_a^{*2} + a^{*2}} \right) - \gamma_c^* c^* + D_c^* \nabla^2 c^* \,, \tag{2.11}$$

where now the damage function depends on spatial coordinates, x^*, as well as time, t^*. For simplicity, we here seek solutions on the one-dimensional spatial domain $x^* \in [0, L^*]$; this is a natural pre-cursor to more complex two-dimensional simulations,

which we examine later in the thesis. We seek solutions that are periodic on the interval $x^* \in [0, L^*]$. .

2.2.1 Parameter values

Parameter values are derived from the literature, where already available, with most of them in this work taken from Dunster *et al.* (2014), and are reported in Table 2.1. Due to modelling constraints and simplifications, not all the parameters have a straightforward biological correspondence in terms of either experimental data or estimation. This is due to limitations in measurements on one hand (constraints on timescales and instrumentation) and the lack of straightforward correspondence between modelling parameters and quantifiable biological processes on the other.

As for the diffusion constants, which are not considered by Dunster *et al.* (2014) and are only introduced here, the available scientific literature does not provide much in this regard because of two main reasons. On one hand, researchers have traditionally focused on the temporal dynamics of inflammation, while the importance of its spatial spread and its dependence on localised concentrations has only recently emerged and prompted more in-depth studies. Furthermore, there is a lack of simple and standard tools to measure diffusion coefficients experimentally, while estimation of these parameters through mathematical models has proven non-trivial. Despite measurements of spatial parameters being relatively sparse in previous literature in comparison to the vast numbers of published temporal studies of the inflammatory response, some measures of these parameters are available from both experimental studies and inferred from mathematical models. It should be noted, however, that these measurements are subject to variability across tissues. Rates of mediator diffusion reported in previous literature generally lie in the range $10^{-8} - 10^{-6}$ $\text{cm}^2 \cdot \text{s}^{-1}$ (Warrender *et al.*, 2006; Weidemann *et al.*, 2011; Ross & Pompano, 2018). In gen-

Parameter	Definition	Range of values	References
χ_n^*	maximal rate of neutrophil influx	$10^6 - 10^7\ cell \cdot pg^{-1} \cdot day^{-1}$	(Kim *et al.*, 2008)
ν^*	neutrophil apoptosis rate	$12 - 72\ day^{-1}$	(Hannah *et al.*, 1998), (Summers *et al.*, 2010)
γ_a^*	rate of necrosis of apoptotic neutrophils	$9.6 - 48\ day^{-1}$	(Mare *et al.*, 2005)
ϕ^*	rate of apoptotic neutrophil removal by macrophages (secondary necrosis)	$10^{-3}\ cell^{-1} \cdot mm^3 \cdot day^{-1}$	(Dunster *et al.*, 2014)
χ_m^*	maximal rate of macrophages influx	$0.1 \cdot 10^6 - 1.17 \cdot 10^6\ cell \cdot pg^{-1} \cdot day^{-1}$	(Furth, 1985)
α^*	mediator production rate	$pg \cdot mm^{-3} \cdot day^{-1}$	
k_a^*	mediator concentration produced by apoptotic neutrophils	$pg \cdot mm^{-3}$	
β_a^*	apoptotic neutrophils saturation constant (concentration of apoptotic neutrophils required for half maximal release of $c^*(t)$)	$cell \cdot mm^{-3}$	
γ_m^*	rate at which macrophages leave the tissue	$0.2\ day^{-1}$	(Waugh & Sherratt, 2007)
γ_c^*	rate of mediator decay	$0.7 - 20\ day^{-1}$	(Smith *et al.*, 2011), (Su *et al.*, 2009)
D_n^*	active neutrophil diffusion constant	$mm^2 \cdot day^{-1}$	
D_m^*	macrophage diffusion constant	$8.64 \cdot 10^{-7} - 8.64 \cdot 10^{-1}\ mm^2 \cdot day^{-1}$	(Lauffenburger & Kennedy, 1983), (Sozzani *et al.*, 1991), (Owen & Sherratt, 1997), (Owen *et al.*, 2004)
D_c^*	pro-inflammatory mediator diffusion constant	$8.64 \cdot 10^{-2} - 8.64\ mm^2 \cdot day^{-1}$	(Warrender *et al.*, 2006), (Weidemann *et al.*, 2011), (Ross & Pompano, 2018)

Table 2.1: Parameters appearing in system (2.8)–(2.11). When available, ranges of parameter values are inferred from relevant literature, as specified.

eral, we expect the rates of cell migration to be slower than those of inflammatory mediators, with previous publications reporting macrophages to move diffusively at rates of order $10^{-13} - 10^{-7}$ $\mathrm{cm}^2 \cdot \mathrm{s}^{-1}$ (Lauffenburger & Kennedy, 1983; Sozzani *et al.*, 1991; Owen & Sherratt, 1997; Owen *et al.*, 2004). Neutrophils, on the other hand, are expected to move more rapidly owing to their smaller size.

Similarly, for the remaining parameters, we investigate results for a range of values within the physiological scales, as provided in the scientific literature.

2.2.2 Nondimensionalisation

Restoring diffusive terms and considering the original PDE system (2.8)–(2.11) introduces the critical problem of evaluating appropriate values for diffusion constants. As already discussed in Section 2.2.1, valuable data can be inferred from the relevant scientific literature where available, although spatial parameters are generally difficult to quantify. Furthermore, in our simulations, we are interested in studying the system upon varying spatial constants in order to characterise the model's behaviour spatially and to assess if and how localised damage can invade the surrounding healthy tissue. In doing so, we also aim to evaluate if the system can sustain spatially inhomogeneous steady states.

An accurate investigation of the available literature, as already exposed in Section 2.2.1, reveals the difficulties and spuriousness of defining specific values for the diffusive constants. In general though, in line with the range of values reported in Table 2.1, diffusion terms are relatively small, as proposed by Pigozzo *et al.* (2013) for a model studying the spatio-temporal dynamics of the human immune system. Furthermore, it would be desirable to infer a relationship between the three diffusion constants D_n, D_m and D_c characterising model (2.13)–(2.16). Although a general relationship cannot be directly assumed from the available literature (Weavers *et al.*,

2016; Graham *et al.*, 2012), at this initial stage it is expected that $D_m < D_n < D_c$ to hold, that is, it is considered that pro-inflammatory mediators (c) diffuse faster than active neutrophils (n), which in turn are quicker than macrophages (m). This assumption is further backed by the set of values provided by Pigozzo *et al.* (2013).

We, here, have the flexibility to tune both the domain size L^* and the timescale γ_c^* in our model, to enable us to relate our simulations to some specific inflammatory condition. However, since we are more interested in examining the general case here, we begin by defining a baseline set of dimensionless spatial parameters, which we use in our simulations in the following sections. Considering a domain of width $L^* = 10$ cm, taking $\gamma_c^* = 3$ day^{-1} (as in Dunster *et al.* (2014)), and taking typical (dimensional) rates of diffusion of mediators and macrophages to be 10^{-7} cm^{2}s^{-1} and 10^{-10} cm^{2}s^{-1} respectively provides approximate dimensionless estimates of $D_c = 10^{-4}$ and $D_m = 10^{-6}$. Since we expect neutrophils to move more quickly than macrophages but slower than mediators, we prescribe $D_n = 10^{-5}$.

To simplify the analysis, we nondimensionalise (2.8)–(2.11) as follows. Let

$$n^* = \frac{\chi_n^* k_a^*}{\gamma_c^*} n, \quad a^* = \frac{\chi_n^* k_a^*}{\gamma_c^*} a, \quad m^* = \frac{\chi_m^* k_a^*}{\gamma_c^*} m, \quad c^* = k_a^* c, \quad x^* = L^* x, \quad t^* = \frac{t}{\gamma_c^*}. \tag{2.12}$$

Having rescaled variables as above, substitution of these expressions into (2.8)–(2.11) leads to the following dimensionless system:

$$\frac{\partial n}{\partial t} = c - \nu n + D_n \nabla^2 n, \tag{2.13}$$

$$\frac{\partial a}{\partial t} = \nu n - \gamma_a a - \phi m a, \tag{2.14}$$

$$\frac{\partial m}{\partial t} = c - \gamma_m m + D_m \nabla^2 m, \tag{2.15}$$

$$\frac{\partial c}{\partial t} = \alpha f(x,t) + \gamma_a \left(\frac{a^2}{\beta_a^2 + a^2} \right) - c + D_c \nabla^2 c \quad , \tag{2.16}$$

Parameter	Approximate Range	Standard values used in simulations in this chapter
ν	$0.001 - 0.6925$	10^{-1}
γ_a	$0.55 - 1$	1
γ_m	$10^{-2} - 1.2375 \cdot 10^{-2}$	10^{-2}
ϕ	$0.001 - 1.38$	10^{-3}
β_a	$0.01 - 0.1$	10^{-1}
α	$5 \cdot 10^{-2}$	$5 \cdot 10^{-2}$
D_n	$10^{-5} - 10^{-3}$	10^{-5}
D_m	$10^{-6} - 10^{-3}$	10^{-6}
D_c	$10^{-4} - 10^{-3}$	10^{-4}

Table 2.2: Dimensionless parameter values appearing in the model of (2.13)–(2.16).

where

$$\phi = \frac{\phi^* \chi_m^* k_a^*}{{\gamma_c}^2{}^*}, \quad \nu = \frac{\nu^*}{\gamma_c^*}, \quad \alpha = \frac{\alpha^*}{\gamma_c^* k_a^*}, \quad \beta_a = \frac{\beta_a^* \gamma_c^*}{\chi_n^* k_a^*}, \quad \gamma_a = \frac{\gamma_a^*}{\gamma_c^*}, \quad \gamma_m = \frac{\gamma_m^*}{\gamma_c^*},$$
$$D_c = \frac{D_c^*}{L_x^{*2} \gamma_c^*}, \quad D_n = \frac{D_n^*}{L_x^{*2} \gamma_c^*}, \quad D_m = \frac{D_m^*}{L_x^{*2} \gamma_c^*}. \tag{2.17}$$

Values for all dimensionless parameters are summarised in Table 2.2.

The initial conditions provided in (2.7) are also updated to their dimensionless correspondents:

$$n(0) = a(0) = m(0) = c(0) = 0. \tag{2.18}$$

2.3 Numerical approach

In order to solve the PDEs in (2.13)–(2.16), different approaches can be considered. A straightforward method would consist of fully discretizing the system, both in time and space; for example, by applying the three point formula of finite difference approximations for second derivatives, thus computing the results by manually setting an appropriate space step ($\mathrm{d}x$) and iterating by time steps ($\mathrm{d}t$). A quite restrictive stability condition applies, however; for one-dimensional systems of parabolic PDEs such as (2.13)–(2.16), we require:

$$D\frac{dt}{dx^2} < \frac{1}{2}, \tag{2.19}$$

with D being the diffusion coefficient. Equation (2.19) guarantees stability for the Forward-Time Central-Space (FTCS) scheme applied to PDEs (LeVeque, 2007).

Nevertheless, this method has an obvious underlying limitation, binding computational efficiency to numerical stability, through the time step value and spatial mesh. Therefore, this approach has been discarded in favour of a more suitable computational method, as described below.

2.3.1 Method of lines

The method of lines offers an appreciably efficient solving approach, by discretizing all but one dimension, thus reducing the PDE system to a system of ODEs.

In order to implement the method of lines, equations (2.13)–(2.16) are discretized in space, as follows:

$$\frac{dn_i(t)}{dt} = -\nu n_i(t) + c_i(t) + D_n\left(\frac{n_{i+1}(t) - 2n_i(t) + n_{i-1}(t)}{\Delta x^2}\right), \tag{2.20}$$

$$\frac{da_i(t)}{dt} = \nu n_i(t) - \gamma_a a_i(t) - \phi m_i(t) a_i(t), \tag{2.21}$$

$$\frac{dm_i(t)}{dt} = -\gamma_m m_i(t) + c_i(t) + D_m\left(\frac{m_{i+1}(t) - 2m_i(t) + m_{i-1}(t)}{\Delta x^2}\right), \tag{2.22}$$

$$\frac{dc_i(t)}{dt} = \alpha f_i(t) + \gamma_a \frac{a_i(t)^2}{a_i(t)^2 + \beta_a^2} - c_i(t) + D_c\left(\frac{c_{i+1}(t) - 2c_i(t) + c_{i-1}(t)}{\Delta x^2}\right), \quad (2.23)$$

with $i = 0, 1, \ldots, N$, where N is the number of spatial meshpoints.

In order to efficiently implement it, the dimensionless system (2.20)–(2.23) is rewritten in a more compact way, by writing (2.20)–(2.23) in vectorised form in Matlab (details omitted).

The Matlab ODE solver `ode15s` is particularly useful when dealing with stiff problems, as in this case. Generally, stiffness occurs when some solution components present a much faster dynamics than others; it strongly affects stability in a way such that the step length is constrained more by stability requirements rather than accuracy (Ashino *et al.*, 2000). It is a variable order algorithm, based on the Backward Differentiation Formulae (BDF) method, the step size is adapted during implementation with error estimation given by the local truncation error (Celaya *et al.*, 2014). The system of vectorised equations is then computed through Matlab function `ode15s`, with initial conditions as in (2.18) and time spans $[0 \quad 10^4]$ (Section 2.4.1) and $[0 \quad 7000]$ (Section 2.4.3). Matlab code for this model is available online via Github[1].

2.4 Simulations

2.4.1 No spatial dependence

We here examine solutions to (2.13)–(2.16) for the case $D_n = D_m = D_c = 0$. In particular, we are looking to recover the ODE results of Dunster *et al.* (2014), as a code validation task. A first implementation of the dimensionless system (2.13)–(2.16) offers graphical evidence of two possible inflammation outcomes, as presented by Dunster *et al.* (2014), regulated by the damage level through the parameter A,

[1] `https://github.com/atihana/basic_inflammation_pde`

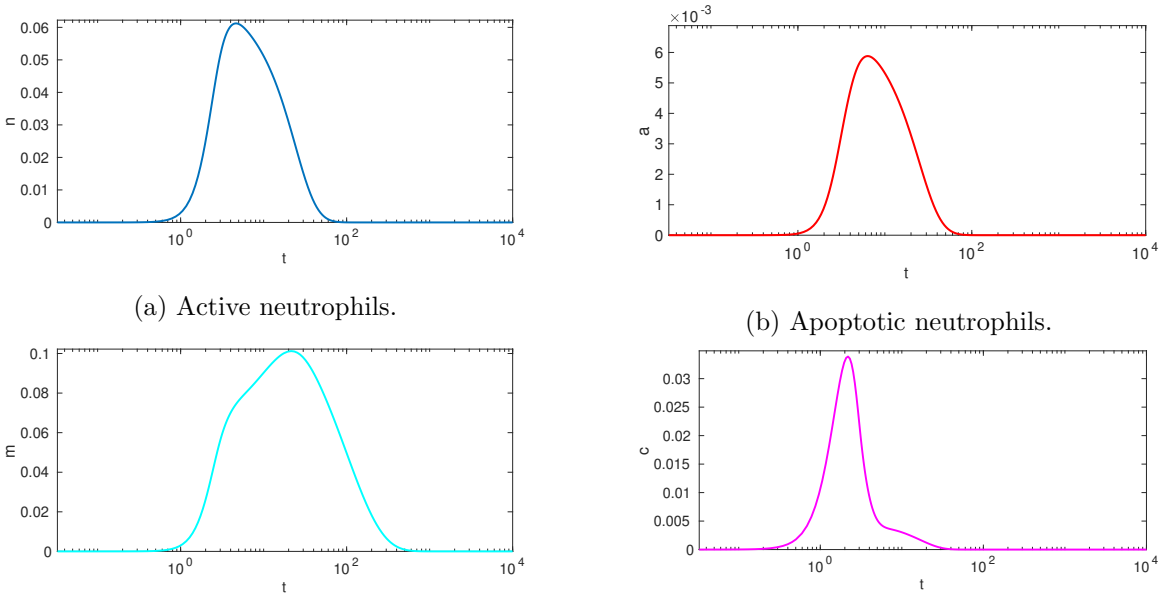

(a) Active neutrophils.

(b) Apoptotic neutrophils.

(c) Macrophages.

(d) Pro-inflammatory mediators.

Figure 2.2: Solution of (2.13)–(2.16) for $f(\mathbf{x}, t) = H(t)\sin^2(t)$, periodic boundary conditions and initial conditions as per (2.18), with parameters values as in Table 2.2. Since $f(\boldsymbol{x}, t)$ is independent of $\mathbf{x}$, solutions are homogeneous; setting $A = 1$ here prompts a resolution of inflammation.

as shown in Figure 2.2 and Figure 2.3. Both figures are obtained with parameters from Table 2.2 and by only varying the number of cycles of damage A, with $A = 1$ in Figure 2.2 and $A = 4$ in Figure 2.3. Computation of (2.13)–(2.16) (with zero diffusion) highlights, as expected, a sensitive increase of pro-inflammatory mediators in response to damage in both Figure 2.2 and Figure 2.3. Macrophages and neutrophils also appear in correspondence with this rise, with the former being in turn partially cleared by apoptotic neutrophils. The biological meaning of the solution in Figure 2.2 is that of resolved inflammation, in which all cell populations and mediators return to healthy physiological levels (zero). On the other hand, for a prolonged damage stimulus ($A = 4$), inflammation cannot be resolved, thus profiling a chronic inflammatory state, as is evident from Figure 2.3, in which both apoptotic neutrophils and pro-

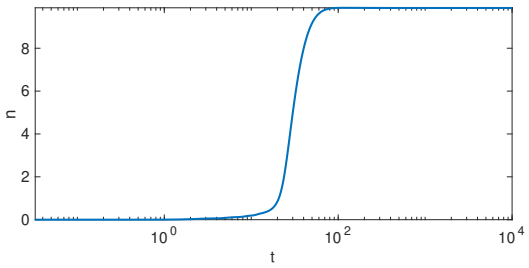

(a) Active neutrophils.

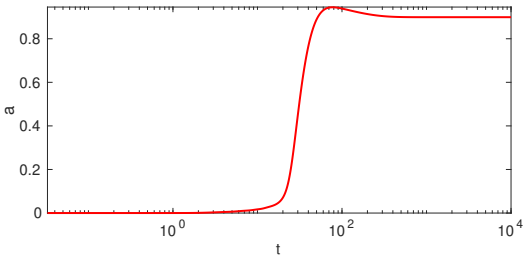

(b) Apoptotic neutrophils.

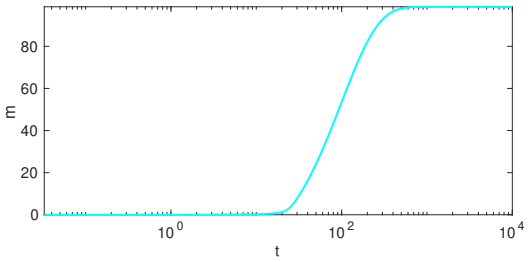

(c) Macrophages.

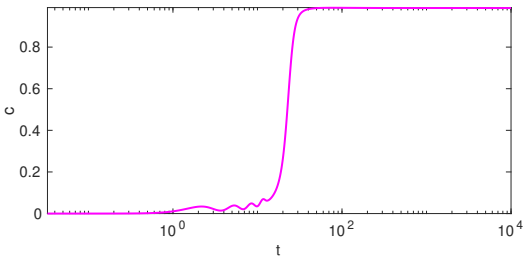

(d) Pro-inflammatory mediators.

Figure 2.3: Solution of (2.13)–(2.16), for $f(\mathbf{x}, t) = H(t)\sin^2(t)$, periodic boundary conditions and initial conditions as per (2.18), with parameters values as in Table 2.2. Since $f(\boldsymbol{x}, t)$ is independent of $\mathbf{x}$, solutions are homogeneous; setting $A = 4$ here prevents full resolution, causing inflammation to be chronic.

inflammatory mediators maintain high levels of concentration, thus resulting in a continuous action of macrophages and active neutrophils.

The interest in investigating the impact of parameter ϕ upon the model's behaviour comes from the paper of Dunster *et al.* (2014) in which manipulation of the rate of the phagocytosis of apoptotic neutrophils is recognised as a possible therapeutic target in resolving inflammation. An analogous analysis can be made by testing different values of parameter the ϕ. Having fixed $A = 4$, that is configuring a context of initially sustained damage, we vary ϕ to elucidate the effect of the macrophage clearance rate instead. We expect to have a prompt and more effective resolution of inflammation for increasing values of ϕ, while choosing ϕ too small should compromise the healing process, eventually resulting in a chronic state of inflammation. The results in Figure 2.4–2.6 confirm these predictions, showing that regulation of the parameter ϕ is key to how quickly and effectively the inflammation is resolved. In particular, increasing ϕ from the nominal value given in Figure 2.2, generally improves the system's response to inflammation, with $\phi = 0.09$ providing damped oscillations but still a chronic outcome (Figure 2.4), $\phi = 0.2$ resulting in full resolution (Figure 2.5) and $\phi = 0.4$ resolving inflammation with even lower levels of cells and mediators (Figure 2.6).

All of the above results recover the results of Dunster *et al.* (2014) exactly; this provides us with confidence that the numerical code use to attain these results is valid. We examine spatially-inhomogeneous solutions to our model using this code in Section 2.4.3, after first examining the stability of the steady states observed above from a theoretical perspective below.

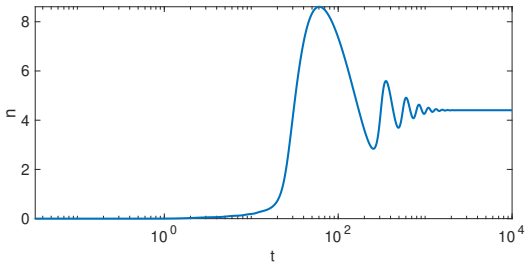

(a) Active neutrophils.

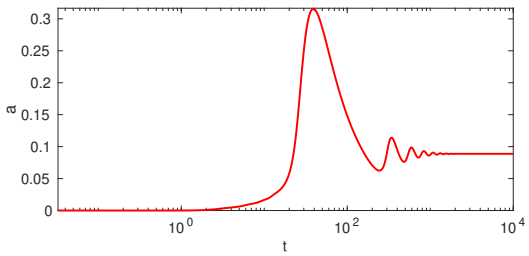

(b) Apoptotic neutrophils.

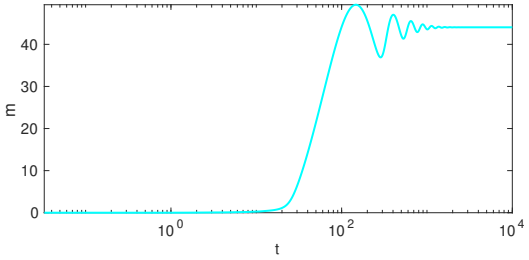

(c) Macrophages.

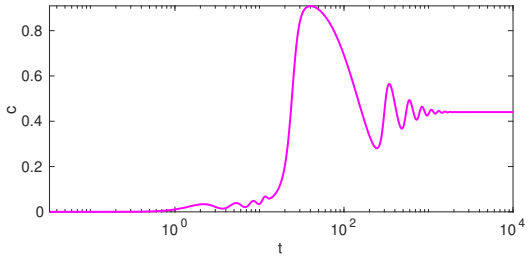

(d) Pro-inflammatory mediators.

Figure 2.4: Solution of (2.13)–(2.16) for $f(\mathbf{x},t) = H(t)\sin^2(t)$, periodic boundary conditions and initial conditions as per (2.18), with $A = 4$, $\phi = 0.09$ and all other parameters values as in Table 2.2. Since $f(\boldsymbol{x},t)$ is independent of $\mathbf{x}$, solutions are homogeneous; setting $\phi = 0.09$ provides damped oscillations, but does not yield complete resolution of inflammation.

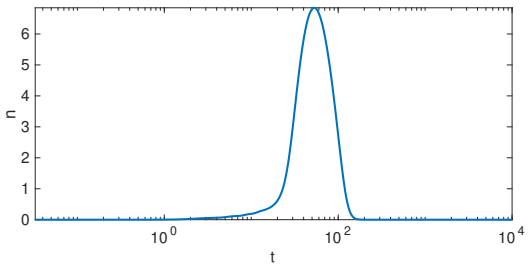

(a) Active neutrophils.

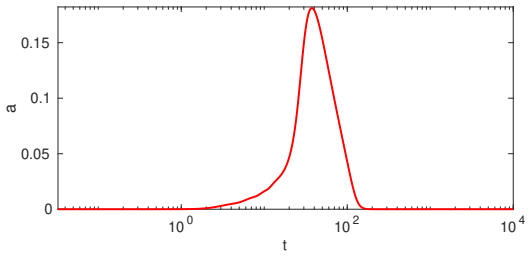

(b) Apoptotic neutrophils.

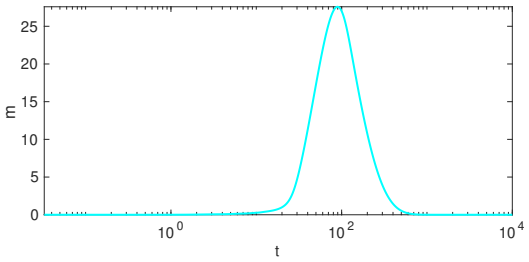

(c) Macrophages.

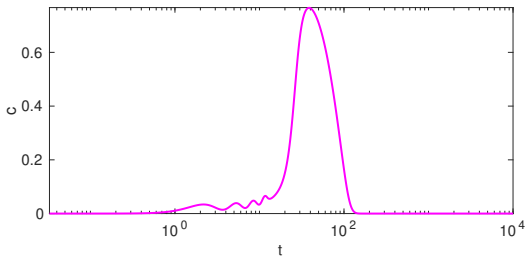

(d) Pro-inflammatory mediators.

Figure 2.5: Solution of (2.13)–(2.16) for $f(\mathbf{x}, t) = H(t)\sin^2(t)$, periodic boundary conditions and initial conditions as per (2.18), with parameters values as in Table 2.2, fixed damage duration with $A = 4$. Since $f(\boldsymbol{x}, t)$ is independent of $\mathbf{x}$, solutions are homogeneous; setting $\phi = 0.2$ results in full inflammation resolution.

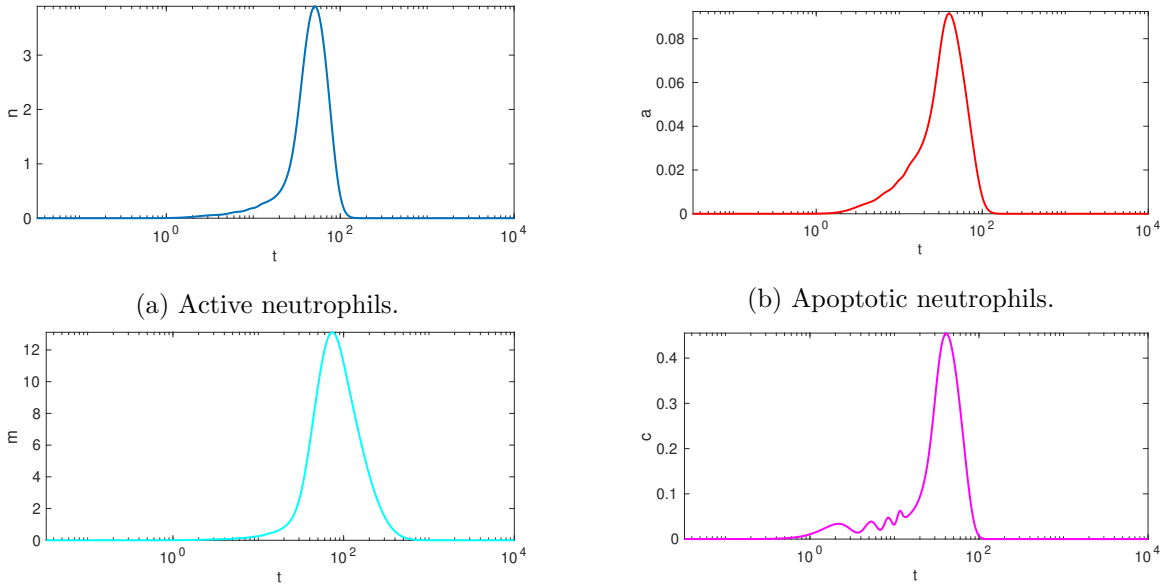

(a) Active neutrophils.

(b) Apoptotic neutrophils.

(c) Macrophages.

(d) Pro-inflammatory mediators.

Figure 2.6: Solution of (2.13)–(2.16) for $f(\mathbf{x},t) = H(t)\sin^2(t)$, periodic boundary conditions and initial conditions as per (2.18), with parameters values as in Table 2.2, fixed damage duration with $A = 4$. Since $f(\boldsymbol{x},t)$ is independent of $\mathbf{x}$, solutions are homogeneous; setting $\phi = 0.4$ prompts here a more effective resolution of the inflammatory state. We note that overall cell numbers and mediator concentrations are lower than those attained for $\phi = 0.2$ in Figure 2.5 due to the enhanced phagocytic action of macrophages here.

2.4.2 Stability analysis

To fully determine how the system responds to varying values of key parameters, the stabilities of steady state solutions are analysed below. In general, the stability of the system is guaranteed to be stable if and only if all real parts eigenvalues are negative.

By computing the fixed points of (2.13)–(2.16) and evaluating the corresponding Jacobian matrix at each point, three generic solutions and corresponding sets of eigenvalues can be found. The latter can assume different values and particularly vary in sign depending on some of the parameters, with the Jacobian matrix associated to the system:

$$\mathcal{J} = \begin{pmatrix} -\nu & 0 & 0 & 1 \\ \nu & -\gamma_a - \phi\, m & -\phi\, a & 0 \\ 0 & 0 & -\gamma_m & 1 \\ 0 & \dfrac{2a\gamma_a\beta_a^2}{(\beta_a^2 + a^2)^2} & 0 & -1 \end{pmatrix}. \tag{2.24}$$

The matrix $\mathcal{J}$ depends on the stationary points and, for each group of solutions, the associated eigenvalues can thus be computed according to the values of parameters ν, γ_a, ϕ, γ_m and β_a.

In order to assess how the stability evolves with respect to these critical parameters, bifurcation diagrams for each variable are plotted, as shown in Figures 2.7–2.11. These plots assess in fact the existence and stability of steady state solutions with reference to a range of values for each parameter featuring in the Jacobian matrix (2.24), thus potentially affecting stability. In these figures, solid lines represent stable steady states and dashed lines represent unstable steady states. In this sense, the absence of any evident bifurcation point in both Figures 2.7–2.9 suggests that (for biologically feasible choices of parameters) the respective parameters ν, γ_m and γ_a do not have direct effect the stability of steady states. Conversely, plots for parameters β_a (Figure 2.10) and ϕ (Figure 2.11) exhibit bifurcations indicating a change in the

number/stability of steady states, by marking the transition from unstable steady states (dashed lines) to stable ones (solid lines). The bifurcation analysis thus suggests that the most interesting parameters to investigate, with the greatest impact to the system's behaviours, are β_a and ϕ. More generally, we are interested in studying the stability of the states as an indicator of the solutions we expect the ODE system associated to (2.13)–(2.16) to exhibit. In particular, solid lines representing stable solutions are captured by the simulations in the form of either resolution to the healthy state (corresponding to the trivial zero steady state) or a chronic state of inflammation (non-zero steady states). Dashed lines represent unstable solutions that the system theoretically supports but that, given their instability, cannot be captured in simulations. The additional presence of bifurcation points further informs on possible oscillations exhibited by the ODE system, depending on the nature of the bifurcation. In particular, Figure 2.10 presents a saddle node of bifurcation at $\beta_a \simeq 0.45$, with the system admitting three possible solutions lying on the left of the bifurcating point, two stable, corresponding to the healthy (zero steady state) and unhealthy (non-trivial steady state) outcomes and one unstable which the system cannot exhibit in simulations. For $\beta_a \gtrsim 0.45$, inflammatory damage is guaranteed to resolve. The bifurcation diagrams shown in Figure 2.11 instead present a Hopf bifurcation at $\nu \simeq 0.1$, where the state of the solutions switches from stability (solid lines) to instability (dashed lines). In general, Hopf bifurcations are also associated with the existence of sustained temporal oscillations; however,the Hopf bifurcation in Figure 2.11 is subcritical, so these oscillations are unstable in this case.

2.4.3 Spatial spread of damage and inflammation

We are particularly interested in regions of parameter space for which the ODE model is bistable, since these regions exhibit the greatest scope for inhomogeneous solutions.

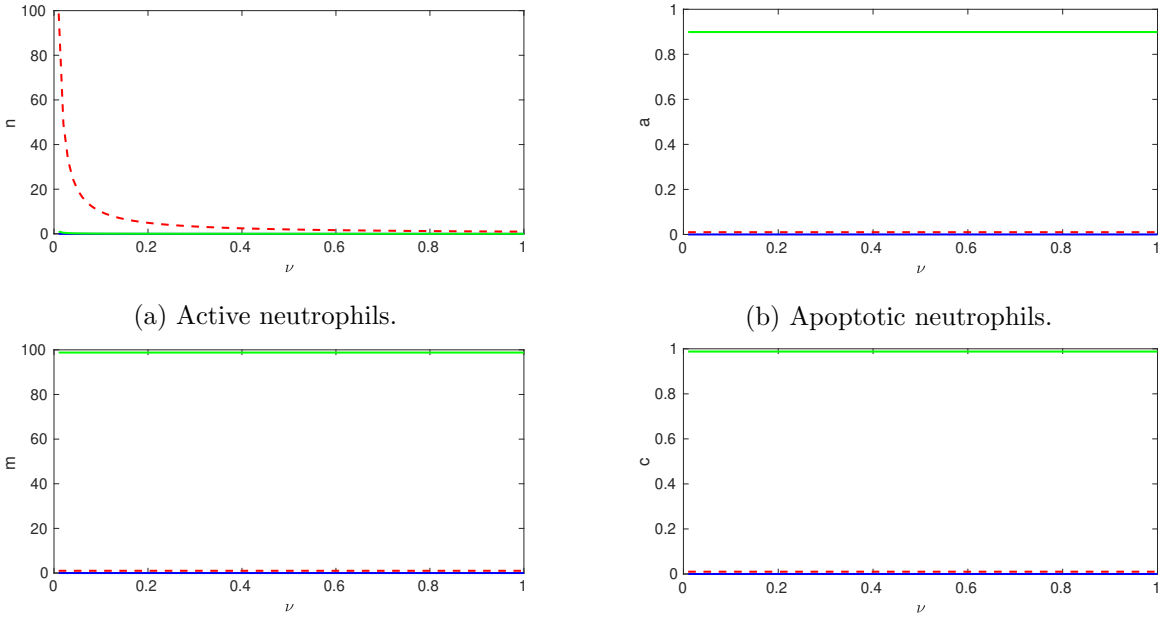

(a) Active neutrophils.

(b) Apoptotic neutrophils.

(c) Macrophages.

(d) Pro-inflammatory mediators.

Figure 2.7: Stability analysis for system (2.13)–(2.16), in function of parameter $\nu \in [0, 1]$. All other parameters values are set as in Table 2.2. Each colour represents one set of 3 stationary points. The three corresponding eigenvalues present either negative real part (stable, solid lines) or positive real part (unstable, dashed lines).

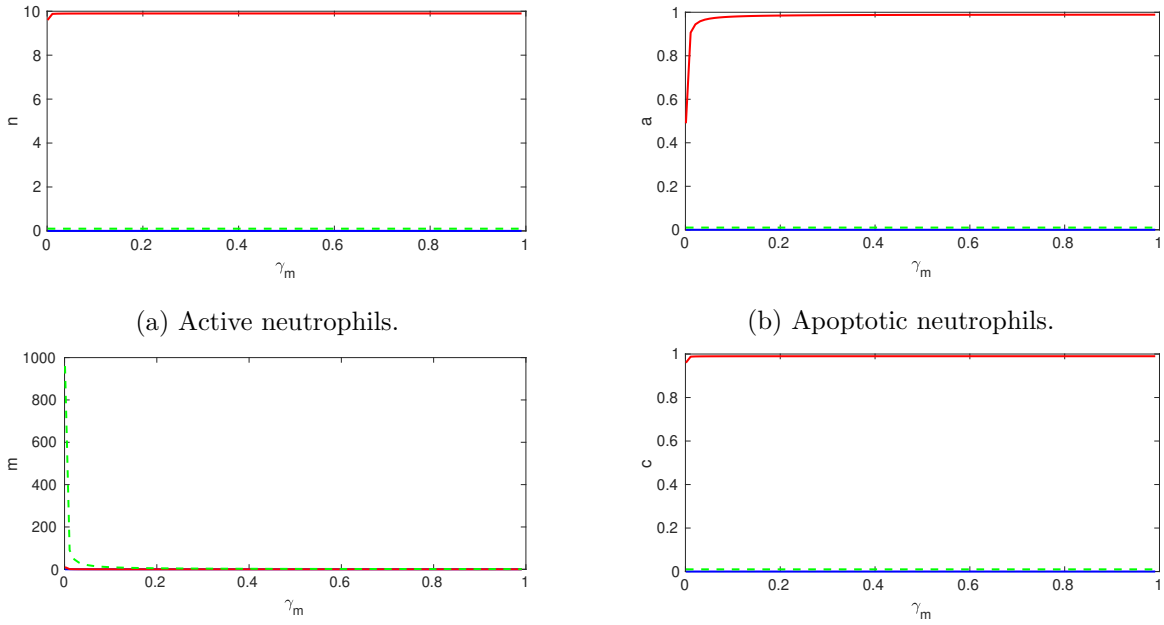

(a) Active neutrophils.

(b) Apoptotic neutrophils.

(c) Macrophages.

(d) Pro-inflammatory mediators.

Figure 2.8: Stability analysis for system (2.13)–(2.16), in function of parameter $\gamma_m \in [0, 1]$. All other parameters values are set as in Table 2.2. Each colour represents one set of 3 stationary points. The three corresponding eigenvalues present either negative real part (stable, solid lines) or positive real part (unstable, dashed lines).

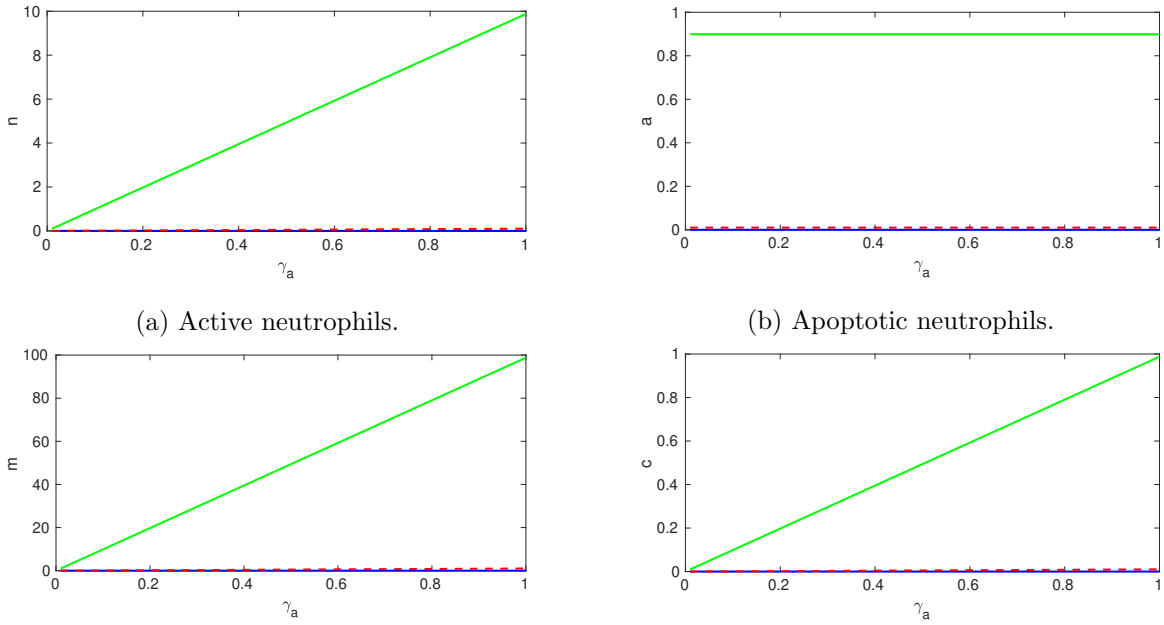

(a) Active neutrophils.

(b) Apoptotic neutrophils.

(c) Macrophages.

(d) Pro-inflammatory mediators.

Figure 2.9: Stability analysis for system (2.13)–(2.16), in function of parameter $\gamma_a \in [0, 1]$. All other parameters values are set as in Table 2.2. Each colour represents one set of 3 stationary points. The three corresponding eigenvalues present either negative real part (stable, solid lines) or positive real part (unstable, dashed lines).

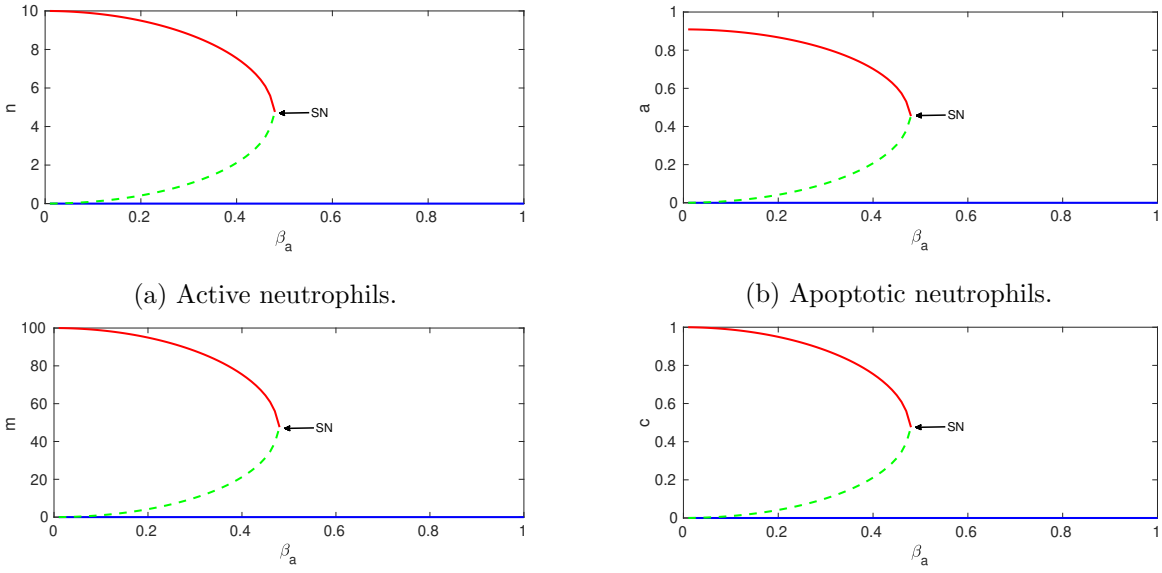

(a) Active neutrophils.

(b) Apoptotic neutrophils.

(c) Macrophages.

(d) Pro-inflammatory mediators.

Figure 2.10: Stability analysis for system (2.13)–(2.16), in function of parameter $\beta_a \in [0, 1]$. All other parameters values are set as in Table 2.2. Each colour represents one set of 3 stationary points. The three corresponding eigenvalues present either negative real part (stable, solid lines) or positive real part (unstable, dashed lines).

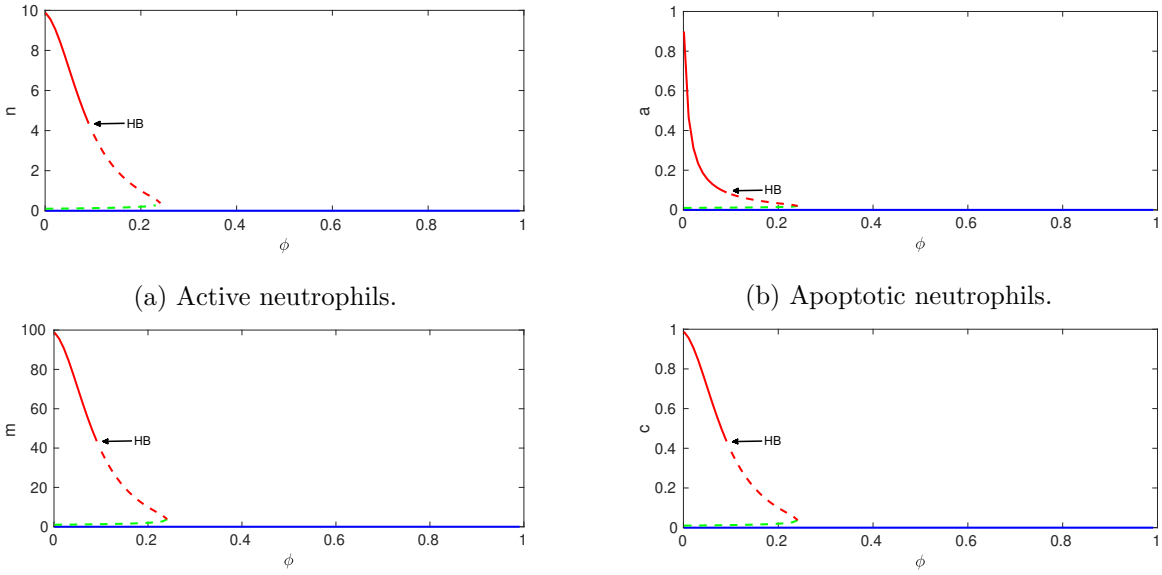

(a) Active neutrophils.

(b) Apoptotic neutrophils.

(c) Macrophages.

(d) Pro-inflammatory mediators.

Figure 2.11: Stability analysis for system (2.13)–(2.16), in function of parameter $\phi \in [0, 1]$. All other parameters values are set as in Table 2.2. Each colour represents one set of 3 stationary points. The three corresponding eigenvalues present either negative real part (stable, solid lines) or positive real part (unstable, dashed lines).

We note, here, that our choices of β_a and ϕ in Table 2.2 (in particular) are positioned in the bistable regime.

In order to study the model's spatial behaviour, numerous simulations have been run, by varying key parameter values and assessing the correspondent system's outcome, similarly to the analysis carried in Section 2.4.1. To this purpose, the damage function introduced in (2.5)–(2.6) is here updated to include spatial dependence:

$$f(x,t) = H(t)\frac{1}{\sqrt{\sigma^2 2\pi}}e^{-\frac{(x-\mu)^2}{2\sigma^2}} \tag{2.25}$$

where $\mu = 0.5$, $\sigma = 0.1$ and

$$H(t) = \begin{cases} 1 & \text{if } t < t_{max}/3 \\ 0 & \text{if } t > t_{max}/3. \end{cases} \tag{2.26}$$

with t_{max} denoting the final time of the simulation. The function $f(x,t)$ is thus modelled as a Gaussian shaped damage, persisting for one third of the total inflammatory time. The model's spatial behaviour is finally enhanced by restoring the diffusive behaviour that had been neglected in the previous analysis for sake of simplicity. As such, it is considered that mediators diffuse with $D_c = 10^{-4}$, while we set neutrophil and macrophage diffusions at $D_n = 10^{-5}$ and $D_m = 10^{-6}$ respectively. The analysis of the spatial spread of inflammation shows continuity with the dynamical analysis of the previous section in terms of parameter's regulation and effects on the model. This is particularly evident by varying the rate of apoptotic neutrophil clearance by macrophages, ϕ, with its enhancement providing a prompter and more effective resolution of inflammation. Figure 2.12, analogously to Figure 2.3, highlights how upon the initial damage 2.25, the nominal value of ϕ is too small to prevent the chronicity of inflammation. Similarly to Figures 2.4–2.5, the simulations in Figures 2.13–2.14 also confirm the healing effects of enhancing the apoptotic neutrophils clearance. On the other side, the addition of spatial dependence in terms of both the initial damage

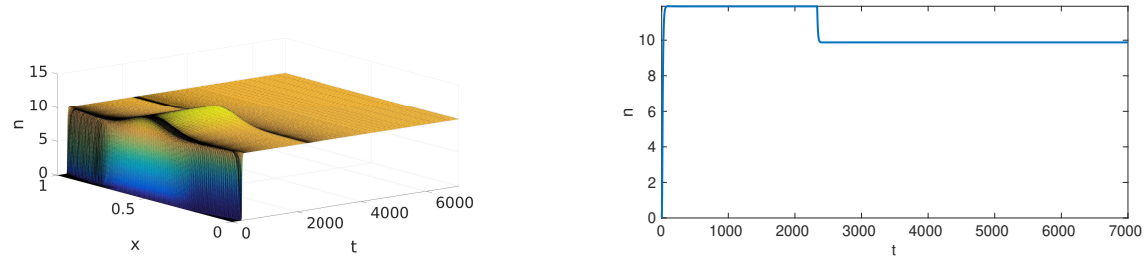

(a) Active neutrophils

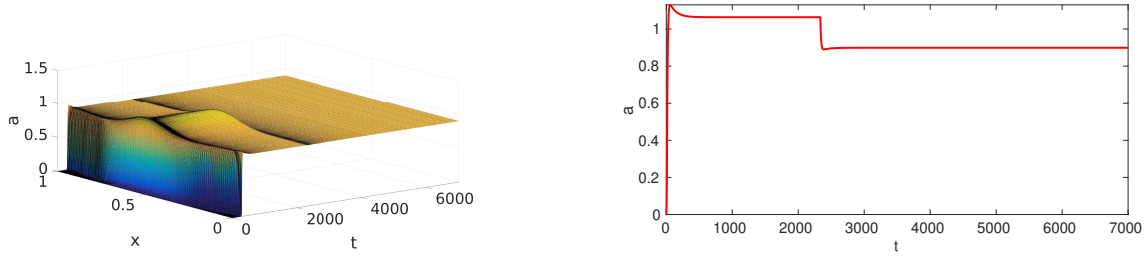

(b) Apoptotic neutrophils

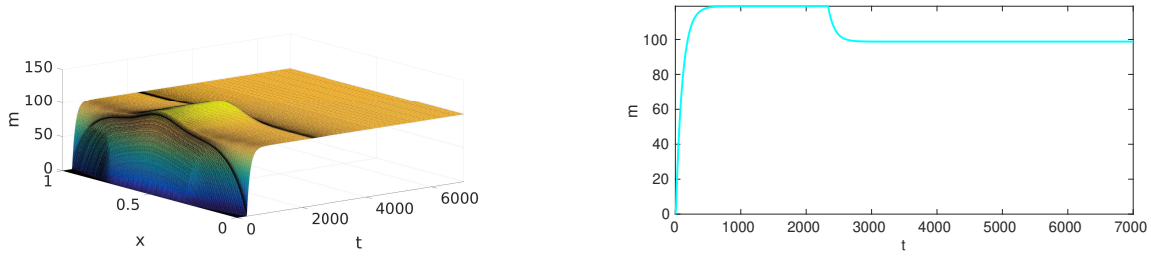

(c) Macrophages

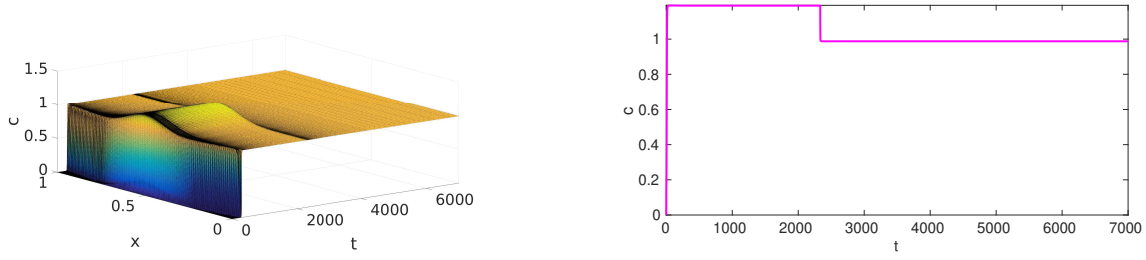

(d) Pro-inflammatory mediators

Figure 2.12: Solution of (2.13)–(2.16), with damage modelled as in (2.25)–(2.26), $\phi = 0.001$ and all other parameters values as in Table 2.2, initial conditions as per (2.18) and periodic boundary conditions. Figures on the left panel correspond to the variables' spatial representation at each time step, the right column presents plots of the dynamics of the same variables in the middle of the spatial domain. The nominal value of $\phi = 0.001$ prevents full resolution, causing inflammation to be chronic.

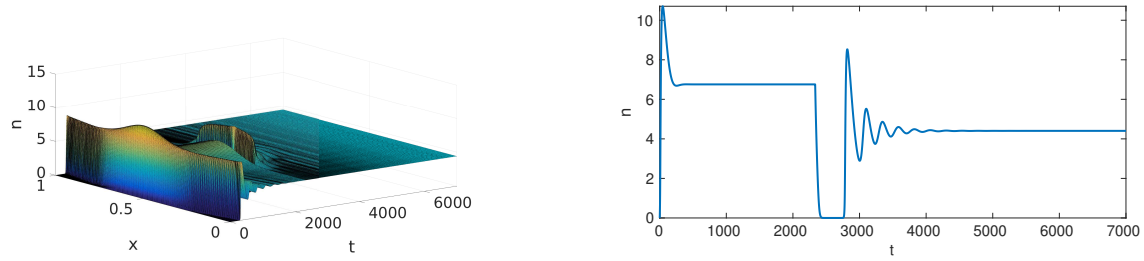

(a) Active neutrophils

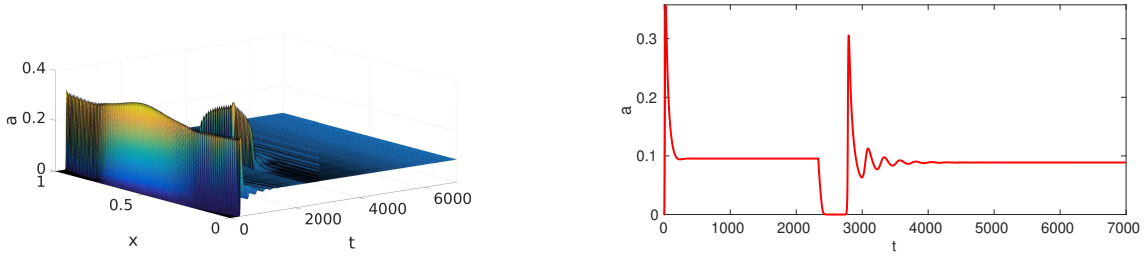

(b) Apoptotic neutrophils

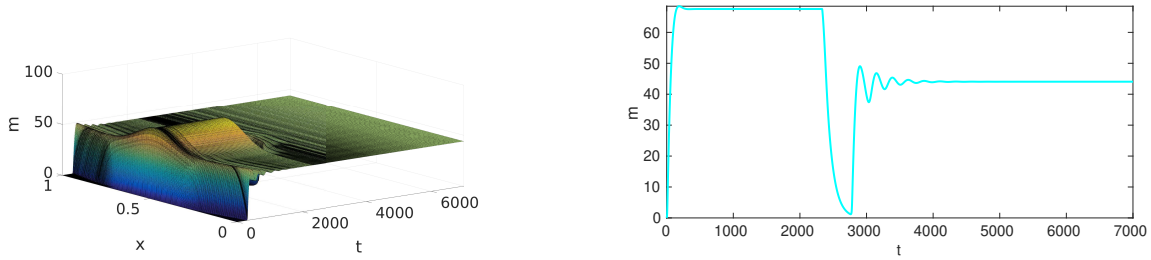

(c) Macrophages

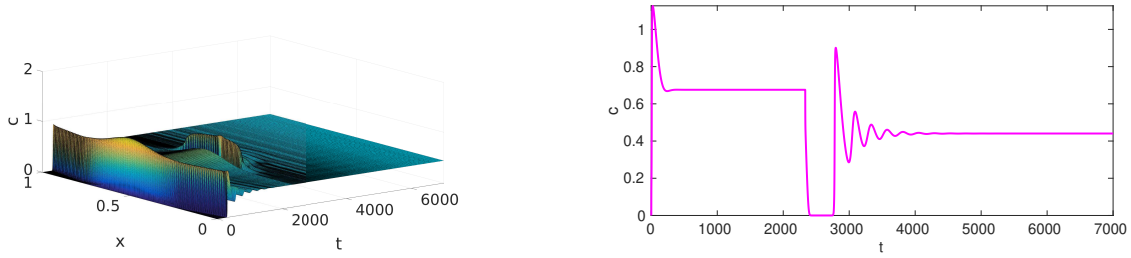

(d) Pro-inflammatory mediators

Figure 2.13: Solution of (2.13)–(2.16), with damage modelled as in (2.25)–(2.26), with $\phi = 0.09$ and all other parameters values as in Table 2.2, initial conditions as per (2.18) and periodic boundary conditions. Figures on the left panel correspond to the variables' spatial representation at each time step, the right column presents plots of the dynamics of the same variables in the middle of the spatial domain. Setting $\phi = 0.09$ provides damped oscillations, but does not yield complete resolution of inflammation.

(a) Active neutrophils

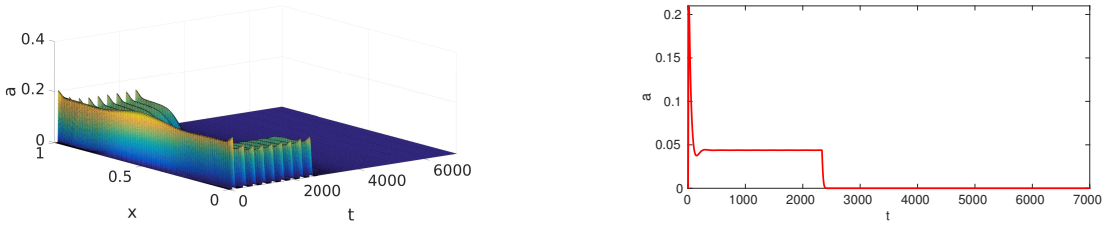

(b) Apoptotic neutrophils

(c) Macrophages

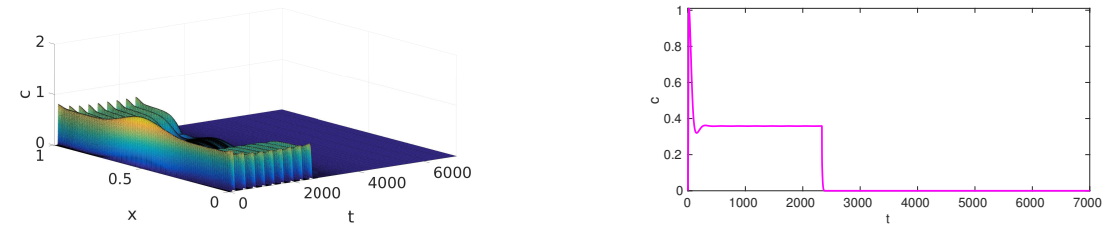

(d) Pro-inflammatory mediators

Figure 2.14: Solution of (2.13)–(2.16), with damage modelled as in (2.25)–(2.26), with $\phi = 0.2$ and with all other parameters values as in Table 2.2, initial conditions as per (2.18) and periodic boundary conditions. Figures on the left panel correspond to the variables' spatial representation at each time step, the right column presents plots of the dynamics of the same variables in the middle of the spatial domain. Setting $\phi = 0.2$ results in full inflammation resolution.

and the mediators diffusion is evident in the left panel graphs of Figures 2.12–2.14, with a preliminary spatial heterogeneity given by the gaussian shaped damage eventually diffusing and settling to a homogeneous steady state. In general, throughout our simulations, we observe that the damage triggering the inflammatory response initially spreads within the tissue, persisting for a limited time and eventually being cleared, restoring a homogeneously healthy state.

In each of Figures 2.12–2.14, we observe a rapid decline in the levels of each of our model components at $t \simeq 2333$. This occurs due to the sudden change in the damage function imposed by (2.26). Prior to this point, the damage function provides constant stimulus to the model in the centre of the domain, resulting in the damage in this region being sustained. At $t \simeq 2333 = t_{max}/3$, the damage function in (2.26) switches off, and we observe a short period of time over which the damage spreads to become homogeneous. After homogeneity is reached, the results recover the results of the corresponding ODE model of Dunster *et al.* (2014) exactly; however, the model of Dunster *et al.* (2014) does not capture intermediate, spatially inhomogeneous configurations.

An important key point arising from the spatial analysis of system (2.13)–(2.16) is that, regardless of parameters, all long-term solutions are homogeneous. As observed in the above figures, variations in key parameter values can cause changes in the way that damage spreads across the tissue, and can ultimately yield switching between globally healthy and globally chronic outcomes. Crucially, for the parameters studied here, there is no emergence of persistent spatial patterns. We investigate the potential for spatial patterns for more general parameter choices via Turing instability analysis below.

2.5 Turing instability analysis

We here conduct a Turing instability analysis to ascertain whether the model of (2.13)–(2.16) can support spatially inhomogeneous steady states.

Analogously to the procedure and notation used in appendix A to identify Turing instabilities and spatial pattern formation, let us firstly consider the system (2.13)–(2.16) referring to its relevant homogeneous steady state, corresponding to solutions of the system

$$n_t = -\nu n + c \equiv f_1(n, a, m, c) = 0\,, \tag{2.27}$$

$$a_t = \nu n - \gamma_a a - \phi m a \equiv f_2(n, a, m, c) = 0\,, \tag{2.28}$$

$$m_t = -\gamma_m m + c \equiv f_3(n, a, m, c) = 0\,, \tag{2.29}$$

$$c_t = \alpha f(t) + \gamma_a \frac{a^2}{\beta_a^2 + a^2} - c \equiv f_4(n, a, m, c) = 0\,. \tag{2.30}$$

By linearising around the steady state (n_0, a_0, m_0, c_0), (2.27)–(2.30) can be rewritten as

$$\underbrace{\begin{pmatrix} n_t \\ a_t \\ m_t \\ c_t \end{pmatrix}}_{\mathbf{w_t}} = \underbrace{\begin{pmatrix} f_{1_{n_0}} & 0 & 0 & f_{1_{c_0}} \\ f_{2_{n_0}} & f_{2_{a_0}} & f_{2_{m_0}} & 0 \\ 0 & 0 & f_{3_{m_0}} & f_{3_{c_0}} \\ 0 & f_{4_{a_0}} & 0 & f_{4_{c_0}} \end{pmatrix}}_{\mathcal{A}} \underbrace{\begin{pmatrix} n - n_0 \\ a - a_0 \\ m - m_0 \\ c - c_0 \end{pmatrix}}_{\mathbf{w}}, \tag{2.31}$$

with $\mathcal{A}$ being the Jacobian matrix evaluated at the steady state, having introduced the notation

$$f_{1_{n_0}} = \left.\frac{\partial f_1}{\partial n}\right|_{n_0, a_0, m_0, c_0}, \tag{2.32}$$

and similarly for $f_{1_{a_0}}$, $f_{1_{m_0}}$ and $f_{1_{c_0}}$ and following rows.

Here, the matrix $\mathcal{A}$ introduced in (2.31) is given by

$$\mathcal{A} = \begin{pmatrix} -\nu & 0 & 0 & 1 \\ \nu & -\gamma_a - \phi\, m_0 & -\phi\, a_0 & 0 \\ 0 & 0 & -\gamma_m & 1 \\ 0 & \dfrac{2a_0\gamma_a\beta_a^2}{(\beta_a^2 + a_0^2)^2} & 0 & -1 \end{pmatrix}. \tag{2.33}$$

For the homogeneous steady state to be stable, we require

$$\Re(\lambda_i(\mathcal{A})) < 0 \qquad i = 1, \ldots, 4. \tag{2.34}$$

The bifurcation analysis of Section 2.4.2 has already shown that the system supports up to two stable homogeneous steady states. Our interest here is in ascertaining whether these steady states can be destabilised by diffusion, potentially resulting in stable patterns.

By restoring diffusion in the model of (2.13)–(2.16), the system can accordingly be rewritten, analogously to expression in (2.31), as:

$$\underbrace{\begin{pmatrix} n_t \\ a_t \\ m_t \\ c_t \end{pmatrix}}_{\mathbf{w_t}} = \underbrace{\begin{pmatrix} f_{1_{n_0}} & 0 & 0 & f_{1_{c_0}} \\ f_{2_{n_0}} & f_{2_{a_0}} & f_{2_{m_0}} & 0 \\ 0 & 0 & f_{3_{m_0}} & f_{3_{c_0}} \\ 0 & f_{4_{a_0}} & 0 & f_{4_{c_0}} \end{pmatrix}}_{\mathcal{A}} \underbrace{\begin{pmatrix} n - n_0 \\ a - a_0 \\ m - m_0 \\ c - c_0 \end{pmatrix}}_{\mathbf{w}} + \underbrace{\begin{pmatrix} D_n & 0 & 0 & 0 \\ 0 & 0 & 0 & 0 \\ 0 & 0 & D_m & 0 \\ 0 & 0 & 0 & D_c \end{pmatrix}}_{\mathcal{D}} \nabla^2 \underbrace{\begin{pmatrix} n - n_0 \\ a - a_0 \\ m - m_0 \\ c - c_0 \end{pmatrix}}_{\mathbf{w}}, \tag{2.35}$$

or, in its compact matrix form

$$\mathbf{w_t} = \mathcal{A}\mathbf{w} + \mathcal{D}\nabla^2\mathbf{w}. \tag{2.36}$$

Assuming a spatial dependence of the form described in Appendix A (equation (A.17)),

with wave number k, we obtain the associated Jacobian

$$\mathcal{A}_k = \begin{pmatrix} f_{1_{n_0}} - k^2 D_n & 0 & 0 & f_{1_{c_0}} \\ f_{2_{n_0}} & f_{2_{a_0}} & f_{2_{m_0}} & 0 \\ 0 & 0 & f_{3_{m_0}} - k^2 D_m & f_{3_{c_0}} \\ 0 & f_{4_{a_0}} & 0 & f_{4_{c_0}} - k^2 D_c \end{pmatrix}, \tag{2.37}$$

or equivalently

$$\mathcal{A}_k = \begin{pmatrix} -\nu - k^2 D_n & 0 & 0 & 1 \\ \nu & -\gamma_a - \phi m_0 & -\phi a_0 & 0 \\ 0 & 0 & -\gamma_m - k^2 D_m & 1 \\ 0 & X & 0 & -1 - k^2 D_c \end{pmatrix}, \tag{2.38}$$

with X conveniently denoting $(2a_0\gamma_a\beta_a^2)/(a_0^2 + \beta_a^2)^2$, as originally appeared in (2.33).

The characteristic polynomial of $\mathcal{A}_k$ is given by

$$\begin{aligned} p_k(\lambda) = (\nu + k^2 D_n + \lambda)[(\gamma_a + \phi m_0 + \lambda)(\gamma_m + k^2 D_m + \lambda)(1 + k^2 D_c + \lambda) + \phi a_0 X] \\ - \nu(\gamma_m + k^2 D_m + \lambda)X. \end{aligned} \tag{2.39}$$

By conveniently renaming the factors as

$$t_1 = \nu + k^2 D_n, \tag{2.40}$$

$$t_2 = \gamma_a + \phi m_0, \tag{2.41}$$

$$t_3 = \gamma_m + k^2 D_m, \tag{2.42}$$

$$t_4 = 1 + k^2 D_c, \tag{2.43}$$

$$t_5 = \phi a_0 X, \tag{2.44}$$

$$t_6 = \nu X, \tag{2.45}$$

and rearranging the terms, the characteristic polynomial can be expressed as

$$p_k(\lambda) = \lambda^4 + \underbrace{(t_1 + t_2 + t_3 + t_4)}_{s_1}\lambda^3 + \underbrace{(t_1t_2 + t_1t_3 + t_1t_4 + t_2t_3 + t_2t_4 + t_3t_4)}_{s_2}\lambda^2 + \\ + \underbrace{[t_1t_2(t_3 + t_4) + t_3t_4(t_1 + t_2) + t_5 - t_6]}_{s_3}\lambda + \underbrace{t_1t_2t_3t_4 + t_1t_5 - t_3t_6}_{s_4}, \tag{2.46}$$

having further simplified the notation, by introducing the terms s_1, s_2, s_3 and s_4 that allow a shorter and straightforward representation of $p_k(\lambda)$:

$$p_k(\lambda) = \lambda^4 + s_1\lambda^3 + s_2\lambda^2 + s_3\lambda + s_4. \tag{2.47}$$

Observation 1. *Recalling that all elements in $\mathcal{D}$ as well as all the model parameters and variables are positive, it follows that $t_1, t_2, t_3, t_4, t_5, t_6 > 0$.*

Observation 2. *From observation 1 it follows that*

$$s_1 = t_1 + t_2 + t_3 + t_4 > 0 \tag{2.48}$$

$$s_2 = t_1t_2 + t_1t_3 + t_1t_4 + t_2t_3 + t_2t_4 + t_3t_4 > 0. \tag{2.49}$$

Similarly to the analysis carried out in appendix A.2, the existence of *spatial instability* is related to the system having eigenvalues with positive real part. This problem is thus equivalent of studying the signs of the real parts of the polynomial roots $\lambda_i\,, i = 1, \ldots, 4$. In order to do so, the Routh-Hurwitz criterion is applied (see appendix B), with the associated Routh matrix (defined in B.2) being

$$R = \begin{pmatrix} 1 & s_2 & s_4 \\ s_1 & s_3 & \\ \frac{s_1s_2 - s_3}{s_1} & s_4 & \\ \frac{s_1^2s_4 + s_3^2 - s_1s_2s_3}{s_3 - s_1s_2} & & \\ s_4 & & \end{pmatrix}. \tag{2.50}$$

In particular, according to the Routh-Hurwitz criterion, the number of eigenvalues with positive real part is related to the number of sign changes within the elements of the first column of R. Therefore, analysing the signs of elements r_{i1}, $i = 1, \ldots, 5$ of the Routh matrix determines the system's homogeneity in space. The analysis of the actual elements r_{i1} of matrix (2.50) first column yields

$$r_{11} = 1 > 0, \quad r_{21} = s_1 > 0, \quad r_{51} = s_4 > 0,$$

with

$$r_{31} = \frac{s_1 s_2 - s_3}{s_1} \tag{2.51}$$

and

$$r_{41} = \frac{s_1^2 s_4 + s_3^2 - s_1 s_2 s_3}{s_3 - s_1 s_2} \tag{2.52}$$

requiring further study. From expressions (2.51)–(2.52) it is clear that the sign of $s_1 s_2 - s_3$ eventually characterises both matrix elements. For simplicity, let us consider the trivial steady state for which all variables are equal to zero, and thus $X = 0$ and $t_5 = t_6 = 0$ also. We can then write

$$\begin{aligned} s_1 s_2 - s_3 = {} & (t_1 + t_2 + t_3 + t_4)(t_1 t_2 + t_1 t_3 + t_1 t_4 + t_2 t_3 + t_2 t_4 + t_3 t_4) + \\ & - t_1 t_2 (t_3 + t_4) - t_3 t_4 (t_1 + t_2), \end{aligned} \tag{2.53}$$

which, in turn, can be rewritten as

$$\begin{aligned} s_1 s_2 - s_3 = {} & t_1 t_2 (t_1 + t_2) + t_3 t_4 (t_3 + t_4) + \\ & + (t_1 + t_2 + t_3 + t_4)(t_1 t_3 + t_1 t_4 + t_2 t_3 + t_2 t_4) + \\ & + t_1 t_2 (t_3 + t_4) + t_3 t_4 (t_1 + t_2) - t_1 t_2 (t_3 + t_4) - t_3 t_4 (t_1 + t_2), \end{aligned} \tag{2.54}$$

prompting the cancellation of all negative terms and resulting in

$$\begin{aligned} s_1 s_2 - s_3 = {} & t_1 t_2 (t_1 + t_2) + t_3 t_4 (t_3 + t_4) + \\ & + (t_1 + t_2 + t_3 + t_4)(t_1 t_3 + t_1 t_4 + t_2 t_3 + t_2 t_4), \end{aligned} \tag{2.55}$$

which, comprising only positive terms, is always positive. Thus, also $r_{31} > 0$.

An analogous analysis of element r_{41} requires studying the sign of its numerator since we know from above that its denominator is negative. Noting (2.55), we have

$$\begin{aligned} s_1^2 s_4 - s_3(s_1 s_2 - s_3) = (t_1+t_2+t_3+t_4)^2(t_1t_2t_3t_4) + \\ - [t_1t_2(t_3+t_4) + t_3t_4(t_1+t_2)][t_1t_2(t_1+t_2) + t_3t_4(t_3+t_4) + \\ + (t_1+t_2+t_3+t_4)(t_1t_3+t_1t_4+t_2t_3+t_2t_4)] . \end{aligned} \tag{2.56}$$

Convenient arrangements of the terms provide the following:

$$\begin{aligned} s_1^2 s_4 - s_3(s_1 s_2 - s_3) = (t_1+t_2+t_3+t_4)^2(t_1t_2t_3t_4) + \\ - (t_1+t_2)^2(t_1t_2t_3t_4) - (t_3+t_4)^2(t_1t_2t_3t_4) + \\ - (t_1^2t_2^2 + t_3^2t_4^2)(t_1+t_2)(t_3+t_4) + \\ - (t_1t_3+t_1t_4+t_2t_3+t_2t_4)(t_1+t_2+t_3+t_4)[t_1t_2(t_3+t_4) + t_3t_4(t_1+t_2)], \end{aligned} \tag{2.57}$$

from which it follows that

$$\begin{aligned} s_1^2 s_4 - s_3(s_1 s_2 - s_3) = (t_1+t_2)^2(t_1t_2t_3t_4) + (t_3+t_4)^2(t_1t_2t_3t_4) + \\ + 2(t_1t_3+t_1t_4+t_2t_3+t_2t_4)(t_1t_2t_3t_4) + \\ - (t_1+t_2)^2(t_1t_2t_3t_4) - (t_3+t_4)^2(t_1t_2t_3t_4) + \\ - (t_1^2t_2^2 + t_3^2t_4^2)(t_1t_3+t_1t_4+t_2t_3+t_2t_4) + \\ - (t_1t_3+t_1t_4+t_2t_3+t_2t_4)(t_1+t_2+t_3+t_4)[t_1t_2(t_3+t_4) + t_3t_4(t_1+t_2)] . \end{aligned} \tag{2.58}$$

Cancelling terms where possible then provides:

$$\begin{aligned} s_1^2 s_4 - s_3(s_1 s_2 - s_3) = (t_1t_3+t_1t_4+t_2t_3+t_2t_4)\{2(t_1t_2t_3t_4) - (t_1^2t_2^2 + t_3^2t_4^2) + \\ - (t_1+t_2+t_3+t_4)[t_1t_2(t_3+t_4) + t_3t_4(t_1+t_2)]\}, \end{aligned} \tag{2.59}$$

Which we may rearrange as follows:

$$\begin{aligned} s_1^2 s_4 - s_3(s_1 s_2 - s_3) = -(t_1t_3+t_1t_4+t_2t_3+t_2t_4)\{(t_1t_2 + t_3t_4)^2 + \\ + (t_1+t_2+t_3+t_4)[t_1t_2(t_3+t_4) + t_3t_4(t_1+t_2)]\}, \end{aligned} \tag{2.60}$$

which is always negative, thus ensuring that $s_1^2 s_4 - s_1 s_2 s_3 + s_3^2 < 0$. This result, combined with (2.55) implies that

$$r_{41} = \frac{s_1^2 s_4 - s_1 s_2 s_3 + s_3^2}{s_3 - s_1 s_2} > 0.$$

Finally, recalling that all elements $r_{i1},\ i = 1, \ldots, 5$ present the same sign, thus preventing any change in sign between consecutive elements, the stability of the healthy, homogeneous steady state is guaranteed, with all the associated eigenvalues having negative real parts (appendix B).

This also implies that, even when diffusion values would lead to spatial instability at the two remaining critical sets of fixed points, this instability eventually settles and the stability guaranteed by the fixed points at zero prevail.

As such, this detailed analysis proves that, regardless of diffusion constants D_n, D_m and D_c values, there is no scope for the model of (2.13)–(2.16) to support Turing instabilities.

2.6 Conclusions

In this chapter an initial spatially-dependent model of inflammation developed by Dunster *et al.* (2014) has been presented and analysed. We then extended this model, adding the spatial description of the inflammatory response. In particular, we modelled diffusion of mediators, active neutrophils and macrophages, neglecting apoptotic neutrophils as dead cells thus unable to move.

The key results emerging from the associated ODE system and the bifurcation analysis regard the system's stability, with the model being either bistable or monostable, depending on the parameters. While a number of parameters regulate the wide range of biological interactions between the system's variables (namely active neutrophils n, apoptotic neutrophils a, macrophages m and pro-inflammatory mediators

c), two main parameters emerge as critical, from both preliminary simulations in Section 2.4.1 and the bifurcation analysis in Section 2.4.2; that is, ϕ and β_a, accounting for the apoptotic neutrophil removal rate and saturation constant respectively. In particular, as Figures 2.4–2.6 show, an enhanced clearance of apoptotic neutrophils by macrophages results in a more effective resolution of inflammation, while, on the other hand, both parameters ϕ and β_a show the most significant effects on the model, in terms of stability of the steady states, as represented in the bifurcation diagrams of Figures 2.10 and 2.11. Overall, for large values of β_a, the model is monostable, since fewer apoptotic neutrophils release pro-inflammatory mediators, meaning that resolution is guaranteed. Analogously, the system is monostable also for large values of ϕ, since apoptotic neutrophils are cleared by macrophages at a higher rate, thus prompting the resolution of inflammation.

Analysing the numerical results, we observed how localised damage can spread to neighbouring healthy tissue. For the parameters studied, we only observe inhomogeneous solutions while damage is being actively stimulated by an inhomogeneous input $f(x,t)$. In the absence of f, long term solutions revert to those of the ODE model. While long-term solutions are always homogeneous, and thus recover the results of Dunster *et al.* (2014) entirely, we note that the ODE model of Dunster *et al.* is unable to capture the intermediate inhomogeneous configurations presented in Figures 2.12–2.14, which illustrate the manner in which localised damage spreads in to neighbouring healthy tissue.

Aiming at studying the models potential for spatial patterning, we investigated the scope for spatial patterns arising through the two most common mechanisms reported in literature, namely Turing instabilities and Hopf bifurcations. In Section 2.5, we illustrated that the structure of this model does not allow diffusion to destabilise the homogeneous steady states of the corresponding ODE model. This eliminates the scope for Turing instabilities to occur. Most pattern formation mechanisms that are

reported to occur at Hopf bifurcations in existing literature do so when these Hopf bifurcations are supercritical and give rise to stable oscillations in the corresponding ODE model. (See, for example, Mazin *et al.* (1996) or Dilao (2005).) However, in this model, the Hopf bifurcation is always subcritical, which seems to eliminate Hopf-based patterns. Therefore, the model does not present any spatial inhomogeneity of the steady states. This in turn prevents the development of possible spatial patterns that would be of interest in biological terms. We note that extensions of the underlying ODE model presented by Dunster *et al.* (2014), which include further biological feedbacks, exhibit changes in the criticality of the Hopf bifurcation, and thus may display scope for inhomogeneous solutions; this is one question that we address in Chapter 3 below.

While we have observed that the model of (2.13)–(2.16) shows relatively limited spatially inhomogeneous behaviour in the absence of sustained inhomogeneous forcing, it is important to note that this model incorporates only a limited number of cellular interactions, and hence lacks some more complex feedbacks that could render spatially inhomogeneous solutions permissible. This model includes only one positive feedback via apoptotic neutrophils and one negative feedback via macrophages. An extension of the underlying ODE model, presented by Dunster *et al.* (2014), incorporates an additional positive feedback via production of pro-inflammatory mediators by active neutrophils, which has significant impact upon the models dynamics, increasing the size of the bistable regime. Furthermore, this model omits anti-inflammatory mediators, which have been shown to play an important role in triggering the resolution of inammatory processes (Serhan *et al.*, 2008; Rinaldi *et al.*, 2011), and provide an additional negative feedback. We anticipate that inclusion of these additional behaviours could enable a broader range of spatially inhomogeneous behaviours, in which localised damage may spread to healthy tissue. In addition, a key limitation of this model is that active neutrophils and macrophages are assumed to move only

diffusively, while *in vivo* the principal motion of these cells is chemotactic migration toward high concentrations of pro-inflammatory mediators. This chemotaxis is omitted here, but may be readily included in an extension of this model. In doing so, we note that our focus upon a one-dimensional domain in this chapter could place some restrictions on the spatial patterns attained. To overcome these limitations, it is essential to widen the current model by adding to its complexity, both spatially (via a $2D$ implementation) and biologically, by including the above described features that will invariably involve a larger number of parameters and variables. We address these deciencies in the following chapter. In particular, we present a thorough review of the limitations of this model, and how they will be addressed in a corresponding extension, in Section 3.1.

Chapter 3

Modelling the effects of anti-inflammatory mediators

In this chapter we extend the previously developed PDE model in order to include the impact of a second group of chemicals upon the system, representing of anti-inflammatory mediators. Furthermore, more refined biological interactions such as neutrophils' inherently pro-inflammatory behaviour (Dunster *et al.*, 2014) and the addition of chemotaxis are also provided in this new model. A new numerical approach is also presented in order to tackle the complications introduced by the inclusion of the chemotactic terms. A two-dimensional version of the model will be implemented, in line with the biological assumption of analysing the surge and resolution of inflammation of a generic two-dimensional tissue. The model will be analysed first in terms of homogeneous steady states and then spatially by investigating the model's ability to support patterning and inhomogeneous oscillations. Results will be gathered and assessed in terms of the manipulation of key parameters and the corresponding impact upon the final inflammatory outcome.

3.1 Limitations and extensions of the model of Chapter 2

The model introduced in Chapter 2 served to provide a basic representation of the main features that characterise the acute inflammatory response. The actual biology of such a complex event presents multiple aspects that have been neglected in the previous model for the sake of simplicity and clarity. These included cells' chemotaxis and neutrophils' contribution to promoting inflammation. While that model yields effective simulations in terms of the dynamical outcome of an inflammatory process, the lack of some significant biological interactions prompts for an extension of the model in order to assess biologically meaningful results by including such features in its mathematical description. Furthermore, the analysis of the model of Chapter 2 also excludes any kind of spatial patterning, while not being sufficiently rigorous in terms of chemical interactions between the main inflammatory variables. Thus, the extension proposed in this chapter, while yielding a more complicated model, takes into account more accurate biological scenarios, possibly providing scope for spatially inhomogeneous outcomes.

The equations provided for the model of Chapter 2 (2.1)–(2.7) configure apoptotic neutrophils as the only active source of pro-inflammatory mediators (initially triggered by generic damage, modelled by $f(t^*)$ as in (2.6)). Biologically though this is not completely accurate, since active neutrophils also serve as a positive feedback in terms of pro-inflammatory events (Xia *et al.*, 2015) by being responsible for an enhanced production of c^*. Furthermore, macrophage activity goes beyond the basic phagocytosing task and presents a much more nuanced response throughout inflammatory processes, by releasing, upon their recognition of apoptotic neutrophils, different specific chemicals that act as anti-inflammatory signals. While the range

of species macrophages release to this scope is quite wide and diversified, both in terms of timing and the specific nature these anti-inflammatory cytokines, there is also a redundancy of the anti-inflammatory signals that are triggered by macrophage activity (Duque & Descoteaux, 2014) that justifies modelling this varied multiple group of mediators as a unique source of anti-inflammatory chemicals. Therefore, in order to model this new sequence of mediators appearing in the inflammatory environment that is being analysed, it is considered that macrophages are responsible for the release of a generic anti-inflammatory mediator, that includes a group of different cytokines and growth factors commonly present in inflammation (Liu *et al.*, 2014).

Moreover, an essential feature that will be incorporated in this extension of the model of Chapter 2 is *chemotaxis*, thus adding to the spatial characterisation of the model as well as replicating a fundamental aspect of *in vivo* inflammatory processes.

In general, in chemical and biological systems, the phenomenon of cellular directional motion up chemical gradients is named chemotaxis (Delves & Roitt, 1998). This is a common feature of many cells, including unicellular organisms such as bacteria (Schaechter, 2009), but, with regards to inflammation, it is most prominently expressed by leukocytes which are diverted from blood stream into the injured area (Tani *et al.*, 2001). A large group of chemicals, including small proteins and chemokines, have been recognised to act as chemotactic agents, although the exact mechanisms of signalling and transduction that result in cell migration have not been completely clarified yet (Jin *et al.*, 2008). Nonetheless, upon injury, as part of the initial cascade of reactions and interactions triggered by the occurred damage, this variety of particles, partly present on-site and partly released in response to the insult, selectively attract neutrophils (in the earliest stages) and macrophages (during the ongoing response), prompting their recruitment and deployment in the inflammatory activity. The tightly controlled mechanisms of chemotaxis during inflammation and their high specificity ensure the triggering and promotion of an effective and physio-

logic acute inflammatory response. On the other hand, slight defects in this complex and delicate cell signalling could easily result in chronic inflammation and possible pathological complications (Turner *et al.*, 2014).

3.2 The model

We extend the model of Chapter 2 to account for the above limitations by following the corresponding model developments of Dunster *et al.* (2014), as described below. Furthermore, we extend the existing ODE model of Dunster *et al.* (2014) to include spatial information via diffusive and chemotactic terms in the governing equations. The biological interactions described above are introduced into the model by denoting with k_n^* the maximal rate of production of pro-inflammatory mediators by neutrophils. We assume this feedback to be saturating in nature in the same manner as production by apoptotic neutrophils was modelled in Chapter 2; we denote with β_n^* the associated half-maximal concentration level. A new equation accounting for the anti-inflammatory mediators, g^*, is also added to the model; we introduce the new parameters k_g^* as the concentration of anti-inflammatory mediators produced upon macrophage engulfment of apoptotic neutrophils, and γ_g^* as the linear decay rate. The anti-inflammatory activity affects in turn the apoptotic process that neutrophils undergo by increasing the apoptosis rate through a saturation constant β_g^* that acts on anti-inflammatory mediators. Conversely, upon a concentration of pro-inflammatory mediators of β_c^* the apoptosis rate decreases. In this context, pro-inflammatory mediators c^* further prolong neutrophils' lifespan (McCracken & Allen, 2014). To model these effects, the apoptosis rate ν^* is amended such as to include the contributions of both the anti-inflammatory mediators g^* through the parameter β_g^* and the pro-inflammatory mediators c^* through the parameter β_c^* respectively. The effect of the newly introduced anti-inflammatory mediators is further reflected on the neutrophils

influx with parameter β^*_{gc} controlling the concentration over which this rate decreases. These additional interactions, introduced in 'Model 3' of Dunster *et al.* (2014), are illustrated in Figure 3.1, which updates upon Figure 2.1 in Chapter 2. Once again, we expand upon this existing ODE model via the addition of spatial terms, following the procedure of Chapter 2. In order to incorporate spatial information for the new variable g^*, a diffusion constant D^*_g is introduced, thus considering anti-inflammatory mediators as moving diffusively.

In order to mathematically incorporate chemotaxis, both active neutrophils n^* and macrophages m^* are considered to move towards higher concentrations of pro-inflammatory mediators c^*. This movement of cells towards high concentrations of pro-inflammatory mediators results in additional flux terms that are proportional to both the local cell concentration and the gradient of the pro-inflammatory mediator concentration. That is, we obtain the highest level of chemotactic flux when both the cell number and the mediator gradient are large. We denote the associated chemotaxis constants for neutrophils and macrophages by θ^*_n and θ^*_m respectively.

Our extended model is therefore generated by the following equations:

$$\frac{\partial n^*}{\partial t^*} = -\nu^* \frac{1+\frac{g^*}{\beta^*_g}}{1+\frac{c^*}{\beta^*_c}} n^* + \chi^*_n \frac{c^*}{1+\frac{g^*}{\beta^*_{gc}}} + D^*_n \nabla^2 n^* - \theta^*_n \nabla \cdot (n^* \nabla c^*), \tag{3.1}$$

$$\frac{\partial a^*}{\partial t^*} = \nu^* \frac{1+\frac{g^*}{\beta^*_g}}{1+\frac{c^*}{\beta^*_c}} n^* - \gamma^*_a a^* - \phi^* m^* a^*, \tag{3.2}$$

$$\frac{\partial m^*}{\partial t^*} = \chi^*_m c^* - \gamma^*_m m^* + D^*_m \nabla^2 m^* - \theta^*_m \nabla \cdot (m^* \nabla c^*), \tag{3.3}$$

$$\frac{\partial c^*}{\partial t^*} = \alpha^* f(x^*, t^*) + k^*_n \left(\frac{n^{*2}}{\beta^{*2}_n + n^{*2}} \right) + k^*_a \gamma^*_a \left(\frac{a^{*2}}{\beta^{*2}_a + a^{*2}} \right) - \gamma^*_c c^* + D^*_c \nabla^2 c^*, \tag{3.4}$$

$$\frac{\partial g^*}{\partial t^*} = k^*_g \phi^* m^* a^* - \gamma^*_g g^* + D^*_g \nabla^2 g^* \quad , \tag{3.5}$$

We retain the cells' spatial description with active neutrophils and macrophages freely diffusing within the tissue. As previously explained in Chapter 2, we do not prescribe apoptotic neutrophils with diffusive motion assuming that the extent to which these

inanimate particles could diffuse (despite varying dependent upon their local environment, size and temperature) will always be negligibly small compared to that of active neutrophils and macrophages.

We highlight, once again, that in the absence of diffusive and chemotactic terms in (3.1)–(3.5) we recover the ODE model labelled as 'Model 3' in Dunster *et al.* (2014).

In Chapter 2 we initially modelled damage through a time dependent function $f(t^*)$, (2.5), and subsequently a spatially dependent one $f(x^*, t^*)$, (2.25), that triggers the inflammatory response. We retain f in (3.4) to make a comparison with Chapter 2, but in later sections we set $f = 0$ and consider damage driven by initial conditions.

3.3 Parameter values

The newly introduced parameters are presented in Table 3.1, with ranges of values inferred from the available literature where possible. As can be seen from Table 3.1, the scientific literature for diffusion constant of the anti-inflammatory mediators D_g^* gives a comparable range to the one provided for the diffusion of pro-inflammatory mediators D_c^* and reported in Table 2.1 of Chapter 2. As such, we consider the anti-inflammatory mediators to diffuse at equivalent rate of pro-inflammatory mediators.

As for the chemotactic constants, as an initial point of reference we assume that chemotaxis parameters are of a similar order to those of leukocytes' diffusion that remain unchanged from the considerations of Section 2.2.1, with specific dimensionless values detailed in the following section.

3.4 Nondimensionalisation

Analogously to Section 2.2.2, we nondimensionalise (3.1)–(3.5) by substituting the rescaled dimensionless variables of (2.12) as well as the new scaling $g^* = \beta_{gc}^* g$, the

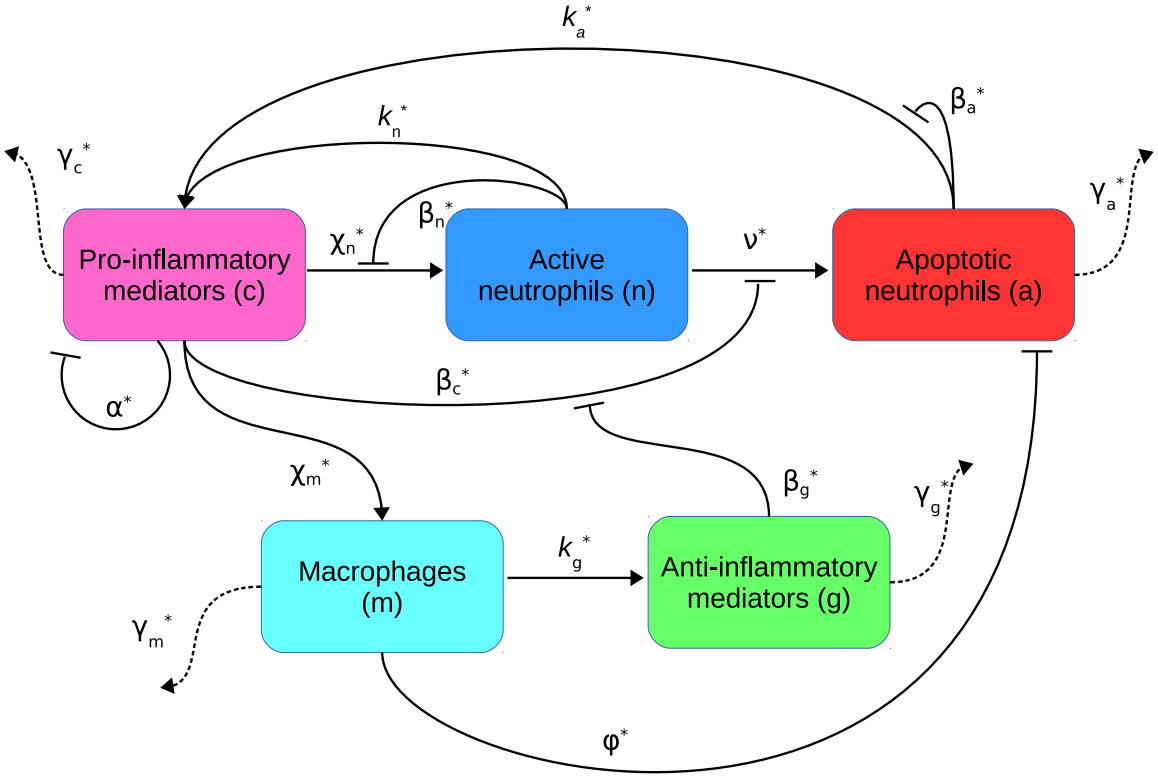

Figure 3.1: Schematic diagram showing the spatially-independent interactions in 'Model 3' of Dunster *et al.* (2014), which form the basis of the PDE model presented in (3.1)–(3.5). The model includes populations of healthy neutrophils (n^*), apoptotic neutrophils (a^*) and macrophages (m^*), interacting in response to pro- and anti-inflammatory mediators (c^* and g^*) with associated parameters as shown. Arrowheads indicate up-regulation; flat-headed arrows indicate down-regulation; dashed arrows indicate natural decay.

Parameter	Definition	Range of values	Unit measure
k_n^*	pro-inflammatory mediators production from active neutrophils (rate of $c^*(t)$ concentration produced in response active neutrophils presence)	$750 - 4000$ (Dumas *et al.*, 2016)	$[pg \cdot mm^{-3} \cdot day^{-1}]$
β_n^*	active neutrophils saturation constant (concentration of active neutrophils required for half maximal release of $c^*(t)$)		$[cell \cdot mm^{-3}]$
k_g^*	anti-inflammatory mediators production from macrophages (concentration of $g^*(t)$ produced in response macrophages presence)	$10 - 750$ (Miles *et al.*, 2009)	$[pg \cdot cell^{-1}]$
β_{gc}^*	inflammatory mediators saturation constant (concentration scale over which neutrophils influx rate decreases)		$[pg \cdot mm^{-3}]$
β_g^*	anti-inflammatory mediators saturation constant (concentration of anti-inflammatory mediators over which apoptosis rate increases)		$[pg \cdot mm^{-3}]$
β_c^*	pro-inflammatory mediators saturation constant (concentration of pro-inflammatory mediators over which apoptosis rate decreases)		$[pg \cdot mm^{-3}]$
γ_g^*	rate of anti-inflammatory mediators decay	$3.6 - 52.56$ (Reynolds *et al.*, 2006)	$[day^{-1}]$
D_g^*	anti-inflammatory mediators diffusion constant	$8.64 \cdot 10^{-2} - 8.64$ (Busse *et al.*, 2010) (Sherratt & Murray, 1990) (Ross & Pompano, 2018)	$[mm^2 \cdot day^{-1}]$
θ_n^*	active neutrophils chemotaxis constant		$[mm^2 \cdot day^{-1}]$
θ_m^*	active macrophages chemotaxis constant		$[mm^2 \cdot day^{-1}]$

Table 3.1: New parameters appearing in the model (3.1)–(3.5). When available, ranges of parameter values are inferred from relevant literature, as specified.

new dimensionless parameters are defined as

$$\begin{gathered}\beta_g = \frac{\beta_g^*}{\beta_{gc}^*}, \quad \beta_c = \frac{\beta_c^*}{k_a^*}, \quad \gamma_g = \frac{\gamma_g^*}{\gamma_c^*}, \quad k_g = \frac{\chi_n^* k_a^*}{\beta_{gc}^* \gamma_c^*} k_g^*, \\ D_g = \frac{D_g^*}{L_x^{*2}\gamma_c^*}, \quad k_n = \frac{k_n^*}{k_a^* \gamma_c^*}, \quad \beta_n = \frac{\gamma_c^*}{\chi_n^* k_a^*}\beta_n, \quad \theta_n = \frac{\theta_n^*}{L_x^{*2}\gamma_c^*}, \quad \theta_m = \frac{\theta_m^*}{L_x^{*2}\gamma_c^*}\end{gathered} \tag{3.6}$$

As the expressions in (3.6) show, we follow the nondimensionalisation applied in Chapter 2, by scaling time on $1/\gamma_c^*$, taking $\gamma_c^* = 3$ day^{-1}, as in Dunster *et al.* (2014), with γ_c^* being the rate of decay of pro-inflammatory mediators. As in Chapter 2, we scale space considering a domain of width $L^* = 10$ cm. The dimensional ranges given by literature and reported in tables 2.1 and 3.1 allow us to provide dimensionless estimates for both spatial and non-spatial dimensionless parameters as shown in Table 3.2. The corresponding dimensionless system is then given by

$$\frac{\partial n}{\partial t} = -\nu \frac{1 + \frac{g}{\beta_g}}{1 + \frac{c}{\beta_c}} n + \frac{c}{1+g} + D_n \nabla^2 n - \theta_n \nabla \cdot (n \nabla c), \tag{3.7}$$

$$\frac{\partial a}{\partial t} = \nu \frac{1 + \frac{g}{\beta_g}}{1 + \frac{c}{\beta_c}} n - \gamma_a a - \phi m a, \tag{3.8}$$

$$\frac{\partial m}{\partial t} = c - \gamma_m m + D_m \nabla^2 m - \theta_m \nabla \cdot (m \nabla c), \tag{3.9}$$

$$\frac{\partial c}{\partial t} = \alpha f + \gamma_a \frac{a^2}{\beta_a^2 + a^2} + k_n \frac{n^2}{\beta_n^2 + n^2} - c + D_c \nabla^2 c, \tag{3.10}$$

$$\frac{\partial g}{\partial t} = k_g \phi m a - \gamma_g g + D_g \nabla^2 g \quad . \tag{3.11}$$

The above described system retains the periodic boundary conditions while the zero initial conditions (2.18) provided for the model of Chapter 2 will later be updated and presented throughout this chapter such as to include initial damage, as discussed in Section 3.8.

From here on we will first proceed with a section investigating spatially-independent simulations driven by the damage function f in (3.10). The computational implementation of (3.7)–(3.11) for this first set of simulations will thus be analogous to the one presented in Section 2.3.1. We then analyse the homogeneous steady states that

Parameter	Approximate Range	Standard values used in simulations in this chapter
ν	$0.001 - 0.6925$	0.1
γ_a	$0.55 - 1$	1
γ_m	$10^{-2} - 1.2375 \cdot 10^{-2}$	0.01
ϕ	$0.001 - 1.38$	0.1
β_a	$0.01 - 0.1$	0.1
D_n	$10^{-5} - 10^{-3}$	10^{-5}
D_m	$10^{-6} - 10^{-3}$	10^{-6}
D_c	$10^{-4} - 10^{-3}$	10^{-4}
$\mathbf{k_n}$	$1.9 \cdot 10^{-3} - 4 \cdot 10^{-2}$	0.01
$\boldsymbol{\beta_n}$	0.1	0.1
$\boldsymbol{\beta_g}$	$8.33 \cdot 10^{-6} - 10^{-2}$	10^{-2}
$\boldsymbol{\beta_c}$	0.12	0.12
$\mathbf{k_g}$	$0.1 - 0.7128$	0.1
$\boldsymbol{\gamma_g}$	$1 - 2.25$	1
$\mathbf{D_g}$	$10^{-4} - 10^{-3}$	10^{-4}
$\boldsymbol{\theta_n}$	$10^{-6} - 10^{-4}$	10^{-5}
$\boldsymbol{\theta_m}$	$10^{-6} - 10^{-4}$	10^{-6}

Table 3.2: Dimensionless parameter values appearing in the model of (3.7)–(3.11). New parameters introduced in this chapter are presented in bold.

the model admits in the absence of spatial terms, and present a bifurcation analysis to illustrate how the stability of these states depends upon model parameters. This assessment is crucial in guiding us in through a further set of simulations in which the spatial behaviour of both mediators and leukocytes is evaluated thoroughly. Furthermore, the implementation and simulation of a two-dimensional version of (3.7)–(3.11) is anticipated by the introduction of a more robust numerical method that takes into account the challenges posed by working with the chemotactic terms on a range of parameter values. The following two-dimensional simulations, presented in Section 3.8 will thus be implemented according to the newly defined numerical approach. Finally the results will be analysed and commented and conclusions to the chapter provided.

3.5 Spatially-independent simulations

The model described in (3.7)–(3.11) presents added complexity, particularly in terms of neutrophil apoptosis and inflammatory mediator interactions. We here aim to draw comparisons with the model analysed in Chapter 2. In order to properly analyse the newly introduced terms and assess how they affect the system, we first present simulations in which all diffusion and chemotaxis terms are omitted and different values of critical parameters are tested. In this preliminary spatially-independent analysis the damage function (2.5) is retained, and the initial conditions of (2.18) are extended to include the new anti-inflammatory mediators such that:

$$n(0) = a(0) = m(0) = c(0) = g(0) = 0. \tag{3.12}$$

Firstly, it is of interest to evaluate how damage duration and possible repetition affects the inflammatory outcome. In fact, with nominal values for the parameters, it is expected from Chapter 2 that upon one single cycle of damage the inflammation would resolve naturally, while the system would not be able to recover when under repeated or continuous damage. However, this is not completely true, as is evident from

the results of Figures 3.2 and 3.3, which both show a similar pattern of a persistent inflamed state, regardless of the damage duration. A key point of comparison here with respect to the model of Chapter 2 is that the introduction of pro-inflammatory mediator production by active neutrophils (with parameter k_n) results in a previously healthy outcome (as shown in Figure 2.2) becoming chronic, as shown in Figure 3.2, with both systems being under one cycle of damage only. This is because of the addition into the extended model of k_n, whose inclusion causes a change of behaviour and an immediate impact upon the system, with Figure 3.2 confirming that the additional pro-inflammatory mediators provided by active neutrophils can be sufficient to prevent resolution. Similarly to the results of Figure 2.3, variables also reach a chronic steady state following four cycles of damage, as shown in Figure 3.3.

In order to better understand the model's behaviour, different parameter values are tested, indicating how some of these parameters are actually key to the progression and evolution of inflammation. In particular, the simulations in Figure 3.4 show how the tuning of parameters ϕ and k_g regulates the oscillatory behaviour of the system. Thus, for sensitive values of ϕ and k_g, the introduction of the anti-inflammatory mediator g provides a negative feedback loop that results in oscillations that are not found in the model of Chapter 2. By further analysing (3.7)-(3.11), new simulations highlight that the rate of mediator production due to active neutrophils (k_n) also impacts on the inflammation's outcome. In this regard, for a smaller choice of k_n ($k_n = 1.9 \cdot 10^{-2}$), the inflammatory outcome is dependent on the duration of the damage; a healthy state is recovered upon a single cycle of damage, while there is no resolution for consecutive damaging events. Therefore, for smaller values of k_n the results of Chapter 2 are recovered, with figures here omitted for brevity.

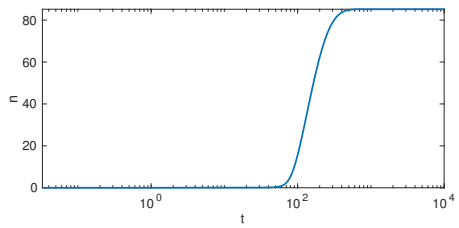

(a) Active neutrophils.

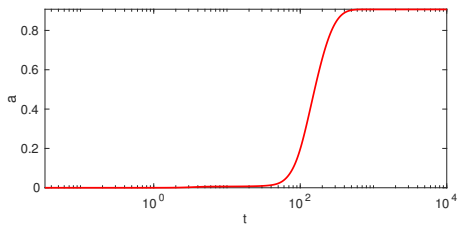

(b) Apoptotic neutrophils.

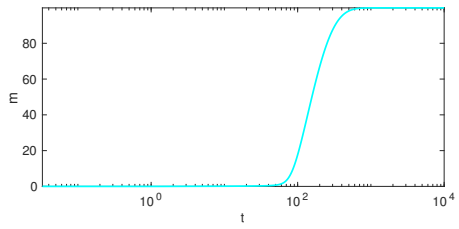

(c) Macrophages.

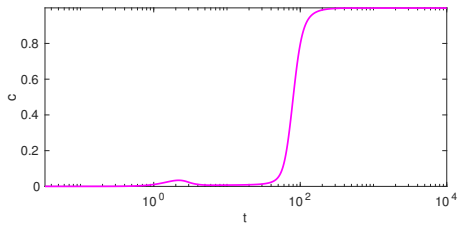

(d) Pro-inflammatory mediators.

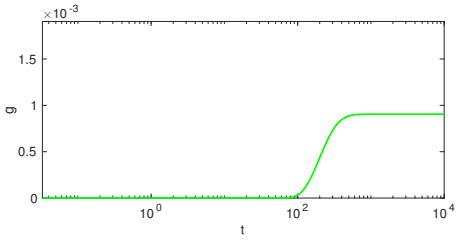

(e) Anti-inflammatory mediators.

Figure 3.2: Solution of (3.7)–(3.12) in the absence of spatial terms, with one damage cycle applied ($A = 1$). All parameters values are as given in Table 3.2.

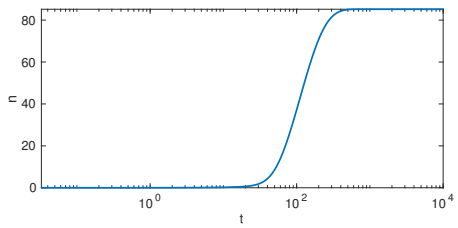

(a) Active neutrophils.

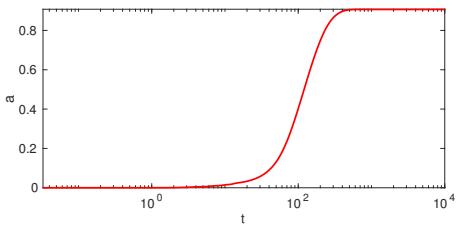

(b) Apoptotic neutrophils.

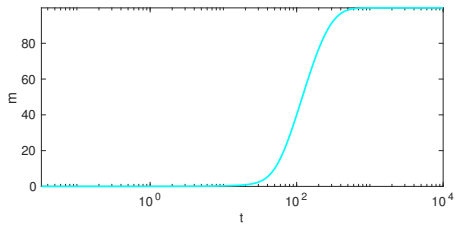

(c) Macrophages.

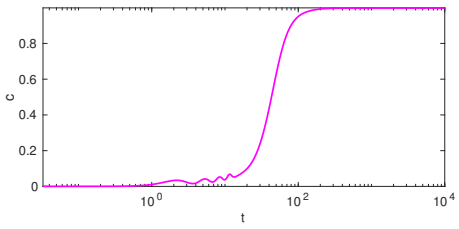

(d) Pro-inflammatory mediators.

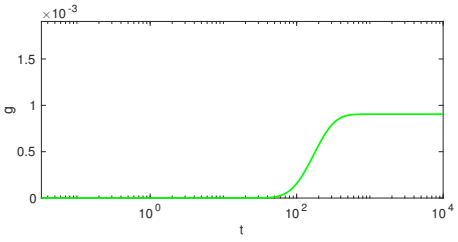

(e) Anti-inflammatory mediators.

Figure 3.3: Solution of (3.7)–(3.12), in the absence of spatial terms, with four damage cycles applied ($A = 4$). All parameters values are as given in Table 3.2.

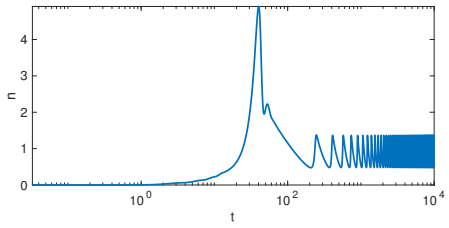

(a) Active neutrophils.

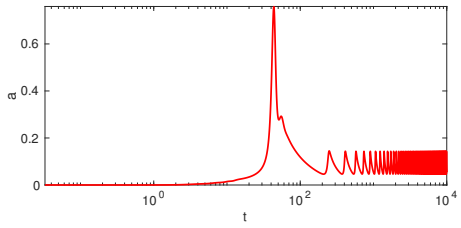

(b) Apoptotic neutrophils.

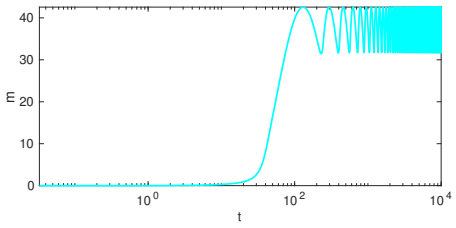

(c) Macrophages.

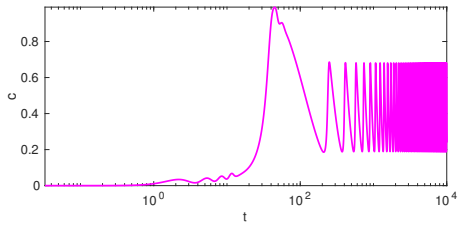

(d) Pro-inflammatory mediators.

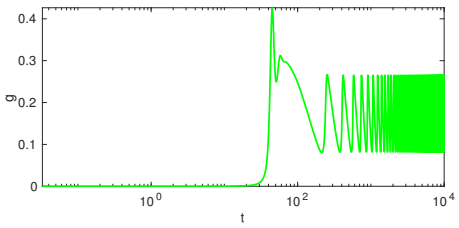

(e) Anti-inflammatory mediators.

Figure 3.4: Solution of (3.7)–(3.12), in the absence of spatial terms, with four damage cycles applied (A=4), for $\phi = 0.08$ and $k_g = 0.65$, and all remaining parameters as given in Table 3.2. For these parameter values, the model exhibits sustained oscillatory behaviour.

3.6 Analysis of homogeneous solutions

We examine how the nature of the homogeneous steady states in (3.7)–(3.11) depends upon choices of key parameters. We analyse a subset of the model's parameters, including a focus on the newly introduced ones. In particular, from the parameters already featuring in Chapter 2, we retain here the stability analysis for the key parameters ϕ and ν and extend it to include the newly introduced anti-inflammatory parameters k_n and k_g, while neglecting the bifurcation diagrams for the remaining ones, already analysed in 2.4.2. It is important to consider how the bifurcation analysis explains the stability of the solutions of the associated ODE system. As exposed in Section 3.5, the system can either exhibit bistability (with healthy or chronic steady states), be excitable (with sustainable oscillations) or monostable (with the healthy steady state the only possible homogeneous outcome). Key parameters directly affect the stability of the system's fixed points.

In the following sections, we present bifurcation diagrams in terms of ν, ϕ, k_n and k_g in turn, holding all other parameters fixed at the values in Table 3.2.

3.6.1 Varying rates of neutrophil apoptotis and macrophage phagocytosis

In Figure 3.5 we show bifurcation diagrams that plot the coordinate of the steady-state pro-inflammatory mediator concentrations, c, as functions of (a) ϕ and (b) ν. Solid black curves illustrate stable steady states, dashed black curves illustrate unstable steady states, and red curves illustrate the amplitudes of stable oscillations. In Figure 3.5a, for $\nu = 0.1$, a supercritical Hopf bifurcation occurs at $\phi = \phi_{HB} \simeq 0.09$. In 3.5b, for $\phi = 0.1$, this same supercritical Hopf bifurcation occurs at $\nu = \nu_{HB} \simeq 0.07$. For values of ϕ or ν that lie to the left of the Hopf bifurcation in either of

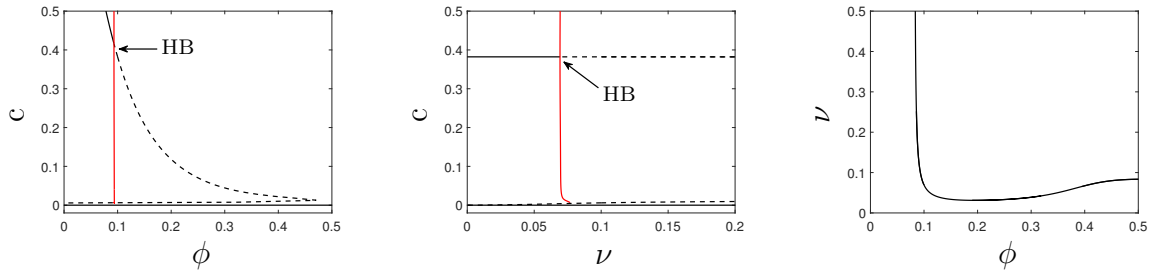

(a) (b) (c)

Figure 3.5: Bifurcation diagrams for parameters ν and ϕ representing the rates at which active neutrophils undergo apoptosis and are phagocytosed by macrophages, respectively, as appearing in system (3.7)–(3.11), with respect to pro-inflammatory mediators (a,b) and combined (c). All other parameters values are set as in Table 3.2. Stable/unstable steady states are plotted in solid/dashed respectively, with stable oscillations indicated in red.

these figures, the system is bistable, since both healthy and chronic steady states are stable; the magnitude of the initial damage acts as a switch between these two configurations. For values of ϕ or ν that lie to the right of the Hopf bifurcation, the chronic steady state is unstable and the only permissible homogeneous configuration is one of complete resolution of damage. In Figure 3.5c, we show the coordinates of the Hopf bifurcation in (ϕ, ν)–space. For parameter values below the illustrated curve, the system is bistable; for parameter values above this curve, the system is monostable since the chronic steady state is unstable.

3.6.2 Varying the neutrophil feedback rate

The model of (3.7)– (3.11) incorporates a positive feedback loop owing to the production of pro-inflammatory mediators by active neutrophils, the associated rate constant being denoted k_n. In Figure 3.6, we briefly examine the extent to which this positive feedback loop impacts upon potential solutions. As discussed above, the facet

of the model that is key in determining the long-term outcome is the position of the Hopf bifurcation. For parameter combinations that lie prior to the Hopf bifurcation, the model is bistable and we have the potential to obtain either healthy or chronic steady states dependent upon initial conditions; for parameter choices beyond the Hopf bifurcation, the only permissible solutions are the healthy homogeneous configuration or outcomes not captured by the associated ODE system. In Figure 3.6, we illustrate how the position of the Hopf bifurcation depends upon our choice of k_n. In Figures 3.6a–3.6b we present two-parameter bifurcation diagrams that illustrate how the ϕ– and ν–coordinates of the Hopf bifurcations evolve as k_n is varied; the non-trivial homogeneous steady state is stable for parameter combinations that lie above the illustrated curves. As k_n is increased from our baseline value of $k_n = 0.01$, there is a narrowing window of ϕ–values (for fixed ν) for which the non-trivial steady state is unstable (Figure 3.6a). As such, the enhanced pro-inflammatory mediator production by neutrophils essentially acts to enhance the stability of the non-trivial steady state, hence increasing the potential of attaining a chronic state. Holding ϕ fixed and varying k_n, the position of the Hopf bifurcation is an increasing function of ν, since the enhanced apoptosis of neutrophils acts to counter the pro-inflammatory mediator production by active neutrophils (Figure 3.6b). For the parameter values of Table 3.2, choices of $k_n \gtrsim 0.07$ result in the Hopf bifurcation being eliminated completely. Figure 3.6c illustrates the curve in (ϕ, ν)–space on which the Hopf bifurcation lies, for various choices of k_n. Below the illustrated curves, the model attains either healthy or chronic outcomes, identifying a region of bistability. Conversely, increases in k_n push the system toward the monostable region where the system's stable outcome is chronic.

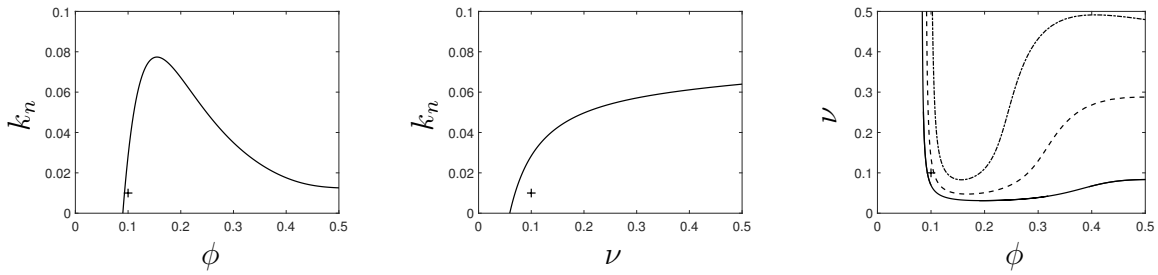

Figure 3.6: Bifurcation diagrams illustrating the effects of the neutrophil feedback parameter k_n upon locations of Hopf bifurcations as functions of (a) ϕ and (b) ν. In (a,b), the non-trivial steady state is stable for parameter combinations above the black curves. In (c) we show the position of the Hopf bifurcation in (ϕ, ν)–space for $k_n = 0.01$ (solid line), $k_n = 0.04$ (dashed line) and $k_n = 0.07$ (dash-dotted line). The non-trivial steady state is stable below the illustrated curves; the areas of parameter-space above the curves exhibit potential for inhomogeneous solutions. The cross symbols demark the baseline parameter values of Table 3.2.

3.6.3 The role of anti-inflammatory mediators

A further focus on the role of anti-inflammatory mediators is provided by Figure 3.7, in which the impact of the manipulation of the parameter k_g on the stability of homogeneous steady states is assessed. In particular, Figure 3.7a illustrates how the regions of stability vary with respect to the production of anti-inflammatory mediators k_g, with those lying below and above the curves representing bistable and monostable outcomes of the system respectively. The region of monostability grows by increasing values of k_g, with the healthy steady state being the only permissible stable steady state for a wider range of parameters in (ϕ, ν)-space. Figure 3.7b illustrates the location of the Hopf bifurcation with respect to parameters k_g and k_n, while fixing all other parameter values according to Table 3.2. Here, the region corresponding to bistability of the solutions lies above the curve with both healthy and chronic homogeneous outcomes being permissible. Below this curve, the only permissible homogeneous solution is one of uniformly resolved damage. Analogously, bifurcation analysis of the anti-inflammatory parameters γ_g and β_g shows a qualitatively similar impact on the system's stability, with the corresponding Hopf bifurcations approaching the dashed curve of Figure 3.7a (results are here omitted for brevity).

3.7 Incorporating chemotaxis: a modified numerical approach

The inclusion of chemotaxis in our model poses a non-trivial numerical challenge. The typical qualitative behaviour chemotaxis prescribes is best represented by hyperbolic PDEs (Gerisch *et al.*, 2001). Such equations, contrary to purely diffusive parabolic PDEs, can present discontinuities even with smooth initial conditions (Rozhdestvenskii, 1960), thus requiring careful numerical approaches in their approximation. Here

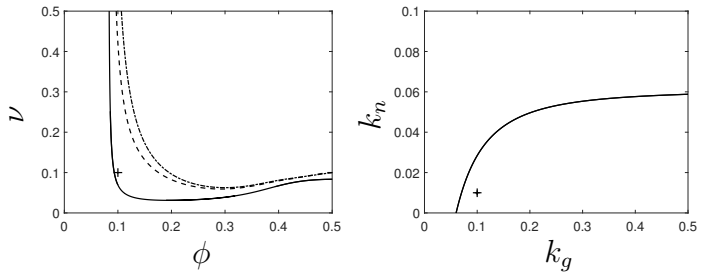

Figure 3.7: Bifurcation diagrams illustrating the role of the anti-inflammatory mediator. In (a) we show the position of the Hopf bifurcation in (ϕ, ν)–space for $k_g = 0.1$ (solid line), $k_g = 0.01$ (dashed line) and $k_g = 0$ (dash-dotted line). The non-trivial steady state is stable below the illustrated curves; the areas of parameter-space above the curves exhibit potential for inhomogeneous solutions. In (b), we illustrate the location of the Hopf bifurcation in (k_g, k_n)–space. The cross symbols demark the baseline parameter values of Table 3.2.

we introduce an effective numerical method that is specifically structured to tackle the shortcomings that traditional finite difference methods face in order to provide a robust approximation of systems comprising both diffusion and chemotaxis. What follows in this section is directly taken from the methods developed and presented by Gerisch *et al.* (2001). To this end, let us consider a generic hyperbolic-parabolic system of the form:

$$\frac{\partial u}{\partial t} = -\nabla \cdot (uG(w)\nabla w) + g_1(u, w) \tag{3.13}$$

$$\frac{\partial w}{\partial t} = \nabla^2 w + g_2(u, w) \tag{3.14}$$

with $u(x, y, t)$ and $w(x, y, t)$ unknown functions defined in a unit square domain in space and for $t \in [0, t_f]$. The functions G, g_1 and g_2 generalise the relationships occurring between the quantities u and w. In order to analyse possible numerical approaches to tackling the discontinuities of (3.13)–(3.14), we supply the sys-

tem with appropriate initial conditions $u_1(x, y, 0) = u_{1_0}(x, y)$, $u_2(x, y, 0) = u_{2_0}(x, y)$ and periodic boundary conditions in order to be consistent with the inflammatory model (3.7)–(3.11). The variable u moves chemotactically up gradients of w, which in turn diffuses within the domain. Such a system represents a simplified and generic version of the interactions we are most interested in, focusing the attention on the diffusion of one variable, namely w, as per (3.14), and the chemotaxis of the other, formally defined as the convection of u by a velocity field and considering a nonlinear dependence on variable w. As such, the sign of $G(w)$ determines the direction of convection, thus reflecting the choice of a positive unitary constant for this function with respect to the inflammatory model object of this investigation. Following the analysis of Gerisch *et al.* (2001) and exploiting the parabolic-hyperbolic nature of system (3.13)–(3.14), we tailor a dual numerical approach in the approximation of these PDEs such that the hyperbolic and parabolic terms are decoupled and treated separately, through explicit methods for the former and implicit ones for the latter. Furthermore, we impose an additional constraint limiting the admissible solutions to non-negative ones only. This is motivated by the biological nature of our problem that refers particularly to concentrations of cells and chemicals within the inflamed tissue, thus representing necessarily positive quantities only.

By splitting equations (3.13)–(3.14), we consider solving the diffusive equation (3.14) through the numerical approach presented in Section 2.3, while for the new chemotactic interactions introduced in (3.13) we follow the *flux-limited* second order approximation proposed in Gerisch *et al.* (2001). By denoting with $i, j = 1, \ldots, N$ the meshpoints x_i and y_j respectively, $u_{i,j}$ and $w_{i,j}$ represent approximations of $u(x_i, y_j, t)$ and $w(x_i, y_j, t)$ respectively. In the analysis of Gerisch *et al.* (2001), (3.13) is dealt with using flux limiters or numerical flux functions, that is functions conveyed in a form as to prevent converging to non-solutions (LeVeque, 1999). We now restrict our analysis to the x-dimension only, for the sake of clarity in the following notation,

with the extension to the second dimension being straightforward. In particular, by conveniently renaming $v(x, y, t) = G(w)\nabla w$, (3.13) can be rewritten in terms of the convection of the quantity u by the velocity field v, that is

$$\frac{\partial u}{\partial t} = -[v(x, y, t)u(x, y, t)]_x \tag{3.15}$$

having preserved periodic boundary conditions for the newly introduced variable $v(x, y, t)$, neglected the additional function $g_1(u, w)$ and assuming a unitary constant value for the term $G(w)$. Following Gerisch *et al.* (2001), we define the semi-discrete flux function as

$$f_{i,j}(t) = v(x_i, y_j, t)u_{i,j}(t)\,. \tag{3.16}$$

By denoting with $F_{i+1/2,j}$ the approximation of the flux function (3.16), in compliance with the constraint of allowing positive solutions only, the general flux function for positive velocity fields is given by

$$F_{i+1/2,j} = f_{i,j} + \frac{1}{2}\Phi(r_{i+1/2,j})(f_{i,j} - f_{i-1,j})\,, \tag{3.17}$$

while, conversely, for negative velocities, we refer instead to

$$F_{i+1/2,j} = f_{i+1,j} + \frac{1}{2}\Phi(r^{-1}_{i+3/2,j})(f_{i+1,j} - f_{i+2,j})\,. \tag{3.18}$$

The general flux functions (3.17) and (3.18) are defined with respect to the ratio r, which regulates the flux's smoothness and is given by

$$r_{i+1/2,j} = \frac{f_{i+1,j} - f_{i,j}}{f_{i,j} - f_{i-1,j}}\,. \tag{3.19}$$

As for the flux limiter Φ, Sweby (1984) presents a comprehensive class of limiters, by analysing both theoretical and numerical features. Among these, Gerisch *et al.* (2001) select and propose the Van Leer flux limiter (Van Leer, 1974), carefully chosen as to be Lipschitz continuous, continuously differentiable for all $r \neq 0$ and preserving the positivity of the solutions:

$$\Phi(r) = \frac{|r| + r}{1 + |r|}\,. \tag{3.20}$$

Thus, the discretisation of (3.15) in the form

$$\frac{\mathrm{d}u_{i,j}(t)}{\mathrm{d}t} = -\frac{1}{h}(F_{i+1/2,j} - F_{i-1/2,j}) \tag{3.21}$$

yields a forward/backward scheme depending on the sign of the velocity field through the approximations

$$\frac{\mathrm{d}u_{i,j}(t)}{\mathrm{d}t} = -\frac{1}{h}\left[\left(1 + \frac{1}{2\Phi(r_{i+1/2,j})}\right) - \frac{\Phi(r_{i-1/2,j})}{2r_{i-1/2,j}}\right](f_{i-1,j} - f_{i,j}) \tag{3.22}$$

and

$$\frac{\mathrm{d}u_{i,j}(t)}{\mathrm{d}t} = -\frac{1}{h}\left[\left(1 + \frac{1}{2\Phi(r^{-1}_{i+1/2,j})}\right) - \frac{\Phi(r^{-1}_{i+3/2,j})}{2r^{-1}_{i+3/2,j}}\right](f_{i+1,j} - f_{i,j}) \tag{3.23}$$

respectively.

With the discretising scheme for convecting equations provided in (3.22)–(3.23), the mixed hyperbolic-parabolic system (3.13)–(3.14) is rewritten here in vector form as

$$\frac{\partial}{\partial t}\begin{pmatrix} u \\ w \end{pmatrix} = \underbrace{\begin{pmatrix} -\nabla\cdot(uG(w\nabla w)) \\ 0 \end{pmatrix}}_{\mathbf{f_1}} + \underbrace{\begin{pmatrix} g_1(u,w) \\ \nabla^2 w + g_2(u,w) \end{pmatrix}}_{\mathbf{f_2}}; \tag{3.24}$$

that is

$$\frac{\partial \mathbf{u}}{\partial t} = \mathbf{f_1} + \mathbf{f_2}\,. \tag{3.25}$$

Such a representation allows us to distinguish the purely convective contribution of $\mathbf{f_1}$ to the system in contrast to its reactive-diffusive stiff part, given by $\mathbf{f_2}$. In particular, (3.25) poses contrasting challenges in its resolution, with $\mathbf{f_1}$ best dealt with via explicit methods allowing for restrictions on the time-step to preserve positivity of the approximations, while $\mathbf{f_2}$ requires an implicit approach due to stability and stiffness concerns. As such, instead of approximating (3.25) with a global numerical approach, a splitting method is employed, by dealing with $\mathbf{f_1}$ and $\mathbf{f_2}$ separately, in the form of:

$$\mathbf{u}(t_k + \tau) = \mathbf{u_k} + \int_{t_k}^{t_k+\tau} [\mathbf{f_1}(\mathbf{u}(t)) + \mathbf{f_2}(\mathbf{u}(t))]\,\mathrm{d}t$$

$$= \mathbf{u_k} + \int_{t_k}^{t_k+\frac{\tau}{2}} \mathbf{f_1}(\mathbf{u}(t))\,\mathrm{d}t + \int_{t_k}^{t_k+\tau} \mathbf{f_2}(\mathbf{u}(t))\,\mathrm{d}t + \int_{t_k+\frac{\tau}{2}}^{t_k+\tau} \mathbf{f_1}(\mathbf{u}(t))\,\mathrm{d}t\,. \quad (3.26)$$

Thus, at each time step, vectors $\mathbf{f_1}$ and $\mathbf{f_2}$ are approximated separately, through explicit methods the former (Runge Kutta 4 in the implementation of our code) and implicit ones the latter (through Matlab's builtin solver `ode15s`). The numerical scheme proposed in (3.26) guides the approximation of $\mathbf{u}(t_k+\tau)$ through intermediate steps consisting of

- $\mathbf{z_1}'(t) = \mathbf{f_1}(\mathbf{z_1}(t))$, with initial condition $\mathbf{z_1}(\mathbf{t_k}) = \mathbf{u_k}$, approximating $\mathbf{z_1}(t_k+\tau/2)$;
- $\mathbf{z_2}'(t) = \mathbf{f_2}(\mathbf{z_2}(\mathbf{t}))$, with initial condition $\mathbf{z_2}(t_k) = \mathbf{z_1}(t_k+\tau/2)$, approximating $\mathbf{z_2}(t_k+\tau)$;
- $\mathbf{z_3}'(t) = \mathbf{f_1}(\mathbf{z_3}(t))$, with initial condition $\mathbf{z_3}(t_k+\tau/2) = \mathbf{z_2}(t_k+\tau)$, approximating $\mathbf{z_3}(t_k+\tau)$.

The stability and positivity of this Implicit-Explicit (IMEX) scheme is guaranteed as detailed in Gerisch *et al.* (2001). Furthermore, particular attention is dedicated to the time-step size: a fixed time step is avoided in favour of a variable one, allowing us to keep its size large enough to be computationally effective and efficient while also maintaining it small enough to prevent numerical errors and stability issues. In practice, this is implemented by selecting time-step sizes for which the approximation's local error is within a fixed tolerance and considering an adaptive time-step τ_k controlling the step size $t_{k+1} = t_k + \tau_k$, with $t_0 = 0$ and $k = 0, 1, \ldots$. Approximations of $\mathbf{u}(t_k+\tau_k)$ providing solutions to the splitting scheme (3.26) are computed with a time-step τ_k, resulting in $\mathbf{u}_{\boldsymbol{\tau_k}}$, and two time-steps $\frac{\tau_k}{2}$ generating $\mathbf{u}_{\mathbf{2}\times\frac{\boldsymbol{\tau_k}}{\mathbf{2}}}$. The size of time-step τ_k is then evaluated against a scaled error measure ρ defined as

$$\rho = \frac{1}{2^n-1}\sqrt{\frac{1}{m}\sum_{i=1}^{m}\left(\frac{(\mathbf{u}_{\mathbf{2}\times\frac{\boldsymbol{\tau_k}}{\mathbf{2}}})_i - (\mathbf{u}_{\boldsymbol{\tau_k}})_i}{\mathrm{atol}_i + \mathrm{rtol}_i\,|(\mathbf{u_k})_i|}\right)^2}\,, \quad (3.27)$$

with n being the order of the ODE solver, m the dimension of the ODE system (3.25), and `atol` and `rtol` being tolerances for the absolute and relative errors, respectively. If $\rho \leqslant 1$, the new step-size $\tau_{k_{new}}$, computed as

$$\tau_{k_{new}} = \tau_k \cdot \min\{2, \max\{0.8\rho^{-\frac{1}{2^n-1}}, 0.25\}\} \tag{3.28}$$

is accepted and $\mathbf{u_{k+1}} = \mathbf{u_{2\times\frac{\tau_k}{2}}}$ is identified as the more accurate n^{th} order approximation. Otherwise, if $\rho > 1$, the step-size is rejected and recomputed accordingly. Matlab code for this model is available online via Github[1].

3.8 Two-dimensional simulations

Considering the interactions of cells and chemicals in a two-dimensional spatial domain allows for a better representation of a generic tissue. The introduction of a second spatial dimension does not change the formal representation of the system, with the corresponding two-dimensional model still defined by equations (3.7)–(3.11), but by explicitly defining the two independent dimensions x and y, each variable's dynamics is now analysed in terms of N^2 mesh points, namely $n(x_i, y_j, t)$, $a(x_i, y_j, t)$, $m(x_i, y_j, t)$, $c(x_i, y_j, t)$ and $g(x_i, y_j, t)$ with $i, j = 0, 1, \ldots, N$. With reference to (3.7)–(3.11), the damage function f is neglected in favour of a set of two-dimensional initial conditions that trigger the dynamics.

The full integration of chemotaxis into the model (3.7)–(3.11), along with the fundamental biological implications discussed in Section 1.2, directly impacts the implementation of our system, requiring the careful numerics introduced in Section 3.7. The validity of this more refined numerical approach, as already presented in Gerisch *et al.* (2001), is further tested and confirmed by multiple simulations run using initial conditions that are independent of one spatial coordinate, with the results then being

[1] `https://github.com/atihana/inflammation_pde`

compared to equivalent $1D$ simulations. These simulations confirmed the validity of the two-dimensional code, with further details of this analysis omitted here for brevity.

Various initial conditions and parameter values have been tested to evaluate the overall behaviour of (3.7)–(3.11) and assess its response towards different stimuli. Initial values have been inferred from steady state values associated with the homogeneous form of the model (3.7)–(3.11). While it is not possible to analytically solve the corresponding system of equations, explicit steady state values different than the trivial $ss1 = (0, 0, 0, 0, 0)$ were derived by the numerical solution provided by Matlab inbuilt function `fsolve` and are here indicated as the set of points $ss2 = (\bar{n}, \bar{a}, \bar{m}, \bar{c}, \bar{g})$. The set of values $ss1$ and $ss2$ are then used to configure different sets of initial conditions. The model's assessment thus allows us to analyse how both diffusion and chemotaxis affect the system behaviour, with a particular interest to a possible emergence of spatial patterns. The results presented in this section account for simulations run with initial conditions considering variable-dependent damages shaped as a circular area of uniform damage of radius $r = 0.25$ and height $(\bar{n}, \bar{a}, \bar{m}, \bar{c}, \bar{g})$ (corresponding to the values from the set of points $ss2$) centred in a unit-square domain, as specified here below:

$$(n, a, m, c, g) = (\bar{n}, \bar{a}, \bar{m}, \bar{c}, \bar{g}), \qquad \text{for } (x - 1/2)^2 + (y - 1/2)^2 \leqslant 1/4^2 \tag{3.29}$$

$$(n, a, m, c, g) = (0, 0, 0, 0, 0), \qquad \text{for } (x - 1/2)^2 + (y - 1/2)^2 > 1/4^2. \tag{3.30}$$

A first representation of two-dimensional results is provided in Figure 3.8 in which active neutrophils' spatial behaviour at four specific time steps is shown. Active neutrophils are initially concentrated in the middle of the two-dimensional domain, as to model the occurred insult triggering the inflammatory response (Figure 3.8a). During intermediate times the spatial distributions of active neutrophils continuously evolves, as is evident from Figure 3.8b–3.8d, with prolonged simulations also showing

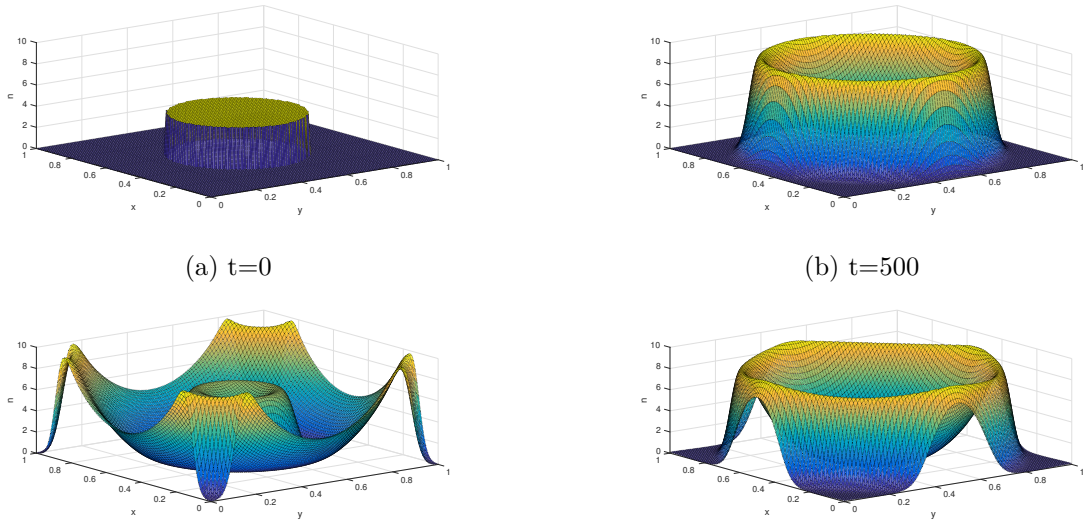

(a) t=0

(b) t=500

(c) t=1000

(d) t=1600

Figure 3.8: Solution of the two-dimensional system (3.7)–(3.11) with respect to variable n. All parameters are as in Table 3.2; initial conditions are as in (3.29).

that the system undergoes sustained spatially inhomogeneous oscillations.

A variety of parameter combinations have been tested and assessed, with particular attention also to diffusion and chemotaxis constant values. The preliminary detailed analysis of the corresponding $1D$ model and new extensive assessment of parameter values of the full two-dimensional system allowed to recognise fixed nominal values for a group of parameters, while evaluating the model's behaviour in response to variations of the remaining key parameters, as illustrated in the following sections.

3.8.1 Effects of non-spatial parameters

Firstly, the system's ability to support spatially inhomogeneous oscillations upon sensitive ranges of its spatial parameters is tested and evaluated against two key non-spatial parameters, the phagocytosis rate ϕ and the apoptosis rate ν. The bifurcation diagrams in Figure 3.5 exhibit how sensitive the system is to variations of

non-spatial parameters ν and ϕ in particular. The choice of specifically focusing on the two parameters ϕ and ν, accounting for the phagocytosis and apoptosis rates respectively, is driven by the direct biological relevance of such features in the inflammatory dynamics, while also being central in the analysis of Dunster *et al.* (2014) in their corresponding ODE model.

As a convenient representation of the two-dimensional system's dynamics, a set of plots exhibiting both the cross-sectional concentrations in time and snapshots of the spatial profiles at specific times are shown in the context of the variation of our identified key parameters, *i.e.* ν and ϕ, rates of apoptosis and phagocytosis, respectively.

In the results presented in Figures 3.9–3.11 it is of particular interest to observe how the system is susceptible to the key parameter ν accounting for the apoptosis rate and how diffusion regulates spatial behaviour. The long-term outcome in Figure 3.9 (in which $\nu = 0.1$) corresponds to a spatially homogeneous steady state at zero, or in biological terms to the resolution of inflammation throughout the tissue. With reference to the bifurcation diagram in Figure 3.5b, we see that, for $\nu = 0.1$, the non-trivial (chronic) steady state is unstable and in this case the model attains the stable, healthy steady state.

In Figure 3.10, we plot solutions corresponding to $\nu = 0.05$, and observe that, in this case, the system attains a homogeneous chronic steady state in which all variables are non-zero and the inflammatory damage persists. Comparing this with Figure 3.5b, we see that the homogeneous system is bistable when $\nu = 0.05$, which means that the system may attain either chronic or homogeneous steady states. The selection of which state is attained depends upon our choice of initial conditions. In Figure 3.11, we plot solutions for $\nu = 0.075$ – a choice of ν which lies immediately to the right of the Hopf bifurcation in Figure 3.5b, for which the chronic homogeneous steady state is unstable. In this case we observe that the system displays sustained spatially-

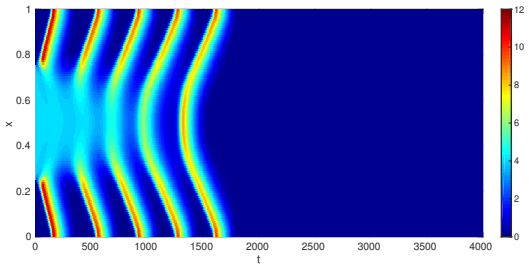

(a) Active neutrophils.

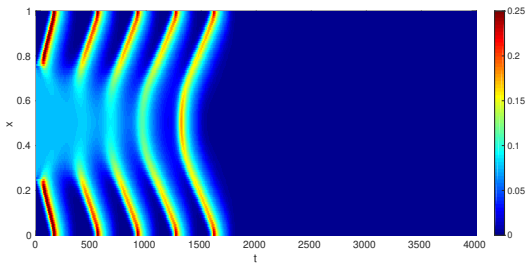

(b) Apoptotic neutrophils.

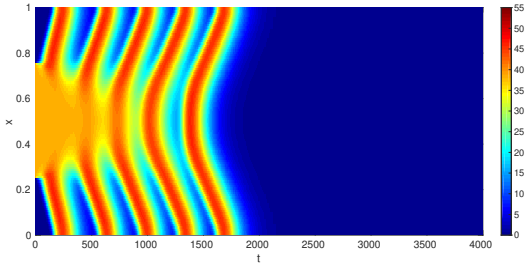

(c) Macrophages.

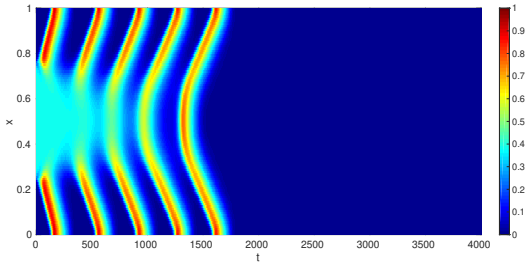

(d) Pro-inflammatory mediators.

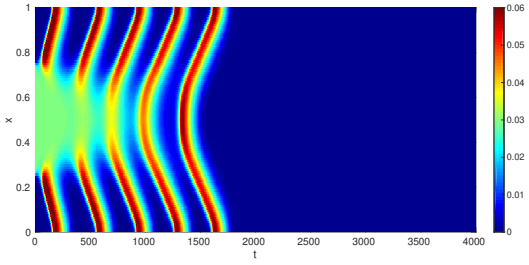

(e) Anti-inflammatory mediators.

Figure 3.9: Solution of (3.7)–(3.11) on the cross-section $y = 0$, with initial conditions as in (3.29) and all parameters as in Table 3.2. The model attains a healthy steady homogeneous steady state.

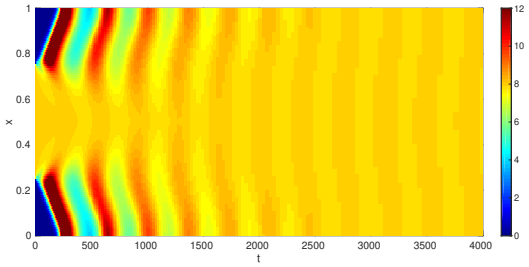

(a) Active neutrophils.

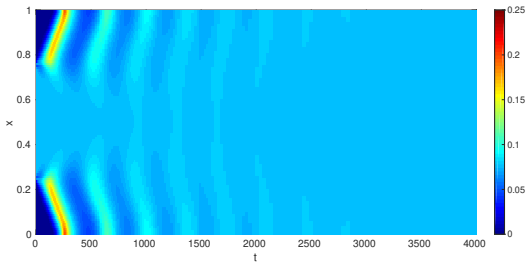

(b) Apoptotic neutrophils.

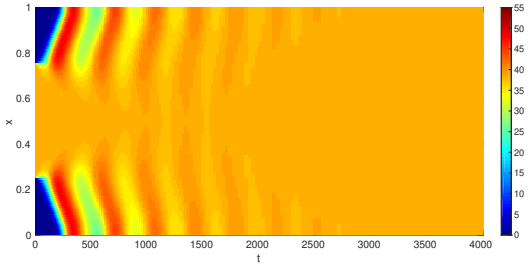

(c) Macrophages.

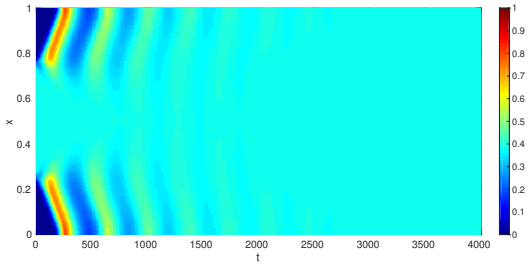

(d) Pro-inflammatory mediators.

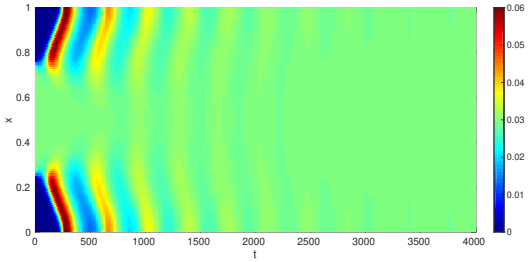

(e) Anti-inflammatory mediators.

Figure 3.10: Solution of (3.7)–(3.11) on the cross-section $y = 0$, with initial conditions as in (3.29). The rate of neutrophil apoptosis is updated to $\nu = 0.05$; all other parameters are as in Table 3.2. The model attains a homogeneous steady state that represents chronic damage.

inhomogeneous oscillations solutions which are not permissible in the corresponding ODE model or the analysis of Section 3.6. Figures 3.12 and 3.13 show snapshots of the corresponding spatial profile at $t = 100$ and $t = 2000$ respectively.

In Figure 3.14, we summarise where in (ν, ϕ)–space we find each of the broad solution types above, with the remaining parameters fixed at the values given in Table 3.2. For all choices of ν and ϕ that fall to the left (or below) the Hopf bifurcation curve (shown in black in Figure 3.14), the system converges to a stable homogeneous steady state corresponding to uniform damage (demarked by green triangles in the figure). For the majority of parameter choices that fall significantly to the right (or above) the Hopf bifurcation curve, the system ultimately progresses toward the trivial homogeneous steady state at zero, corresponding to damage being uniformly resolved (as shown by black circles in the figure). We note that in these areas of parameter space, the non-trivial homogeneous steady state is unstable, so uniform chronic damage is not a permissible configuration. However, for suitable choices of ϕ, there exists a narrow region of parameter-space immediately beyond the Hopf bifurcation in which long-term spatially inhomogeneous configurations exist. For the parameter choices represented by red squares in Figure 3.14, these configurations display oscillations temporally as well as spatially; however, spatially inhomogeneous steady states can also be permissible for some choices of parameters. We note that these spatially inhomogeneous configurations do not fall into the classical class of solutions that typically arise through Turing instabilities, given their temporally oscillating nature (in most cases), and that they do not result from changes in the stability of the homogeneous steady states in the corresponding ODE model. These results are akin to similar patterns driven by Hopf bifurcation in other models, such as that of Penner *et al.* (2012), for example. Below, we examine how variations in the choices of spatial parameters affect the spatially-dependent configurations observed here.

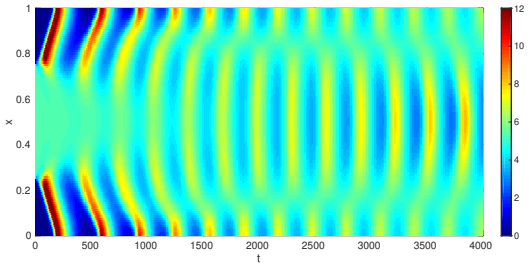

(a) Active neutrophils.

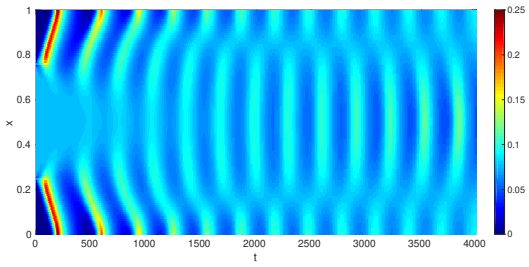

(b) Apoptotic neutrophils.

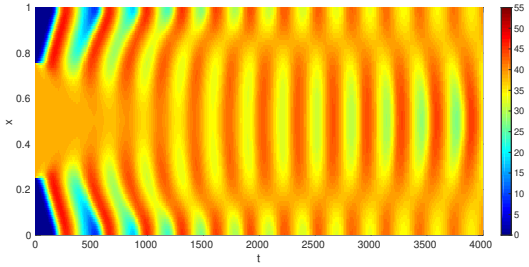

(c) Macrophages.

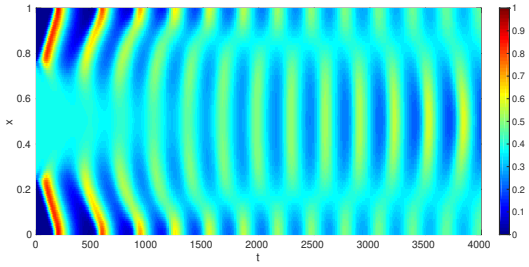

(d) Pro-inflammatory mediators.

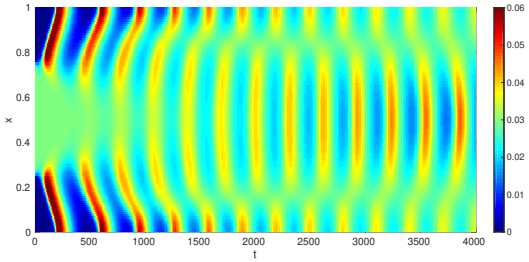

(e) Anti-inflammatory mediators.

Figure 3.11: Solution of (3.7)–(3.11) on the cross-section $y = 0$, with initial conditions as in (3.29). The rate of neutrophil apoptosis is updated to $\nu = 0.075$; all other parameters are as in Table 3.2. The model displays sustained spatially-inhomogeneous oscillations.

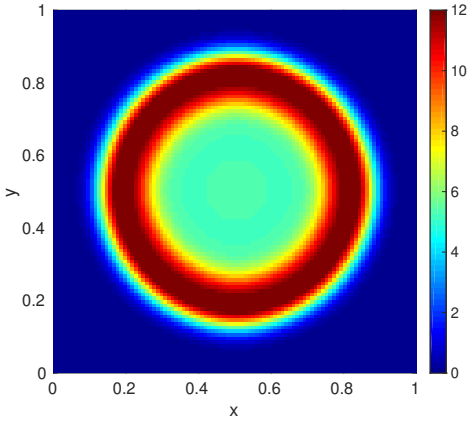

(a) Active neutrophils.

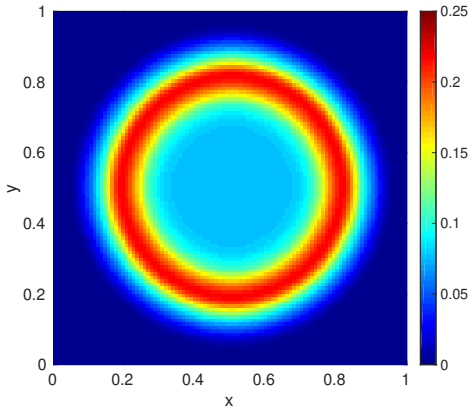

(b) Apoptotic neutrophils.

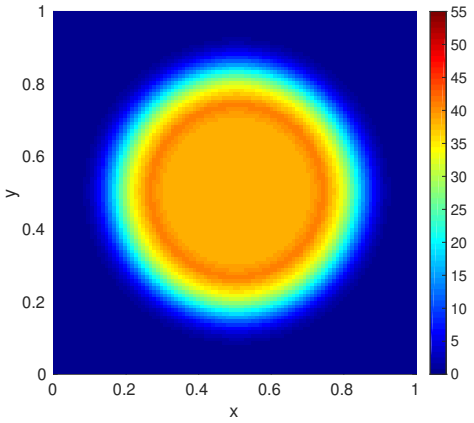

(c) Macrophages.

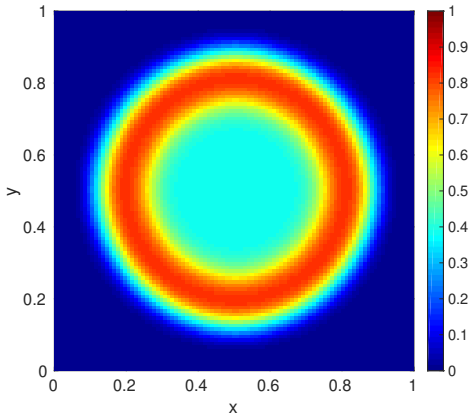

(d) Pro-inflammatory mediators.

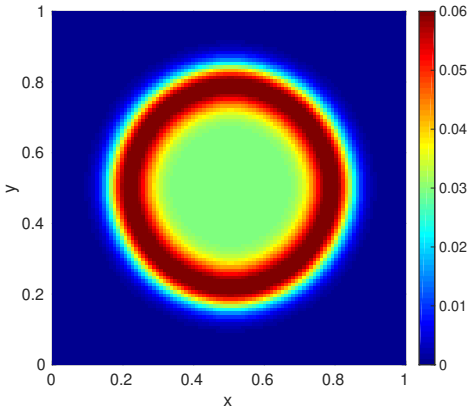

(e) Anti-inflammatory mediators.

Figure 3.12: Snapshot of the spatial profile at $t = 100$ corresponding to the solution of (3.7)–(3.11) in Figure 3.11, with initial conditions as in (3.29). The rate of neutrophil apoptosis is updated to $\nu = 0.075$; all other parameters are as in Table 3.2.

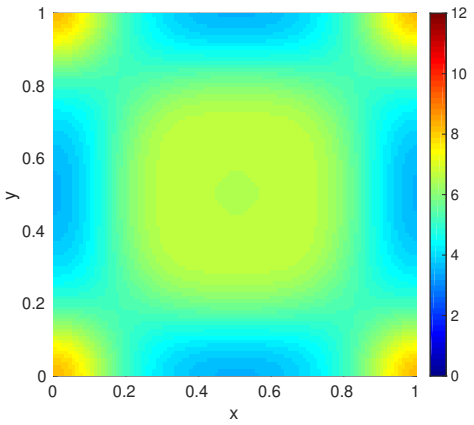

(a) Active neutrophils.

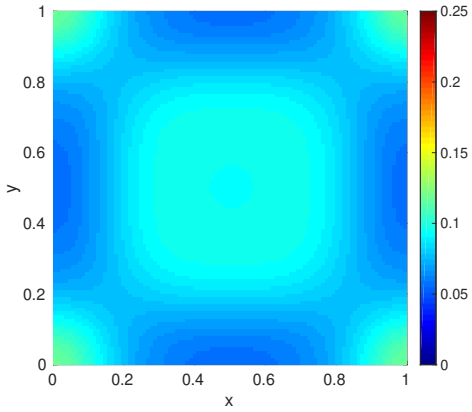

(b) Apoptotic neutrophils.

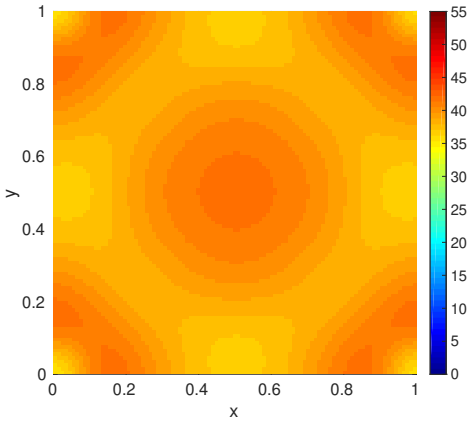

(c) Macrophages.

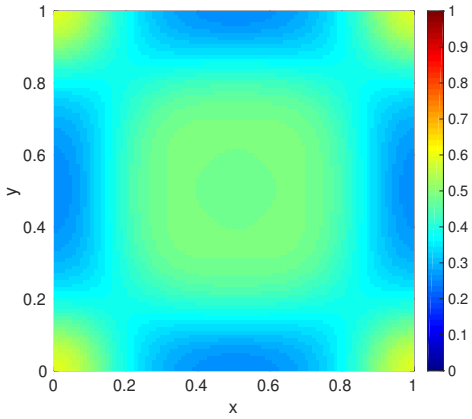

(d) Pro-inflammatory mediators.

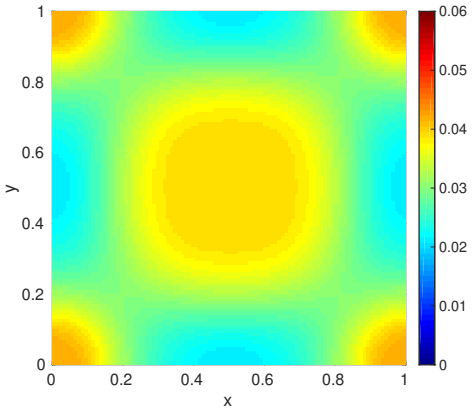

(e) Anti-inflammatory mediators.

Figure 3.13: Snapshot of the spatial profile at $t = 2000$ corresponding to the solution of (3.7)–(3.11) in Figure 3.11, with initial conditions as in (3.29). The rate of neutrophil apoptosis is updated to $\nu = 0.075$; all other parameters are as in Table 3.2.

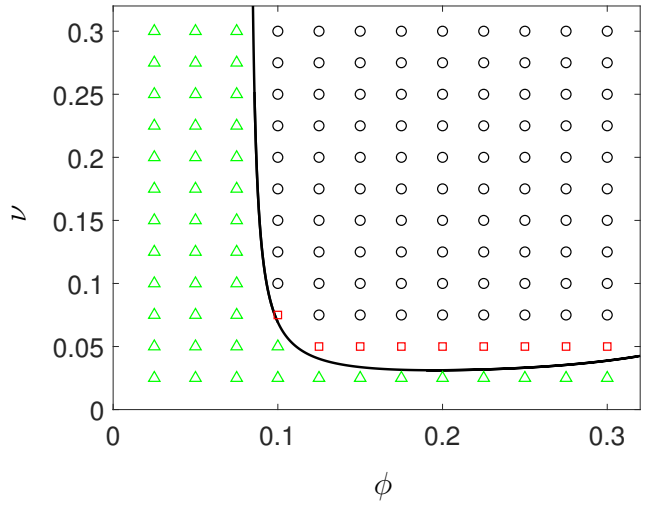

Figure 3.14: Summary of the types of solutions omitted by (3.7)–(3.7) for various choices of ν and ϕ, and all other parameter values as given in Table 3.2. Green triangles indicate that the system attains the non-trivial (chronic) homogeneous steady state given by the ODE model; red squares indicate that the model exhibits spatially inhomogeneous temporal oscillations; black circles indicate that the damage is resolved uniformly. The black curve marks the location of the Hopf bifurcation.

3.8.2 Effects of spatial parameters

The model is thoroughly evaluated with respect to its spatial parameters in order to further expose and analyse arising spatially inhomogeneous outcomes. To this end, we run an extensive set of simulations for varying values of both mediators' and cellular diffusion constants as well as chemotaxis parameters, holding all other parameters at the same values given in Table 3.2. The inflammation outcomes were shown to vary accordingly, as reported in Figure 3.15, with Figure 3.15a in particular studying conditions for patterning depending on the diffusion of chemicals. When either pro- or anti-inflammatory mediators diffuse relatively quickly, namely quicker than $D = 10^{-4}$, inflammation is homogeneously resolved, while spatially inhomogeneous oscillations are appreciable upon smaller diffusion constants. Figure 3.15b further investigates the spatial response of the model to the cellular activity, with larger populations of macrophages in particular leading the way to heterogeneous steady states and enhanced presence of neutrophils, conversely, smoothening the system to the homogeneous resolution of inflammation. Decoupling the values accounting for diffusion and chemotaxis, as in Figures 3.15c and 3.15d leads to mixed results. While either a stronger attraction of neutrophils to sources of pro-inflammatory activities or their quicker diffusivity within the tissue is enough to resolve to damage uniformly, as visible in Figure 3.15c, the same does not hold for macrophages. Figure 3.15d in fact exhibits a more complex structure of results in which larger values of macrophagic diffusion lead to spatially inhomogeneous steady states, in accordance to the results of Figure 3.15b, while a range of values for spatially inhomogeneous oscillations is also individuated.

These results are biologically of particular relevance, providing a detailed spatial characterisation of the tissue configuration upon healing times. Notably, we observe that by individuating the ranges of cellular and mediators diffusivity upon which

the system attains the spatially homogeneous trivial steady state, we determine the conditions that guarantee a global recovery and the restoration of a healthy state. This suggests that promoting the diffusivity of mediators within the tissue, as well as that of neutrophils, is key to prevent the inflammation from becoming chronic. Similarly, defects in the mediators' and cells' ability to diffuse causes the tissue to be pervaded by inflammation without eventually recovering. Another important result that emerges from the spatial analysis illustrated in Figure 3.15 is the peculiarity of the role of macrophages in the healing process. In particular, given their larger size and overall slower velocity (Barros-Becker *et al.*, 2017), to ensure a homogeneous healthy recovery, the therapeutic action on these cells in terms of diffusivity and chemotactic strength, is shown to be effective on smaller scales compared to that of neutrophils (Figure 3.15d).

3.8.3 Domain effects and dependence upon initial conditions

We, here, briefly assess the extent to which the patterns identified above are sensitive to our choice of domain. Numerical simulations conducted on a number of rectangular domains of varying aspect ratio, with $\nu = 0.075$ ($\nu > \nu_{HB}$) and all other parameters as in Table 3.2, reveal that the regions of parameter-space in which we attain uniformly resolved, uniformly damaged, or spatially inhomogeneous configurations are exactly as illustrated in Figure 3.14. (Results omitted for brevity.) However, changes in the shape of the domain can impact on the resultant patterns themselves. In Figure 3.16, we illustrate snapshots of two solutions attained on domains with y restricted to the intervals (a) $[0.15, 0.85]$ or (b) $[0.25, 0.75]$ (with $x \in [0, 1]$ as previously). Comparing these results to those attained on the square domain (Figure 3.13d), we observe that moving to a domain with a higher aspect ratio can predispose the system to striped patterns such as that shown in Figure 3.16b. Additional simulations also reveal

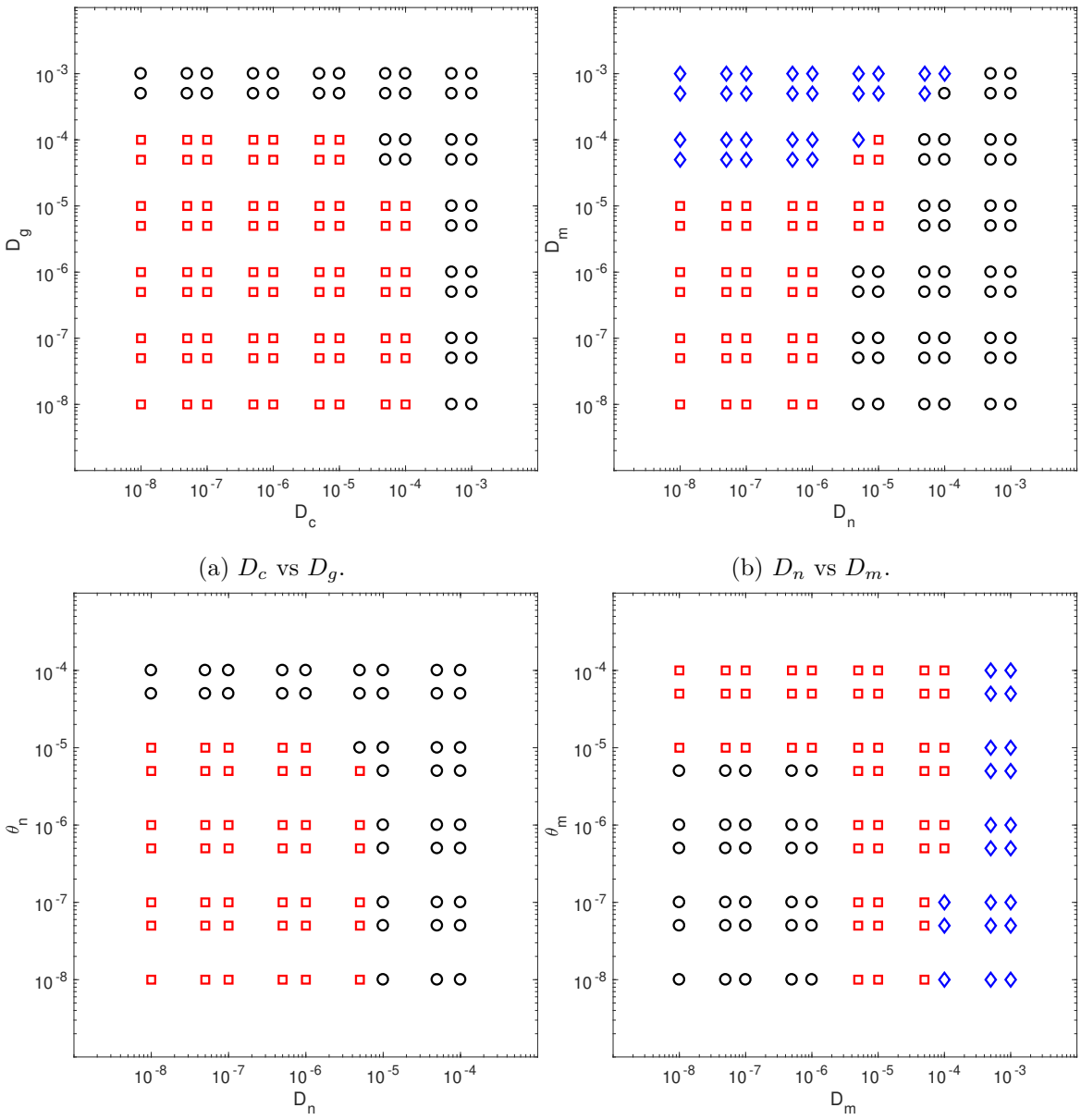

(a) D_c vs D_g.

(b) D_n vs D_m.

(c) D_n vs θ_n.

(d) D_m vs θ_m.

Figure 3.15: Tables of simulations for varying spatial parameters, all other parameters are as in Table 3.2. Red squares correspond to spatially inhomogeneous oscillations, black circles to the zero steady state, blue diamonds to spatially inhomogeneous steady states.

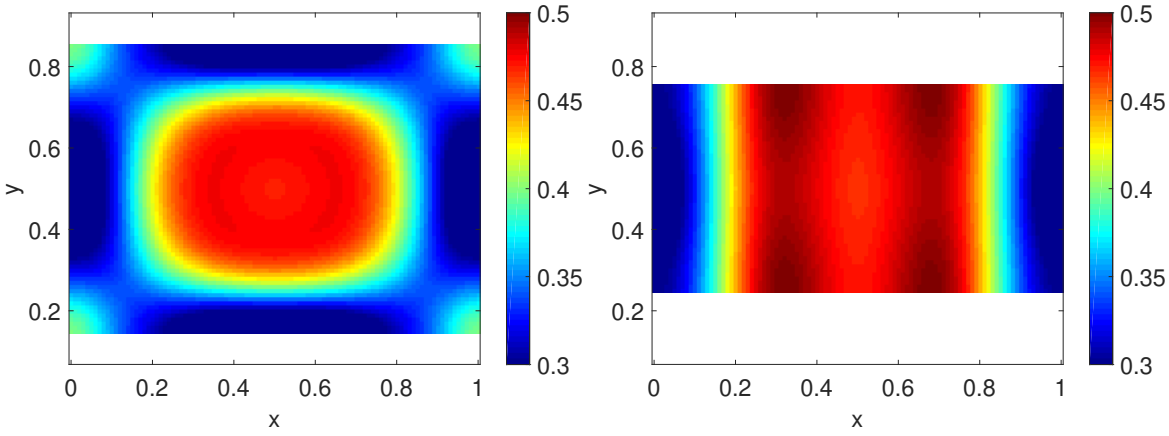

(a) (b)

Figure 3.16: Snapshots (at time $t = 2000$) of temporally oscillating, spatially inhomogeneous configurations attained on rectangular domains comprised of $x \in [0, 1]$ and (a) $y \in [0.15, 0.85]$, and (b) $y \in [0.25, 0.75]$, for $\nu = 0.075$ and all other parameter values as given in Table 3.2. Moving from a square domain (Figure 3.13d) to a narrowing rectangular domain can drive the system from spotted to striped patterns.

that replacing periodic boundary conditions by Neumann boundary conditions on all boundaries has negligible impact upon permissible patterns. (Once again, results are omitted for brevity.)

In Figure 3.17, we examine the sensitivity of patterns to the size of the area of damage imposed via the initial conditions described above. In the figure, we set $\nu = 0.075$ and $\phi = 0.1$ (a parameter choice for which we have demonstrated, in Figure 3.14, that temporally oscillating patterns are permissible), fix all other parameters at the values used given in Table 3.2, and examine results for various choices of the radius of the initially damaged area. As the figure shows, while variations in the radius of the initial damage give rise to some differences in the short term, long-term patterns are largely insensitive to the size of the initially-damaged area. Starting with uniform damage of course results in spatially homogeneous results (not shown), but since this

configuration is unstable in the ODE model, introducing even a small amount of healthy tissue is sufficient to allow the PDE system to diverge from the unstable homogeneous configuration and instead attain stable, spatially-inhomogeneous periodic orbits. Similar simulations (not plotted here for brevity) reveal that the model is also largely insensitive to changes in the magnitude of the initial damage. For example, on making all the initial conditions used above ten times larger or smaller, we attain qualitatively equivalent spatially inhomogeneous solutions in the long-term, despite some small variations in initial behaviour.

3.9 Conclusions

In this chapter the inflammation model has been further developed in order to include important features that improve upon the model of Chapter 2. Firstly, key cellular interactions have been included, by modelling the positive feedback of active neutrophils to the pro-inflammatory mediators and studying how the contribution of anti-inflammatory mediators, g, affects the system's behaviour. Chemotaxis has also been added with cells modelled to move preferentially towards higher concentrations of pro-inflammatory mediators.

The inclusion of chemotaxis, in particular, required a careful numerical approach involving flux-limited approximations and a tailored use of implicit-explicit schemes, as proposed by Gerisch *et al.* (2001) in order to ensure positivity and smoothness of solutions.

Finally, the full system (3.7)–(3.11), comprising all the main biologically relevant features of an inflammation process, has been implemented in a unit-square two-dimensional domain, with the corresponding results assessed both in terms of dynamics and spatial dependence. Guided by an existing focus in the literature upon targeting the phagocytosing ability of macrophages (ϕ) in the hunt for new thera-

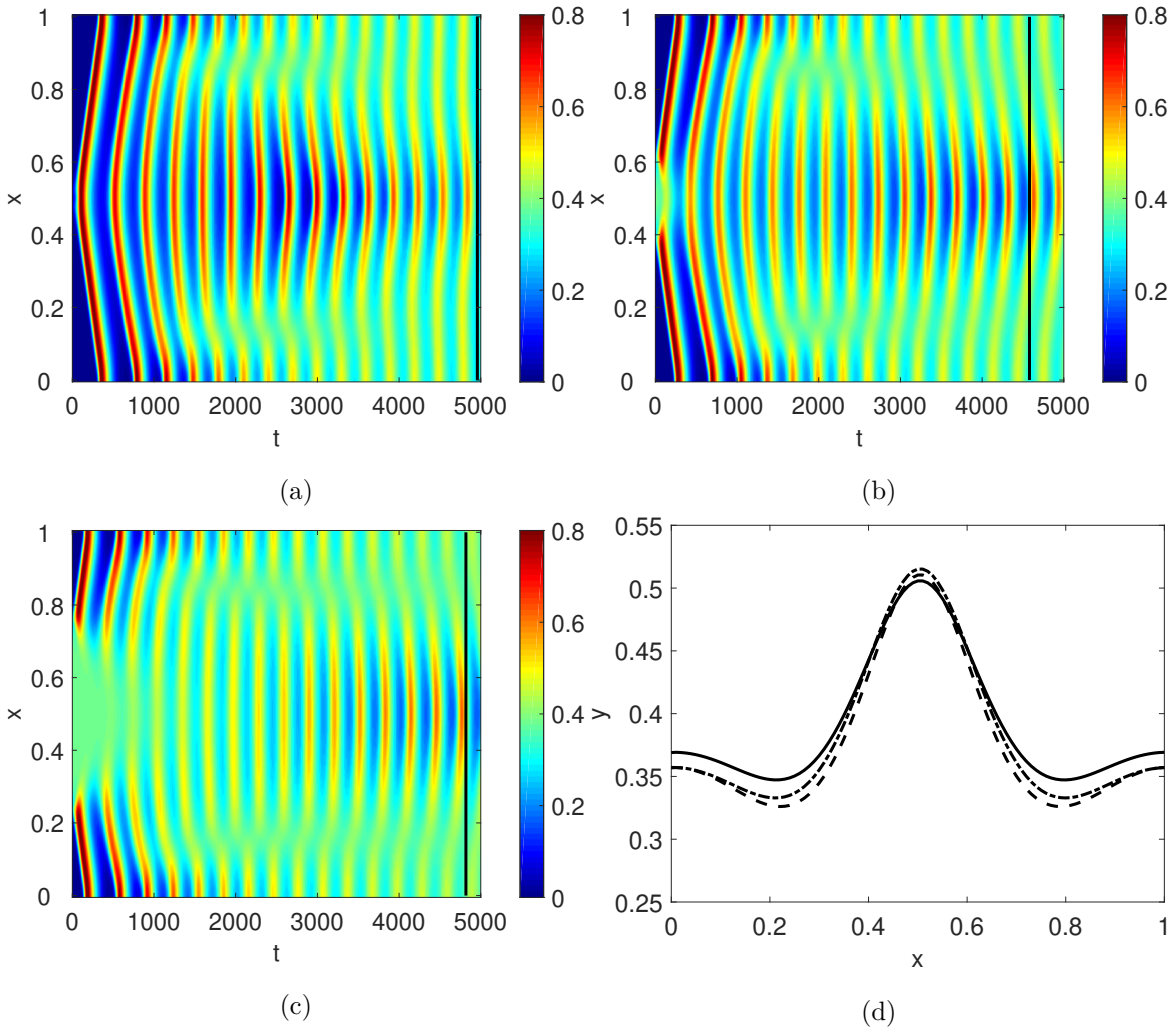

Figure 3.17: The effect of changing the radius of the initial damage upon pro-inflammatory mediator concentrations, c, for $\nu = 0.075$ and $\phi = 0.1$. In (a-c) we plot the concentrations of c on the cross-section $y = 0$ as functions of time, with initially damaged areas of radius (a) 0.01, (b) 0.1, and (c) 0.25. In (d) we plot the mediator distributions at the times demarked by the black lines in (a-c), with solid, dashed and dash-dotted lines relating to panels (a), (b) and (c) respectively. The long-term profiles are qualitatively similar for all three configurations.

peutic strategies (see *e.g.* Porcheray *et al.* (2005), Serhan (2017)), together with the fact that the analysis of Dunster *et al.* (2014) identified the neutrophil apoptosis rate (ν) as a key parameter in determining the nature of long-term outcomes, our analysis initially focused upon how variations in these two parameters can facilitate or inhibit spatially inhomogeneous outcomes. While the ODE model shows that variations in these two parameters that result in crossing the Hopf bifurcation curve in Figure 3.5c act as a switch from bistability to monostability (*i.e.* guaranteed resolution of inflammation), simulations of our spatially-dependent model illustrate (in Figure 3.14) that crossing the same Hopf bifurcations can move the model into an area of parameter space for which persistent spatially-inhomogeneous solutions exist – both steady state solutions and solutions that oscillate temporally. These chronically inflamed solutions lie in an area of parameter space for which the ODE model predicts full resolution of damage. For the majority of parameters studied, our spatially inhomogeneous solutions comprise disparate areas of damage whose severity oscillates temporally; while one area of damage may be resolving, in that pro-inflammatory mediator levels are reducing, other areas of damage are worsening due to the feedback from both active and apoptotic neutrophil populations. Oftentimes, monitoring the pro-inflammatory mediator concentrations alone would seem to indicate resolution, yet responses from the other components of the system yield further flares of damage in due course. In this sense, the temporal patterns that we observe are reminiscent of inflammatory conditions that have relapsing–remitting characteristics, such as Crohn's disease or rheumatoid arthritis (Tibble *et al.*, 2000; Firestein, 2003).

With the introduction of the neutrophil feedback, large values of the parameter k_n that controls this added feature can cause previously healthy outcomes of Chapter 2 to become chronic. We here examined the extent to which the balance between the pro-inflammatory feedback from active neutrophils (with rate k_n) and the counteracting role of the anti-inflammatory mediator (g) can have a key influence upon

biassing the system toward globally inflamed (homogeneous) or spatially inhomogeneous solutions (as illustrated in Figures 3.6 and 3.7). For large choices of k_n or small concentrations of anti-inflammatory mediator (*e.g.* in the limit $k_g \to 0$), spatial patterns can be eliminated and the results of the corresponding homogeneous model are recovered. While some drugs in current usage (such as methotrexate, sulphasalazine and FK506) do act to mitigate against inflammation by triggering the synthesis of anti-inflammatory mediators (Gilroy *et al.*, 2004; Hasko & Cronstein, 2004), manipulation of anti-inflammatory mediators remains an active area of focus in the hunt for new therapeutic targets (Henson, 2005; Barnig *et al.*, 2018; Back *et al.*, 2019). Our results indicate that, while increasing the concentrations of anti-inflammatory mediators can move the homogeneous system from a bistable regime (in which chronic outcomes are permissible) to a healthy state, intermediate levels of anti-inflammatory mediators can yield spatially inhomogeneous, non-resolving outcomes.

For spatially-independent parameter values that allow the model to emit spatially inhomogeneous solutions, we have explored (in Figure 3.15) the extent to which variations in spatial parameters can influence the solutions obtained. For rapidly spreading mediators (D_c and D_g large), the initial damage rapidly spreads to fill the entire domain, triggering a global response that results in a homogeneous, healthy outcome. Similarly, large choices of the neutrophil motility parameters (D_n and θ_n) or small choices of macrophage motility parameters (D_m and θ_m) result in a rapid spread of damage driven by the apoptosis and eventual necrosis of neutrophils, the associated positive feedback in pro-inflammatory mediator concentrations once again triggering a global response that restores the healthy state. For small to moderate choices of the neutrophil diffusion parameter D_n, our simulations reveal that strong neutrophil chemotaxis (θ_n large) can drive resolution of inflammation, while weaker neutrophil chemotaxis can result in a persisting spatially inhomogeneous outcome (Figure 3.15d). The role of neutrophil migration in many different inflammation-related pathologies

is of increasing interest (Brubaker *et al.*, 2013; Cecchi *et al.*, 2018); there is strong evidence in the biological literature that a reduction in the rate of neutrophil chemotaxis occurs under trauma and ageing and results in an otherwise healthy inflammatory response being pushed into a persistent inflammatory response (Sapey *et al.*, 2014b). Indeed, neutrophil migration is now thought to be an attractive therapeutic target for diseases such as chronic obstructive pulmonary disease, a chronic lung disease characterised by aberrant neutrophil migration (Sapey *et al.*, 2011; Jasper *et al.*, 2019).

It is pertinent to remark briefly that, while the model presented here incorporates a reasonably thorough catalogue of biological interactions, this comes at the expense of restricting the use of some key mathematical analyses that would commonly be used in analysing pattern-forming systems. For example, our model does not lend itself to travelling wave analysis, and does not allow spatially interesting configurations to be determined analytically; we are therefore restricted to the use of robust numerical schemes in order to identify the model's spatially-dependent solutions. This is in contrast to a broad range of existing models, the construction of which can often omit key biological feedbacks in order to facilitate greater analytical progress. Furthermore, we note that, while we regard the model described here to include the majority of crucial biological interactions at play in a typical inflammatory response, there is certainly scope for inclusion of further, more detailed mechanisms. To do so within the confines of a PDE-based model would likely result in a model that is not easily penetrable via mathematical analysis. This potentially motivates the need for a shift to an alternative modelling paradigm, via which the full remit of biological interactions can be easily incorporated. In Chapter 4 we further investigate this through agent based models, where cells are accounted for individually, allowing us to study their interactions with greater insight.

Chapter 4

Modelling the inflammatory response via agent based models

In this chapter, a new modelling approach will be introduced in which the cells featuring in the inflammatory process will be accounted for individually. This new 'agent-based' model of inflammation will replicate and extend all the biological interactions outlined in the model of Chapter 3, in order to investigate further those inflammatory mechanisms that still remain unclear from both the available literature and the analysis presented in the previous chapters. More importantly, by modelling the inflammatory process under conceptually and mathematically different terms to the PDE framework, we investigate how sensitive the conclusions are to the modelling approach.

4.1 Introduction

Agent-based modelling is a parallel computational paradigm based on a uniform, locally detailed and synchronous structure. Agent-based modelling provides a robust and innovative alternative to differential equation based dynamical systems represen-

tations, by relying on a fundamentally simple concept of cell units updating their states according to synchronised local sets of rules, underlying the potential complexity in structures and dynamics that such a paradigm delivers (Schiff, 2008). As such, while analogous to PDEs in purpose, that is in representing complex systems, agent-based modelling presents important advantages in terms of stability, convergence and approximation of the results (Hoekstra *et al.*, 2010). In addition, this valuable modelling approach provides a reliable and valid bridge between the microscopic level and emerging patterns or behaviours of interest. This further underlines how ABMs are not necessarily substitutes for PDE ones but can actually offer an integrating approach in clarifying specific conditions that arise from microscopic mechanisms that would otherwise be missed or remain under appreciated.

Formally, ABM are defined as discrete, both in time and space, dynamical systems in which single cells (*automata*) exhibit one from a finite set of states according to homogeneous local rules of interactions (Kari, 2013). More precisely, let $d \in \mathbb{N}$, then

$$\mathcal{L} = \mathbb{Z}^d \tag{4.1}$$

is a discrete cellular space, with elements of $\mathcal{L}$ being cells. Let S be a finite state set; then elements $\sigma \in S$ are called states. The local value space S basically defines all the possible states for each cell of $\mathcal{L}$. The ABM configuration of the d-dimensional ABM is then defined as the function

$$c : \ \mathbb{Z}^d \to S \,, \tag{4.2}$$

with c describing all possible compositions of all cells within the state space $\mathcal{L}$. For additional clarity, let us highlight that when referring to ABM, the entity 'cell' does not necessarily refer to a biological cell, and has to be intended instead as a single agent or basic unit of the model. With respect to the topology of each individual cell, a neighbourhood $\mathcal{N}$ is determined as the set of its N neighbouring cells. The definition

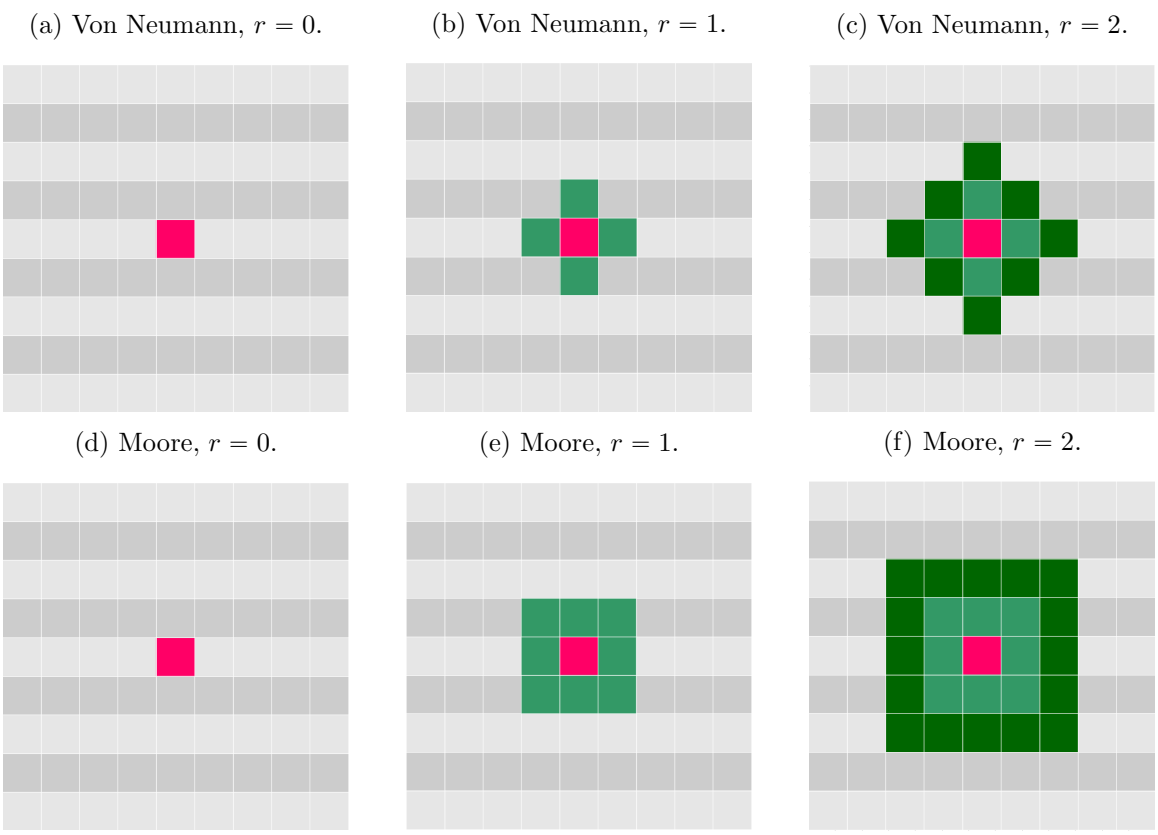

Figure 4.1: Examples of different $2D$ neighbourhood configurations with varying ranges r. Von Neumann neighbourhoods (first row) are diamond-shaped and include $1 + 2r(r + 1)$ cells, while Moore neighbourhoods (bottom row) are square-shaped with the total number of cells given by $(2r + 1)^2$.

of neighbourhoods can vary according to their shapes and ranges, with examples of typical configurations shown in Figure 4.1. Configurations are in turn determined with respect to the boundary conditions that can be periodic, reflective or fixed (Hoekstra *et al.*, 2010). Periodic boundary conditions implement a periodic extension of the lattice, thus simulating an infinite lattice (in $2D$ this corresponds to the topology of a torus). Reflective boundary conditions, as the name suggests, implement the reflex of the lattice at the boundary, providing the equivalent to Neumann boundary conditions typical of diffusive systems, while fixed boundary conditions implement the Dirichlet

conditions within the ABM frame, by setting a fixed value at each boundary cell. A further step in determining the ABM paradigm consists in specifying a transition (or local update) rule ϕ defined as the function describing the change in state that cells in the N-sized neighbourhood undergo:

$$\phi : \ S^N \rightarrow S \, . \tag{4.3}$$

All cells follow the same transition rule simultaneously, according to an external time step (tick). Therefore, a cellular automata A is defined as the $4-$tuple

$$A = (d, S, \mathcal{N}, \phi) \, , \tag{4.4}$$

with respect to a dimension $d \in \mathbb{N}$, a finite state set S, a neighbourhood $\mathcal{N}$ and a transition rule ϕ.

4.1.1 Implementation

Agent based modelling implies a shift in the typical modelling approach in which agents are structured with respect to their activity, rather than attributes and methods (Abar *et al.*, 2017). In practice, this translates into building the model around agents' responses, with their behaviour being characterised in terms of cells' actions instead of their defining properties. As such, agent-based modelling can be seen as an extension of object-oriented programming, by defining agents as objects in control of their execution (Abar *et al.*, 2017). More specifically, with agents being characterised as objects, their behaviour is shaped and controlled through sets of states and functional rules.

There is a wide choice of available agent-based modelling software tools, with mostly similar capabilities but varying features and programming language implementations. While Abar *et al.* (2017) provide an exhaustive review of eighty-five agent-based toolkits, including non-commercial, academic-focused packages, all our

ABMs and simulations are implemented with the **Repast Simphony** software tool. This software relies on Java as source code, with object-oriented agents, and allows for both $2D$ and $3D$ simulations (North *et al.*, 2007, 2013).

4.1.2 Agent based models in inflammation – a literature review

ABMs offer a varied set of desirable features that allow us to investigate specific mechanisms that more traditional modelling approaches often fail to take into account. As such, ABM are increasingly deployed in many multidisciplinary research areas, including economics, biology, ecology, sociology, just to name a few, by defining the complex systems of interest in function of the interactions of their agents (seen as entities). The versatility of the ABM paradigm allows for the integration of a variety of modelling strategies, with the set of rules defining the agent states spanning from simple Boolean interactions to full approximation of PDE. The integration of PDEs in ABMs results in Hybrid Cellular Automata (HCA). These models are of particular importance in the investigation of biological problems by providing both accuracy and effectiveness in capturing mechanisms of interest typically arising in many of these areas involving both spatial and temporal dynamics such as cancer treatment efficacy (Ribba *et al.*, 2004), bone remodelling and synthesis upon mechanical stimuli (Tovar *et al.*, 2004), tumour growth (Gerlee & Anderson, 2007), cartilage regeneration within a porous scaffold (Cassani & Olson, 2018). This adaptability is of great use in many different biological applications, capturing multi-scale interactions and complex dynamics that are often missed in traditional equation-based models. As such, there is growing interest in modelling a variety of biological systems for which previous and on-going research based on more traditional tools does not offer an exhaustive understanding of more subtle and key mechanisms that still remain unclear. This

is particularly true for all those applications that rely on cells' self-organisation and multi-scale dynamics (Alber *et al.*, 2003), two of the key features of ABMs. One such phenomenon is morphogenesis; that is, the complex and ordered way in which cells organise, through controlled proliferation and motility, practically shaping an organism since the earlier embryological stages of its formation. Alber *et al.* (2003) present a detailed analysis of various morphogenetic processes in their review of ABMs of cell aggregation and migration. An account of many ABM capabilities in describing a variety of biological events is given by Ermentrout & Edelstein-Keshet (1993). In particular, the authors illustrate the suitability of agent-based models in the field of developmental biology. An *et al.* (2009) provides an insight into different ABMs that have been crucial in determining mechanisms that could not be otherwise captured by traditional equation-derived models. Again, the key feature in such breakthroughs is the simultaneous consideration of both spatial and multi-scale dependency that agent-based models typically offer. More specifically, this approach has successfully been used to determine a number of molecular mechanisms in the intracellular signalling occurring at cytoplasm level, as well as clarifying the role of cells' spatial propagation as a leading event in a variety of physiological and pathological processes such as morphogenesis, angiogenesis, inflammation, tumour growth and infections (An *et al.*, 2009).

Of more direct relevance to this project, a number of researchers have also been working on ABM based models to study a variety of pathophysiological issues that closely involve inflammatory mechanisms, ranging from wound healing to infection and acute inflammation, amongst others. With respect to infectious mechanisms in particular, Gorochowski *et al.* (2012) develop a ABM-based tool to model bacterial populations. This framework accounts for both lower-scale interactions such as gene regulatory networks and cell to cell dynamics and the heterogeneous behaviours at population level that arise from such mechanisms, with simulations capturing the

expression of both single cells and the collective population. The ABM system presented by An (2001) models the inflammatory response at the capillary level, with agents accounting for different groups of both cells and molecules. A first class of cells for endothelial agents exhibits either a healthy or injured state, with the latter triggering adhesion mechanisms, practically modelling the mediators' behaviour, with the system's damage assessed as a measure of the agents in an injured state. Agents representing neutrophils are characterised by a lifespan after which the cells die and random movement. They exhibit sequential states in response to the local endothelial agents' activity, with the last of such states acting as chemoattractant for a third class of agents accounting for mononuclear cells. Mononuclear agents' activity is in response to the endothelial agents' damage that, in turn, is cleared by mononuclear cells, resetting the endothelial ones back to the uninjured state. Another class of agents representing Reactive Oxygen Species (ROS) is also included, promoting the spread of damage within the different cells. This model accounts for both damage related inflammations and infections, with the former triggered by the initial distribution of injured epithelial agents and the latter by a class of infectious carrier agents as vectors that are in turn cleared by the agents representing ROS. This last interaction highlights the dual nature inflammatory-driven mechanisms in which the promotion and spread of damage is key to the activation of the resolution pathways. The model is assessed by qualitatively comparing the simulations resulting from both the infectious and sterile injury as well as analysing the system's outcome upon varying degrees of each injury type. The high degree of abstraction of this model only allows for preliminary qualitative analysis of the results, with the authors suggesting the need for models describing the inflammatory response with greater detail and to be validated against the available experimental data. In particular, this ABM of inflammation lacks any anti-inflammatory mechanism, as well as the system's pro-inflammatory feedback and the repercussions of apoptosis on the

healing process. Building up from this model, An (2008) extended this ABM system to a multi-scale architecture to include tissue and organ functioning levels, along with the cell to cell interactions described in An (2001). In particular, the former model is extended by including the pro-inflammatory mechanisms and agents representing epithelial cells. Finally, another ABM system representing individual organs and their systemic inflammation leading to failure is introduced and implemented as a layered configuration of the previous models accounting for cells and tissues respectively. The resulting model simulates inflammatory mediators acting on a barrier of epithelial cells which, in turn, respond to the inflammatory trigger with a disruption in both shape and functioning, signalling the local failure of the epithelial junction. Following the same scheme, a further extension linking two layered ABM working in parallel is proposed as a multi-organ model. The relative simulations focus on specific scenarios replicating gut ischemia and a generic inflammatory pulmonary disease. These models, though, do not provide any new insight into the biological mechanisms they simulate and are intended instead as a qualitative tool in representing relevant multi-scale problems.

As discussed above, existing agent-based models of inflammatory systems generally place significant focus upon specific tissues or inflammatory conditions. However, as discussed in Chapter 1, the fundamental mechanisms that underlie the acute inflammatory response are broadly consistent across scenarios. There is a lack of existing agent-based models of inflammation that incorporate a full repertoire of cellular interactions, while also being suitably generic to be transferrable to multiple conditions. Thus, in the following section, we construct a novel ABM aiming to investigate the emergence and spread of inflammation by accounting for neutrophils and macrophages separately and by highlighting the nuanced role each of these groups of cells has in initiating the anti-inflammatory response. In doing so, we are also interested in addressing the question of whether the conclusions of previous chapters

are sensitive to the modelling approach. We thus draw direct comparison between the ABM developed below and the corresponding PDE model of Chapter 3 in particular, once again examining the extent to which localised tissue damage can invade neighbouring healthy tissue, and the extent to which spatial aspects of the inflammatory response contribute to the switch between healthy and chronically inflamed outcomes.

4.2 Model construction

We, here, describe the assembly of a hybrid PDE-ABM of the inflammatory response. Such an approach improves upon the PDE-based models of the previous chapters by modelling the behaviour of individual cells in function of their location and *neighbourhood* within the modelled tissue.

Our model incorporates components that replicate each of the variables featured in the model of (3.7)–(3.11). In particular, variables accounting for cell groups n, m and a (active neutrophils, macrophages and apoptotic neutrophils respectively) are replaced by an agent-based description involving instances of the classes `Neutrophil`, `Macrophage` and `Apoptotic`. Chemical mediators (both pro- and anti-inflammatory) are modelled within a separate class named `Environment` in which the PDE descriptions of Chapter 3 are retained and implemented. This class, as suggested by its name, also implements those methods that directly act on cellular concentrations in response to the mediators' interactions (*i.e.* recruitment of neutrophils and macrophages in response to damage). Finally, a class `InflammationBuilder` is also defined, which has the role of setting up the spatial domain in terms of dimensions, boundaries and visualisation, implementing the initial conditions of the model at time (*tick*) $t = 0$, instantiating the required agents, and scheduling their interactions. In practice, the definition of classes and their methods closely follows the interactions highlighted in equations (3.7)–(3.11). These are summarised for clarity in Table 4.1 and explained

in detail in the following sections.

Finally, to summarise the structure of the ABM outlined below, Figures 4.2 and 4.3 provide a graphical representation of the system's main features, parameters, links to the previous PDE model and intrinsic functioning. Figure 4.2 in particular describes the structure of the model in terms of agents and parameters, by highlighting the points of control of inflammation. Figure 4.3 represents a flow chart with a schematic illustration of the model's general structure, while the set of changes that agents undergo at each tick according to their state and the class they belong to will be presented in figures 4.4–4.6 and discussed in later sections.

4.2.1 Domain and initial conditions

The above classes define a framework to create objects (agents), each with a specific set of properties, whose behaviour is characterised by methods that are called in response to interactions with other agents. Agents are placed within a square region that represents the model's spatial domain. Formally, this is defined as a combination of a *grid* that contains the agents with respect to cartesian coordinates and allows for queries within their Moore neighbourhood (i.e. the central cell and its eight surrounding cells) and a *continuous space* in which the cells are visualised in simulations, neglecting, as the name suggests, the domain's discretisation. The square domain is subject to periodic boundary conditions, with initial conditions slightly differing from those described in (3.29). In particular, the system is initialised with the inflammatory response triggered by the presence of pro-inflammatory mediators concentrated initially in the centre of the domain, modelling a circular damage of radius r and severity c_0. In contrast with Chapter 3, the system's initial conditions do not include any concentration of anti-inflammatory mediators or leukocytes in the ABM starting configuration.

Class methods	ENVIRONMENT		NEUTROPHIL	MACROPHAGE	APOPTOTIC	Methods called
	c	*g*				
NEUTROPHIL						
run						becomeApoptotic moveChemotactically releasePro
moveChemotactically	in					moveRandomly
moveRandomly						
releasePro	+					
die			−			
becomeApoptotic					+	die
MACROPHAGE						
run						moveTowardApoptotic phagocytoseApoptotic releaseAnti makeLeaveDecision die
die				−		
moveRandomly						
moveTowardApoptotic					in	moveChemotactically
moveChemotactically	in					moveRandomly
phagocytoseApoptotic						apoptotic.die
releaseAnti		+				
makeLeaveDecision	in					die
APOPTOTIC						
run						releasePro
die					−	
releasePro	+					die
ENVIRONMENT						
run	in	in				getProconcentration getAntiConcentration
getProConcentration	in					
setProConcentration	in					
increaseProConcentration	+					
getAntiConcentration		in				
setAntiConcentration		in				
increaseAntiConcentration		+				
recruitNeutrophil	in	in	+			
recruitMacro	in			+		

Table 4.1: Scheme of the ABM interactions. Columns marked with *in* represent instances of that object sensed within the execution of the method. Plus/minus signs correspond to increase/decrese in the number of objects within the grid. Methods can be scheduled (italics) and be called upon probabilities (blue).

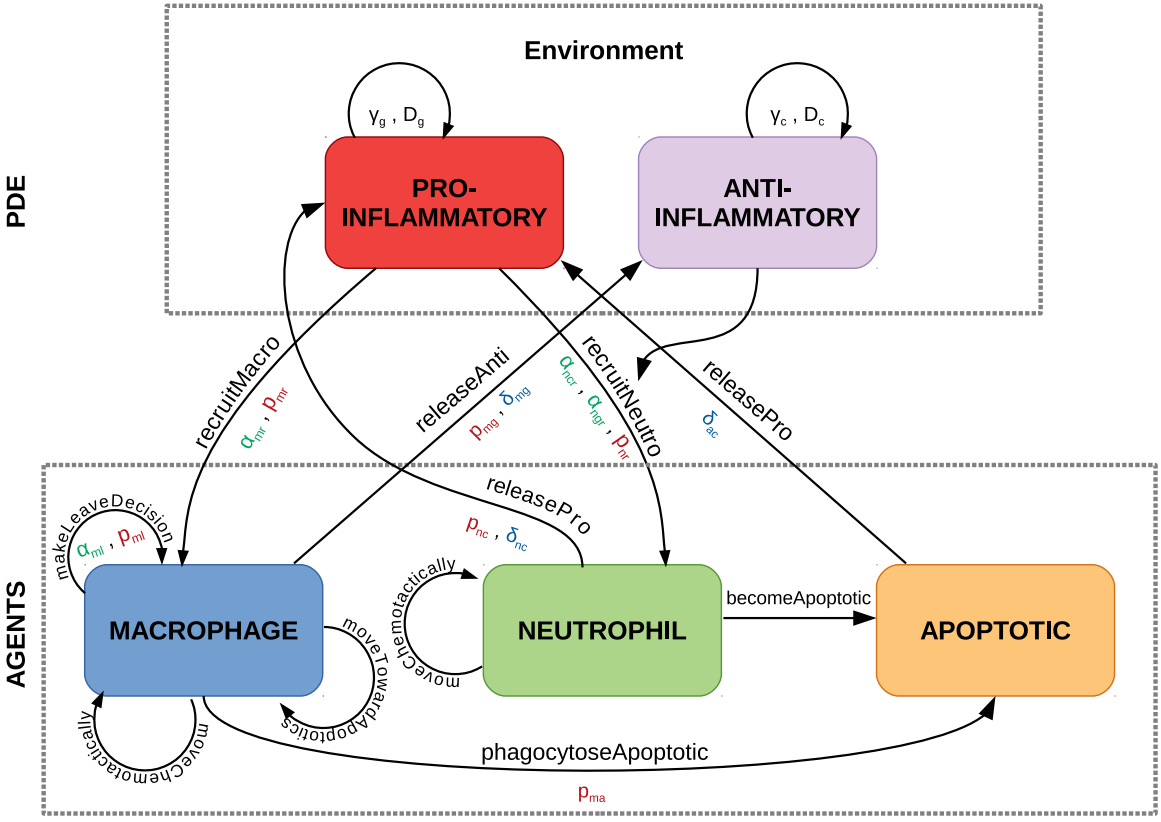

Figure 4.2: Schematic diagram representing the ABM of inflammation and illustrating the constituent interactions between populations of healthy neutrophils, apoptotic neutrophils and macrophages, modelled as agents, in response to pro- and anti-inflammatory mediators, modelled through PDEs. Interactions are shown by arrows and can be in turn regulated by parameters. Parameters are differentiated by colour and refer to probabilities in red, increments in blue, thresholds in green, with PDE parameters in black.

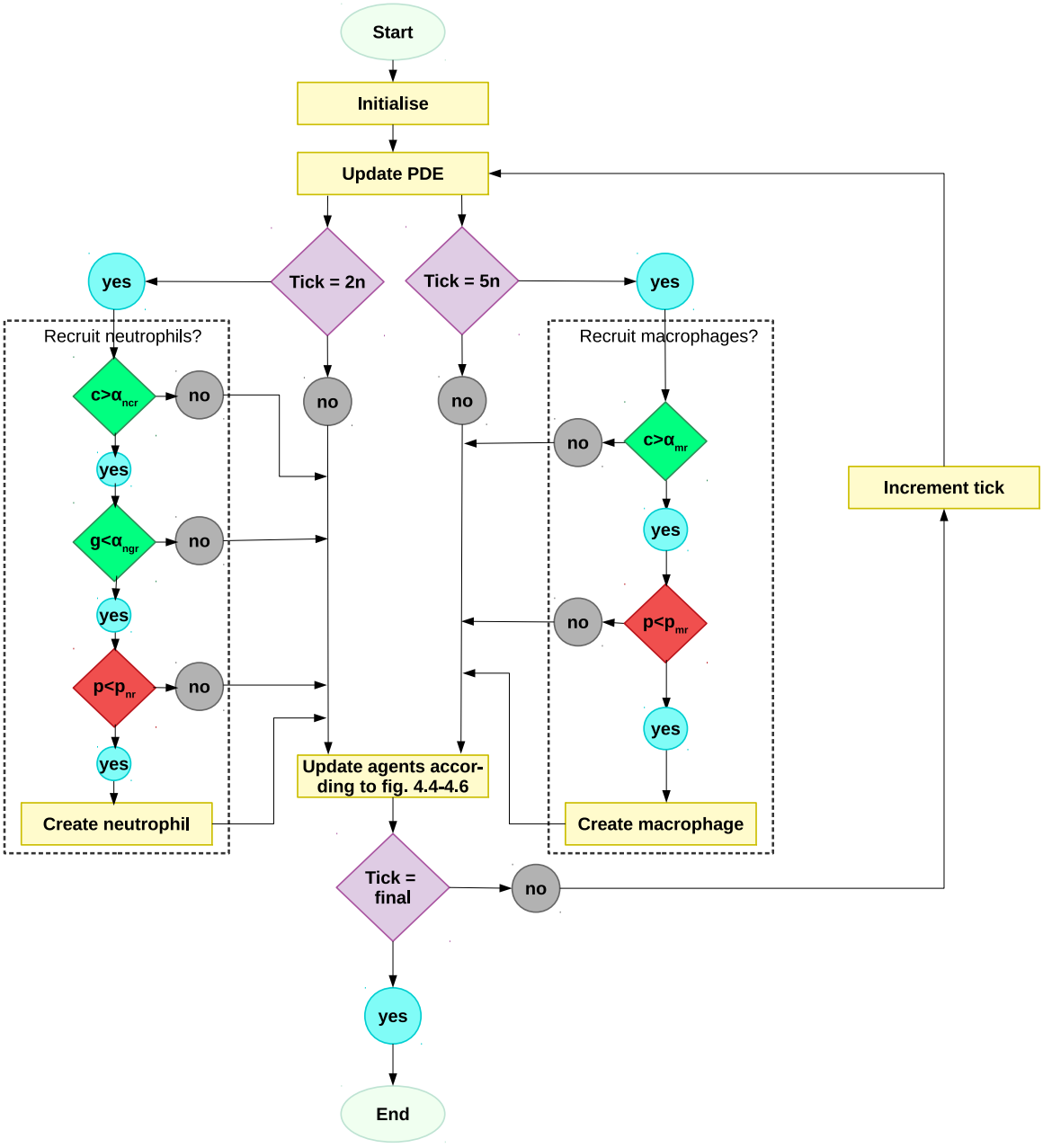

Figure 4.3: Flow chart representing the ABM of inflammation and illustrating the cyclic chain of actions with respect to the tick count. Diamonds represent decision points, green diamonds represent thresholds, red diamonds represent probabilities. Here, p represents a random number drawn uniformly from the interval $[0, 1]$.

4.2.2 Modelling mediators

The mediators' behaviour is rendered by explicitly defining the expression of both pro- and anti-inflammatory properties through PDEs. Their representation, and the inflammatory properties that can either promote the acute response or dampen it according to the ongoing cellular interactions, are thus regulated with respect to both decay rates for pro- and anti-inflammatory mediators, modelled through tunable parameters γ_c and γ_g respectively, and diffusive behaviour controlled by parameters D_c and D_g respectively. These parameters relate directly to their counterparts in the model of Chapter 3, both theoretically but also practically, being implemented in a similar fashion. In particular, to model pro-inflammatory mediators c, we implement a finite difference approximation of the PDE

$$\frac{\partial c}{\partial t} = D_c \nabla^2 c - \gamma_c c + \Gamma_c \,, \tag{4.5}$$

by retaining the numerical approach first used in Section 2.3.1. Equivalently, the distribution of anti-inflammatory mediators g is governed by

$$\frac{\partial g}{\partial t} = D_g \nabla^2 g - \gamma_g g + \Gamma_g \,. \tag{4.6}$$

In the above, Γ_c and Γ_g incorporate any sources/sinks in the mediator concentrations owing to the actions of the agents described below.

Equations (4.5) and (4.6) are solved numerically on the discrete grid described in Section 4.2.1, in exactly the same manner as was described in Chapter 3. The numerical scheme employs a five-point Laplacian for the diffusive term as before, and an associated timestep dt. Note that we tune dt to ensure numerical stability, and in doing so take multiple numerical timesteps per tick.

Finally, the remaining classes, detailed in the following subsections, define the agents' behaviour through *scheduled* methods, that is methods that are called at fixed intervals, starting from an initial tick t. This allows us to characterise each

agent with respect to both its intrinsic biological properties and possible interactions with other agents, according to specific conditions and/or probabilities for an action or method to be called.

4.2.3 Macrophages

Overview

Macrophages are defined with respect to a grid location, a continuous space location and an integer field named `lifespan`. While the first two fields are intrinsic to the ABM system's setting, the latter describes the duration for which leukocytes are in a biologically active state (Parihar *et al.*, 2010). This is typically within days and in general is observed to be longer than for neutrophils (Patel *et al.*, 2017). We will discuss the implications of these scales in the parametrisation of our model in the following dedicated Section 4.3. At each tick the Macrophage agent carries out four actions: it decides whether to move (and, if so, where to); it attempts to remove apoptotic neutrophils in its neighbourhood; it attempts to release anti-inflammatory mediators, and it decides whether to vacate the tissue (if inflammation is sufficiently resolved). We expand upon how these behaviours are implemented below.

Macrophage recruitment

Reflecting the biological implications of the mediators' activity, in response to the enhanced concentration of active neutrophils prompted by pro-inflammatory mediators, macrophages are recruited to effectively counteract the inflammation. The recruitment, scheduled at every $t = 5$ ticks in order to best model the delayed feedback in the anti-inflammatory response initiated by macrophages, becomes effective only subject to both a probability p_{mr} and if the punctual concentration of pro-inflammatory mediators c at the grid point being considered is greater than a threshold value α_{mr}.

In substance, at each grid point and at every 5 ticks, if $c > \alpha_{mr}$, macrophage agents are recruited with probability p_{mr}.

Finally, to avoid the biologically unrealistic event of infinite recruitment and accumulation of cells, we prescribe a maximum global number of macrophages m_{max} to be recruited within the tissue. We will infer this saturation level threshold from the available experimental data, as explained in Section 4.3, below.

Chemotactic motion

Macrophage motion is regulated such that agents move preferentially towards a neighbouring location containing apoptotic neutrophils. Such behaviour is in itself of chemotactic nature, driven by chemicals released by apoptotic neutrophils and reflecting a fundamental biological aspect with respect to the more subtle details at play during the phagocytosing process and its wider implications on the inflammatory outcome, as exposed by Hawkins & Devitt (2013). This feature had been neglected in the PDE models of the previous chapters, in which macrophage chemotaxis is directed toward pro-inflammatory mediators only, but is now included in this new ABM, thus marking an important difference both in terms of practical implementation between the two systems but also more importantly rendering the model subject of this chapter more interesting, by adding a biological behaviour that is central to the inflammatory response but was missing in PDE analysis.

In the absence of any apoptotic neutrophils in the macrophage's neighbourhood, its preferential action is that of sensing pro-inflammatory mediators (always considering neighbourhood proximity), practically implementing leukocytes' chemotaxis towards higher concentrations of pro-inflammatory chemicals. For a given macrophage m_i, we begin by examining the pro-inflammatory mediator concentrations in each position in its neighbourhood $\mathcal{N}_i$. For each position $j \in \mathcal{N}_i$, the macrophage moves

to position j with probability

$$p_j = \frac{c_j}{\sum\limits_{k \in \mathcal{N}_i} c_k}, \tag{4.7}$$

where c_j denotes the pro-inflammatory mediator concentration at position j.

Finally, in the absence of both apoptotic neutrophils and pro-inflammatory mediators in the agent's neighbourhood, the macrophage moves to a random neighbouring location. Such a characterisation of the macrophage movement within the domain reflects their biological activity in being highly responsive to the presence of apoptotic neutrophils, in order to phagocytose them, and to generally move chemotactically towards pro-inflammatory mediators.

Phagocytosis

Macrophages also act to clear apoptotic neutrophils, implemented through a dedicated method that models the phagocytosing action, and in doing so can promote the anti-inflammatory response. The phagocytosis of apoptotic neutrophils by macrophages is scheduled at every tick and simply consists, for each individual macrophage, of randomly selecting an apoptotic agent at its current position, if there are any, and removing it with probability p_{ma}.

Release of anti-inflammatory mediators

The active initiation of the anti-inflammatory feedback mediated by macrophages occurs in response to the change in phenotype these leukocytes undergo upon environmental stimuli (Ponzoni *et al.*, 2018). We thus model the release of anti-inflammatory mediators subject to macrophages' engulfment of apoptotic neutrophils, individuating in a macrophage first phagocytic action the switch to its anti-inflammatory activity, *i.e.* macrophages do not release any g before their first phagocytosis. On removing an apoptotic cell, the macrophage yields an anti-inflammatory response by enabling

this change in phenotype such that, after the first phagocytosis event, macrophages steadily increase the concentration of anti-inflammatory mediators by a quantity δ_{mg} (per tick) at the macrophage agent's grid location, with probability p_{mg}. This behaviour echoes the function of parameter k_g in (3.7)–(3.11). It thus models the macrophage's active role in initiating the anti-inflammatory response by prompting the release of anti-inflammatory mediators (Wynn *et al.*, 2016). It is also important to highlight how the ability of macrophages to release anti-inflammatory mediators is not intrinsic to these agents and is only activated upon their first phagocytosing action, indicating the change in their phenotype.

Macrophage death/departure

Finally, a specific method is created for macrophage agents to decide whether to leave the tissue. In order to do so, the total concentration of pro-inflammatory mediators in the agent's neighbourhood is assessed and if this is below a threshold α_{ml} the macrophage agent leaves the tissue with probability p_{ml}.

Summary

In summary, macrophages retain all their main features from the previous PDE model of Chapter 3, with the added behaviour of chemotactically moving towards apoptotic neutrophils preferentially. In particular, each agent individually carries out (or attempts to carry out, in hierarchical order of priority) the following set of actions at every tick:

- move chemotactically towards apoptotic neutrophils;
- move chemotactically towards pro-inflammatory mediators;
- phagocytose an apoptotic neutrophil at its current position;

- release anti-inflammatory mediators;
- leave the tissue.

Additionally, at every $t = 5$ ticks, large concentrations of pro-inflammatory mediators result in the recruitment of new macrophage agents that are added to the inflamed tissue in order to counteract the acute inflammation and in particular the enhanced concentration of active neutrophils prompted by it.

The illustration of the macrophage agents' action is further summarised in the flow chart represented in Figure 4.4.

Finally, it is important to highlight that macrophages, or agents in general, do not implement a diffusive behaviour immediately comparable to the one defined in model (3.7)–(3.11). In fact, more in line with the definition of ABMs, agents of the `Macrophage` class move at each tick according to the set of actions and rules described above. Agents accounting for active neutrophils are treated analogously and introduced below.

4.2.4 Active neutrophils

Overview

Analogously to macrophage cells, active neutrophils are also defined in terms of the cells' motion and activity within the domain. In particular, at each tick the active neutrophil agent moves chemotactically towards higher concentrations of pro-inflammatory mediators and, upon depletion of its lifespan, it becomes apoptotic. Neutrophils have widely been observed to have considerably short lifespans, in the range of hours to few days but overall shorter than that of macrophages (McCracken & Allen, 2014; Bekkering & Torensma, 2013). Further details are given below in Section 4.3.

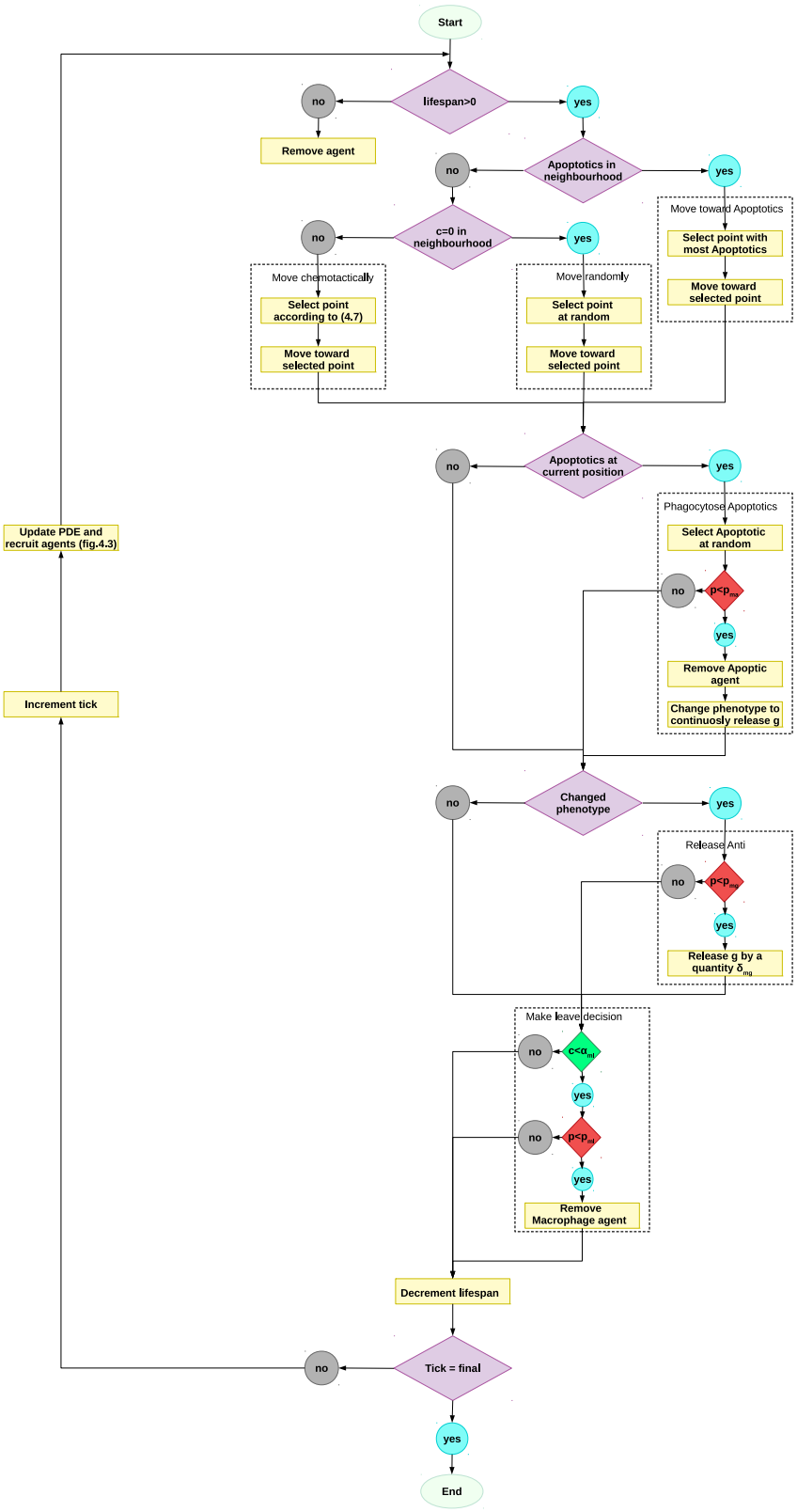

Figure 4.4: Flow chart representing the cyclic chain of actions each agent of the Macrophage class undergoes according to its state at each tick count. Green triangles represent thresholds and red triangles represent probabilities. Here, p represents a random number drawn uniformly from the interval $[0, 1]$.

Neutrophil recruitment

During the acute inflammatory response, as a feedback to higher concentrations of pro-inflammatory mediators, we, again, prescribe the enhanced recruitment of active neutrophils. The implementation is slightly different to the one described for the recruitment of macrophage agents though. In particular, the recruitment of neutrophil agents is scheduled at every $t = 2$ ticks via the preliminary assessment of both a minimum threshold of pro-inflammatory mediators α_{ncr} and a maximum threshold of anti-inflammatory mediators α_{ngr} and takes place only if both $c > \alpha_{ncr}$ and $g < \alpha_{ngr}$ hold. Under this condition, subject to a further probability p_{nr}, the pro-inflammatory activity is further enhanced by creating a new instance of the neutrophil agent. In practice, at each grid point, every 2 ticks, upon a preliminary assessment of the levels of pro- and anti-inflammatory mediators, if $c > \alpha_{ncr}$ and $g < \alpha_{ngr}$, then neutrophils are recruited with probability p_{nr}.

Similarly to macrophages, neutrophils are also capped at a critical level n_{max} to avoid the infinite recruitment and accumulation of cells within the tissue. Further details and the proportionality to the maximum number of macrophages are provided in the dedicated parametrisation Section 4.3.

Chemotactic motion

In a similar fashion to macrophages, the chemotactic motion of neutrophils is modelled by analysing, for each cell n_i, the concentrations c_j of pro-inflammatory mediators at each position j of the neighbourhood $\mathcal{N}_i$. The final choice of the new position to move to, dictated by levels of chemoattractant within the cell's neighbourhood, is based upon probability (4.7).

Release of pro-inflammatory mediators

In line with their biological function of promoting inflammation and echoing a key feature from the PDE model of Chapter 3, we identify neutrophil agents as a source of pro-inflammatory mediators. At each tick, active neutrophils release an increment δ_{nc} of pro-inflammatory chemicals with probability p_{nc}.

Apoptosis

Finally, the physiological cellular death that neutrophils naturally undergo is described by a dedicated method. The biological implications of a neutrophil's apoptosis in the inflammatory context are multiple and directly affect the complex chain of cellular and chemical interactions, as already highlighted in Section 1.2.1. The cell's death through apoptosis is modelled by removing the original agent from the system and replacing it with a new agent from the `Apoptotic` class (described below) instead.

Summary

In conclusion, at every tick, agents from the `Neutrophil` class

- move chemotactically towards pro-inflammatory mediators;
- release pro-inflammatory mediators;
- decide whether to become apoptotic.

Moreover, neutrophils are prescribed with the added feature of a background release of pro-inflammatory mediators, in order to further promote inflammation. This behaviour reflects the additional terms introduced in the extension of the PDE model from Chapter 2 to Chapter 3 as well.

A schematic representation of the set of rules regulating each neutrophil's activity is provided in Figure 4.5.

4.2.5 Apoptotic neutrophils

Overview

Once again, apoptotic neutrophils are defined with respect to a grid, a continuous space and a lifespan, in this case representing the delay between the cell becoming apoptotic and necrotic. At the point of necrosis, the cell releases its toxic content and further promotes the inflammatory activity, provided they have not already been phagocytosed by macrophages.

Necrosis

At each tick, the Apoptotic agent's lifespan is consumed and, upon complete depletion, the cell finally becomes necrotic, with a dual action of incrementing the concentration of pro-inflammatory mediators at the agent's location by a quantity δ_{ac}, and the apoptotic cell being finally removed from the system. It is important to observe that, unlike the release of pro-inflammatory mediators by active neutrophils, the splurge of chemicals by apoptotic neutrophils upon necrosis is not subject to a probability and is generally intended to be more disruptive. While the release of pro-inflammatory mediators by active neutrophils is physiological and a fundamental part of the chain of interactions that regulate the acute inflammatory response, apoptotic neutrophils are ideally efficiently cleared and phagocytosed by macrophages, with their necrosis playing a major role only in critical pathological contexts.

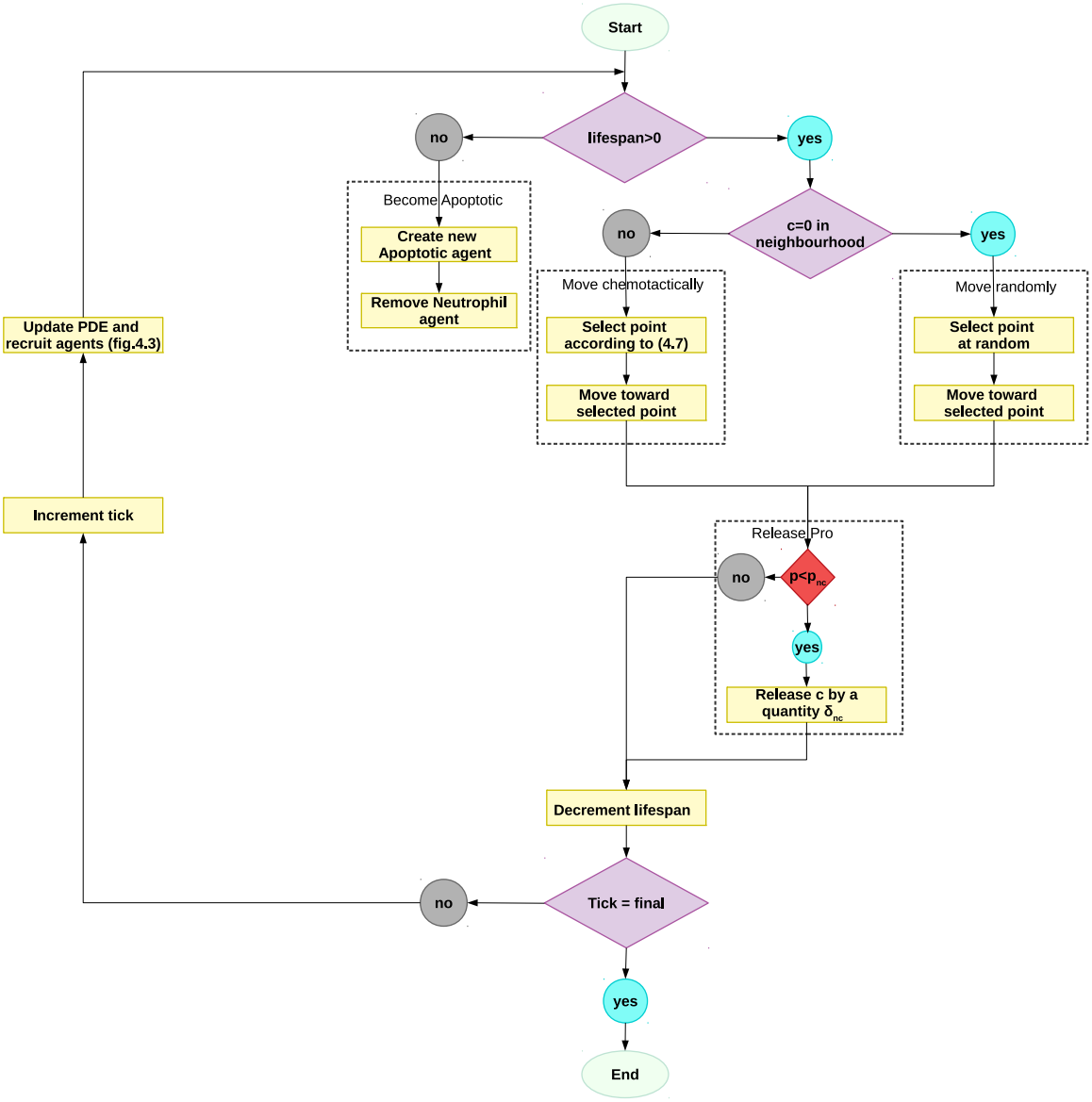

Figure 4.5: Flow chart representing the cyclic chain of actions each Neutrophil agent undergoes according to its state at each tick count. Red triangles represent probabilities. Here, p represents a random number drawn uniformly from the interval $[0, 1]$.

Summary

In short, apoptotic neutrophils do not move but if not phagocytosed by the time they become necrotic, spill their toxic content, further enhancing the inflammatory activity by releasing new pro-inflammatory mediators. Figure 4.6 summarises the limited activity of apoptotic neutrophils with respect to the system's tick count.

4.3 Parametrisation

We here pay particular attention to the spatial and temporal scales associated with the agent based model described above, to both ensure biological realism and facilitate comparison of results with the model of Chapter 3.

It should be noted here that the spatial scale associated this model is much smaller than that of Chapter 3, since we are interested in the interactions of individual cells. Within our agent based model, it is natural to consider the resolution of the grid to be such that each grid space corresponds to one cell diameter. We choose to set each grid space to correspond to the diameter of a macrophage, which is approximately 20 μm. For a 100×100 grid, this corresponds to a square domain of width 2 mm. When considering the nondimensionalisation required to arrive at the dimensionless PDEs (4.5) and (4.6) from a dimensional analogue, it is computationally convenient to scale lengths against the size of one grid space (since this provides a mesh with unit spacing that can be coupled easily to the agent-based portion of the model). We therefore choose $L^* = 20\mu$m (as opposed to the larger choice $L^* = 10$cm in Chapter 3) and run simulations on the domain $[0, 100] \times [0, 100]$.

Similarly, we are required to choose an appropriate scaling of time, T^*. In doing so, we configure the cell velocities against data reported in the literature. As summarised in Table 4.2, macrophage velocities are reported to lie in the range $0.5 - 30$ μm min^{-1}.

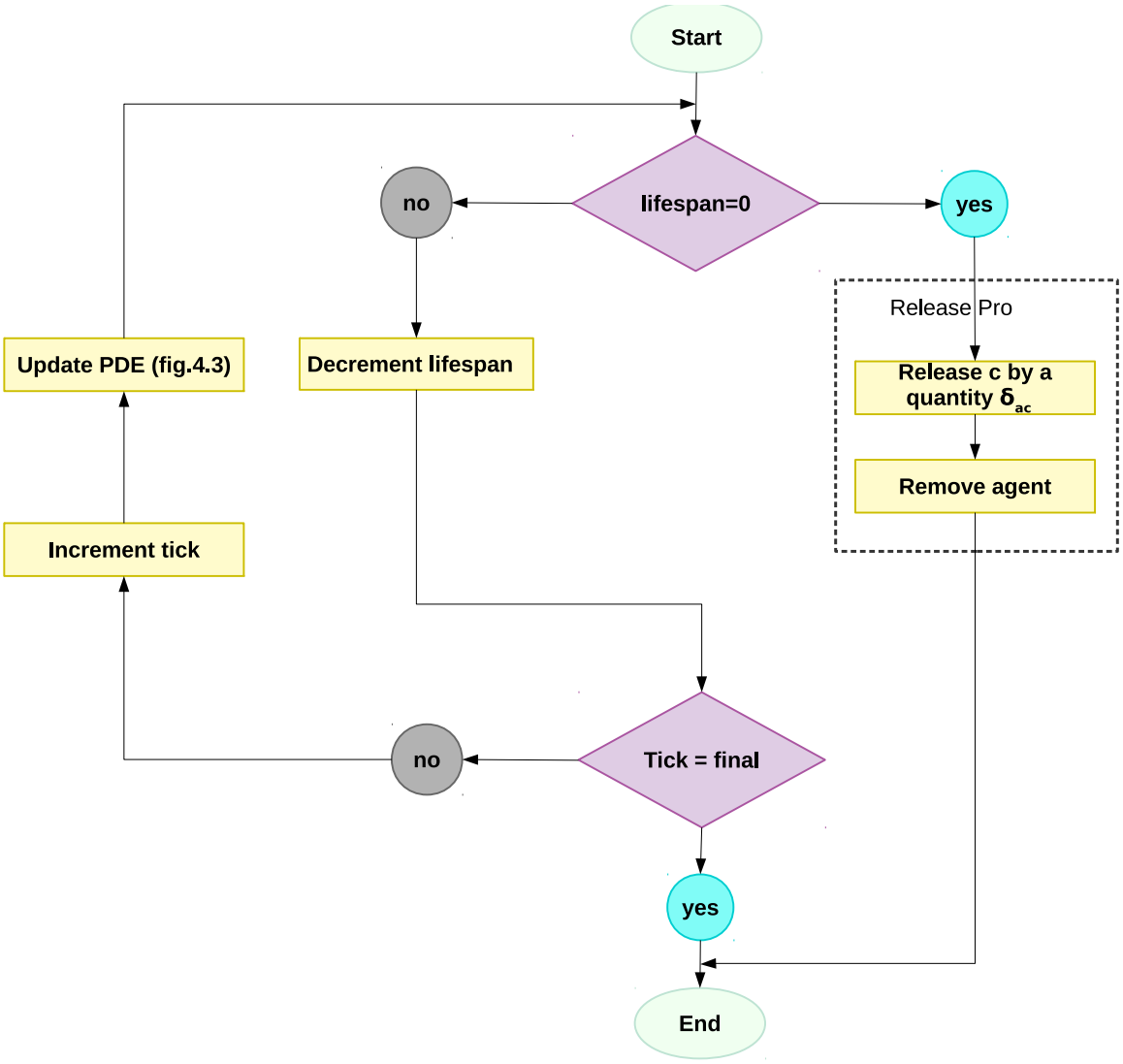

Figure 4.6: Flow chart representing the cyclic chain of actions each agent of the Apoptotic class undergoes according to its state at each tick count.

We therefore set each tick to be equivalent to 1 minute (*i.e.* $T^* = 1$ min) and allow macrophages to move once per tick, resulting in a typical macrophage velocity of 20 μm min^{-1}. Meanwhile, neutrophils are reported to move roughly twice as fast as macrophages, as the data in Table 4.2 shows, with average velocities between 4.5 – 63.5 μm min^{-1}. We therefore allow neutrophils to move twice per tick with a corresponding neutrophil velocity of 40 μm min^{-1}. We note that, through this rescaling of time, 1 unit of dimensionless time in the model of Chapter 3 corresponds to 480 ticks in this model.

As discussed in previous chapters, typical (dimensional) mediator diffusion rates are reported to be of order $D_c^* \simeq D_g^* \simeq 10^{-7}\text{cm}^2/\text{sec} \equiv D^*$. Following the nondimensionalisation procedure described in previous chapters, but with the new length and time scales described above, we calculate appropriate dimensionless diffusion coefficients as

$$D_c = D_g = \frac{D^* T^*}{L^{*2}} = 1.5. \tag{4.8}$$

We take this as our standard baseline value for D_c and D_g in the simulations below. Similarly, the decay rate parameter γ_c in (4.5) is related to its dimensional equivalent according to $\gamma_c = \gamma_c^* T^*$. Since we know from the literature that $\gamma_c^* \simeq 3$ day^{-1} Dunster *et al.* (2014), we have $\gamma_c \simeq 0.002$. Again, we take this as our baseline value for γ_c in simulations below, and for ease we also assume $\gamma_g = \gamma_c$.

It then remains to consider the scaling of mediator concentrations themselves. In Chapter 3, pro-inflammatory mediator concentrations were scaled against the parameter k_a^*, which is related to the production of pro-inflammatory mediator by apoptotic neutrophils on necrosis. Whilst it is difficult to recover this scaling exactly, we can make a qualitative comparison by setting the amount of pro-inflammatory mediator released by an apoptotic neutrophil (δ_{ac}) equal to one in our model. It is then intuitive to trigger our simulations with an initial condition that represents an intermediate level of damage. We therefore choose our initial conditions to include a

central circular area of damage of radius r in which $c = c_0$ ($c_0 \in [0, 1]$), surrounded by healthy tissue in which $c = 0$. For ease, we assume that there is no anti-inflammatory mediator initially, so that $g = 0$ everywhere in the domain.

The remaining parameters in our model are not known exactly, but some can be inferred qualitatively from biological intuition. For example, we expect the production of pro-inflammatory mediators by active neutrophils to be on a scale much smaller than that by apoptotic neutrophils, so $\delta_{nc} \ll \delta_{ac}$. Similarly, due to the scaling of mediator concentrations, we intuitively expect $\delta_{mg}, \alpha_{nr}, \alpha_{mr}, \alpha_{ml} \in [0, 1]$. We investigate the sensitivity of the model to variations in key parameters in Section 4.5 below.

Furthermore, in order to ensure that a finite number of cells is recruited, we prescribe both macrophage and active neutrophils agents with a maximum number of instances within the domain, as mentioned in Sections 4.2.3 and 4.2.4. In order to infer a biologically realistic proportionality between the maximum number of macrophages and neutrophils within the tissue, we refer to standard measurements of human differential white blood cells. In particular, neutrophils account for 40% to 80% of the total leukocyte population while macrophages have considerably lower proportions, with typical values between $2\% - 10\%$ (Curry, 2015). As such, by recalling that gridpoints are scaled with respect to the diameter of macrophages ($\sim 20\mu$m) and that we operate over a $2\,\text{mm} \times 2\,\text{mm}$ domain, we fix the maximum number of macrophages at $m_{max} = 1000$ and a limit number of neutrophils four times larger at $n_{max} = 4000$.

Finally, we consider appropriate choices for leukocyte lifespans. As already reported in Sections 4.2.3 and 4.2.4, macrophages and neutrophils are typically active for a variable amount of time that depends on the tissue and phase of inflammation, with the former spanning from several days to months (Takahashi, 2001) and the latter being considerably shorter, from within hours to few days (Pillay *et al.*, 2010; Tak *et al.*, 2013). Thus, recalling that according to our parametrisation one

Literature reference	Neutrophil velocity ($\mu m\, min^{-1}$)	Literature reference	Macrophage velocity ($\mu m\, min^{-1}$)
Qasaimeh *et al.* (2018)	4.77 ± 2.27	Hind *et al.* (2014)	$5 - 20$
Hoang *et al.* (2013)	19 ± 6	Shi *et al.* (2018)	$2 - 30$
Rainger *et al.* (1997)	9.8 ± 0.95	Toth *et al.* (2014)	≈ 1
Jung *et al.* (1996)	63.5 ± 41.32	Nguyen-Chi *et al.* (2015)	$0.5 - 1$
Skoge *et al.* (2016)	18	Li *et al.* (2017)	$8 - 12$
Raymond *et al.* (2017)	12.7		
Burton *et al.* (1987)	21.7 ± 6.2		

Table 4.2: Leukocyte velocities in the literature.

tick is equivalent to one minute, we model this information by randomly assigning `lifespan` a value taken from a uniform distribution on the interval $[1440, 86400]$ for macrophages and the interval $[60, 1440]$ for neutrophils, respectively. For apoptotic neutrophils, there is a lack of experimental methods to properly detect and measure the necrosis timescales (Iba *et al.*, 2013), but it is generally understood that this a rapid process (Vanden Berghe *et al.*, 2010). We thus prescribe an approximate lifespan for apoptotic neutrophils randomly assigned from a uniform distribution on the interval $[60, 720]$.

4.4 Simulations

The implementation of the ABM described above provides the opportunity to assess multiple simulations. The model's response is modulated through a set of parameters that can be manipulated in order to lead the system towards either the resolution of inflammation or its chronicity. In this sense it is interesting to observe that the intrinsic structure of the ABM paradigm provides a degree of randomness to each simulation, thus replicating those natural biological features that do not necessarily follow a strict set of fixed numerical parameters. As such, while the tuning of pa-

rameters affects the overall outcome of batches of simulations, it is nonetheless not surprising that a fraction of those simulations could yield an opposing result than the one set by the parameter values. In the analysis that follows we run batches of 100 repeated simulations per parameter set and report the main outcomes. All the parameters controlling the ABM behaviour are defined in Table 4.3. Through careful regulation of the parameter values and assessment of the resulting simulations, two main behaviours emerged: the overall resolution of inflammation (which we define as the simultaneous elimination of active/apoptotic neutrophils and pro-inflammatory mediators), detailed in Section 4.4.2, and a chronic non-resolved outcome, as described in the following section. Table 4.4 summarises the parameter values used in the following simulations and, as it can be observed from the bold rows, the shift in the overall outcome of the acute inflammatory response is achieved by manipulating those parameters that directly regulate the inflammatory activity. In particular a number of parameters that specifically target the severity of the initial damage (c_0), the size of the initial damage (r), the regulation of neutrophil recruitment (α_{ncr}, α_{ngr}), and the efficiency of macrophages recruitment (α_{mr}) provide a switch between the chronicity of inflammation and the restoration of a healthy state. This further reinforces on one hand the impact of the initial damage upon the spatial spread of inflammation and its eventual outcome and on the other hand the key role of neutrophils in promoting inflammation and macrophages in actively resolving it, which is tightly dependant on the mediator's presence and action.

4.4.1 Chronic outcome

While each single simulation plays out differently in terms of the agent locations and the interactions conditioned by probabilities, fixing the parameters accordingly with the second column of Table 4.4 provides a set of baseline values that yield an overall

Parameter	Definition	Class
c_0	initial pro-inflammatory mediators concentration (damage severity)	InflammationBuilder
r	initial damage radius (damage size)	InflammationBuilder
D_c	diffusion of pro-inflammatory mediators	Environment
D_g	diffusion of anti-inflammatory mediators	Environment
γ_c	decay of pro-inflammatory mediators	Environment
γ_g	decay of anti-inflammatory mediators	Environment
δ_{ac}	increment of pro-inflammatory mediators upon apoptotic neutrophils undergoing necrosis	Apoptotic
δ_{nc}	increment of pro-inflammatory mediators upon active neutrophils activity	Neutrophil
δ_{mg}	increment of anti-inflammatory mediators upon macrophagic activity	Macrophage
p_{nr}	probability of recruitment of new neutrophils	Environment
p_{nc}	probability conditioning release of pro-inflammatory mediators upon neutrophils activity	Neutrophil
p_{mr}	probability of recruitment of new macrophages	Environment
p_{mg}	probability upon which macrophages initiate the anti-inflammatory response	Macrophage
p_{ml}	probability at which macrophages leave the tissue	Macrophage
p_{ma}	probability at which macrophages phagocytose apoptotic neutrophils	Macrophage
α_{ncr}	threshold of pro-inflammatory mediators above which new neutrophils are recruited	Environment
α_{ngr}	threshold of anti-inflammatory mediators below which new neutrophils are recruited	Environment
α_{mr}	threshold of pro-inflammatory mediators above which new macrophages are recruited	Environment
α_{ml}	threshold of pro-inflammatory mediators below which macrophages leave the tissue	Macrophage

Table 4.3: Parameters of the ABM inflammatory model.

Parameter	Chronic outcome (baseline values)	Healthy outcome (switch: damage severity)	Healthy outcome (switch: damage size)	Healthy outcome (switch: neutrophil recruitment via c)	Healthy outcome (switch: neutrophil recruitment via g)	Healthy outcome (switch: macrophage recruitment)
$\boldsymbol{c_0}$	**1**	**0.5**	1	1	1	1
$\boldsymbol{r}$	**10**	10	**5**	10	10	10
D_c	1.5	1.5	1.5	1.5	1.5	1.5
D_g	1.5	1.5	1.5	1.5	1.5	1.5
γ_c	0.002	0.002	0.002	0.002	0.002	0.002
γ_g	0.002	0.002	0.002	0.002	0.002	0.002
δ_{ac}	1	1	1	1	1	1
δ_{nc}	0.001	0.001	0.001	0.001	0.001	0.001
δ_{mg}	0.001	0.001	0.001	0.001	0.001	0.001
p_{nr}	0.02	0.02	0.02	0.02	0.02	0.02
p_{nc}	0.5	0.5	0.5	0.5	0.5	0.5
p_{mr}	0.04	0.04	0.04	0.04	0.04	0.04
p_{mg}	0.8	0.8	0.8	0.8	0.8	0.8
p_{ml}	0.8	0.8	0.8	0.8	0.8	0.8
p_{ma}	1	1	1	1	1	1
$\boldsymbol{\alpha_{ncr}}$	**0.05**	0.05	0.05	**0.1**	0.05	0.05
$\boldsymbol{\alpha_{ngr}}$	**0.015**	0.015	0.015	0.015	**0.0015**	0.015
$\boldsymbol{\alpha_{mr}}$	**0.25**	0.25	0.25	0.25	0.25	**0.05**
α_{ml}	0.02	0.02	0.02	0.02	0.02	0.02

Table 4.4: Parameter values modelling the resolution of inflammation (third to seventh column) and its chronicity (second column).

behaviour towards the chronic state of inflammation that clearly emerges through multiple simulations. Snapshots of one such simulation, as shown in Figure 4.7, provide a visual understanding of the biological mechanisms unfolding at tissue level that cannot otherwise be easily captured by PDE models. Setting the parameters as in the second column of Table 4.4 disrupts the physiological progression of acute inflammation, resulting in continuous neutrophil activity which in turn further enhances the pro-inflammatory mediators' action, thus eventually preventing the resolution of inflammation and leading to its periodic recurrence or non-resolution altogether.

In order to appreciate how the system's outcome is modulated by the parameter values, a series of 100 simulations were run, in which the agent counts of cells (active neutrophils, macrophages, apoptotic neutrophils) and maximum concentrations of pro- and anti-inflammatory mediators were monitored. Figure 4.8 thus results from the averaging of all the collected data, highlighting a trending behaviour for each

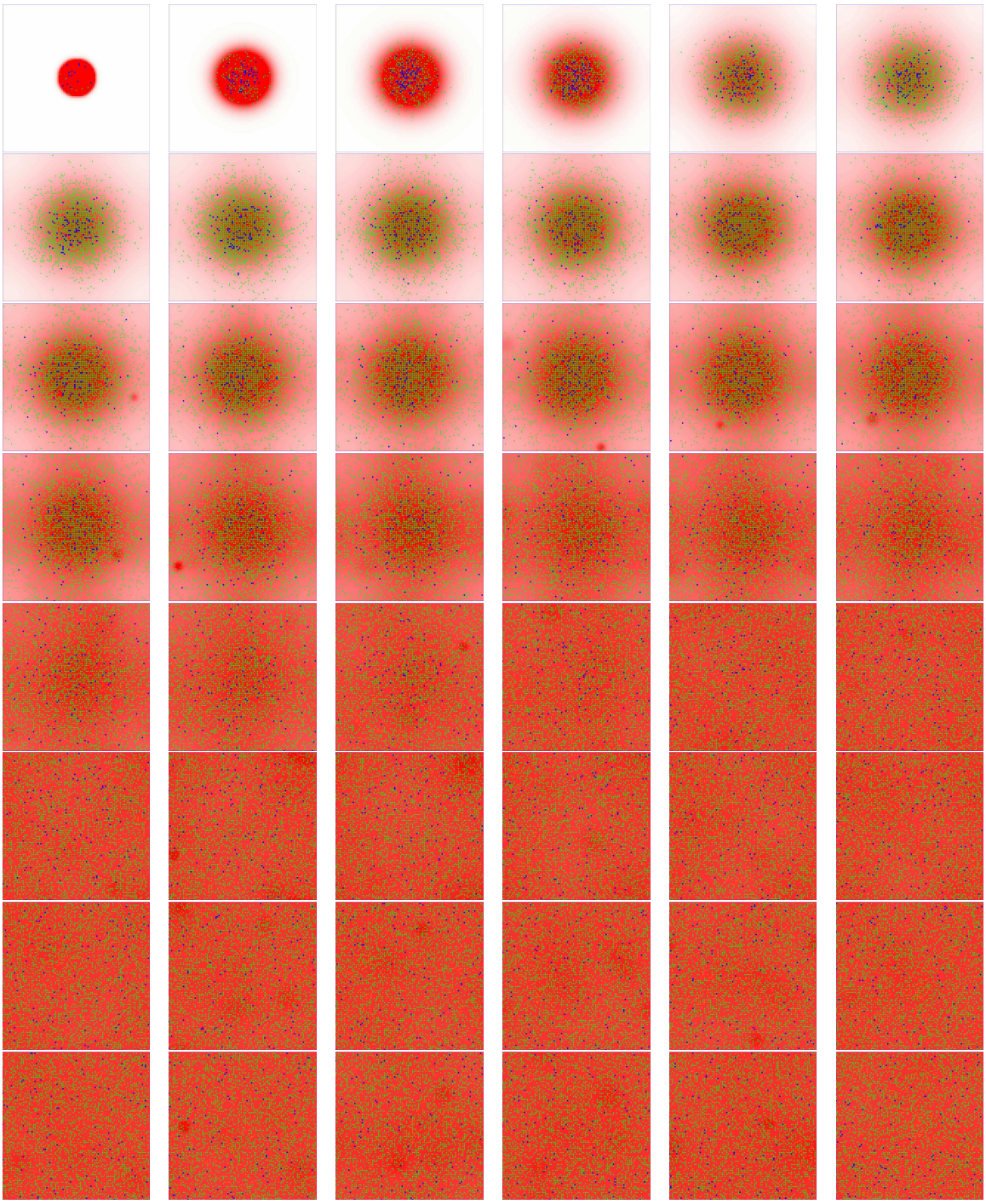

Figure 4.7: Simulation of the chronic outcome of the ABM running from $t = 0$ (upper left corner) to $t = 5000$ (bottom right corner), with parameters as in the second column of Table 4.4. Macrophages are represented with blue circles, active neutrophils with green triangles and apoptotic neutrophils with orange triangles.

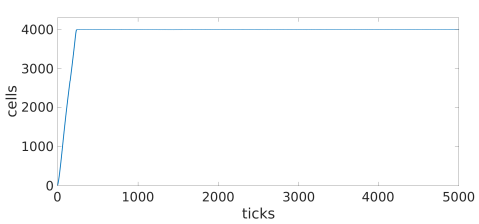

(a) Active neutrophils.

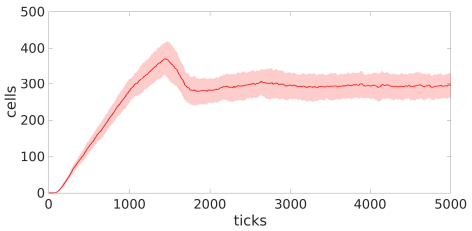

(b) Apoptotic neutrophils.

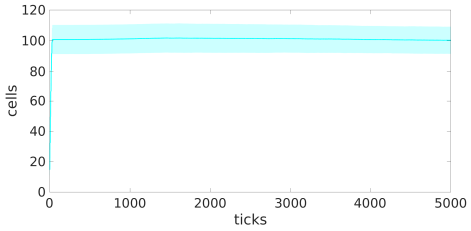

(c) Macrophages.

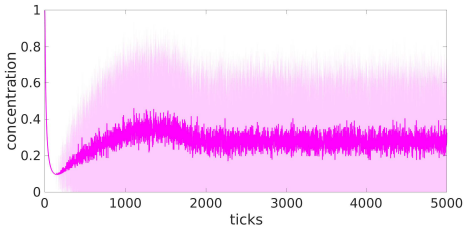

(d) Pro-inflammatory mediators.

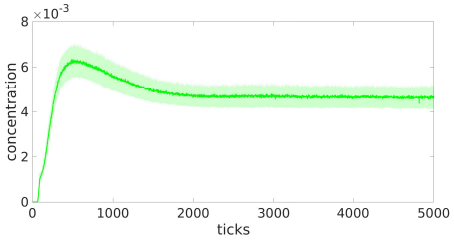

(e) Anti-inflammatory mediators.

Figure 4.8: Plots for the ABM corresponding to the average results of the batch of 100 simulations, with parameters as in the second column of Table 4.4. Shades around the plots represent standard deviations.

group of cells and mediators that could not otherwise be captured and analysed. Figures 4.8a and 4.8c in particular highlight how both neutrophils and macrophages exhibit a steady increase, rapidly settling to constant levels that are maintained throughout the simulations. Apoptotic neutrophils start appearing gradually with a delay corresponding to the lifespan of active neutrophils (Figure 4.8b). Inflammatory mediators present a different temporal pattern, in line with their specific biological behaviour. Figure 4.8d shows an immediate drop of pro-inflammatory mediators corresponding to the combined effect of diffusion and decay from the initial concentra-

tion modelling the damage. The levels of c are then sustained by neutrophils' activity, as prescribed by the background release of pro-inflammatory mediators provided by these cells and described in Section 4.2.4. Recurrent peaks of pro-inflammatory mediators signal the necrosis of an apoptotic neutrophil and the resulting spilling of its toxic content within the tissue, causing further disruption and promoting the pro-inflammatory activity. Conversely, anti-inflammatory mediators (Figure 4.8e) start appearing in the system only via mature macrophages, *i.e.* macrophages that have already phagocytosed apoptotic neutrophils and have thus undergone a change in phenotype. Such behaviour signals the active role of these leukocytes in promoting healing. The stable level of anti-inflammatory mediators observed in prolonged times of simulations is contrasted by the continuous recruitment of neutrophils and their pro-inflammatory activity that effectively counteracts the anti-inflammatory action. This results in an impaired healing process, with both cells and mediators maintaining high levels of concentration throughout, eventually preventing the resolution of inflammation. We note that, while the pro-inflammatory mediator concentration in Figure 4.8d occasionally approaches or reaches zero in some simulations, this does not signify a switch to a healthy outcome since (in all simulations) there is a sustained presence of both active and apoptotic neutrophils (Figures 4.8a and 4.8b), which result in damage persisting. As such, these low levels of pro-inflammatory mediators are not representative of emergent behaviours here.

4.4.2 Healthy outcomes

The crucial role of macrophages in promoting the resolution of inflammation (Hesketh *et al.*, 2017) suggests that, in order to model an effective healing process, leading to the resolution of inflammation, those parameters that regulate the anti-inflammatory mediators' action are key to switching the system's behaviour. Similarly, with neu-

trophils enhancing the pro-inflammatory activity, a careful modulation of the levels of neutrophils infiltrating the injured tissue emerges as decisive point of control for the resolution of inflammation (Ortega-Gomez *et al.*, 2013). As such, two main parameters from the ones listed in Table 4.3 are individuated to best tackle the disruption of the healthy state prompted by the physiological acute response and promote recovery, namely the threshold of pro-inflammatory mediators upon which neutrophils are recruited (α_{ncr}) and the threshold of pro-inflammatory mediators allowing recruitment of macrophages (α_{mr}). Furthermore, we also investigate the effects of the initial damage on the final outcome of the inflammatory response, by focusing on its severity, c_0, and its initial initial radius, r. Through manipulation of each of these parameters individually, we determine sets of key parameter values that act as switches between chronic and healthy scenarios, as highlighted in Table 4.4 and further detailed in the sections below.

Finally, we will investigate the efficacy of phagocytosis in the healing process, by assessing how the tuning of parameter p_{ma} impacts upon the resolution of inflammation.

Neutrophil recruitment

The careful assessment of repeated simulations resulting in non-resolved inflammation, as well as the biological evidences highlighting the prime role of active neutrophils in enhancing the release of pro-inflammatory mediators motivate us to focus our attention on the recruitment of these cells as a possible target for resolution of inflammation. Simulations reveal that increasing α_{ncr} from 0.05 to 0.1 results in a sufficiently reduced neutrophil recruitment to generate a healthy outcome. Figure 4.9 shows the initial trigger of acute inflammation, in response to the immediate release of pro-inflammatory mediators at the site of injury and its progression in time. Firstly, it is straightforward to observe how the resolution of inflammation is reached well

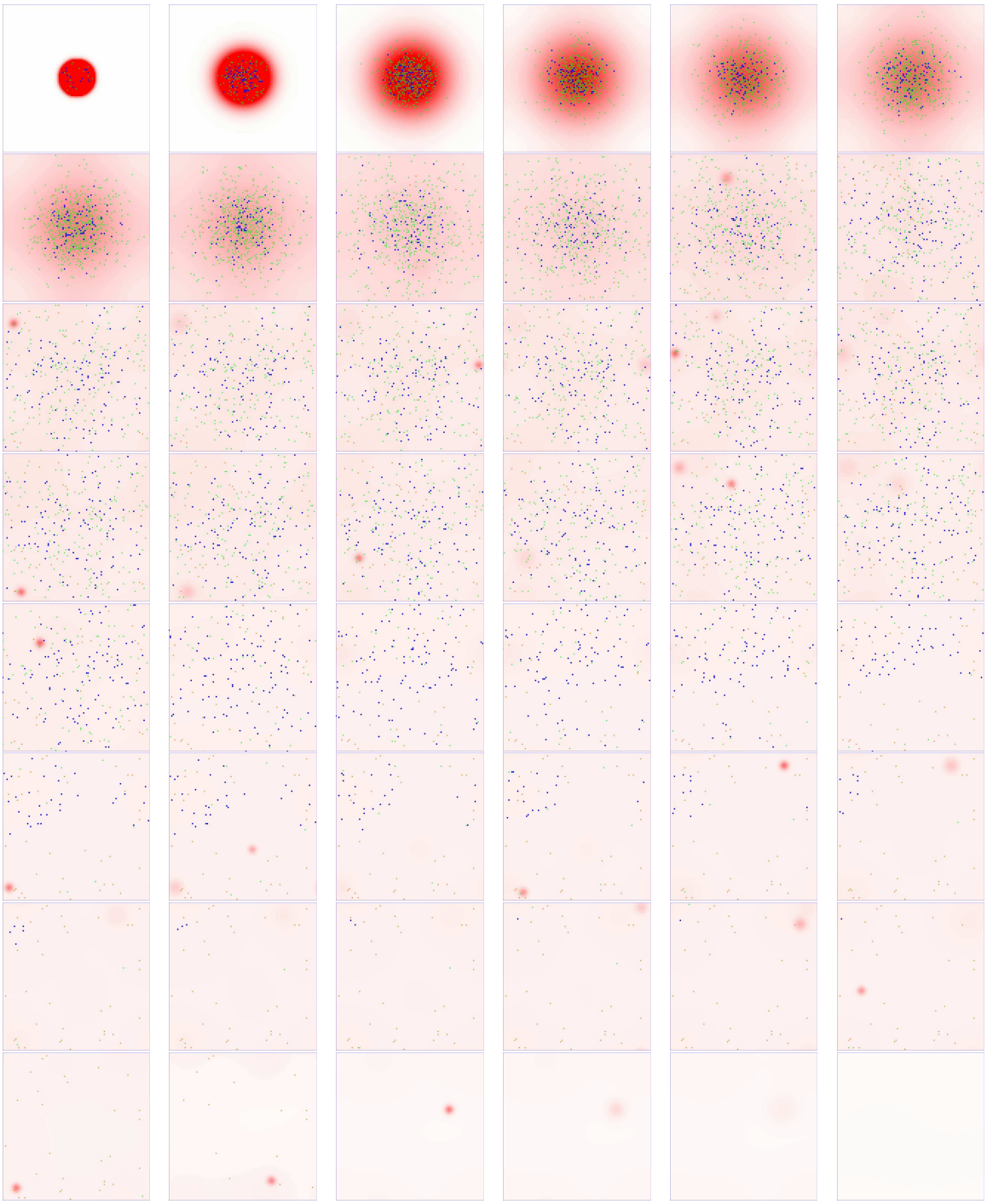

Figure 4.9: Simulation of of the chronic outcome of the ABM running from $t = 0$ (upper left corner) to $t = 5000$ (bottom right corner), with parameters as in the fifth column of Table 4.4, where $\alpha_{ncr} = 0.1$. Macrophages are represented with blue circles, active neutrophils with green triangles and apoptotic neutrophils with orange triangles. Increases in concentrations of pro-inflammatory mediators in red are gradually dampened by anti-inflammatory chemicals.

before the end of the simulation at $t = 5000$, as the last row of Figure 4.9 shows, with lower levels of pro-inflammatory mediators prompting the remaining macrophages to leave the tissue. When not phagocytosed in time, apoptotic neutrophils can also be seen undergoing necrosis and releasing additional quantities of pro-inflammatory mediators, as represented by the red bursts visible throughout Figure 4.9. The occasional necrosis of neutrophils does not prevent the overall resolution of inflammation thanks to the efficient recruitment and action of macrophages that preferentially move toward apoptotic cells. The controlled recruitment of neutrophils prevents a surge in the background level of pro-inflammatory mediators, with the increasing levels of anti-inflammatory mediators released by mature macrophages proving decisive in the healing process and final healthy outcome.

Similarly, simulations resulting from decreasing α_{ngr} from 0.015 to 0.0015 exhibit a resolved inflammatory outcome. Restoration of health is, in this case, prompted by lowering the threshold of anti-inflammatory mediators, g, that controls the recruitment of neutrophils. Thus, significantly smaller amounts of g are enough to signal the system is headed towards the resolution of inflammation and no new neutrophils are needed at the site of the original injury.

Overall, this dynamic balance between pro- and anti-inflammatory activity, obtained by adjusting the recruitment of neutrophils in response to local concentrations of c and g, eventually leans towards the anti-inflammatory mediators that prompt the resolution of inflammation and restoration of a healthy state.

Macrophage recruitment

Conversely, macrophages actively lead to the resolution of inflammation. Thus, from our simulations it emerges that decreasing the minimum threshold value of pro-inflammatory mediators required for the recruitment of macrophages to $\alpha_{mr} = 0.05$, *i.e.* enhancing the recruitment of macrophages, the system's behaviour switches from

a previously chronic outcome to the healthy one. In practice, as soon as the local concentration of c is above this updated threshold of $\alpha_{mr} = 0.05$ (less constraining than the original baseline value of $\alpha_{mr} = 0.25$), new macrophages are recruited, with their additional contribution of anti-inflammatory mediators eventually proving key to the resolution of inflammation.

Damage severity

As the baseline values reported in Table 4.4 suggest, an initial damage of radius $r = 10$ and concentration of pro-inflammatory mediators of $c_0 = 1$ is enough to prompt an inflammatory response, with the system yielding a perpetual inflamed state. In investigating the impact of the severity of the initial damage over the strength of the inflammatory response, we observe that upon a diminished quantity of pro-inflammatory mediators within the injured site the overall outcome can also be affected, prompting the restoration of a healthy state. As such, through simulations we determined that a decreased initial concentration of $c_0 = 0.5$, while keeping all other parameters unchanged, as visible in Table 4.4, is enough to ensure a healthy outcome.

Damage size

Similarly, by manipulating the radius of the initial damage, from a baseline set of parameter values resulting in a non-resolved inflammation, we can provide the system with a switch to a healthy outcome by only tuning the initial radius of the damage to $r = 5$. Thus, as reported in Table 4.4, halving the size of injury ensures the clearance of inflammation and restoration of the healthy state.

Phagocytosis

As already emerged in Section 1.2 and largely confirmed in the results from Chapter 2–3, the phagocytosing actions of macrophages and their role in clearing apoptotic neutrophils is key in the inflammatory process. In particular, analogously to the analysis of the previous PDE model in which a specific focus was put on the effects of parameter ϕ accounting for the rate at which macrophages phagocytose apoptotic neutrophils, we here investigate the impact of parameter p_{ma}, which represents the probability of the phagocytosing action. By considering each of the parameter sets that results in a healthy scenario, as reported in Table 4.4, we reassess and compare the results yielded by tuning the probability of phagocytosis to $p_{ma} = 0.01$, from its original baseline value of $p_{ma} = 1$. In doing so, we drastically affect the macrophage efficiency in clearing apoptotic neutrophils, with expecting deteriorating results to the inflammatory outcome. Interestingly, all simulations with either set of parameters ensuring restoration of the healthy state, when run with the updated value of parameter $p_{ma} = 0.01$ continued to guarantee the complete resolution of inflammation with the introduction of a considerable delay in the healing process. The longer healing times are caused by the drastic inhibition of the phagocytic action of macrophages that move preferentially toward apoptotic neutrophils and when fetching them are not able to immediately engulf them. In fact, in this new scenario, phagocytosis happens with probability $p_{ma} = 0.01$, thus causing a delay between the time a macrophage moves to and reaches an apoptotic neutrophil and the time that probability p_{ma} is met, when the former can finally phagocytose the latter. These delays accounted for an approximate number of 500 ticks, with the overall healing period varying depending on the specific healthy scenario that was being tested, as detailed in table. It should be noted that the timespans reported in Table 4.5 provide approximate intervals and not exact durations of simulations. This further highlights

	Approximate standard healing time (ticks)	Approximate delayed healing time (ticks) (via $p_{ma} = 0.01$)
Healthy outcome (via damage severity)	$1500 - 2000$	$2500 - 3000$
Healthy outcome (via damage size)	$1000 - 1500$	$1500 - 2000$
Healthy outcome (via neutrophil recruitment over c)	$1000 - 1500$	$1500 - 2000$
Healthy outcome (via neutrophil recruitment over g)	$3000 - 3500$	$3500 - 4000$
Healthy outcome (via macrophage recruitment)	$2000 - 2500$	$2500 - 3000$

Table 4.5: Approximate healing times upon individual tuning of selected parameters.

the random component in the ABM paradigm, marking a strong difference with the PDE modelling approach in which all the analyses, even upon repeated simulations, yields strictly deterministic results.

4.4.3 Discussion

In addition to exposing the role of the effects of phagocytosis on the inflammatory response, Table 4.5 also provides an assessment of the efficacy of each individual parameter in the resolution of inflammation, namely those accounting for the initial damage (c_0 and r) and the ones modelling the recruitment of leukocytes (α_{ncr}, α_{ngr} and α_{mr}) as possible therapeutic targets and their benefit in terms of healing times. In particular, we can conclude that therapies acting on the controlled recruitment of neutrophils and the enhanced recruitment of macrophages can potentially have a dramatic impact on the outcome of the acute inflammatory response, prompting the restoration of the healthy state in an otherwise chronic scenario. Furthermore, as shown in Table 4.5 the effectiveness of the manipulation of the recruitment of

neutrophils (through parameter α_{ncr}) appears to be slightly more beneficial in terms of healing time, compared to the tuning of parameter α_{mr}. Conversely, the impact of manipulation of parameter α_{ngr}, while still effective, is considerably delayed compared to other parameters. Similarly, our results suggest that strategies acting on limiting the initial damage, both in size and severity, can prove determinant in preventing inflammation from becoming chronic. This, while not providing an immediate therapeutic target in terms of pharmacological action, points at the importance of controlling the initial tissue damage, which, in case of sterile inflammations such as in the scope of our models, has a direct impact on surgical techniques and strategies to reduce the inevitable tissue injury upon surgery as much as possible.

The manipulation of the parameters key to the resolution of inflammation, as detailed in Table 4.4, results in simulations where the initial damage is effectively tackled, limited in spread and eventually resolved, as represented in Figure 4.9 where healing is prompted via regulation of neutrophils' recruitment, effectively fixing either $\alpha_{ncr} = 0.1$ or $\alpha_{ngr} = 0.0015$. Simulations of the remaining healing scenarios reported in Table 4.4, namely the ones obtained by decreasing the damage size (r) and severity (c_0) and the ones achieved by improving the macrophage recruitment (α_{mr}) and neutrophil recruitment via g (α_{ngr}), provide visually similar results in terms of final outcome to the one showed in Figure 4.9 referring to the manipulation of parameter α_{ncr}. They vary though in the overall healing times, with the average total number of ticks required for the inflammation to be cleared and resolved differing from one scenario to the other, as already discussed and reported in Table 4.5. Interestingly, we also observe variations in the number of cells recruited and concentrations of mediators involved. These differences are illustrated in Figure 4.10, where results from each set of simulations are averaged and compared. The results shown in Figure 4.10 provide a temporal analysis of the concentrations of both groups of cells and chemicals and, while neglecting the spatial distribution of agents, offer nonetheless a

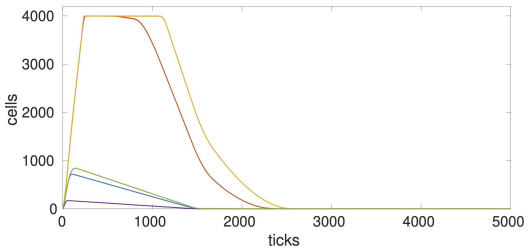

(a) Active neutrophils.

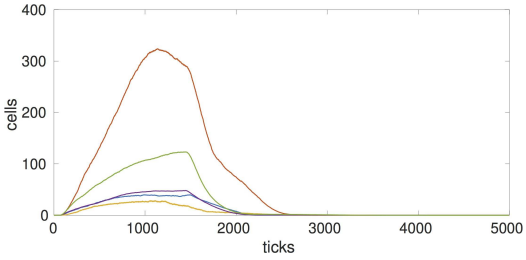

(b) Apoptotic neutrophils.

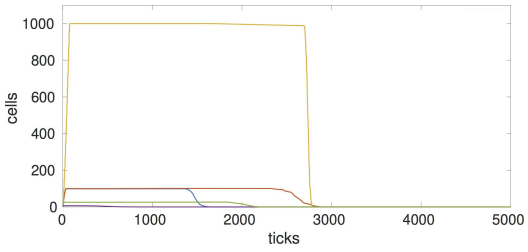

(c) Macrophages.

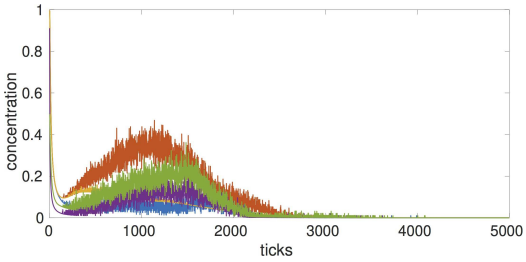

(d) Pro-inflammatory mediators.

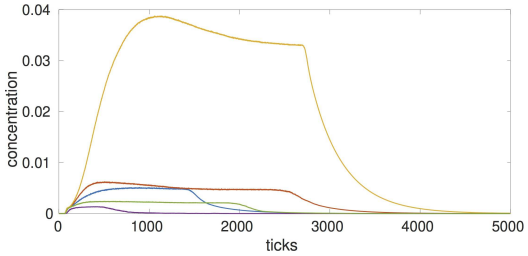

(e) Anti-inflammatory mediators.

Figure 4.10: Plots for the ABM corresponding to the average results of batches of 100 simulations, with resolution obtained by increasing α_{ncr} from 0.05 to 0.1 (blue), decreasing α_{ngr} from 0.015 to 0.0015 (red) and decreasing α_{mr} from 0.25 to 0.05 (yellow), r from 10 to 5 (purple) and c_0 from 1 to 0.5 (green); all other parameters as in the second column of Table 4.4.

valuable assessment of the progression and final outcome of the acute inflammatory response by highlighting the tight interactions between leukocytes and mediators. Firstly, we observe that the overall healing profiles, achieved via manipulation of α_{ncr}, α_{ngr}, α_{mr}, r and c_0 respectively, share specific patterns in terms of dynamics. In particular, we observe how the number of active neutrophils (Figure 4.10a) at each tick is closely followed by that of apoptotic neutrophils (Figure 4.10b), as expected, since all active neutrophils eventually undergo apoptosis. The macrophagic activity (Figure 4.10c) on the other hand is expressed in response to the presence of both apoptotic neutrophils and pro-inflammatory mediators. This explains why peaks of macrophage presence within the inflamed tissue are delayed compared to active neutrophils. Conversely, the pro-inflammatory mediator concentration is enhanced in correspondence to those apoptotic neutrophils that become necrotic before being effectively phagocytosed by macrophages, thus releasing their toxic content and further promoting the inflammatory activity. This is well reflected in Figure 4.10d in which the surge in concentration of pro-inflammatory mediators follows the same timescale pattern of the increase in apoptotic neutrophils. Finally, the production and release of anti-inflammatory mediator is actively promoted by the phagocytosis of apoptotic neutrophils by macrophages. Thus, Figure 4.10e should be read as the result of the joint interaction of these two agents that eventually leads towards the resolution of inflammation, with all the variables plotted in Figure 4.10 exhibiting zero concentrations by the end of the simulation at $t = 5000$ accordingly.

Additionally, interesting differences emerge with respect to each healing strategy employed. In particular, Figure 4.10 shows how decreasing the size of the initial damage r is the most effective target, as represented by the plots in yellow, with the number of active neutrophils and macrophages involved being minimised and the anti-inflammatory response being in turn of a considerably lower scale. Adjustments to neutrophils' recruitment (α_{ncr}, plotted in blue) and the decrease in the initial damage

severity (c_0, plotted in purple) provide instead similar benefits in terms of healing times and levels of cells and mediators involved, but are sensibly larger than the results achieved via manipulation of r. Finally, while still effective in resolving inflammation, changing the value accounting for the recruitment of macrophages through parameter α_{mr}, provides an inflammatory response of a considerably larger scale, with respect to both healing times and concentrations of leukocytes and mediators featured, as shown in the plots in red.

4.4.4 Comparison with the PDE model of Chapter 3

Given that the modelling approach proposed by the ABM paradigm is substantially different to the one offered by PDEs, it is interesting to compare the results provided by both sets of models. To this end, Figures 4.11–4.12 present a combination of results from the inflammation model described in Chapter 3 and the ABM introduced in this chapter. Both models depend on sets of parameters representing the main cellular and chemical interactions; the accurate tuning of some sensitive and biologically significant ones provides different outcomes in terms of the resolution of inflammation, as shown throughout Chapters 3–4. We note, here, that the model of Chapter 3 and the ABM constructed in this chapter operate on very different spatial scales: the model of Chapter 3 is applied on a square domain of width 10 cm, while the ABM of this chapter uses a smaller domain of width 2 mm (as discussed in Section 4.3). For this reason, the numbers of cells reported for the PDE model of Chapter 3 are typically at least one order of magnitude higher than those of the ABM in Figures 4.11–4.12.

Figure 4.11 combines results from Figures 3.9 (by appropriately rearranging the data and plotting at each time step the total number of cells and the maximum concentration of mediators) and 4.10, from the PDE and ABM simulations respectively. While the plots for each cellular and chemical group do not overlap exactly, the over-

all behaviour is similar in presenting a surge in each variable upon injury and their eventual dampening, with the restoration of a healthy state. Similarly, Figure 4.12 compares simulations from Figures 3.11 and 4.8. The immediate visual comparison between the two sets of plots is straightforward in highlighting the persistent high levels of both white blood cells and inflammatory mediators, typical of chronic inflammation. More importantly, regardless of the modelling approach, the outcome of these simulations is directed and controlled by a careful manipulation of the models' parameters. As such, the PDE model's outcome (left panel) is obtained by tuning the parameters accounting for the rate at which active neutrophils undergo apoptosis (ν). Simulations of the ABM yield the chronic outcome by changing either of the parameters that act as switch between resolved and chronic outcomes, namely the threshold of pro-inflammatory mediators upon which new neutrophils and macrophages are recruited (α_{ncr}, α_{ngr} and α_{mr}), and the damage size and severity (r and c_0 respectively). In particular, it is crucial to observe that in both the PDE and the ABMs, the inflammation outcome changes from a healthy state to a chronic one by manipulating the neutrophil activity, which in turns affects the release of pro-inflammatory mediators and the level of disruption within the tissue. The mechanisms are specific to the modelling approach, with the PDE model highlighting the role of apoptosis through manipulation of parameter ν and the agent based model with respect to parameters α_{ncr} and α_{ngr}, controlling the recruitment of neutrophils instead.

Analogously, both the PDE and the ABM are susceptible to the regulation of macrophage activity, as addressed in Chapter 3 with respect to the phagocytosing rate ϕ and in Section 4.4.2 of the current chapter via parameter α_{mr} controlling the macrophage recruitment, respectively. Therefore, qualitatively comparable results between the two models are similarly achieved by tuning the macrophagic activity, which directly controls (by either delaying or impairing) the anti-inflammatory mediators action. This aspect highlights the importance of neutrophil's controlled recruitment

and apoptosis on one hand and of macrophages on the other hand in terms of possible therapeutic targets, in addition to the sensible beneficial effects achieved by minimising the initial damage size and severity. This suggests that the manipulation of both the action of leukocytes and the containment of tissue injury could be key to restoring a healthy state and preventing the chronic state of inflammation.

4.5 Parameter sensitivity analysis

In order to provide an exhaustive assessment of the model capabilities and analyse its dependence on individual parameters, we perform a parameter sensitivity analysis. The aim of such study is to individuate parameters that have a key impact on the model's outcome, while also highlighting the marginal role of those remaining parameters whose variation does not significantly affect the system's behaviour.

4.5.1 Set up

We consider the standard chronic outcome outlined in Section 4.4.1 as our reference simulation and investigate, through a systematic set of simulations where individual parameters are changed one at time, differences arising in the final outcome of the inflammatory response. We outline a set of parameter values to be tested with the aim to assess the model's response to significant increases and decreases of each parameter with respect to the reference set of parameter values listed in the second column of Table 4.4. For each parameter individually, increases and decreases of 50% of the reference value are considered. The resulting set of values tested is listed in Table 4.6, with the second column reporting the reference chronic values for convenience and the third and fourth columns exhibiting decreased and increased values respectively. The outline in Table 4.6 provides a guide to the simulations performed for the sensitivity analysis, where the model is systematically set up with all combinations of

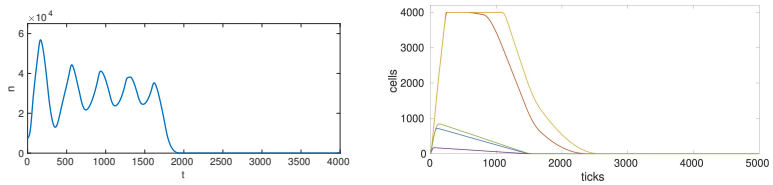

(a) Active neutrophils.

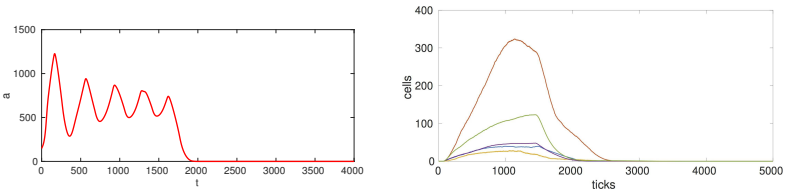

(b) Apoptotic neutrophils.

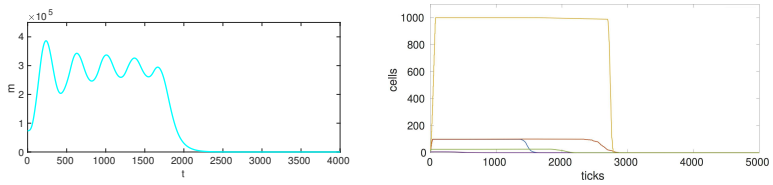

(c) Macrophages.

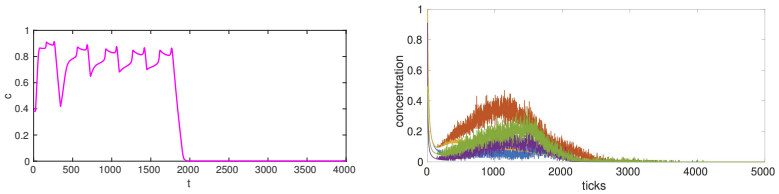

(d) Pro-inflammatory mediators.

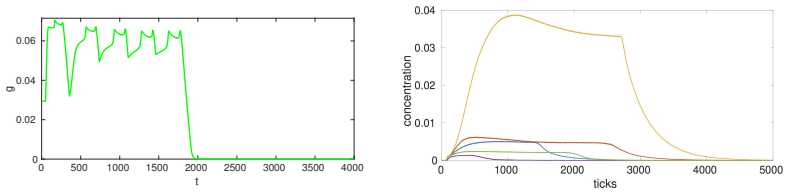

(e) Anti-inflammatory mediators.

Figure 4.11: Left panels: solution of (3.7–3.11, 3.29), with parameters as in Table 3.2. At each time step, we plot the global cell counts and the maximum concentration of mediators. Right panels: plots for the ABM corresponding to the average results of batches of 100 simulations, with parameters as in the third (green), fourth (purple), fifth (blue), sixth (red) and seventh (yellow) columns of Table 4.4.

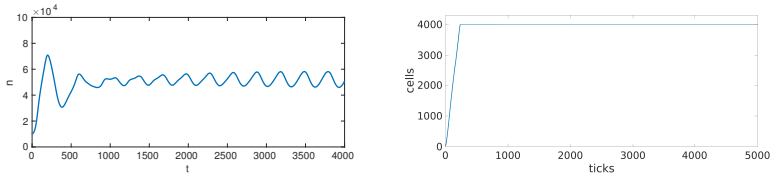

(a) Active neutrophils.

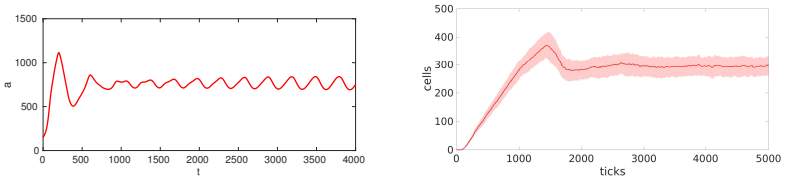

(b) Apoptotic neutrophils.

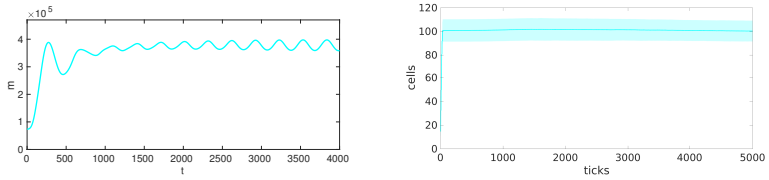

(c) Macrophages.

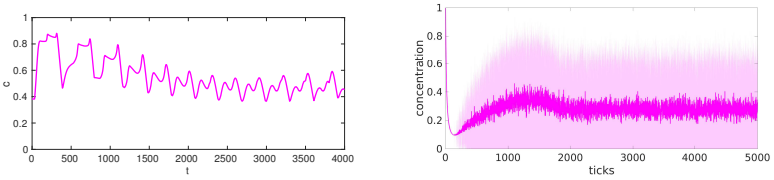

(d) Pro-inflammatory mediators.

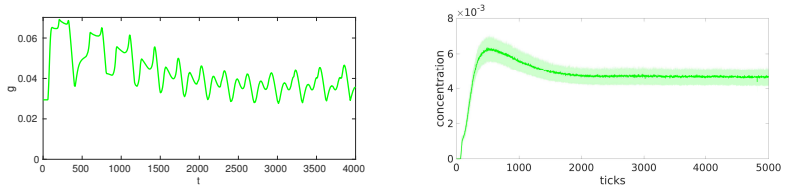

(e) Anti-inflammatory mediators.

Figure 4.12: Left panel: solution of (3.7–3.11, 3.29). At each time step, we plot the global cell counts and the maximum concentration of mediators. The rate of neutrophil apoptosis is updated to $\nu = 0.075$, all other parameters are as in Table 3.2. Right panels: plots for the ABM corresponding to the average results of the batch of 100 simulations, with parameters as in the second column of Table 4.4.

parameters resulting from the reference column and each of the updated parameter values one at time. It is important to observe that parameter δ_{ac}, accounting for the increment of pro-inflammatory mediators in response to apoptotic neutrophils' necrosis, is excluded from the parameter sensitivity analysis. This is due to δ_{ac} being the parameter with respect to which all other parameters are scaled, as detailed in Section 4.3. Additionally, as is visible in Table 4.6, parameter p_{ma}, representing the probability of macrophages to phagocytose apoptotic neutrophils, is only tested in terms of a decrease from its reference value, since the baseline chronic value of $p_{ma} = 1$ is already maximal. The total global concentration of mediators and the number of neutrophils are monitored over 5000 ticks, collected and saved as output in order to be compared against the reference data. In particular, we record the percentage change in these two measures in comparison to the reference data.

4.5.2 Analysis

In order to take into account the randomness within the ABM framework, both the reference simulation and each set of test simulations are analysed over a batch of 100 runs. Upon selection of a timepoint of interest t_p, each set of data is averaged. Variations over single batches of simulations are computed with respect to the percentage change compared to the reference simulation. Figure 4.13 shows the results corresponding to each combination of parameter values from Table 4.6. Simulations corresponding to parameter decreases are marked by red downward-pointing triangles. Conversely, simulations for parameter increases are marked by green upward-pointing triangles. Here, all results are reported at the final tick, so $t_p = 5000$ throughout.

Parameter	Reference values (Chronic outcome)	Decreased values (−50% of reference value)	Increased values (+50% of reference value)
c_0	1	0.5	1.5
r	10	5	15
D_c	1.5	0.75	2.25
D_g	1.5	0.75	2.25
γ_c	0.002	0.001	0.003
γ_g	0.002	0.001	0.003
δ_{nc}	0.001	0.0005	0.0015
δ_{mg}	0.001	0.0005	0.0015
p_{nr}	0.02	0.01	0.03
p_{nc}	0.5	0.25	0.75
p_{mr}	0.04	0.02	0.06
p_{mg}	0.8	0.4	1
p_{ml}	0.8	0.4	1
p_{ma}	1	0.5	n/a
α_{ncr}	0.05	0.025	0.075
α_{ngr}	0.015	0.0075	0.0225
α_{mr}	0.25	0.125	0.375
α_{ml}	0.02	0.01	0.03

Table 4.6: Parameter values for the reference chronic outcome (second column) and for sensitivity study with values to be tested representing decrease in half of reference value (third column) and increase in half of reference value (fourth column).

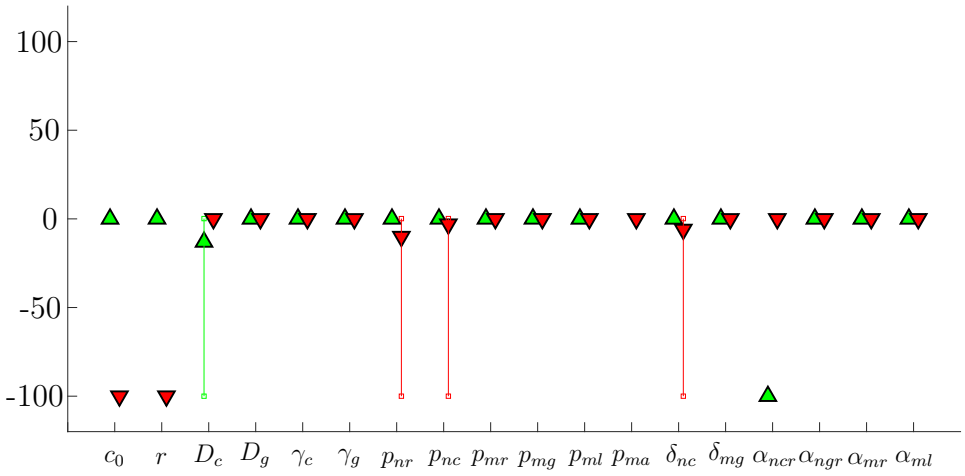

(a) Active neutrophils.

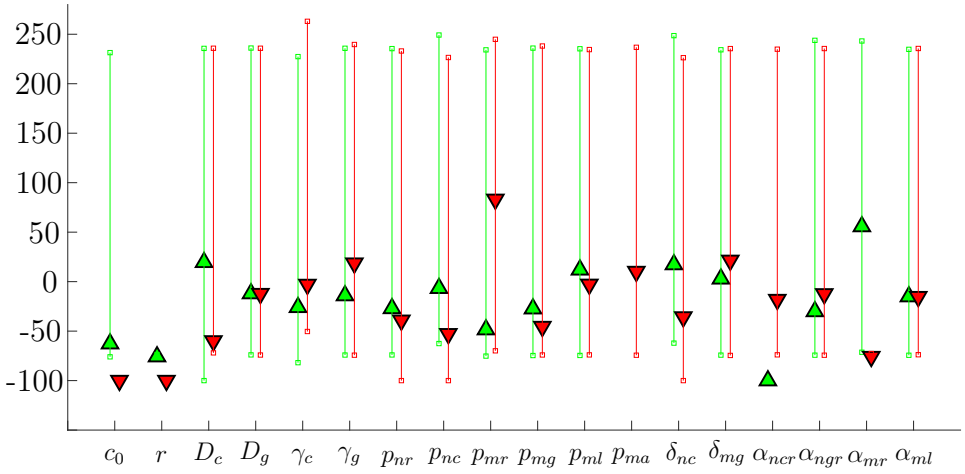

(b) Pro-inflammatory mediators.

Figure 4.13: Parameter sensitivity analysis results showing the percentage change in (a) the number of active neutrophils and (b) the concentration of pro-inflammatory mediators, both with respect to the reference chronic simulation at final tick $t = 5000$, for variations of individual parameters. Green and red triangles represent 50% increases and decreases respectively. Bars indicate change in minimum and maximum changes in percentage over 100 simulations for each parameter. Note that a change in response of -100% corresponds to a switch from a chronic to a healthy outcome.

4.5.3 Discussion

The data collected in the simulations run for the parameter sensitivity study are rich and of complex interpretation, as is evident from the results in Figure 4.13. In particular, the total concentrations of pro-inflammatory mediators and the total number of active neutrophils inform differently upon the acute inflammation outcome. Since the data resulting from each batch of simulations is plotted in terms of percentage changes with respect to the chronic reference, we are interested in the markers' divergence from the chronic baseline at zero. Thus, upward deflections from such baseline correspond to worsening inflammatory conditions, since they represent higher concentrations of mediators and higher numbers of cells involved. Conversely, downward deflections represent improvements in the inflamed tissue, with the presence of lower amounts of mediators and cells compared to the reference data. In this sense, the analysis of Figure 4.13a provides a neat interpretation of the tissue's health state at the end of the simulations at tick $t = 5000$. Markers aligned at zero indicate the absence of any discrepancy with the reference data, meaning that the tested parameter did not change the model's final outcome toward neither healing nor worsening conditions. More importantly, overlapped upward and downward triangle markers highlight how increases and decreases of a specific parameter are irrelevant to the model's overall behaviour. Conversely, markers aligned at -100 indicate a decrease of 100% in the final amount of active neutrophils at tick $t = 5000$ with respect to the reference chronic data, pointing at the resolution of inflammation.

Observing Figure 4.13a, the key parameters affecting the system's outcome and providing a drastic switch from chronic inflammation to its resolution are immediately individuated as c_0, r and α_{ncr}. In particular, a decrease in half from the reference value for either of the parameters controlling the initial damage (*i.e.* its severity c_0 and its radius r), results in the complete resolution of inflammation. Similarly, health

is restored upon an increase in half of the nominal value of parameter α_{ncr} controlling the recruitment of active neutrophils. These results are in complete agreement with the corresponding analysis presented in Section 4.4.2. A notable discrepancy emerges with respect to the system's sensitivity to parameter α_{mr}, controlling the recruitment of macrophages, which does not appear to be determinant in the model's outcome when decreased by half of its reference value $\alpha_{mr} = 0.25$, but is proved to provide a switch from chronicity to health when set at a considerably lower value of $\alpha_{mr} = 0.05$, as presented in 4.4.2. The apparent incongruity on the role of parameter α_{mr} arises from forcibly pushing the system toward resolution through a decrease of 80% from the reference chronic value of α_{mr}, while a decrease in 50% of its nominal value does not provide any sensitive anti-inflammatory impact.

Similarly, the role of parameter α_{ngr} as a possible switch between chronic and resolved outcomes is not entirely caught by the parameter sensitivity analysis. As exposed in Section 4.4.2, a significant decrease in the threshold value controlling the recruitment of neutrophils upon levels of anti-inflammatory mediators is necessary in order to push the system toward resolution. Such variation is in order of 90% from the chronic reference of 0.015 to the updated 0.0015 and does thus not feature in the sensitivity analysis results, where variations of $\pm 50\%$ are only considered.

As already highlighted in Section 4.4.3, within this model, parameters α_{ncr}, α_{ngr} and α_{mr} are individuated as possible therapeutic points of control, suggesting that their manipulation via targeted drugs could be beneficial to the resolution of inflammation. From the additional parameter sensitivity analysis we further infer that such drugs would have a stronger impact when aimed at the recruitment of neutrophils and, conversely, an enhanced action on the recruitment of macrophages is required for the resolution of inflammation.

More interesting points of discussion emerge from observing Figure 4.13a, focusing on the system's behaviour when increasing the diffusion of pro-inflammatory

mediators D_c and upon decreasing the probability of recruiting neutrophils p_{nr}, the probability of neutrophils to release pro-inflammatory mediators p_{nc} or the increment in pro-inflammatory mediators by neutrophils δ_{nc}. In particular, the markers for these specific tested parameters are very closely aligned to the reference data, indicating the persistence of the chronic outcome, but exhibiting significant variations that signal the occasional resolution of inflammation in a fraction of the batch simulations. This is significant in highlighting once more the non-deterministic nature of the ABM framework, which thus results better suited to describe complex biological processes whose nuanced interactions are not always captured in full by the deterministic approaches provided by ODEs and PDEs.

The parameter sensitivity analysis on pro-inflammatory mediators (4.13b) presents a more complex result. In particular, the main considerations about the decreases in key parameters c_0, r and increase in α_{ncr} are retained, with the respective markers aligned at -100, thus indicating a switch from the chronic reference outcome to full recovery. Conversely, the level of inflammation severity with respect to the chronic baseline is of more difficult interpretation, with most markers presenting a significant divergence from the reference data. The high variations provide an understanding for such behaviour, explaining the strong variability in the concentration levels of pro-inflammatory mediators at every stage of inflammation, depending in first instance by the presence of active neutrophils which provide a continuous background release (as explained in Section 4.2.4) and more importantly to the surges of c upon necrosis of apoptotic neutrophils (as described in Section 4.2.5). Thus, overall, levels of global concentrations of pro-inflammatory mediators appear to be more informative in terms of the severity of inflammation, rather than being an indicator for its resolution.

Another important observation arising from the parameter sensitivity analysis is with respect to probabilities. In particular, as evident from the results in Figure 4.13, the model is largely insensitive to choices of most probabilities, thus overcoming the

biological uncertainty in identifying suitable values for such parameters.

4.6 Conclusions

In this chapter we introduced a new modelling framework, defining the ABM paradigm and presenting related applications of biological relevance. We then proceeded to model acute inflammation taking into account the response of white blood cells, differentiating between neutrophils and macrophages and their action, as well as that of both pro- and anti-inflammatory mediators. Both groups of leukocytes of the ABM implement chemotaxis and direct their motion within the domain accordingly. The system's behaviour, including that of each group of agents, is controlled through parameters that can be tuned to simulate both healthy and unresolved outcomes of the inflammatory event. Key parameters around which such behaviour is modulated find a direct correspondent both biologically and with respect to the PDE model of Chapter 3, to which a comparative analysis in terms of results was also carried out. A key result from this novel model is that of accounting for cells individually while also retaining the diffusive and chemotactic behaviours introduced in the previous chapter. This better reflects the heterogeneous response of cells that exhibit varied responses according to their location and particular environment, rather than acting as a homogeneous group as implied in the definition of the PDE model.

The main focus of our analysis has been on highlighting how parameters of high biological significance, namely the size and severity of damage and the efficiency of leukocyte recruitment, can have a determining impact on the inflammatory outcome, acting as a switch between healthy and chronic scenarios. We also investigated the effects of phagocytosis on the healing process, assessing recovery times in correspondence of the tuning of the parameter controlling the likelihood of macrophages effectively clearing apoptotic neutrophils. This detailed analysis allowed us to individ-

uate these biological interactions as key targets for possible therapeutic interventions, suggesting tailored strategies for drugs either enhancing macrophage recruitment or controlling neutrophil recruitment and surgical procedures at aiming in minimising size and severity of the tissue damage. Additionally, our analysis shows that all these strategies would be sensibly affected in terms of recovery times upon macrophages impaired phagocytosing action. Finally, a parameter sensitivity analysis was performed, to gain further insight into the role of individual parameters in controlling the system's behaviour. In response to systematic increases and decreases of parameter values from their reference chronic set, the model results are robust to variations of the probabilities regulating leukocytes' behaviour and to inflammatory mediators' increments, diffusivity and decay rates. Conversely, manipulation of parameters controlling the initial damage and cells' recruitment have a regulatory action on the system's outcome in terms of resolution of inflammation. This is also in accordance with the results presented in earlier Sections 4.4.2–4.4.3 and further suggests the benefits of targeting tissue damage and neutrophil recruitment as key mechanisms of the inflammation's outcome. In this regard, an important observation emerges from the impact of cell's recruitment, with the parameter sensitivity analysis exposing the system's stronger response to recruitment of neutrophils than macrophages. Evaluating this result in terms of therapeutic targets, drugs aiming at controlling macrophage's recruitment would need an enhanced action to tackle effectively inflammation and promote its resolution.

We note that, in this model, there is a degree of choice over the exact manner in which a tick of the model is defined. For convenience, we have assumed that all cellular decisions are implemented every tick, with the exception of the recruitment of neutrophils and macrophages, which we recruit every two and five ticks respectively in order to account for delays in cell recruitment *in vivo*. We note that the definition of a tick in the agent-based component of our model does not impact upon

the numerical solution of the PDEs describing mediator concentrations, since the numerical timestep used to solve these PDEs is implemented separately, with multiple numerical timesteps occurring per tick. It is well-known that neutrophils are recruited more rapidly than macrophages *in vivo*, which motivates our choices of recruitment frequencies used here; however, it is intuitive to expect that variations in these recruitment frequencies could have an impact upon the results obtained. Naïvely, we may expect more frequent neutrophil recruitment to move the model toward chronic outcomes, while more frequent macrophage recruitment may promote restoration of health. However, since the pro- and anti-inflammatory effects of these cells are delicately connected, the effects of varying these parameters may be somewhat more complex. We briefly revisit the question of how the scheduling of cell recruitment impacts upon model observations in the following chapter.

Going forward in our analysis we aim to capture with greater detail the chemotactic mechanisms that drive the motion of leukocytes, in order to help elucidate its role within the physiologic inflammatory response and individuate points of control to prevent impairment and defects in cells' collective motility.

Chapter 5

An enhanced model of directed neutrophil motility

In this chapter our objectives focus on modelling chemotaxis with greater detail, by calibrating our model against available experimental data and to evaluate the impact of the improved leukocytes motion within the inflammatory ABM. We further aim to investigate the inflammatory pathology Chronic Obstructive Pulmonary Disease (COPD) as a case study for model validation.

Numerous inflammatory conditions are associated with aberrant migration of neutrophils, in particular, while detrimental changes in neutrophil migration have also been observed in ageing, with neutrophils generally exhibiting reduced chemotaxis (Wagner & Roth, 1999; Sapey *et al.*, 2014b; Jasper *et al.*, 2019). The in-vitro study of Sapey *et al.* (2011) used time-lapse photography to record trajectories of healthy and COPD-affected neutrophils migrating up gradients of interleukin-8 (IL-8), demonstrating that healthy neutrophils chemotax more efficiently, while impaired neutrophils can have weaker sensitivity to the local chemoattractant gradient, which we associate with an impaired ability to resolve tissue damage. We use the quantitative measurements of directed neutrophil motility given by Sapey *et al.* (2011) to

calibrate our description of leukocyte chemotaxis in the model presented below.

To include a novel calibrated description of chemotaxis, we will firstly introduce biological aspects of cells' directed motion, particularly focusing on leukocyte migration under physiological conditions. After a brief review of the relevant literature in terms of both experimental and mathematical models of cell motility, an agent-based model of neutrophil migration under a chemoattractant source is presented and thoroughly analysed, with the aim to simulate and replicate experimental data obtained from the available literature, with key parameters providing a switch between healthy and pathogenic scenarios. In particular, our main focus is comparing cell walks exhibited by our model to appropriate experimental data. We further characterise the model of neutrophils' directed motion in terms of balance between chemical attraction to a source of mediators and cells' persistence of motion. The aim for such characterisation directly arises from the observed features of leukocyte migration, as laid out in the work of Foxman *et al.* (1999). More in detail, we model cells' directed motion in terms of *biased persistent random walk*, to best describe the *in vivo* leukocyte migration described in Taylor *et al.* (2013). Finally, we investigate the implications of impaired chemotaxis on inflammatory mechanisms.

5.1 The biology of cell motility

Cell migration is an essential feature of living organisms, characterising embryogenesis and directly affecting and regulating morphogenesis and inflammation. The organised collective motion cells exhibit persists also in adult organisms and constitutes a key aspect of a variety of physiological processes, including tissue homeostasis and immune responses, amongst others, as well as being essential to many biotechnology applications such as tissue-engineered scaffolds and cellular transplantation. Crucially, cell migration plays a fundamental role also in pathology, acting as a driv-

ing factor for different diseases such as cancer spread, chronicisation of inflammation, mental disorders, arthritis and atherosclerosis (Ridley *et al.*, 2003). Given the dual nature of this phenomenon, with single cells responding to molecular and physical stimuli but also acting in group towards a global directed movement, biologically the motion of cells can be described and analysed with respect to both single-cell and collective cell migration.

Mechanically, a cell moves through a cyclic set of actions characterised by polarisation (in response to extracellular signalling), membrane extension, adhesion of protrusions, contraction, traction and adhesion detachment (Horwitz & Webb, 2003; Lauffenburger & Horwitz, 1996). The velocity and distinctiveness of these stages depend on the cell type, with leukocytes in particular exhibiting a smooth and quick drift over the substratum of migration. The source of polarisation triggering cellular directed motion can vary in nature, with local gradients associated with either chemokinetic (upon variations of the receptor-ligand interface), haptotactic (with concentrations of chemical attractants expressed by the substrate) or chemotactic stimuli (Horwitz & Webb, 2003). The transduction of the relevant signalling internally to the cell results in the physical modifications at the membrane that allow for the movement, with the development of protruding structures known as lamellipodia (broad and flat) and filopodia (thin and cylindrical) that mediate the adherence and detachment of substratum adhesion (Lauffenburger & Horwitz, 1996; Lodish *et al.*, 2008). The attachment site provides a firm focal adhesion between the cell's membrane protrusions and the substrate, leading the way to the cell body translocation through consecutive contraction and traction forces between cell and substratum adhesion points. The practical movement is thus achieved as a result of the mechanical forces exerted by the cellular structures and the resisting forces of the cell-substrate adhesions that, in turn, are rapidly detached at the cell's rear upon movement (Lodish *et al.*, 2008). On the other hand, the understanding of the signalling and coordinated

activity involved in the cell's mechanics remains still unclear, particularly at the biochemical level but also in terms of temporal and spatial behaviour (Lauffenburger & Horwitz, 1996). Such processes are also studied at a larger scale, by considering the temporal and spatial characterisation of *collective* cell migration. The prominence and centrality of collective cell migration in a number of physiological and pathological events, namely morphogenesis, wound healing and cancer, with the latter two directly relating to inflammation, further explains the importance of a clear understanding of this phenomenon. When analysed in its whole, the global directed motion of cells follows a similar pattern to the one of single cells, by polarising with respect to a source of attraction, protruding towards it and eventually moving by balancing contractive and adhesive forces with the surrounding matrix (Trepat *et al.*, 2012). Furthermore, a collective behaviour in terms of cohesiveness, permeability and mechanical cell-to-cell signalling is also exhibited.

Overall, though, it is important to highlight how, in adult organisms, only stem cells, fibroblasts and leukocytes preserve the ability to migrate, along with tumour cells whose spread and metastatisation constitutes a crucial aspect of the disease progression and ultimate lethality (Entschladen & Zanker, 2010). Similarly, as already pointed out in Section 1.2, the effective and prompt migration of leukocytes to sources of inflammation also proves to be essential in the restoration of a healthy state and particularly in tackling chronic inflammation, further motivating our focus on neutrophil motility in this chapter.

5.1.1 Leukocyte motility in health and disease

The role of neutrophils in human physiology is key in a number of issues, including in mediating the innate immune response and most prominently in leading the inflammatory process. In particular, neutrophils constitute the front line response

to tackling tissue injuries or pathogenic intrusions and their prompt and efficient recruitment at the insulted site is central to the restoration of a healthy state. The migrating mechanisms that regulate leukocyte motility follow the pattern described in 5.1 but are specific in the cells' intrinsic polarisation as well as the integrated process of adhesion and release between front and rear cell, resulting in a characteristic gliding motion (Entschladen & Zanker, 2010). Unlike most other cells, neutrophils along with metastatic tumour cells, naturally exhibit the ability to move within varied tissues. Their directed drift towards specific targets, namely sites of inflammation, results from a number of overlapping conflicting but highly coordinated signals. The nature and unfolding of such signals that regulate leukocyte motion is particularly complex and still partially unclear. The network of interactions tightly controlling neutrophils' responsiveness is mediated by both chemicals (including growth factors, hydrogen peroxide and cytokines) and the extracellular matrix. The latter, in particular, functions as an inhibitor of cell migration, directly acting on cells' polarisation, protrusion, adhesion and detachment, effectively regulating their speed. A key counteraction to the promoters of leukocyte motility is provided by pro-inflammatory mediators that, in addition to their role as the main chemoattractant, also act as inhibitors to cell migration, once at the injured site, thus blocking neutrophils within the inflamed tissue and ensuring high optimal concentrations of white blood cells to efficiently neutralise sources of damage (Entschladen & Zanker, 2010).

Given the crucial role of neutrophils in the initiation, promotion and progression of inflammation, impairments of neutrophil motility can have disruptive consequences on the normal physiology, leading to and a number of pathologies. In particular, specific immunodeficiency disorders arise from defects in neutrophil recruitment, typically due to transmutations at genetic level of key receptors, as in the case of diseases such as leukocyte adhesion deficiency, Wiskott-Aldrich syndrome and Whim syndrome, amongst others, with patients affected by either disorder prone to frequent infections

(Entschladen & Zanker, 2010). Chronic inflammatory diseases, including both hereditary and developed disorders such as Crohn's disease, gout, arthritis, just to name a few, while still little understood in terms of pathogenesis, are characterised by a clear overconcentration of neutrophils within the damaged sites. As highlighted in Chapter 1, these leukocytes further promote the pro-inflammatory activity and the their faulty or uncontrolled up-regulation from physiological levels eventually leads to chronic inflammation. While the broader causes that result in impaired leukocyte motility and related diseases have been individuated, it is still challenging to gain an exhaustive comprehension of the defective mechanisms that lead to such abnormalities.

5.2 Models of collective cell movement

The relevance of cell migration in both health and disease has long motivated the great interest of researchers in clarifying intrinsic cellular mechanisms and external signalling activity that prompt and regulate this phenomenon. While the understanding of cell locomotion at the molecular level plays a key role in explaining the chemical and mechanical response underlying cellular motion, it is the complex coordination and regulation of these processes that results in the cells' polarised motion experimentally observed. This highlights the challenges posed by this problem, with mathematical models providing an effective tool to help tackle this multidisciplinary task. More specifically, cells' persistence in motion is analysed in terms of direction (Taylor *et al.*, 2013). Furthermore, there is a clear understanding that *in vivo* and *in vitro* cell migration function differently, particularly in response to chemotactic gradients (Entschladen & Zanker, 2010), with research in this area still failing to provide an exhaustive explanation of the signalling and mechanics that regulate cells' collective motion (Horwitz & Webb, 2003). The mathematical modelling of such phe-

nomena aims therefore to narrow the existing gaps in the understanding, and inform over possible therapeutic targets to tackle impaired cell migration.

5.2.1 Previous models of cell migration

Given the centrality of cell migration in many fundamental biological processes, from embryogenesis to the regulation of the immune system, there is great interest in modelling this phenomenon, with research in this field focusing on capturing different aspects of the collective motion of cells. As such, a number of valuable mathematical models of cell motility have been proposed, providing a valuable resource in terms modelling approaches and new insights into collective cell motion.

In their review, Camley & Rappel (2017) introduce the basics of collective cell modelling, with distinct models capturing only a subset of these aspects, according to each model purpose and specificity. In particular, single cells' velocity and persistence of motion are described in terms of stochastic differential equations, in function of the cell's polarity distribution, *i.e.* the asymmetry in the positioning of signalling components on the cell's surface. Similarly, a number of mathematical representations of cells' shape and mechanics are provided for implementation for models that aim to capture these aspects. Among these, phase field models are introduced, with each cell assigned a region, or phase field, and their motion described as a transition between an inner or outer location of the field. In Camley & Rappel (2017) such transition functions are modelled with respect to both single cells and cell-to-cell energies, while also being straightforwardly extended to account for additional parameters such as the phase field surface's width and cell's membrane bending energies. However, these models are admittedly costly in terms of computation and are more suitable for simulations of small numbers of cells, thus best serving models that aim to investigate biochemical interactions and cells mechanics.

Because of its intrinsic nature, the problem of modelling collective cell motion is commonly tackled by accounting for individual cells as basic units. While ABMs provide a straightforward answer in representing in an accurate and relevant way such scenario, other approaches have also been investigated. In this regard, Palsson (2001) proposed a $3D$ model of cells implementing motion in terms of change in shape and conservation of volume. Cell types are then defined according to a set of parameters accounting for sitffness, adhesion and locomotive force generation, adding to the flexibility of the model and its suitability to describe different multicellular systems. A cell's orientation is configured with respect to both chemotactic gradient and their previous location, upon a threshold value serving as tool in selecting the direction of movement. The cell-to-cell forces exerted upon motion are also accounted for, with adhesive and viscous forces prescribing the cell's deformation and ultimate movement. Simulations from the model are compared to available experimental data, successfully replicating cells sorting and chemotactic collective motion in typical physiologic scenarios but lacking any extension to possible impairments and neglecting more specific interactions at play in wound healing and embryogenetic processes. A more detailed study of cell migration by Palsson & Othmer (2000) focusing on slime mould motion proposes an ABM investigating the cell-to-cell forces at play in collective motion mechanisms. The model is firstly assessed with respect to adhesive forces and cellular mass surface tension in the absence of chemotaxis, subsequently analysing cells' aggregation in response to varying configurations of chemoattractant presence and studying the overall effect of adhesion in cells assembling and collective movement. In particular, validating their model against experimental results, Palsson & Othmer (2000) investigate closer aspects of cell-to-cell interactions, elucidating the cellular deformation mechanisms that can explain cellular aggregation by individuating in cells' increased speed the main drive to collective rotational movements.

Schumacher *et al.* (2016) review modelling approaches that specifically focus on

embryogenesis-driven cell migration, in particular with respect to neural crest cells, a fundamental embryonic structure giving rise to different specialised cells of the peripheral nervous system and heart amongst others. Similarly, Maini & Baker (2014) also assess models of collective cell motion, ranging from a classical PDE-based representation for tumour cell invasion, an agent based system for cells motility in epithelial sheets and a hybrid model for neural crest migration. Starting from energetic considerations in tumour cells metabolism, a mathematical analysis of their competitive behaviour revealed how the invasion of cancerous cells is best described by travelling waves, with the corresponding PDE model accounting for densities of both healthy tissue and pathological cells, as well as concentrations of critical agents promoting tumour invasion. Parameters were estimated from the relevant literature when available, with remaining ones tuned to capture the observed biological behaviour and simulations predicting effective treatment strategies for reducing tissue the metastatisation driven by tumour cells invasion. A model for epithelial cell migration is also presented, with cells represented as polygons sharing edges and grouped through common vertices. The model accounts for the assembling and positioning of such structures, which is crucial in the later stages of embryonic development. Finally, another embryogenic process is modelled in order to study the impact domain's growth on cells' migration. This is achieved by coupling a PDE based model describing concentrations of Vascular Endothelial Growth Factor (VEGF) which diffuses within tissue and, being consumed by cells, practically acts as a chemoattractant agent; cells are instead implemented as single agents, within a ABM framework. The model is then tested upon different scenarios, in order to clarify cellular migratory mechanisms, with the emerging result suggesting that cells at the back are responsive to correspondent cells at the front, rather than to the chemoattractant VEGF. Further experimental investigations confirmed this phenomenon revealing a difference in genetic expression at the base of such behaviour.

Neilson *et al.* (2011) propose a framework for modelling cell migration subject to chemotaxis in the form of reaction-diffusion equations over evolving domains. This approach takes into consideration the cell's shape, with the corresponding PDE's solution driving the cell's motion and morphology. The model is studied with respect to local stimuli and the cell's pseudopods' response to them, with a leading pseudopod emerging from a group of multiple competing ones. The model is further tested by simulating a single cell movement and its repositioning upon the introduction of the chemoattractant. The model compares well to experimental observations but does not include any pathological scenario; furthermore the mechanical forces regulating the cell's crawling do not take into account adhesive interactions, with the authors suggesting such implementation as a natural extension of their model.

Gavagnin & Yates (2018) highlight the duality between the continuum, deterministic PDE-based approach and the discrete stochastic ABM one. By exposing strengths and weaknesses of both, they review a number of relevant past models, including those extending the analysis of collective cell movement to cell proliferation and chemotaxis. In particular, on the latter, they underline the centrality of persistence and diffusiveness in describing these phenomena at population-level. Furthermore, methodologies towards the convergence of the deterministic and stochastic approaches are presented, by framing the diffusive behaviour typically implemented by PDEs within the ABM paradigm.

5.2.2 Modelling motility in terms of cell walks

Computational approaches in the understanding of cell motility are widely used and offer a straightforward tool for the analysis of experimental data and, more crucially, for the assessment of hypotheses that would otherwise remain unexplored with the support of *in vivo* measurements only. In particular, from the mathematical analysis,

computational processing and final elaboration of such data a number of *cellular walk* models have emerged and are now considered as an established part of the basic understanding of cell movement (Read *et al.*, 2016). Providing a mathematical description of directed motility is crucial in a wide range of fields, from biology to ecology; traditionally, models of motion derive from extensions of random walk processes that are in turn based on the principles of Brownian motion, named after the botanist Brown and his work on plants' pollen movement (Brown, 1828). In its simplest form, a model of movement is based on an *uncorrelated* and *unbiased* random walk, highlighting the independence between current and past directions and the lack of a preferred direction, respectively, basically reproducing the behaviour resulting from purely diffusive equations (Codling *et al.*, 2008). Accordingly, *persistent* or correlated random walks refer to the local directional bias of the moving object and a degree of persistence in maintaining a direction of motion. The strength and influence of such persistence can vary, typically modelled as decreasing in time and eventually uniformly distributed in directions. The straightforward biological interpretation of this model of motion is the tendency to keep moving forward, that is when memory of previous moves is relevant in determining the following moves. Further studies by Nava-Sedeno *et al.* (2017) expose the non-trivial role of persistence in affecting the cell's motion, studying the impact of reorientation and highlighting the dynamic non-linear effect of memory. In contrast, a biased random walk is characterised by a global directional bias, usually implemented in terms of probabilities to move to certain preferred directions. An obvious biological correspondent is thus motility subject to chemical gradients, with biased random walks describing a generic chemotactic movement. The two key features of persistence and bias can also be combined, resulting in a *biased persistent random walk* that describes optimal neutrophil motility (Taylor *et al.*, 2013). The coupled effects of persistence and memory in cells' collective motility are further analysed by Foxman *et al.* (1999). In particular, they expose the role of competitive

chemoattractant sources in guiding and diverting the cells' motion, with the overall direction resulting from the vectorial sum of the target orientations. In addition, a cells' persistent walk is also tested in contexts of biased motion, to investigate the role of memory and its relevance upon chemotaxis. Interestingly, it is found that, when subject to complex (multi-sourced) chemotactic fields, cells navigate through chemoattractants sequentially, with such dynamical regulation provided by memory (Foxman *et al.*, 1999).

The lack of inflammatory models based on measured cell trajectories, as exposed in the above literature review, motivates our aim in refining the ABM of Chapter 4 to calibrate the leukocytes motion upon experimental *in vitro* data. In particular, we model cells moves as a regulated combination of persistence in their walk and sensitivity to the chemotactic attractant, calibrated against the experimental data of Sapey *et al.* (2011), for both healthy subjects and patients affected by COPD.

5.3 Model construction

As already outlined in the beginning of this chapter, we aim to closer investigate leukocyte directed motility upon chemotactic gradient. Thus, we firstly start with a preliminary model that includes one type of cell and a fixed chemoattractant gradient. The structuring details of this preliminary model are defined and analysed in this section and later assessed with appropriate simulations. The preliminary model for leukocyte chemotactic motion will be then plugged into the inflammatory ABM framework presented in Chapter 4 in order to analyse the resulting enhanced model of inflammation, with the manipulation of chemotactic-specific parameters controlling physiologic and impaired motion of cells.

With respect to the physiological stages of inflammation, the effective migration of leukocytes to the injured site is a key aspect of the inflammatory process, with

faulty neutrophil recruitment or impaired chemotaxis posing a serious threat to the restoration of the healthy state, possibly prolonging recovery time, evolving into long term chronic inflammation or even giving rise to major pathologies (as described in Section 1.1). Furthermore, while there is an overall understanding of the mechanisms that regulate neutrophil motility in terms of both free movement and migration towards a chemoattractant source, the cell's response to competent signals and its resulting directed motion still remain unclear and need further investigation (Nuzzi *et al.*, 2007). To this end, we build a model comprising of neutrophils subjected to a chemoattractant source in order to provide greater detail into the fundamental mechanisms of leukocytes directed motion described in the previous models of inflammation presented in Chapters 3 and 4.

Similarly to the ABM inflammatory model in Chapter 4, we here describe the initial assembly of an agent based framework to characterise the basic chemotactic interactions between a group of cells and a chemical acting as attractant. A such, two main variables are individuated: neutrophils, described in class `Cell` and chemical mediators acting as a chemoattractant source and characterised in class `Environment`, purposely recalling the class of the same name of the inflammatory model of the previous chapter. The preliminary model has a minimal setup, with the main focus being on providing an accurate characterisation of cells' chemotactic motion.

5.3.1 Domain and initial conditions

As is evident by comparing Figure 4.3, which illustrates the structure of the ABM-based inflammation model of Chapter 4, to Figure 5.1 it is evident how the system we aim to model here focuses on a subsection of the interactions described in previous chapters, particularly characterising with greater detail the motion of neutrophils upon a variety of different stimuli, in order to simulate both physiological and im-

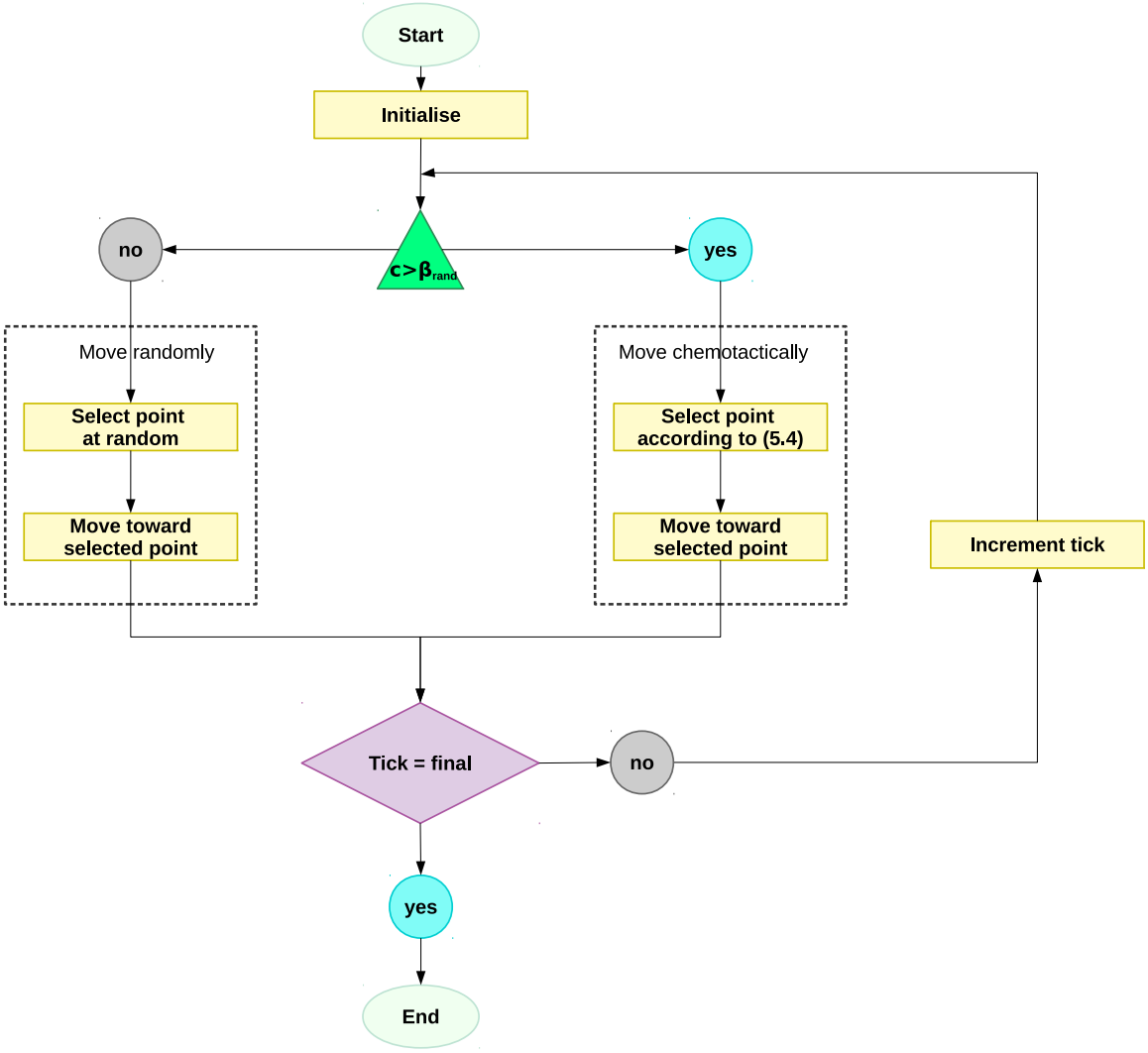

Figure 5.1: Flow chart representing the preliminary ABM of chemotaxis and illustrating the cyclic chain of actions with respect to the tick count. Green triangles represent thresholds, diamonds represent decision points.

paired motility of these cells. We retain the framework from the previous ABM, with the model's agents referred through both a *grid* with relative coordinates and neighbourhood considerations and a *continuous space* for visualisation purposes. Furthermore, our agents' actions (*i.e.* the system's variables), namely `Cell` and `Environment` will be defined according to their state at each tick t.

The formal setting of the chemotactic preliminary model follows the same structure of the ABM inflammatory model of Chapter 4 in terms of domain. In particular, we study the chemotactic motion of agents over a squared domain subject to periodic boundary conditions, initialising the system with a fixed number of cells n_{cells} and a constant gradient of mediators. Mediators' distribution is uniformly localised at the top border of the squared domain with concentration A_{chem}, with a linear decreasing gradient toward the bottom of the domain.

5.3.2 Modelling chemotaxis

In order to take into account the main considerations about neutrophil motility, as outlined in Section 5.1, we model the motion of leukocytes as a combination of random walks: a biased walk, towards a chemoattractant source, and a persistent walk, with cells exhibiting memory properties that preserve past directions (Albrecht & Petty, 1998). By combining these different behaviours, we aim to model a *biased persistent random walk*, as experimentally shown by Taylor *et al.* (2013). To this end, we structure a joint probability p_{chem} describing a cell's likelihood to move from its current position to a neighbouring one as a combination of both the surrounding mediator concentrations (p^{grad}, taking into account the biased component of the walk) and the agent's previous position (p^{mem}, modelling the persistence in walk), with $p_{chem} = p^{grad} \cdot p^{mem}$ being the resulting probability.

The specifics of each cell's behaviour are defined at each tick, upon which the

agent's move is modelled in terms of either a chemotactic motion or a random one. Firstly, the source global concentration in the cell's neighbourhood is sensed and compared against a parameter β_{rand} identifying a threshold for the directed motion to happen. For concentrations smaller than the threshold β_{rand}, the cells will simply move randomly to a neighbouring position. Upon concentrations equal to or exceeding β_{rand}, the cell will instead proceed to move chemotactically. The agent is thus set to move to a direction according to a combined probability of the surrounding concentration gradient and the cell's previous move. To provide greater flexibility in tuning the balance between the effects of chemoattractant gradient and cell memory, for cell i with neighbourhood $\mathcal{N}_i$, we apply a weighting function $w(c_j)$ to the chemoattractant concentrations at all positions $j \in \mathcal{N}_i$. For each position $j \in \mathcal{N}_i$, the probability that the cell moves to position j (in the absence of memory effects) is given by

$$p_j^{grad} = \frac{w(c_j - c_i)}{\sum\limits_{k \in \mathcal{N}_i} w(c_k - c_i)}. \tag{5.1}$$

Here, we consider the exponential weighting function:

$$w(c_k) = e^{k_{grad} c_k}, \tag{5.2}$$

with scaling parameter k_{grad}. The weighting function is thus assessed against each of the eight neighbouring positions of cell i, as illustrated in Figure 5.2.

In terms of a cell's memory, agents of the system are embedded with the record of their previous move, serving as record for the direction from which a cell is coming. This information thus identifies one of the eight possible previous points of origin, as illustrated in Figure 5.3. The probability associated with the cell's memory (p^{mem}) follows a gaussian distribution, with the strongest likelihood associated with the preservation of direction. The likelihood of other directions are directly controlled through the parameter σ_{mem}, referring to the standard deviation of the probability distribution associated to the eight possible points the cell can move to and with mean

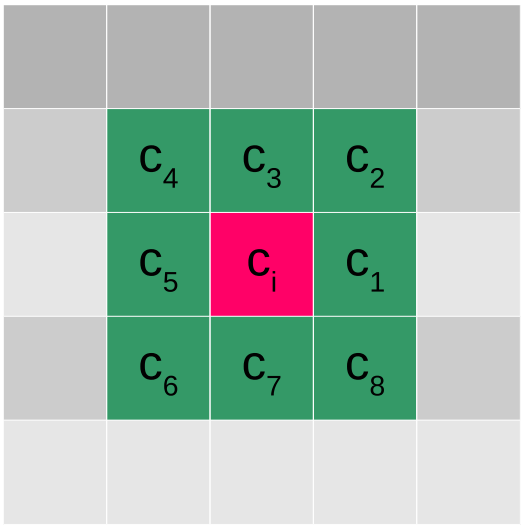

Figure 5.2: Graphic representation of chemoattractant concentration at each cell's neighbouring position. The mediator's concentration c_i at the cell's location i and the neighbouring concentrations c_j, $j = 1, \ldots, 8$ are the arguments of the weighting function w, as defined in (5.2).

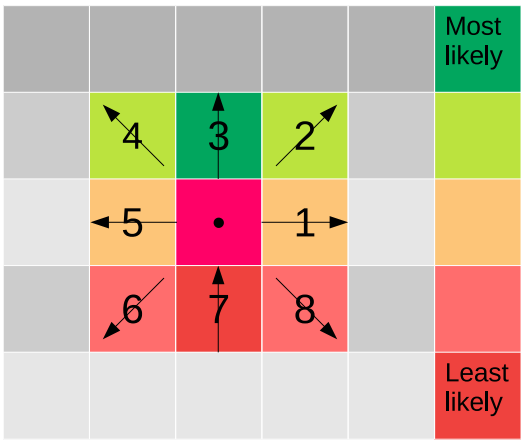

Figure 5.3: Graphic representation of cell's embedded record of its previous move with respect to its Moore's neighbourhood. The likelihood of the cell's next move depend on its previous position, with the two neighbouring positions from the origin being the least likely (in red), followed by the side positions with an increased likelihood (in orange) and the furthest ones with maximum likelihood (in green).

equal to the angle θ_{prev}, representing the information enclosed in the agent's track record of its previous position. Thus, the probability of cell i with neighbourhood $\mathcal{N}_i$ to move with direction prescribed by the angle θ_j, $j = 1, \ldots, 8$ given its previous location represented by θ_{prev} is

$$p_j^{mem} = \frac{1}{K}\left(\frac{1}{\sqrt{2\pi\sigma_{mem}^2}} e^{-\frac{(\theta_j - \theta_{prev})^2}{2\sigma_{mem}^2}}\right), \tag{5.3}$$

where K is a normalising constant that ensures probabilities sum to one. Finally, we construct the joint probability

$$p_j^{chem} = \frac{p_j^{grad} \cdot p_j^{mem}}{\sum_{k \in \mathcal{N}_i} p_k^{grad} \cdot p_k^{mem}} \tag{5.4}$$

determines the cell's new position.

Here, we consider that cells do not die, with the initial (and fixed) number of cells determined through parameter n_{cell} instead. This, though, is coherent with the purposes of this new chemotactic model in which the interactions of interest are studied on a shorter timescale, with particular focus on the nature of cells' movement rather than the mechanisms analysed in the previous chapter. Furthermore, another parameter n_{run} is introduced, regulating the number of times per tick the agents update their state. This parameter is modulated from the Sapey *et al.* (2011) paper, in which neutrophil motions upon different healthy and non-healthy scenarios are studied. In particular, the experimental work presented by the authors highlights how in specific pathological circumstances, affected neutrophils present a more disordered, yet quicker, motion. This data shows that, when compared to healthy scenarios, while there is an increase in the overall non-directed speed of cells, the velocity in approaching the chemotactic target is significantly reduced. Thus, the parameter n_{run} allows to control the switch between a physiological and non-healthy scenario.

The modelling of chemical mediators acting as the chemoattractant source for leukocytes, while having an analogous setup to the corresponding class of the model

Parameter	Definition	Class	Standard value
n_{cell}	number of neutrophils	ChemotaxisBuilder	10
A_{chem}	maximum concentration of chemoattractant	ChemotaxisBuilder	1
n_{run}	number of moves per tick	Cell	1
β_{rand}	threshold minimum concentration of chemoattractant for chemotactic motion	Cell	0.001
σ_{mem}	standard deviation of likelihood of positions within the cell's Moore's neighbourhood with gaussian distribution	Cell	
k_{grad}	scaling parameter appearing in the weighting function of (5.2)	Cell	

Table 5.1: Parameters of the ABM chemotaxis model.

in Chapter 4, presents significant differences in terms of features. In particular, in this case we do not differentiate between pro- and anti-inflammatory mediators, since the main focus in this model is the cells' chemotactic behaviour, rather than the nature of the chemoattractant source. Similarly, the mediators' intrinsic ability to diffuse and decay is here neglected, in favour of a linear gradient of concentration proportional to a fixed parameter A_{chem}, as outlined in Section 5.3.1. Similarly, k_{grad}, β_{rand} and σ_{mem} are identified in order to qualitatively reproduce the physiological motion of neutrophils described in Albrecht & Petty (1998) and Taylor *et al.* (2013). In particular, the specific choice of values for parameters σ_{mem} and k_{grad} is crucial in defining the chemotactic movement of leukocytes as a biased persistent random walked, as observed experimentally (Taylor *et al.*, 2013; Jones *et al.*, 2015). Table 5.1 summarises the model's parameters, providing standard values for all parameters except k_{grad} and σ_{mem}, which we discuss below.

Figure 5.4 illustrates the role of parameter σ_{mem} in calibrating the cells' motion. The value $\sigma_{mem} = 1.75$, for example, (as detailed in Figure 5.4b) ensures that pro-

gressing in the broader direction set by θ_{prev}, that is allowing a maximum shift of $\pm\frac{\pi}{4}$ radians from the cell's previous position, is 54.51% likely, while shifts of $\frac{\pi}{2}$ radians are 25.94% likely and backwards motion (shifts greater than $\frac{3}{4}\pi$ radians) has a likelihood of only 19.55%. The study of the combined effect of both persistence and bias in the cells' movement is presented in Figure 5.5, which shows different motion profiles obtained by varying both σ_{mem} and k_{grad}. Value ranges are chosen as to illustrate extreme and intermediate behaviours, with $\sigma_{mem} = 0.1$ implying that the direction consistent with the cell's θ_{prev} property is picked with probability $p^{mem} = 1$, effectively forcing the cell to never change direction, regardless of the concentration gradient, or, on the other hand, $\sigma_{mem} = 10$ cancelling the effects of persistence on cells' motion, with all directions prescribed by p^{mem} being equally likely, thus selecting the point to move to with respect to the gradient only. Conversely, by varying k_{grad} between $k_{grad} = 1$ and $k_{grad} = 80$, we gradually strengthen the response to the attractant. We describe the manner in which we can select appropriate choices of k_{grad} and σ_{mem}, given suitable experimental data, in the following section.

5.4 Comparison with experimental data

Defects in neutrophil recruitment result in a delayed progression of inflammation, potentially preventing the restoration of a healthy state and leading the way to diseases (as described in 5.1.1). Understanding the conditions that prevent the correct migration of leukocytes to the sources of damage upon an inflammatory event is key to developing effective therapeutic tools, in order to contain and eventually tackle such disorders. The model developed in Section 5.3 is purposefully articulated with respect to different parameters in order to take into account a wide spectre of leukocyte behaviour, ranging from a healthy physiological chemotactic motion to different impairments in motility due to specific disorders. One of such pathological conditions that

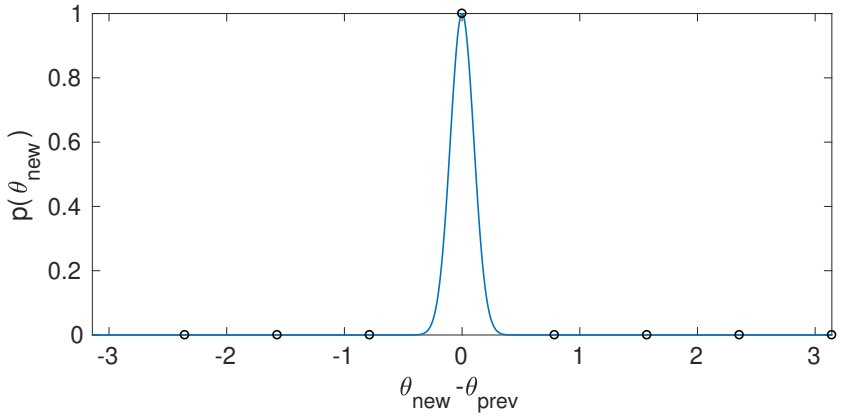

(a) $\sigma_{mem} = 0.1$

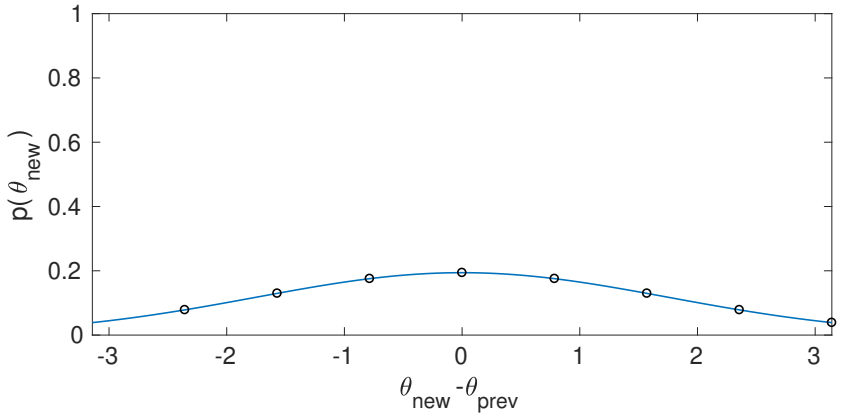

(b) $\sigma_{mem} = 1.75$

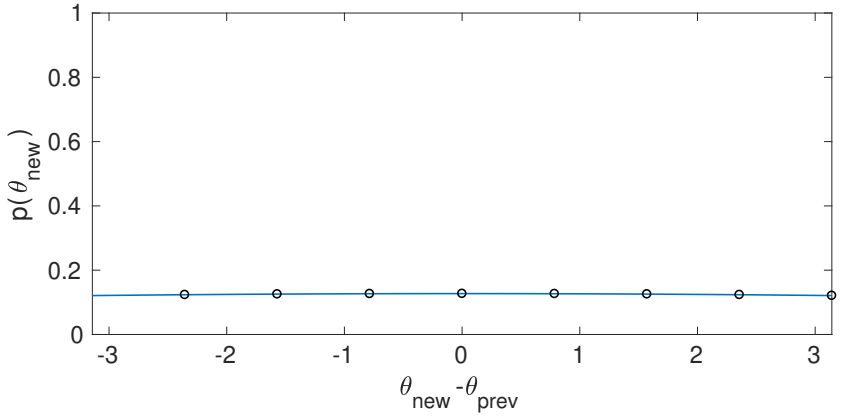

(c) $\sigma_{mem} = 10$

Figure 5.4: Probability distribution of (5.3) for different values of the standard deviation σ_{mem}.

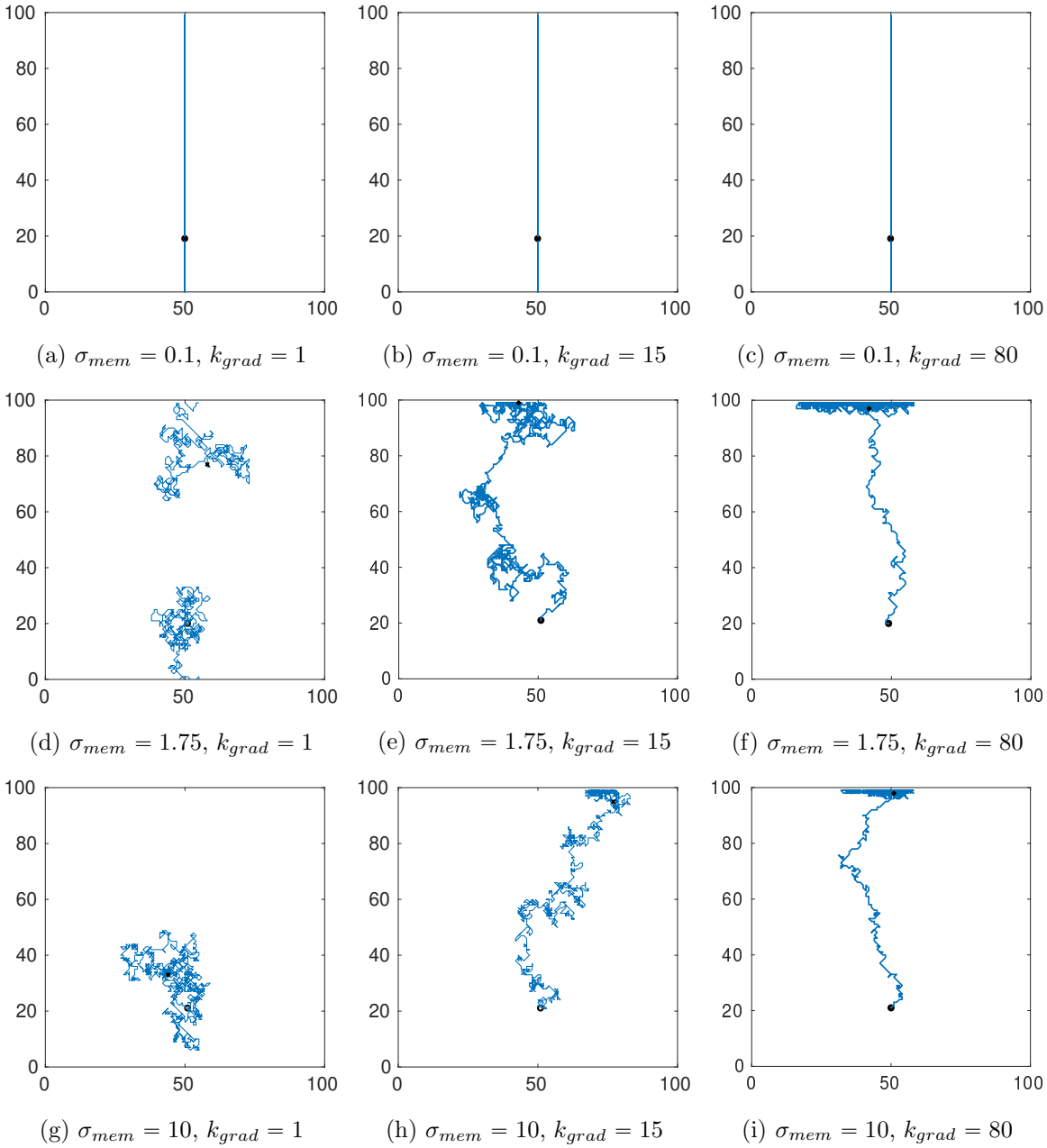

(a) $\sigma_{mem} = 0.1$, $k_{grad} = 1$ (b) $\sigma_{mem} = 0.1$, $k_{grad} = 15$ (c) $\sigma_{mem} = 0.1$, $k_{grad} = 80$

(d) $\sigma_{mem} = 1.75$, $k_{grad} = 1$ (e) $\sigma_{mem} = 1.75$, $k_{grad} = 15$ (f) $\sigma_{mem} = 1.75$, $k_{grad} = 80$

(g) $\sigma_{mem} = 10$, $k_{grad} = 1$ (h) $\sigma_{mem} = 10$, $k_{grad} = 15$ (i) $\sigma_{mem} = 10$, $k_{grad} = 80$

Figure 5.5: Tracking of cell motion from $t = 0$ to $t = 1000$ (initial and final positions marked with black circles and black crosses respectively) for varying choices of σ_{mem} and k_{grad}. The number of cells per simulation is fixed at $n_{cell} = 1$, with all other parameters as in Table 5.1.

we aim here to replicate, in order to provide both an *in silico* correspondent to existing experimental observations and eventually a tool to capture intrinsic aspects that are missed in *in vivo* studies is COPD. COPD is a complex inflammatory disease characterised by both airflow limitations and extrapulmonary systemic manifestations. It is currently individuated as the third global cause of death worldwide (WHO, 2018) and is usually associated with a number of comorbidities that further complicate its treatment and management, while also constituting an important burden in terms of both cost and resources to healthcare services globally (Barnes & Celli, 2009; Mannino & Buist, 2007). COPD develops from systemic persistent low level inflammation, with increased concentrations of leukocytes and pro-inflammatory mediators playing a key role in preserving and pathologically prolonging the inflammatory state (Agusti *et al.*, 2012). The initiating causes that can trigger such an inflammatory state are varied and sometimes unclear, although mainly environmental (smoking, occupational and air pollution, ageing) and, to a minor degree, genetic factors are all distinctive features that are known to pose great risk in the development of this condition (Mannino & Buist, 2007). The relevance and great impact of COPD on morbidities worldwide motivates the interest of researchers in investigating this condition with a particular focus on the wide spectrum of comorbidities and phenotypes that characterise it as well as the underlying biological mechanisms at tissue level that express typical inflammatory patterns. Concentrating on this latter aspect, Sapey *et al.* (2011) determine and highlight the impairments in neutrophil migration suffered from subjects affected by COPD, by investigating through experimental observations and analyses the cells' chemotactic motion with respect to selected case studies, namely healthy non-smoking subjects, healthy smokers, subjects genetically prone to develop COPD and finally subjects already affected by COPD. The results provided by this research allow us to effectively introduce defects and impairments of the cells' chemotaxis to our ABM preliminary model, by carefully calibrating the parameters of Table 5.1 in

order to capture the relevant changes in neutrophil motility exposed by Sapey *et al.* (2011). In their study, Sapey *et al.* (2011) monitor neutrophils of both COPD affected subjects and control groups through videomicroscopy, tracking ten randomly chosen cells over time upon a fixed concentration of chemoattractant. As part of the migration assessment different measures are recorded, including speed cell of movement (indicating the movement in any given direction), cell velocity (in the direction of the chemoattractant) and a chemotactic index, which measures the cells' mean orientation with respect to the chemical gradient. Interestingly, results from this experimental work showed that neutrophils in COPD-affected subjects exhibit greater overall speed compared to healthy subjects, while the cells' directed chemotactically-driven velocity is also considerably reduced, with a significantly smaller chemotactic index as well.

5.4.1 Nondimensionalisation

The implications stemming from defective neutrophil chemotaxis in connection to inflammatory diseases and more specifically to COPD, as exposed in Sapey *et al.* (2011), motivate our aim in linking up the preliminary ABM chemotactic model to experimental *in vitro* data. This allows for a more in depth investigation of the role of leukocyte directed motion in the acute inflammatory response in terms of the cells' spatial localisation, which will be explored in the following sections with the analysis of a new joint ABM of inflammation and chemotaxis.

In order to compare results from Sapey *et al.* (2011) and our ABM chemotaxis framework, we introduce a nondimensionalisation of the model presented in Section 5.3, tailored upon the authors' experimental setup. In particular, by choosing to set each grid space to correspond to $1\,\mu$m and given that the *in vitro* chemotactic chamber in which neutrophils are tracked measures $240\,\mu\text{m} \times 180\,\mu\text{m}$, we consider

a 240×180 rectangular grid as our domain. The recorded speeds of neutrophils in both healthy and COPD affected subjects are available from Sapey *et al.* (2011), with the former group registering an average motion of $3.77\,\mu$m min^{-1} and the latter presenting neutrophils moving significantly faster at $5.12\,\mu$m min^{-1} but, crucially, with a decreased sensitivity to the chemotactic target. We derive a timescale fitting the experimental data in which each tick corresponds to 20 s, and allow cells to move a suitable number of times per tick in a healthy physiological scenario, as prescribed by parameter n_{run}, whose value is calibrated to the available cell velocity data as illustrated in the following section. In the following sections we calculate the expected distance travelled.

5.4.2 Calibration against experimental data

We incorporate the analysis provided in the previous sections into our model by analytically computing the expected number of moves and chemotactic index for any given combination of chemotactic strength k_{grad} and walk persistence σ_{mem}.

The evaluation of the parameter values, based on the nondimensionalisation of Section 5.4.1, is structured upon a mathematical fitting of our preliminary model setup to the experimental data. In particular, Sapey *et al.* (2011) analyse their results with respect to cell speed s (measuring movement in any direction), cell velocity v (speed towards the chemoattractant) and chemotactic index I_{chem} (measuring cells' accuracy in chemotaxis as the cosine of the angle between the cell's direction and the chemotactic gradient's orientation). We consider these indicators of the chemotactic efficacy into our calculations to compare it to the experimental observations reported in Sapey *et al.* (2011). The resulting set of pairs of (σ_{mem}, k_{grad}) that satisfy the constraint given by the cell velocity v is then narrowed by allowing only those combinations that provide a suitable value of the chemotactic index I_{chem}, also reported

in Sapey *et al.* (2011). Finally, we prescribe a value for parameter n_{run} by fitting the experimental data about the total distance travelled by cells recorded over a span of $t = 20$ minutes in terms of the number of moves per tick.

Let us consider a cell's walk in terms of its global motion over a given span of time, its recorded cell velocity and the corresponding chemotactic index. By decomposing such a trajectory into single moves of an agent over gridspaces, let us define m_k as the k^{th} move of a cell. We are thus interested in the probability of the cell to pick move m_k, from the eight possible moves of Figure 5.3, given its previous move m_{k-1}. We define a transition matrix, $\mathcal{P}$, such that, at move k, $p_{i,j}$ represents the probability that the k^{th} move is move j given that the $(k-1)^{th}$ move was move i; *i.e.*

$$p_{i,j} = P\left(m_k = j \,|\, m_{k-1} = i\right), \qquad i, j = 1, \ldots, 8\,. \tag{5.5}$$

Equivalently, we have the following matrix:

$$\mathcal{P} = \begin{pmatrix} P\left(m_k = 1 \,|\, m_{k-1} = 1\right) & P\left(m_k = 2 \,|\, m_{k-1} = 1\right) & \ldots & P\left(m_k = 8 \,|\, m_{k-1} = 1\right) \\ \vdots & \ddots & & \vdots \\ P\left(m_k = 1 \,|\, m_{k-1} = 8\right) & \ldots & & P\left(m_k = 8 \,|\, m_{k-1} = 8\right) \end{pmatrix} \tag{5.6}$$

As described in Section 5.3.2, agents are initialised with a randomly assigned direction of origin, while at subsequent iterations the dependence of the selection of the future move given the previous one is according to probability (5.4). Thus, the initial probabilities of move are equal and defined as

$$\mathbf{\Pi_0} = \begin{pmatrix} \frac{1}{8} & \frac{1}{8} & \frac{1}{8} & \frac{1}{8} & \frac{1}{8} & \frac{1}{8} & \frac{1}{8} & \frac{1}{8} \end{pmatrix}. \tag{5.7}$$

At each stage, represented by move m_k, with $k = 1, \ldots, n$, the statistical description of a cell's motion is described by the Markov chain defined by the transition probability $\mathcal{P}$ and the initial data $\mathbf{\Pi_0}$. Given this initial data, the probability that the k^{th} move is move i is given by

$$P(m_k = i) = \left(\mathbf{\Pi_0} \cdot \mathcal{P}^k\right)_i, \qquad i = 1, \ldots, 8\,. \tag{5.8}$$

Let us now define a new matrtix $\mathcal{Q}$ such that

$$q_{i,k} = P(m_k = i)\,, \tag{5.9}$$

with the right-hand side of (5.9) being computed according to (5.8). Given this matrix, we can calculate the expected distance travelled in the vertical direction after N moves as

$$d_v(N) = \sum_{k=1}^{N} \left(\sum_{i\in\{2,3,4\}} q_{i,k} - \sum_{i\in\{6,7,8\}} q_{i,k} \right). \tag{5.10}$$

Given a target cell velocity, we can infer an expected distance of travel from the experimental data, and by comparing this with (5.10), we prescribe the total number of moves to be carried out within a given simulation. This effectively prescribes the parameter n_{run} in our model, holding fixed the required number of ticks.

Similarly, for each possible move i, let us construct a vector $\boldsymbol{\alpha}$ such that α_i is the angle that the trajectory of move i makes with the vertical, *i.e.*

$$\boldsymbol{\alpha} = \left(\frac{\pi}{2}, \frac{\pi}{4}, 0, \frac{\pi}{4}, \frac{\pi}{2}, \frac{3\pi}{2}, \pi, \frac{3\pi}{2} \right). \tag{5.11}$$

We can then compute the average chemotactic index after N moves according to

$$I_{chem} = \frac{1}{N} \sum_{k} \sum_{i} \cos(\alpha_i) q_{i,k}\,. \tag{5.12}$$

Integrating the data available from Sapey *et al.* (2011), which is summarised in Table 5.2, we are able to tune the parameters k_{grad} and σ_{mem} to values that fit the measured cells' velocity v and chemotactic index I_{chem}. Furthermore, our computation yields the total number of moves required to match the recorded v and I_{chem} for each suitable pair of (k_{grad}, σ_{mem}) identified.

Figure 5.6 illustrates values of the predicted mean chemotactic index resulting from a range of combinations of possible parameter values k_{grad} and σ_{mem}. While initially investigated on a larger scale, the range is here narrowed to sensible choices of these two key parameters, in accordance to the results derived in Section 5.3.2,

Measure	Physiological chemotaxis	COPD-affected chemotaxis
$s\ [\mu m\, min^{-1}]$	3.77	5.12
$v\ [\mu m\, min^{-1}]$	2.14	0.09
I_{chem}	0.39	0.04

Table 5.2: Measured data during studies of neutrophils' migration upon chemotactic gradient, as reported in Sapey *et al.* (2011).

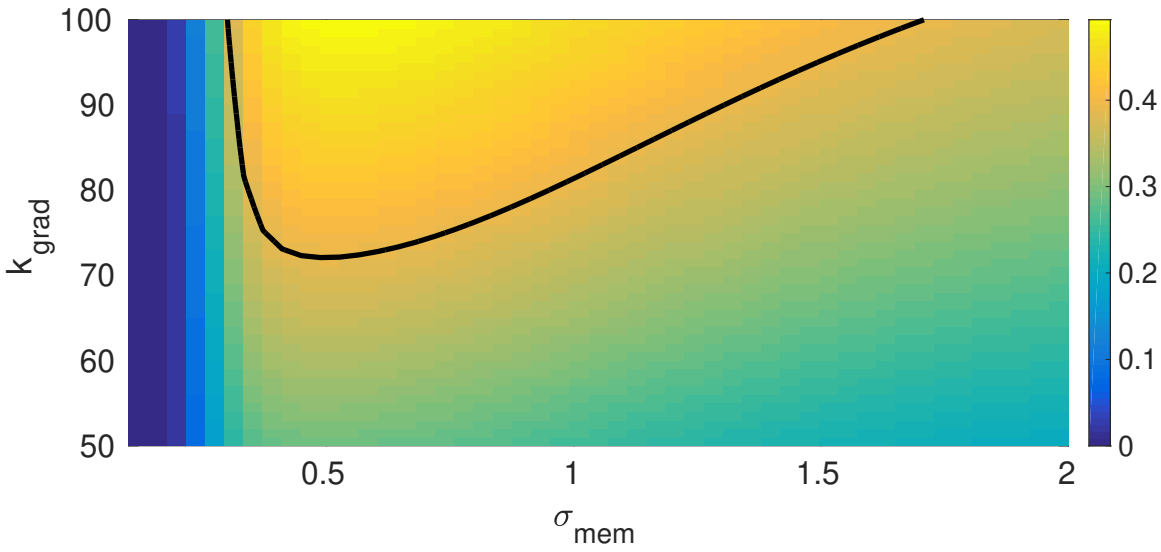

Figure 5.6: Map of values of the predicted mean chemotactic index I_{chem} corresponding to combined values of parameters k_{grad} and σ_{mem}. The black curve highlights the subset of parametric combinations that correspond to the physiologic chemotactic index $I_{chem} = 0.39$, as reported in Sapey *et al.* (2011).

with $k_{grad} \in [50, 100]$ and $\sigma_{mem} \in [0.1, 2]$. To fit the available data to our model, the parameters k_{grad} and σ_{mem} are calibrated to the corresponding physiological chemotactic index, that is $I_{chem} = 0.39$, which is also highlighted in black in Figure 5.6. Thus, any pair of values (k_{grad}, σ_{mem}) sitting on that curve, satisfy the chemotactic index and cell velocity requirements. We choose $k_{grad} = 80$ and $\sigma_{mem} = 1$ to illustrate the behaviour. Since such combination fits a number of total moves of $n = 160$ and given that each tick corresponds to 20 s, as per the nondimensionalisation presented in the previous Section 5.4.1, we prescribe for each agent a number of moves per tick of $n_{run} = 3$.

With an analogous approach, the chemotactic parameters k_{grad} and σ_{mem} are also fitted against the data arising from COPD-affected neutrophils. In particular, as reported in the second column of Table 5.2, the chemotactic strength k_{grad} and the cells' persistence regulated by σ_{mem} are set in accordance to an increase in the overall undirected speed of motion s and a sharp decrease in the chemotactic index I_{chem}. The resulting map of parameter combinations fitting the measured data is shown in Figure 5.7 from which $k_{grad} = 8$ and $\sigma_{mem} = 1.2$ emerge as suitable choices. Furthermore, as already pointed out in Section 5.4.1, in line with the results of Sapey *et al.* (2011), we allow COPD-affected cells to move twice as fast as the healthy cells, thus setting updating the value of parameter n_{run} controlling the number of moves per tick to $n_{run} = 6$. The set of parameter values characterising both physiological and pathological chemotaxis is outlined in Table 5.3.

By initialiasing our chemotactic model with the parameter values informed by the calibration to the data available in Sapey *et al.* (2011), we are able to fully assess its efficacy and reliability in describing both healthy and pathological chemotaxis. Figure 5.8 shows tracks of neutrophil chemotactic motion from both *in vitro* and *in silico* results. The experimental study conducted by Sapey *et al.* (2011) focused on analysing neutrophil chemotaxis from varied groups of individuals, partic-

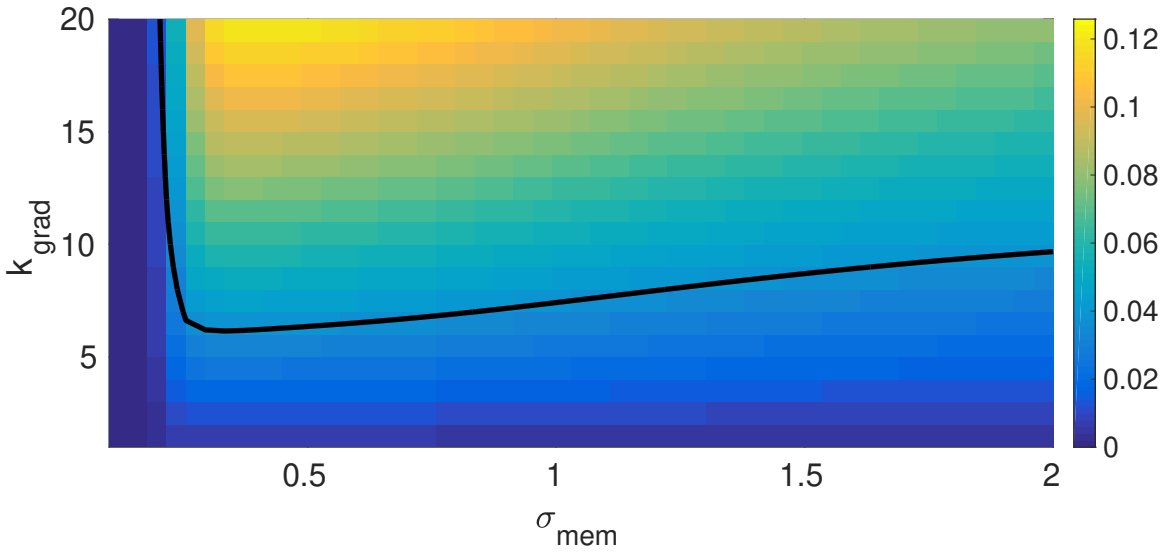

Figure 5.7: Map of values of the expected mean chemotactic index I_{chem} corresponding to combined values of parameters k_{grad} and σ_{mem}. The black curve highlights the subset of parametric combinations that correspond to the physiologic chemotactic index $I_{chem} = 0.04$, as reported in Sapey *et al.* (2011).

Parameter	Definition	Standard physiologic value	Updated value
n_{run}	number of iterations at each tick t	3	**6**
σ_{mem}	standard deviation of likelihood of positions within the cell's Moore's neighbourhood with gaussian distribution	1	**1.2**
k_{grad}	rate parameter of likelihood of positions within the cell's Moore's neighbourhood with exponential distribution	80	**8**

Table 5.3: Updated values for parameters of the ABM chemotactically impaired model. All other parameters retain the values listed in Table 5.1.

ularly healthy, never-smoking subjects and COPD-affected patients amongst others, by recording through videomicroscopy 10 randomly chosen cells for a duration of 20 minutes. Neutrophils were subject to a chemotactic source directed top to bottom, with paths and directions indicated by white arrows (Figures 5.8a and 5.8c). Similarly, our simulations monitor 10 cells at time, for a duration of $t = 60$ ticks (Figures 5.8b and 5.8d). As emerging from both experimental results and model simulations, in healthy scenarios, neutrophils are able to quickly orientate towards the chemoattractant and move smoothly towards it (Figures 5.8a and 5.8b). Conversely, COPD-lead defective neutrophil motion results in significant impairments delaying the cells' ability to promptly direct themselves according to the chemotactic signal. The faulty responsiveness of COPD-affected neutrophils to the chemoattractant disrupts the correct recruitment of leukocytes, enhancing the inflammatory mechanisms towards uncontrolled, eventually pathological, levels. In addition to the qualitative validation of the ABM against the experimental results of Sapey *et al.* (2011) detailed in Figure 5.8, with comparable cell trajectories in both healthy and diseased cases, our agent-based model matches the *in vitro* data also in terms of the quantitative differences arising from the analysis of control and COPD-affected subjects. In particular, in correspondence to the increase in undirected speed, sharp decrease in oriented motion and chemotactic inefficiency quantified by Sapey *et al.* (2011) in COPD-affected neutrophils, our model exhibits also a significant decrease in the value of parameter k_{grad}, responsible for the cells orientation. It is also interesting to observe how parameter σ_{mem}, reflecting the persistence of cells' walk, plays a key role in controlling healthy chemotaxis, while, as highlighted in Figure 5.7, the COPD case is largely insensitive to σ_{mem}. The agent-based model's ability to retain the typical features in terms of behaviour of migrating cells in varying scenarios and its tuning through parameters experimentally measurable and of biological significance is a key point in the validation and effectiveness of this model and leads towards further investigations

in the role of chemotaxis as a point of control and regulation of inflammatory events through this novel approach.

5.4.3 Discussion

Physiological neutrophil motility

The effectiveness of the modelled neutrophil motility, implemented as described in Section 5.3.2, is evaluated with respect to the qualitative behaviour of cells exhibiting a biased persistent walk, as first described in Section 5.2.2. These results in particular show how such characteristic cellular walk is implemented for each cell, by balancing the effects of both parameters k_{grad} and σ_{mem}, controlling bias and persistence respectively, effectively modelling the chemotactic migration described in Figure 5.5f, calibrated to the data inferred from Sapey *et al.* (2011).

In conclusion, through the parameter k_{grad} we are able to control the chemotactic behaviour of cells in our ABM. The effectiveness of this parameter directly depends on the maximum concentration of mediators A_{chem} (located at the top of the domain and linearly decreasing to the bottom), while also being bound to the parameter accounting for the persistence in cells' random walk, ie σ_{mem}. With this regard, we provide values for k_{grad} and σ_{mem} such that the combined probability $p_{chem} = p_{grad} \cdot p_{memory}$ reflects balanced weights for contributions of both bias and persistence of cells' motion. Such tuning of parameters effectively models an ideal healthy scenario, inferred from experimental observations investigated by a number of researchers, in particular by Foxman *et al.* (1999) and Taylor *et al.* (2013) showing the dual conflicting nature between memory and gradient in leukocyte chemotactic motion, and by Sarris *et al.* (2012) with respect to chemical gradients actually limiting leukocyte motility once the cells reach the chemoattractant source. While this setting successfully replicates the healthy behaviour exhibited by leukocytes as analysed by Khandoga *et al.* (2009),

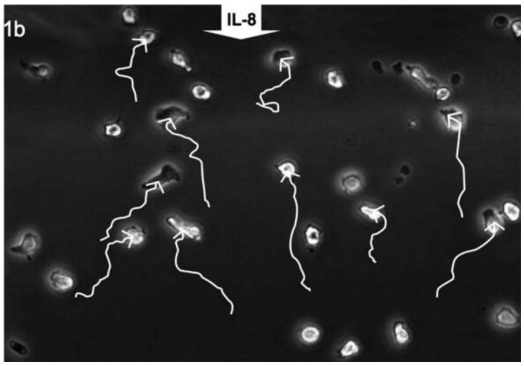

(a) Healthy *in vitro* neutrophils

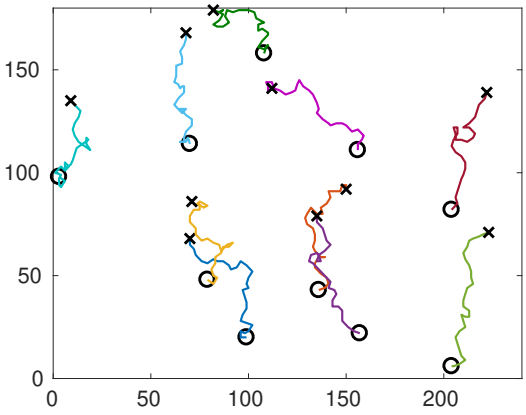

(b) Healthy *in silico* neutrophils

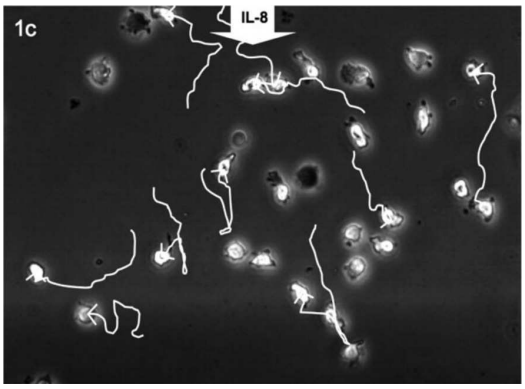

(c) COPD *in vitro* neutrophils

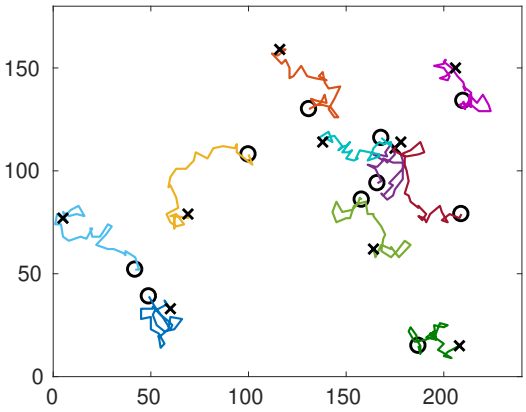

(d) COPD *in silico* neutrophils

Figure 5.8: Comparison between experimental results from Sapey *et al.* (2011) (left column) and simulations from the ABM, with final tick at $t = 60$ (right column). Neutrophils are tracked both in a healthy scenario (first row, ABM parameters as in third column of Table 5.3) and a pathological (COPD) one (second row, ABM parameters updated as in fourth column of Table 5.3).

Sapey *et al.* (2011) and Jones *et al.* (2015), overall confirming the *in vivo* results presented by these researchers, we will now focus on impaired neutrophil motility, at the base of many pathologic conditions, as described in 5.1.1, analysing the results provided by an accurate manipulation of the model's parameters.

Impaired neutrophil motility

With respect to our preliminary model, in order to accurately take into account the qualitative and quantitative changes in leukocyte migration of COPD-affected subjects compared to healthy ones, we focus on three main parameters that provide a switch from a physiological scenario of efficient neutrophil chemotaxis to a pathological one: namely k_{grad}, σ_{mem} and n_{run}. Manipulation of parameter n_{run} serves to reflect the increased undirected speed of impaired neutrophils as reported in Sapey *et al.* (2011), to preserve consistency with simulations in Section 5.4.2, with changes in the value of n_{run} not affecting the system's behaviour. The parameter k_{grad} is considerably decreased to model the loss of accuracy in the cells' chemotactic motion, thus serving as a correspondent to the chemotactic index computed in Sapey *et al.* (2011) study. In particular, the choice for k_{grad} in this setting directly takes into account the tuning provided in Section 5.4.2, by purposefully choosing $k_{grad} = 8$ to correspond to the behaviour described in Figure 5.8d. Here, the chemotactic directioning is less accurate compared to the nominal healthy scenario of Figure 5.8b when $k_{grad} = 80$, as employed instead in calibration of Section 5.4.2. Finally σ_{mem} is also updated in order to effectively model the cells' impairment in sensing the chemotactic signal typical of pathological conditions and exhibiting a stronger persistence in their directed walk as a result. Thus, the correction introduced in σ_{mem} deregulates the cells' chemotactic behaviour.

Upon pathological impairments, while cells preserve the overall tendency to move chemotactically, their migration is defective and highly inefficient. In particular a

fraction of cells do not eventually reach the chemotactic target, while the neutrophils that successfully reach and stay within higher concentrations of mediators do so through a much less smoother path, compared to cells migrating in physiological conditions (Figure 5.8d).

The biological consequences of such inefficiencies in cells' motility are multiple and severely disruptive of the inflammatory process, which in itself opens the way to further complications, as exposed in Section 1.1. The switch from physiological to pathological chemotaxis provided by this model by simply adjusting few key parameters highlights the high sensitivity of cells' behaviour to their microenvironment. Furthermore, the sets of results this model yields also suggest that neutrophils retain their chemotaxis ability in terms of persistent biased random walk even in pathological conditions such as the ones typically prescribed by COPD, with the overall impairment in their migration being subject to greater randomness in direction, at the expenses of bias towards mediators.

5.5 An enhanced inflammatory model

In order to investigate inflammatory mechanisms more thoroughly and to assess the full impact that chemotaxis has on the resolution of inflammation, we integrate the chemotactic model developed in the previous sections into the model of Chapter 4. In particular, our aim is to assess the inflammatory outcomes arising from refined modelling of the chemotactic motion of populations of neutrophils and macrophages with respect to the analysis presented in Section 4.4, where only an elementary version of the cells' chemotaxis was implemented. The resulting new ABM retains the structure and all functionalities of the model of Chapter 4. Additionally, with the inclusion of the improved chemotaxis of cells toward pro-inflammatory mediators, the working scheme of the model is updated to Figure 5.9, where the new chemotactic parameters

are also highlighted.

Figures 4.3–4.6 remain accurate in the description of the new chemotactically enhanced ABM of inflammation. Initialisation and parametrisation of the new model are also inherited from the ABM of Chapter 4. We therefore prescribe an initial damage modelled through a circular concentration of pro-inflammatory mediators centred in a square domain. Parameters retain their scaling with respect to the unitary amount δ_{ac} of pro-inflammatory mediators released by apoptotic neutrophils upon their necrosis, with all the considerations highlighted in Section 4.3 remaining valid. Finally, by describing the leukocytes' motion with higher accuracy, we introduce the two subsets of parameters modelling the neutrophil and macrophage chemotaxis respectively, as detailed in Table 5.4. In particular, when subject to standard physiological chemotaxis and in line with the parametrisation in Chapter 4, we consider neutrophils moving twice per tick, compared to macrophages moving only once per tick, with each tick being equivalent to one minute. Conversely, as inferred by the calibration of Section 5.4.2, in specific pathological conditions such as COPD, neutrophils' chemotaxis is affected and exhibits a greater undirected speed of motion. To reflect this, we prescribe a set of chemotactic parameter values controlling neutrophils' motion in disease accordingly.

With the new inflammation model outlined as above, we investigate the impact of chemotaxis on the mechanisms controlling the resolution of inflammation. In particular, we study a set of scenarios of biological interest by integrating an effectively regulated chemotaxis of neutrophils and macrophages toward pro-inflammatory mediators. In particular, we will assess expected chronic outcomes, as outlined by the model in Chapter 4, against both healthy and impaired chemotaxis. We will further analyse the efficacy of leukocytes' chemotaxis upon expected healthy outcomes, thus exposing the essential contribution of cells' directed motility in resolving inflammation.

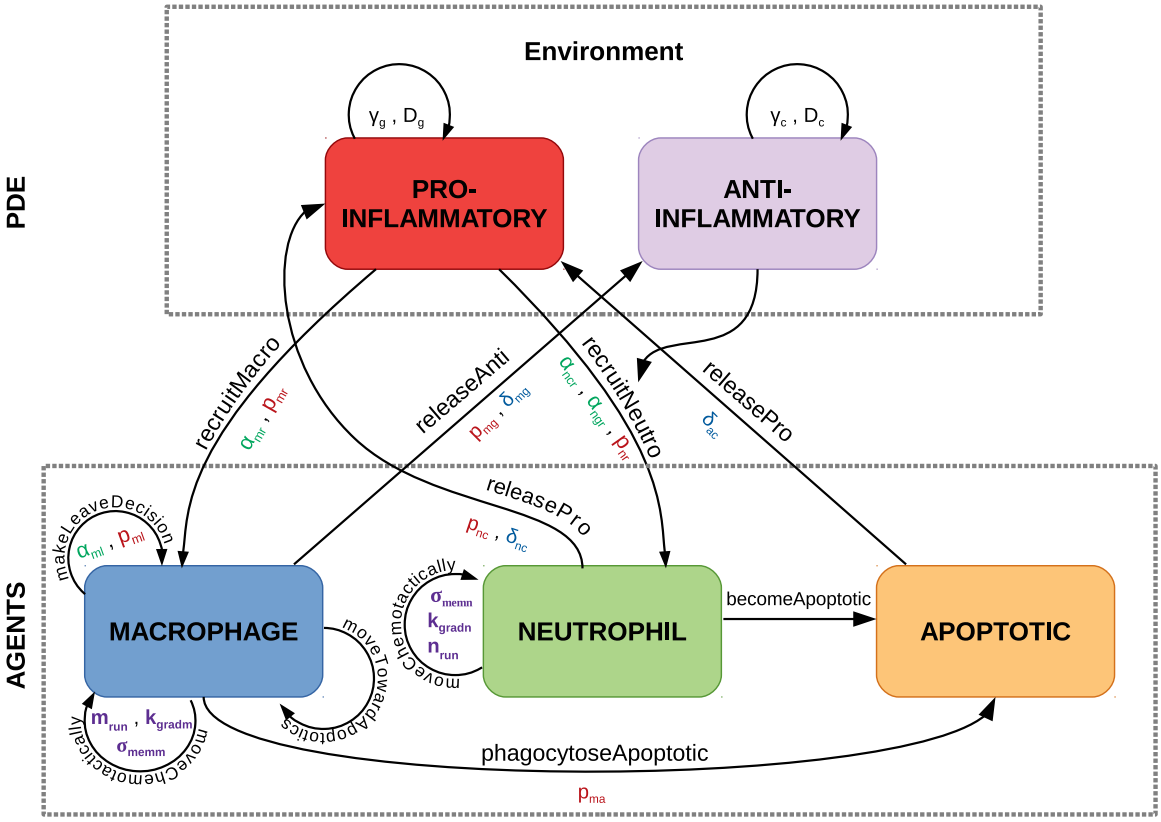

Figure 5.9: Schematic diagram representing the ABM of inflammation with improved chemotaxis and illustrating the constituent interactions between populations of healthy neutrophils, apoptotic neutrophils and macrophages, modelled as agents, in response to pro- and anti-inflammatory mediators, modelled through PDEs. Interactions are shown by arrows and can be in turn regulated by parameters. Parameters are differentiated by colour and refer to probabilities in red, increments in blue, thresholds in green, with PDE parameters in black. Newly introduced chemotactic parameters are in purple.

Parameter	Definition	Standard physiological value	Pathological value
n_{run}	number of neutrophil iterations at each tick t	2	**4**
σ_{memn}	standard deviation of likelihood of positions within the neutrophil's Moore's neighbourhood with gaussian distribution	1	**1.2**
k_{gradn}	rate parameter of likelihood of positions within the neutrophil's Moore's neighbourhood with exponential distribution	80	**8**
m_{run}	number of macrophage iterations at each tick t	1	1
σ_{memm}	standard deviation of likelihood of positions within the macrophage's Moore's neighbourhood with gaussian distribution	1	1
k_{gradm}	rate parameter of likelihood of positions within the macrophage's Moore's neighbourhood with exponential distribution	80	80

Table 5.4: Values for chemotactic parameters, with neutrophils' chemotaxis being affected in disease as inferred from Sapey *et al.* (2011) and reported in the fourth column.

5.5.1 Impaired chemotaxis

We firstly analyse the effects that more refined modelling of chemotaxis have on previously chronic outcomes. By doing so, we initialise our model of inflammation with the set of parameter values given by the second column of Table 4.4, combining these with compromised chemotactic motion of neutrophils, as set out in the fourth column of Table 5.4. The results of this simulation are shown in Figure 5.10, which confirms that the previously chronic outcome of Figure 4.8 remains chronic given pathological choices of chemotaxis parameters here. This is an intuitive result, since taking the limit of small k_{grad} in the model of Section 5.3 qualitatively recovers the chemotaxis model of Chapter 4, provided that σ_{mem} is of $\mathcal{O}(1)$ or larger. Given the calibration exercise of Section 5.4, we could regard the chemotaxis model of Chapter 4 as an accurate model of chemotactically impaired neutrophils in the context of an inflammatory condition (such as COPD); however, there is potential scope for the model of Chapter 4 to omit some healthy outcomes in which resolution is heavily reliant on

efficient chemotaxis of leukocytes. We examine this further below. This result is of particular interest in highlighting the versatility of the original inflammatory system of Chapter 4, which in its current extended version reaches the scope of successfully modelling prominent inflammatory pathologies affecting neutrophils, such as COPD.

5.5.2 Healthy chemotaxis

Healthy inflammatory outcomes

With the aim of investigating the role of chemotaxis in the effectiveness of inflammatory models, we analyse possible changes in the outcome of the acute inflammatory response upon chemotactically enhanced motion of leukocytes. In particular, we configure our enhanced model with inflammatory parameters that, in the absence of refined chemotactic mechanisms, would lead to chronic inflammation, while keeping the chemotactic parameters that prescribe physiological cell motility, as in the third column of Table 5.4. Interestingly, as shown in Figure 5.11, integrating an enhanced description of cellular chemotaxis into the model significantly changes the inflammatory outcome, prompting the restoration of the healthy state. This reinforces the key role of chemotaxis in inflammatory mechanisms and exhibits it as an additional therapeutic target that could not be otherwise captured by the previous model of Chapter 4. As a comparison with the inflammatory model of Chapter 4, its equivalents parameteric configuration, represented in Figure 4.7, where only basic chemotactic mechanisms are modelled, results in a perpetual state of inflammation. Furthermore, it is of interest to observe the spatial configuration of cells at different stages of the inflammatory response. While the central localisation of the initial damage immediately attracts both macrophages and neutrophils at the site of injury, the former group of cells remains chemotactically anchored to higher concentrations of pro-inflammatory mediators and, upon phagocytosing nearby apoptotic neutrophils,

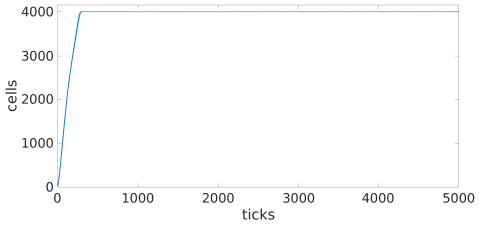

(a) Active neutrophils.

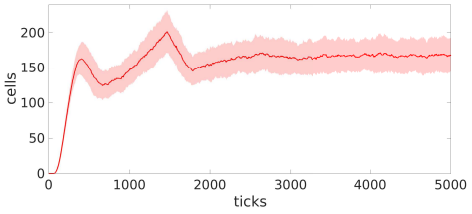

(b) Apoptotic neutrophils.

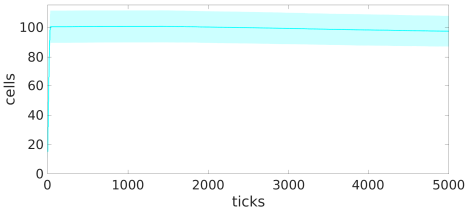

(c) Macrophages.

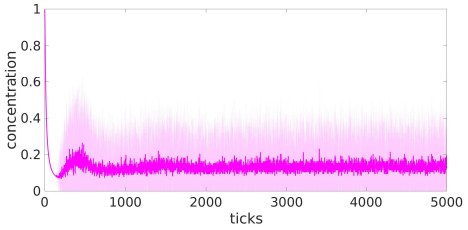

(d) Pro-inflammatory mediators.

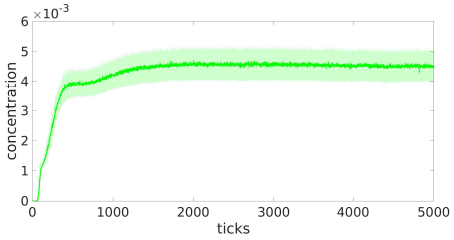

(e) Anti-inflammatory mediators.

Figure 5.10: Plots for the ABM corresponding to the average results of the batch of 100 simulations, with inflammatory parameters as in the second column of Table 4.4 and chemotactic parameters as in the fourth column of Table 5.4. Shades around the plots represent standard deviations.

starts releasing anti-inflammatory mediators. This in turn inhibits the local recruitment of new neutrophils, with existing neutrophils moving chemotactically towards diffusing concentrations of pro-inflammatory mediators. After such initial patterning of different cells, homogeneous levels of pro-inflammatory mediators across the tissue prompt the redistribution of leukocytes, with apoptotic neutrophils eventually cleared and macrophages leaving upon the resolution of inflammation.

To further highlight the effects of taking into account more refined chemotactic mechanisms in the modelling of the inflammatory response, Figure 5.12 shows the overlapped timecourses corresponding to Figures 5.10 and 4.7. In particular, it is evident how defects in the cells' ability to sense the chemoattractant and move towards it accordingly is a crucial aspect in the effectiveness of the immune response. With respect to our model, this mechanism is controlled by parameter k_{grad}, through manipulation of which we can effectively model both physiological inflammatory responses (solid coloured lines) or pathological inflammatory conditions, such as COPD (grey dashed lines).

It is also of interest to assess the new enhanced model of inflammation in scenarios where the more basic model of Chapter 4 was already delivering a healthy outcome. To this end, we consider the sets of parameter values provided in Table 4.4 highlighting the inflammatory mechanisms that shift the system's outcome from chronic to healthy. The key parameters individuated in Chapter 4 providing a switch from chronic to healthy outcomes, namely c_0 and r controlling the initial damage and α_{ncr}, α_{ngr} and α_{mr} regulating the leukocytes' recruitment, are now evaluated in the context of the improved implementation of healthy chemotaxis. Figure 5.13 shows the results of these simulations, overlaid with the corresponding results from Figure 4.10. In particular, the plots illustrated in Figure 5.13 focus on the global count of cells, throughout a timespan of 5000 ticks. As already discussed in Section 4.4.2, manipulation of the key inflammatory parameters provides a switch from

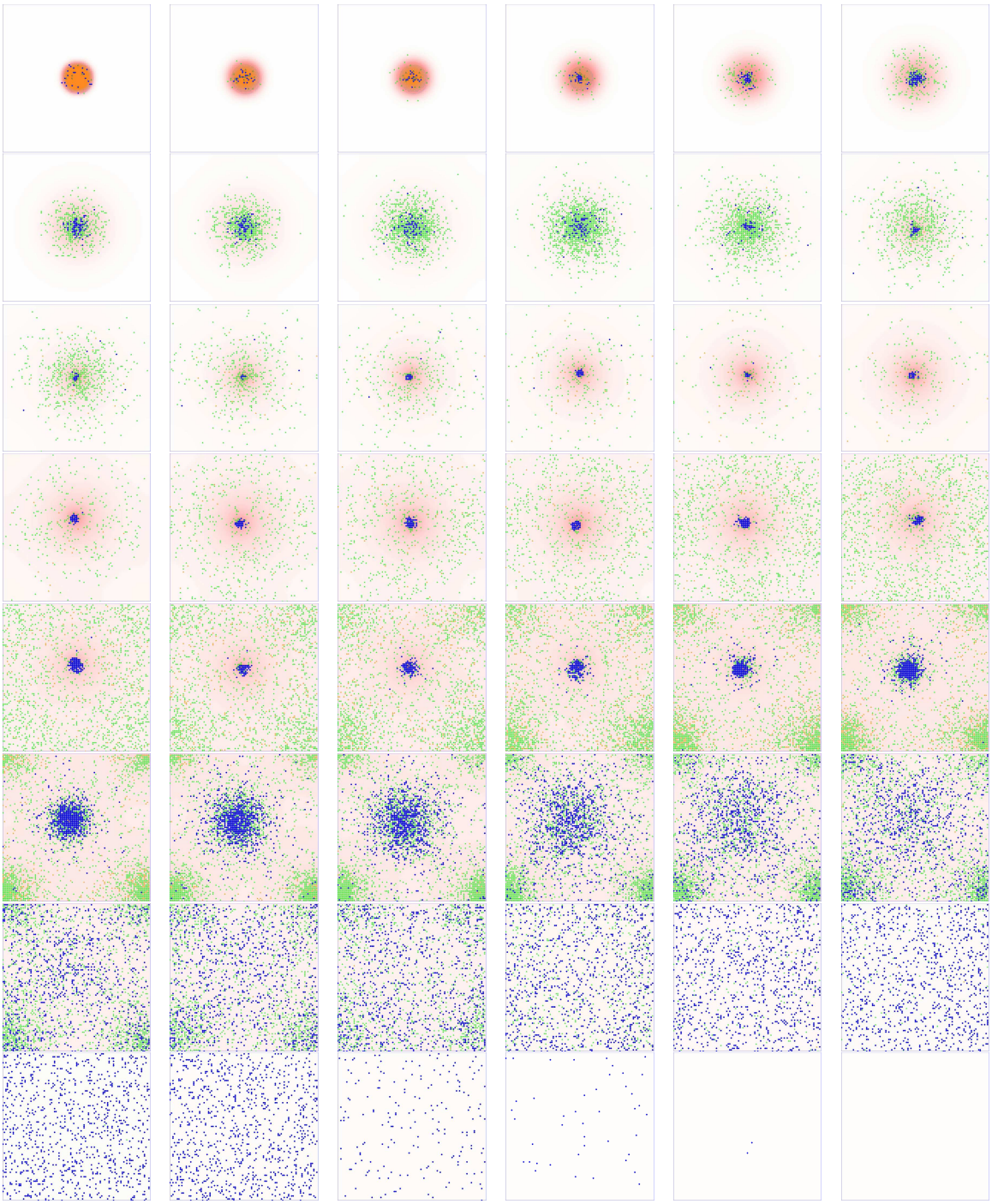

Figure 5.11: Simulation of the ABM running from $t = 0$ (upper left corner) to $t = 5000$ (bottom right corner), with inflammatory parameters as in the second column of Table 4.4 and chemotactic parameters as in the third column of Table 5.4. Macrophages are represented with blue circles, active neutrophils with green triangles and apoptotic neutrophils with orange triangles.

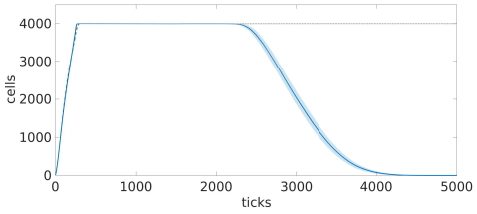

(a) Active neutrophils.

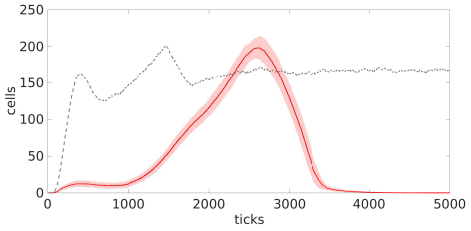

(b) Apoptotic neutrophils.

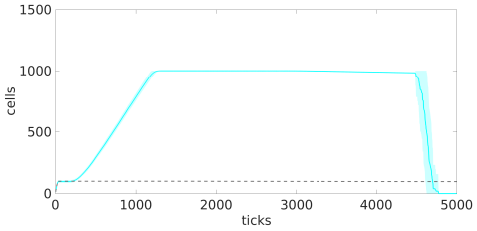

(c) Macrophages.

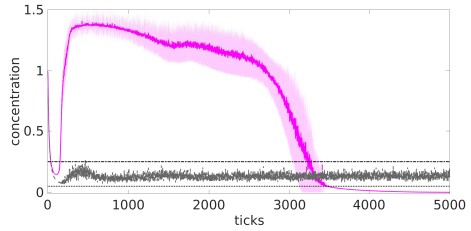

(d) Pro-inflammatory mediators.

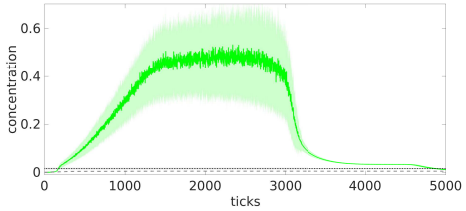

(e) Anti-inflammatory mediators.

Figure 5.12: Plots for the ABM corresponding to the average results of the batch of 100 simulations, with healthy outcomes in solid coloured lines (chemotactic parameters as in the third column of Table 5.4) and pathological ones in dashed grey lines (chemotactic parameters as in the fourth column of Table 5.4). All other parameters are as in the second column of Table 4.4. Threshold values on pro- and anti-inflammatory mediators controlling the recruitment of cells are plotted as dotted (α_{ngr} and α_{ncr}) and dotted (α_{mr}) lines, respectively. Shades around the plots represent standard deviations.

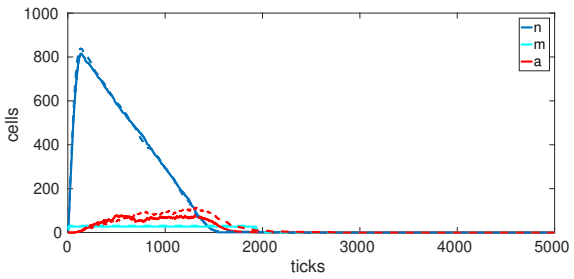

(a) $c_0 = 0.5$.

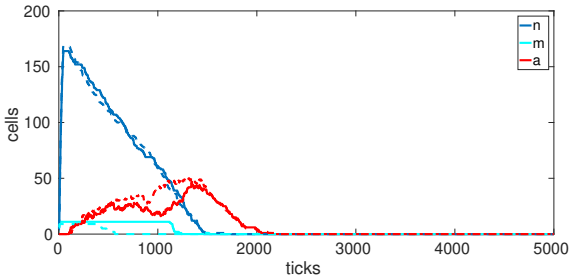

(b) $r = 5$.

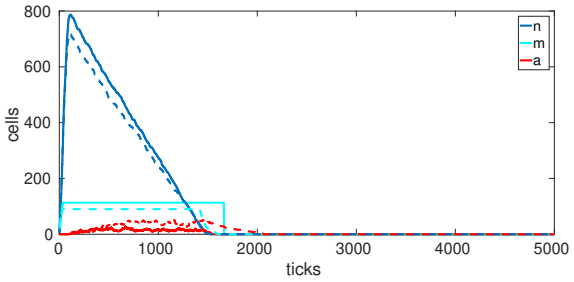

(c) $\alpha_{ncr} = 0.1$.

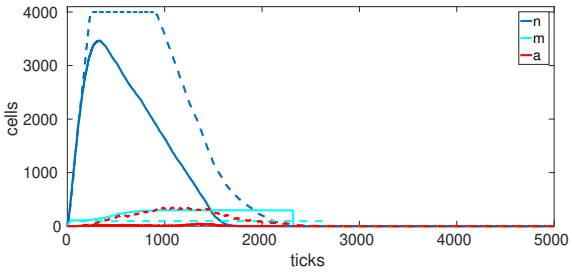

(d) $\alpha_{ngr} = 0.0015$.

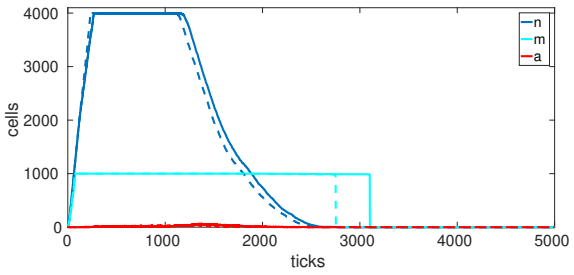

(e) $\alpha_{mr} = 0.05$.

Figure 5.13: Plots for the ABMs with basic (dashed lines) and enhanced (solid lines) models of chemotaxis, with inflammatory parameters as in the third to seventh columns of Table 4.4 (for plots (a) to (e), respectively) and chemotactic parameters as in the third column of Table 5.4.

previously chronic outcomes to healthy ones. This crucial result is retained also in our enhanced model, where, as expected, simulations exhibit the final resolution of inflammation. An important point to observe is that there is not a significant difference in either healing times or severity between the inflammatory model of Chapter 4 and the chemotactically more advanced one of the current chapter. These results indicate that these switches from chronic damage to full resolution are not heavily reliant upon efficient chemotaxis; moreover, it is the delicate balance between neutrophil recruitment due to pro-inflammatory mediators and the competing anti-inflammatory role of macrophages that determines the ultimate outcome for these choices of parameters.

Chronic inflammatory outcomes

It is important to highlight that, even in the presence of physiological (healthy) chemotaxis in this enhanced model, the model still supports both healthy and chronic long-term outcomes. The strength of the chemotactic behaviour is not sufficiently large to out-weigh the other behaviours in the model. We illustrate this briefly in Figure 5.14, in which we increase the parameter regulating the recruitment of macrophages from $\alpha_{mr} = 0.25$ to $\alpha_{mr} = 0.4$. Figure 5.14 illustrates that a disruption of the healing process caused by more significant initial damage and/or detrimental changes to cell recruitment parameters can yield a chronic response, in spite of optimal chemotactic motion of leukocytes. The model hence retains the fundamental bistability of all of the models studied within this thesis, in the presence of our enhanced model of physiological chemotaxis. A qualitatively similar result is obtained upon increasing the parameter accounting for neutrophil recruitment via anti-inflammatory mediators from $\alpha_{ngr} = 0.015$ to $\alpha_{ngr} = 0.02$, with figures omitted for brevity.

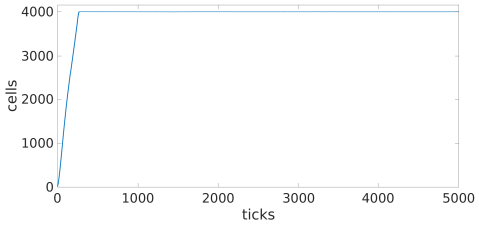

(a) Active neutrophils.

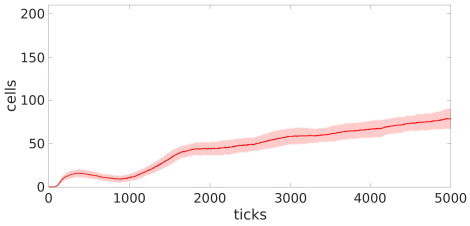

(b) Apoptotic neutrophils.

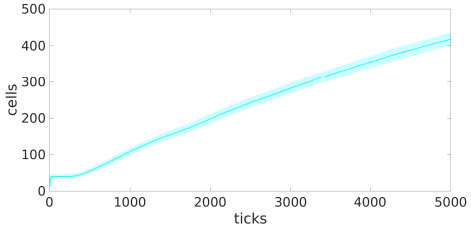

(c) Macrophages.

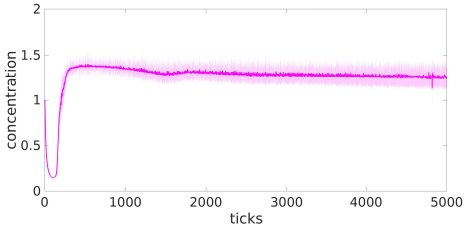

(d) Pro-inflammatory mediators.

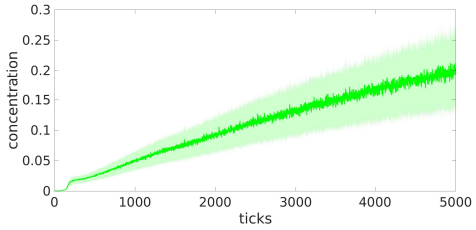

(e) Anti-inflammatory mediators.

Figure 5.14: Plots for the ABM corresponding to the average results of the batch of 100 simulations, with $\alpha_{mr} = 0.4$ and all other inflammatory parameters as in the second column of Table 4.4 and chemotactic parameters as in the third column of Table 5.4. Shades around the plots represent standard deviations.

5.5.3 Parameter sensitivity

In Figure 5.15, we examine the extent to which the inflammatory outcome depends upon our choices of model parameters. Holding chemotactic parameters fixed at the healthy choices calibrated in Section 5.4.2 ($k_{grad} = 80$, $\sigma_{mem} = 1$), we perform simulations with each parameter in Table 5.5 increased by 50% (denoted by upward pointing green triangles in the figure) and decreased by 50% (denoted by downward pointing red triangles in the figure) and record the mean percentage change in the maximal level of pro-inflammatory mediator c and active neutrophils n at $t = 5000$. (We omit the parameter δ_{ac} from this analysis, as this parameter is directly implicated in the non-dimensionalisation of the inflammatory model described in Section 4.3. For parameters representing probabilities for which an increase of 50% would result in a choice greater than one, we instead perform simulations with unit probability.) As usual, all results are averaged across batches of 100 simulations. Since the baseline parameter set of Table 5.5 yields a chronic outcome (Figure 5.14), we are particularly interested in whether changes in parameter values can result in a switch to full resolution (*i.e.* a percentage change of -100% in Figure 5.15).

Intuitively, a reduction in the severity of the initial damage (via either c_0 or r) can result in the inflammation being fully resolved. Interestingly, the model is highly sensitive to variations in the rate of pro-inflammatory mediator diffusion, D_c, in that both high and low choices can drive resolution, by weakening the model's positive feedback or strengthening its negative feedback respectively. For D_c large, the damage rapidly spreads spatially, attaining low levels across the domain. This results in a much weaker neutrophil response, which is ultimately overcome by macrophages. Conversely, for D_c small, the initial damage remains more localised, with greater levels of pro-inflammatory mediator at the site of initial damage. This triggers more rapid recruitment of macrophages, which in turn generate increased release of anti-

Parameter	Reference values (Chronic outcome)	Decreased values (−50% of reference value)	Increased values (+50% of reference value)
c_0	1	0.5	1.5
r	10	5	15
D_c	1.5	0.75	2.25
D_g	1.5	0.75	2.25
γ_c	0.002	0.001	0.003
γ_g	0.002	0.001	0.003
δ_{nc}	0.001	0.0005	0.0015
δ_{mg}	0.001	0.0005	0.0015
p_{nr}	0.02	0.01	0.03
p_{nc}	0.5	0.25	0.75
p_{mr}	0.04	0.02	0.06
p_{mg}	0.8	0.4	1
p_{ml}	0.8	0.4	1
p_{ma}	1	0.5	n/a
α_{ncr}	0.05	0.025	0.075
α_{ngr}	0.015	0.0075	0.0225
α_{mr}	0.4	0.2	0.6
α_{ml}	0.02	0.01	0.03

Table 5.5: Parameter values for the reference chronic outcome (second column) and for sensitivity study with values to be tested representing decrease in half of reference value (third column) and increase in half of reference value (fourth column).

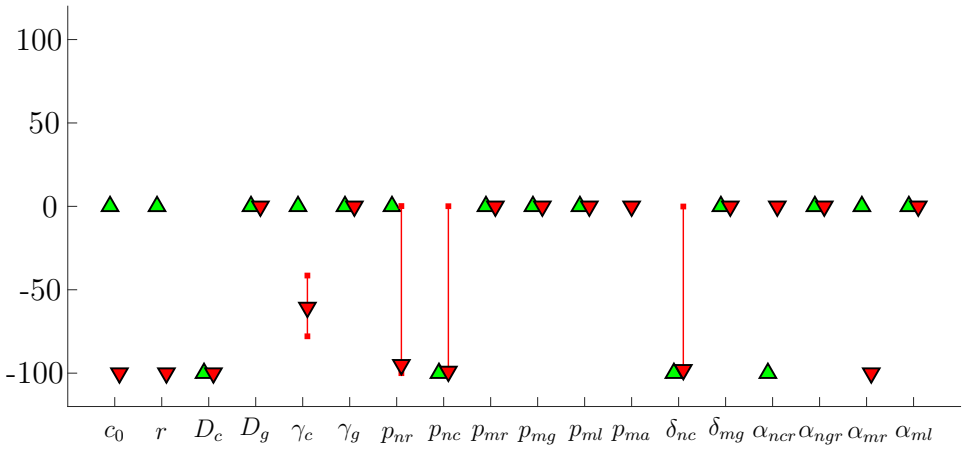

(a) Active neutrophils.

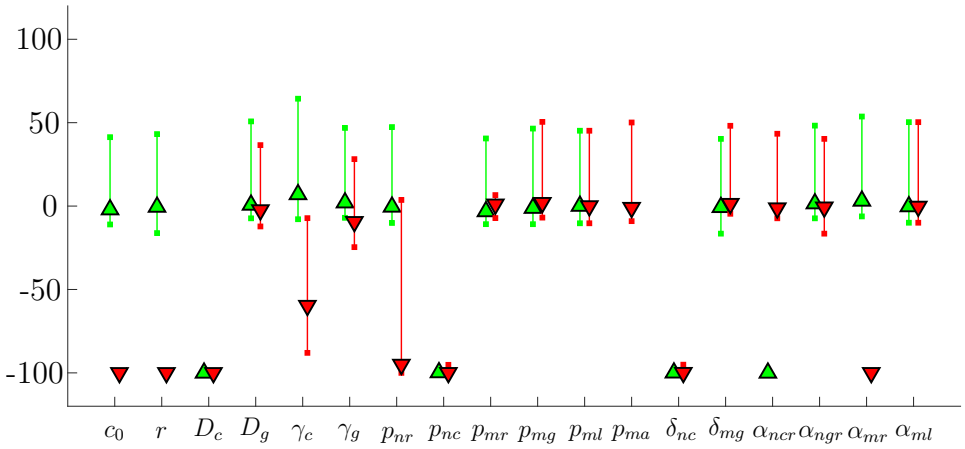

(b) Pro-inflammatory mediators.

Figure 5.15: Parameter sensitivity analysis results showing the percentage change in (a) the number of active neutrophils and (b) the concentration of pro-inflammatory mediators, both with respect to the reference chronic simulation with parameter values given in Table 5.5 at final tick $t = 5000$, for variations of individual parameters. Green and red triangles represent 50% increases and decreases respectively. Bars indicate change in minimum and maximum changes in percentage over 100 simulations for each parameter. Note that a change in response of -100% corresponds to a switch from a chronic to a healthy outcome.

inflammatory mediators, which once again trigger full resolution. Similarly the model exhibits some dependence upon the pro-inflammatory mediator decay parameter, γ_c. For the parameters studied in Figure 5.15, a reduction of γ_c is sufficient to stimulate a greater macrophage response, yielding a long-term reduction in the severity of the damage. The model is much less sensitive to the PDE-parameters associated with anti-inflammatory mediators, D_g and γ_g, for the parameters investigated here.

Reducing the recruitment of neutrophils by increasing α_{ncr} (or decreasing p_{nr}) or stimulating the recruitment of macrophages by reducing α_{mr} can switch the model to a healthy outcome. The model is less sensitive to choices of the neutrophil recruitment parameter α_{ngr}; however, more significant reductions in this parameter can also drive resolution, as illustrated in Figure 5.12. The model exhibits a bidirectional sensitivity to the strength of the pro-inflammatory neutrophil feedback (δ_{nc}, p_{nc}) in the same manner as is described for the diffusion parameter D_c above. The model is largely insensitive to variations in the remaining parameters (for the combinations examined here); in particular, while variations in probabilistic parameters related to macrophages may affect the timescales associated with macrophage recruitment and the anti-inflammatory response, these do not affect the long-term inflammatory outcome here. The parameter α_{ml} does not affect the resolution of damage; only the rate at which macrophages vacate the tissue after damage is resolved.

In comparison with the parameter sensitivity analysis of Chapter 4 (Figure 4.13), we observe how the models' responses to variations of parameters controlling the levels of pro-inflammatory mediators c are driven by chemotaxis strength. In particular, the effects of parameter D_c are less strong in the inflammatory model of Chapter 4, due to the cells' reduced sensitivity to the chemotactic signal. Similarly, the discrepancy in the sensitivity analysis for parameters γ_c, p_{nc} and δ_{nc} between Figures 5.15 and 4.13 is explained by the stronger effect that the spatial distribution of c has in the chemotactically enhanced model.

Finally, in Figures 5.16 and 5.17, we briefly assess the models sensitivity to our implementation behaviours per ticks of the ABM algorithm. We note that varying the definition of a tick does not affect the numerical solution of the PDE portions of the model, since a separate numerical timestep is also implemented. Since all other cellular behaviours are scheduled every tick in our model, we focus, in particular, upon how varying the frequencies of cell recruitment affects the outcome of the model. In all previous simulations we recruit neutrophils every two ticks and macrophages every five ticks to account for the more rapid recruitment of neutrophils *in vivo*. Here (and in Figure 5.16 and 5.17), we label the recruitment frequencies of neutrophils and macrophages as n_{freq} and m_{freq} respectively.

In Figure 5.16, we show how variations in n_{freq} and m_{freq} affect the otherwise healthy outcome obtained for $\alpha_{mr} = 0.05$ (shown in Figure 5.13e). For the choices of n_{freq} and m_{freq} shown, the outcome is still one of full resolution; the scheduling of cell recruitment has negligible effect on the results, and only gives rise to small variations in the time taken to resolve the damage. In Figure 5.17, we perform a similar analysis for the baseline set of parameter values listed in the second column of Table 5.4, for which we usually obtain a chronic outcome. For small variations in the cell recruitment frequencies (*e.g.* $n_{freq} = 3$ or $m_{freq} = 2$, shown in blue and red respectively) we obtain a similar chronic result to that previously obtained in Figure 5.14 (shown in black here). However, for significantly slower neutrophil recruitment (*e.g.* $n_{freq} = 5$; magenta) or significantly more rapid macrophage recruitment (*e.g.* $m_{freq} = 2$; green), we may observe a switch from chronicity to restoration of health. Thus, the model does exhibit some sensitivity to the manner in which behaviours (cell recruitment, in particular) are scheduled; however, in most cases the model parameters listed in Table 5.4 seem to have much greater influence upon model outcomes. We reflect on this further in the discussion below.

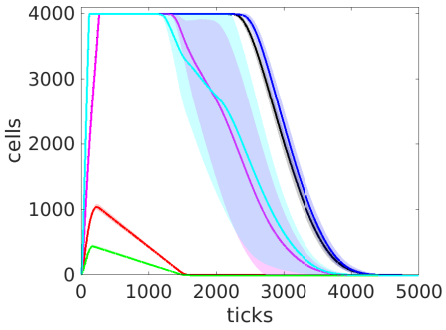

(a) Active neutrophils.

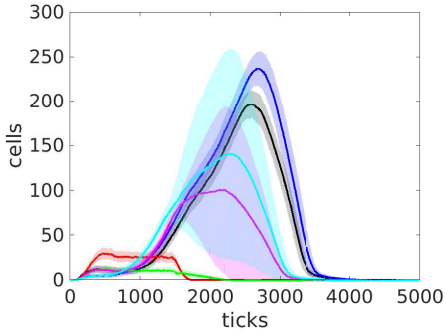

(b) Apoptotic neutrophils.

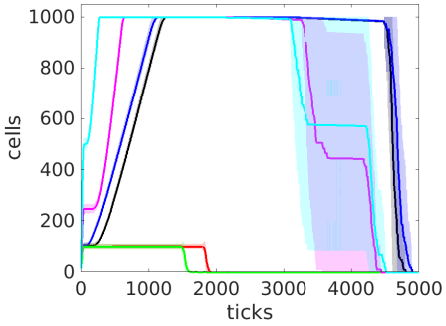

(c) Macrophages.

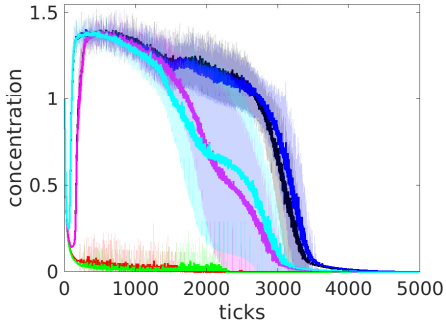

(d) Pro-inflammatory mediators.

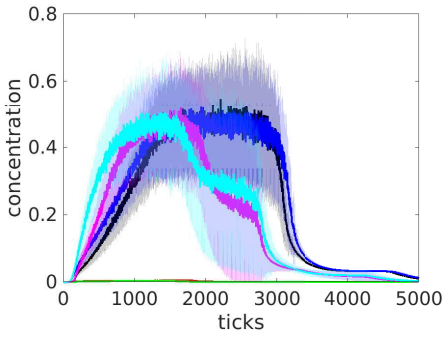

(e) Anti-inflammatory mediators.

Figure 5.16: Results obtained on varying the frequencies of neutrophil and macrophage recruitment (n_{freq} and m_{freq} respectively) for $\alpha_{mr} = 0.05$,with inflammatory parameters as in the seventh column of Table 4.4 and chemotactic parameters as in the third column of Table 5.4. The healthy outcome obtained for our standard choice of $n_{freq} = 2$ and $m_{freq} = 5$ is shown in black. The remaining curves represent the following: $n_{freq} = 1$ and $m_{freq} = 5$ (blue); $n_{freq} = 5$ and $m_{freq} = 5$ (red); $n_{freq} = 10$ and $m_{freq} = 5$ (green); $n_{freq} = 2$ and $m_{freq} = 2$ (magenta); $n_{freq} = 2$ and $m_{freq} = 10$ (cyan). While the time taken to full resolution varies slightly, these parameters have no significant impact on the final outcome.

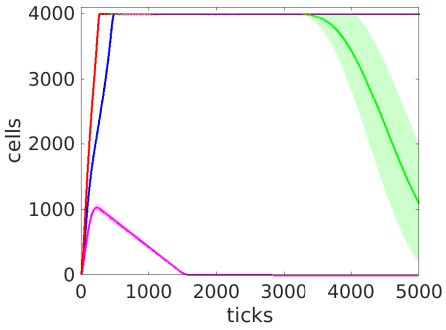

(a) Active neutrophils.

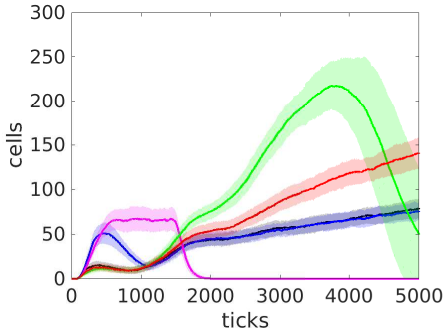

(b) Apoptotic neutrophils.

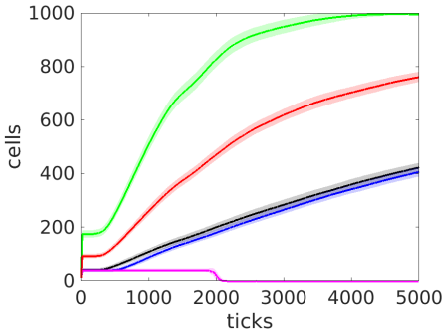

(c) Macrophages.

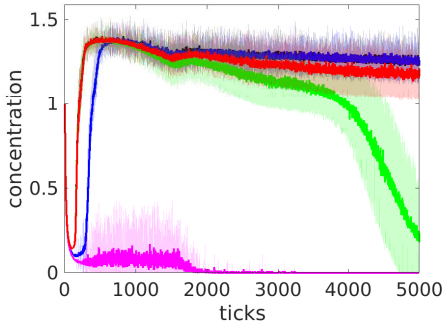

(d) Pro-inflammatory mediators.

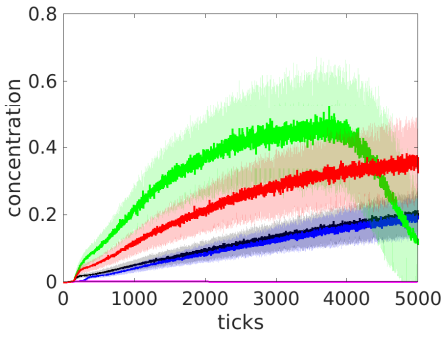

(e) Anti-inflammatory mediators.

Figure 5.17: Results obtained on varying the frequencies of neutrophil and macrophage recruitment (n_{freq} and m_{freq} respectively) for the baseline inflammatory parameters given in the second column of Table 4.4. The chronic outcome obtained for our standard choice of $n_{freq} = 2$ and $m_{freq} = 5$ is shown in black. The remaining curves represent the following: $n_{freq} = 3$ and $m_{freq} = 5$ (blue); $n_{freq} = 2$ and $m_{freq} = 2$ (red); $n_{freq} = 2$ and $m_{freq} = 1$ (green); $n_{freq} = 5$ and $m_{freq} = 5$ (magenta). Small variations in these parameters have negligible impact on the outcome; however, very slow neutrophil recruitment or very rapid macrophage recruitment can switch the outcome from chronicity to health.

5.6 Conclusions

In this chapter we developed a model of leukocyte chemotaxis to better detail the chemotactic mechanisms initially implemented in the previous model of Chapter 4. In particular, the limitations introduced by the simplifications of the previous model were tackled in this chapter by analysing specific features of cells' directed motion. This was done by constructing a more advanced model of chemotaxis that incorporates cells' persistence in motion to better replicate experimental observations.

Firstly, the biological mechanisms regulating cell migration were presented, with a particular focus on leukocyte motility in both physiological and pathological contexts. The relevant scientific literature was reviewed and typical modelling approaches in terms of random walks were also presented. We proceeded by defining an ABM accounting for neutrophils moving to a chemotactic target upon tuning of a set of parameters that reflect significant biological features, namely bias (attraction to the chemoattractant) and persistence (memory of past moves) in the cells' random walk, and are in accordance to the experimental setting of the study conducted by Sapey *et al.* (2011). The model was carefully calibrated against the experimental data published by Sapey *et al.* (2011) for healthy patients and COPD patients, thus allowing us to define sets of chemotactic parameters defining both physiological and pathological (COPD-affected) cellular motility. Variations in the values of such key parameters can shift the model's behaviour from a healthy scenario to a pathological one, with particular reference to COPD. This is a proof of principle demonstrating how our model can be to tuned to accurately describe leukocyte chemotaxis under a specific inflammatory condition. The model retains the distinctive features of neutrophil motility, implemented in the form of a biased persistent random walk. Simulations resulting from both physiological and pathological scenarios are directly comparable to experimental data. The model's assessment is followed by an analysis of the result-

ing simulations, calibrated against the data of Sapey *et al.* (2011), highlighting strong agreement between *in vitro* and *in silico* results, confirming the model's validity and opening up the way to further investigations in this direction and the use of the model as a predictive tool in both health and disease.

Finally, we incorporated our enhanced chemotaxis model into the model of Chapter 4. In fact, while the model of Chapter 4 describes the inflammatory response well in the context of an inflammatory condition with impaired chemotaxis, it omits the observations that some seemingly chronic outcomes can actually be resolved by efficient chemotaxis in healthy patients. This novel ABM, on the other hand, offers an important improvement in the landscape of inflammatory models, by providing an enhanced description of directed cell motility and successfully capturing the inflammatory mechanisms at play upon defective chemotaxis. In particular, we firstly investigated the effects of impaired chemotaxis on the inflammatory outcome. Our simulations show (in Figure 5.10) that in an impaired chemotactic regime, in which cells are equipped with a weaker sensitivity to the chemotactic target (*i.e.* reduced k_{grad}) and a greater persistence in their direction of motion (*i.e.* increased σ_{mem}), an otherwise healthy response can be pushed to a self-perpetuating inflamed state. We then extended the analysis of physiological cellular motility during the acute inflammatory response by determining the different scenarios that determine the resolution of inflammation and, by contrast, its ongoing chronic state. Additionally, we exposed how not all resolution is dependant on chemotaxis. In particular, the long-term inflammatory outcome is determined by a balance between the pro-inflammatory (positive) feedbacks of neutrophils and the anti-inflammatory (negative) feedbacks of macrophages; conditions which enhance the neutrophil response (via *e.g.* δ_{ac}, δ_{nc} large or α_{ncr} small in our model) are more likely to yield a self-perpetuating inflammatory condition, while treatments that enhance the macrophage response (via *e.g.* δ_{mg} large or α_{mr} small) are more likely to stimulate resolution in the long-term. (See

Figures 5.13 and 5.14.) To this end, mediated cell recruitment remains an important therapeutic target, regardless of chemotactic strength. We concluded our investigation of the model by performing a parameter sensitivity analysis, to evaluate the model's dependence on its parameters, exhibiting how initial conditions, cells' recruitment and regulation of pro-inflammatory mediators c can have a driving effect on the resolution of inflammation.

Overall, the hybrid model presented here has facilitated inclusion of a greater array of cell-specific behaviours than is afforded by many previous (mostly ODE- or PDE-based) models. For example, the model includes a description of cells' chemotaxis toward pro-inflammatory mediators that is calibrated against experimental data, and also specifically incorporates the preferential motion of macrophages toward nearby apoptotic neutrophils. Furthermore, the model includes an explicit (while simplistic) description of the activation of the anti-inflammatory macrophage response that can be applied on a cell by cell basis as each macrophage undergoes its first phagocytosis of an apoptotic neutrophil. The precise cellular and sub-cellular mechanisms that initiate production of anti-inflammatory mediators is complex (Dunster & Dransfield, 2016); however, the link between the phagocytosis of apoptotic cells and the phenotypic switch of macrophages from the classically activated M1 phenotype to the alternatively activated, anti-inflammatory M2 phenotype is well documented in existing literature (Schnyder & Baggiolini, 1978; Korns *et al.*, 2011; Hiemstra, 2013). This notwithstanding, it is well-known that the M1/M2 classification of macrophages presents a degree of over-simplification in itself, with the broad range of macrophage phenotypes actually spanning a continuous spectrum Dunster & Dransfield (2016). There is a great degree of scope to extend our model to include more detailed descriptions of macrophage phenotypes and corresponding inflammation-related behaviours going forward. In the model presented here, we include only the anti-inflammatory effects of the M2 macrophage; however, macrophages of the M1 phenotype can also

provide pro-inflammatory stimuli, which are here omitted as we focus on the dominant pro-inflammatory effects of neutrophils. Our model also omits the scope for bidirectional switching between macrophage phenotypes. More refined modelling of the relevant cell signalling cascades that govern phenotypic switching of macrophages remains a target for future study.

Our model exhibits significant scope to be calibrated to model specific inflammatory conditions in specific tissues. An open question, in this context, is that of how to infer some parameter values directly from experiments. While the PDE parameters (D_c, D_g, γ_c, γ_g) can be inferred from existing literature to some extent, and chemotactic parameters (k_{grad}, σ_{mem}) can be inferred from cell tracking experiments as described here, there remains a degree of uncertainty regarding the various threshold parameters controlling cell recruitment (α_{ncr}, α_{ngr}, α_{mr}) and the strengths of the corresponding inflammatory feedbacks (δ_{nc}, δ_{ac}, δ_{mg}). These parameters are likely to vary across both inflammatory conditions and affected tissues. We have the least confidence in the precise values of the probabilistic parameters in the model; however, we have also shown that in most cases the model's outputs are robust to variations in these values (Figure 5.15). Furthermore it is to be expected that our model exhibits some sensitivity to the choice of how cellular responses are scheduled 'per tick', or equivalently how a tick itself is defined. We note that tick definition affects only the agent-based components of our model, since numerical solution of the PDEs is implemented independently. In our implementation, most behaviours are scheduled to occur at every tick. We anticipate that alternative implementations of most behaviours simply correspond to alternative choices of the related probabilities or feedback parameters, and thus would not impact upon the qualitative observations presented here. The only behaviour that is not scheduled every tick here is cell recruitment, which we schedule every two ticks for neutrophils and every five ticks for macrophages to account for more rapid recruitment of neutrophils *in vivo*.

Simulations that experiment with alternative choices of these recruitment frequencies (Figures 5.16 and 5.17) reveal that the model is relatively robust to variations of these values. For parameter choices that yield a healthy outcome here (Figure 5.13), alternative choices of cell recruitment frequencies generally still result in a healthy outcome, but with some small variation in the time taken to achieve full resolution of damage (5.16). For a parameter-set corresponding to a typical chronic simulation (*e.g.* that of Figure 5.14), small variations in recruitment frequencies make minimal difference to model results; however, significantly slower neutrophil recruitment or significantly more rapid macrophage recruitment can yield a switch from chronicity to restoration of health in some cases (5.16). Experimental studies that quantify cell recruitment, in particular, would advance our ability to model accurately specific inflammatory conditions.

Chapter 6

Conclusions

In this work, we have studied a number of mathematical approaches to effectively model a spatio-temporal description at tissue level of the acute inflammatory response. The prominence of inflammation in several pathologies has long been established, with the presence of low persistent levels of inflammation being a key precursor in critical conditions such as neurodegenerative disorders (Alzheimer's, Huntington's, Parkinson's) and cancer, as well as aggravating existing comorbidities such as type-2 diabetes and Chronic Obstructive Pulmonary Disease (COPD), among others. The clear understanding of inflammation and in particular the mechanisms controlling its resolution remains a highly challenging objective for the scientific community, tackled through very multidisciplinary approaches. Overall, our models address the question of how localised damage can invade neighbouring healthy tissue, which is not thoroughly investigated in literature. The clear understanding of such features is a key point in preventing chronic undesired outcomes and, throughout this work, we aimed at identifying the leading mechanisms in resolving damage.

In Chapter 2, we firstly extended an existing ODE model as a starting point for our work. We proceeded by studying the basic underlying interactions between pro-inflammatory mediators and cells, where the damage triggering the acute inflam-

matory response is driven by a function of time f. We assessed the stabilities of the steady states and investigated potential scope for pattern formation. Our thorough analysis of this first simplified PDE model of inflammation revealed the key role of a subset of biologically significant parameters, namely ϕ, the rate at which macrophages phagocytose apoptotic neutrophils, and β_a, a constant representing the saturation level upon which the release of pro-inflammatory mediators depends. The bifurcation analysis along with manipulation of sensitive parameters in simulations and an accurate analysis of Turing instabilities excluded the model's capability of exhibiting spatially inhomogeneous outcomes, which prompted further investigations into addressing this first model's shortcomings.

In Chapter 3, we extended the PDE model of Chapter 2 by including a second group of chemicals acting as anti-inflammatory mediators and adding a direct interaction between active neutrophils and the enhanced presence of pro-inflammatory mediators. Furthermore, we modelled cellular motion as chemotactically driven toward higher concentrations of pro-inflammatory mediators. By investigating the stability of the steady states associated to the correspondent ODE system, we found a pattern-forming regime driven by Hopf bifurcations. In particular, we found that careful manipulation of key parameters ϕ, accounting for the phagocytosing rate, and ν, representing the rate at which neutrophils become apoptotic, yield a range of biologically meaningful outcomes, namely homogeneous resolution and restoration of the healthy state, homogeneous damage and persistent inflammation and, most interestingly, spatially inhomogeneous outcomes, either stationary or oscillatory, representing chronic recurring inflammation. These chronic inhomogeneous solutions lie in an area of parameter space for which the corresponding ODE model predicts full resolution of damage. Having identified the areas of (ϕ, ν)–space that exhibit spatially inhomogeneous solutions, we examined the extent to which the balance between the pro-inflammatory feedback from active neutrophils and the counteracting

anti-inflammatory feedback from macrophages can bias the system toward globally inflamed or spatially inhomogeneous solutions. For strong pro-inflammatory feedback or weak anti-inflammatory feedback, spatial patterns are eliminated and the results of the corresponding homogeneous model are recovered. The anti-inflammatory mediator thus plays a key role in mediating the spatial spread of damage. While the PDE model of Chapter 3 presents a reasonably thorough catalogue of biological interactions, these are not exhaustive. The PDE modelling framework used here is somewhat prohibitive as regards incorporating further interactions, thus motivating a switch to the alternative strategy of agent based modelling.

In Chapter 4 we developed a novel hybrid PDE–ABM framework where cells are accounted for as individual agents, retaining the PDE implementation for inflammatory mediators. In particular, while providing a new modelling framework for modelling the acute inflammatory response, we improved upon the previous PDE-based model by including macrophages' ability to preferentially exhibit chemotaxis toward apoptotic neutrophils and differentiating their role with respect to their contribution of actively releasing anti-inflammatory mediators. The key results that this alternative modelling approach provided included the individuation of a set of parameters of biological significance that acted as switches between undesired chronic outcomes and the resolution of inflammation. In particular, the parameters of interest control the initial damage in terms of both severity (c_0) and size (r) and the recruitment of neutrophils and macrophages (α_{ncr}, α_{ngr} and α_{mr}, respectively). This allowed us to determine such biological features as key targets for therapeutic strategies, suggesting minimising the sterile damage in surgical procedures on one hand and developing tailored drug treatments for enhancing macrophage recruitment and inhibiting neutrophil recruitment on the other hand. The phagocytosing ability of macrophages was also assessed, with manipulation of the phagocytosing rate decreasing the healing time. Finally, a parameter sensitivity analysis was also performed, confirming the

robustness of the model with respect to its parameters.

In Chapter 5 we investigated the role of chemotaxis in inflammatory mechanisms. We developed an initial ABM of chemotaxis, calibrating it against the experimental data reported by Sapey *et al.* (2011). This demonstrated how our model could be tailored to specific conditions. In particular, we modelled leukocytes' chemotaxis in terms of a random biased persistent walk, where cells' motion is regulated by parameters controlling the preference to move toward their chemotactic target and the memory of the direction the are coming from. We then included the improved description of chemotaxis into our ABM inflammatory model. This new chemotactically enhanced model of inflammation improves on the previous model of Chapter 4 by effectively capturing critical inflammatory processes that are eventually resolved because of cells' efficient chemotaxis. A parameter sensitivity analysis further highlighted the stronger response of the model to the spatial distribution of pro-inflammatory mediators c, driven by the enhanced chemotactic mechanisms. Finally, we completed our investigation of the chemotactically improved inflammatory ABM by evaluating the impact of alternative choices of cell recruitment frequencies. In particular, manipulating the frequencies at which neutrophils and macrophages are recruited was shown to have minimal effects on the systems outcome when acting on a set of parameter values that yield a healthy response, with only small variations in the healing times. Conversely, for parameter choices that yield chronic outcomes, only large variations of cell recruitment frequencies can yield the restoration of the healthy state in some cases, via either a significantly increased macrophage recruitment frequency or significantly slowed neutrophil recruitment. The model presented in Chapter 5 is the most robust of the four models presented in this thesis, given that it includes a full repertoire of inflammatory interactions and a description of cell chemotaxis that can be easily calibrated against experimental data (as we have demonstrated here with respect to COPD). The model exhibits significant scope to be tuned to model spe-

cific tissues, ailments or clinical interventions in the future, given the availability of suitable experimental data. The hybrid approach used is advantageous as it is readily accessible to non-theoreticians, and includes stochastic rules that can be easily adjusted to incorporate new biological insights as they arise.

In summary, in this work, we developed spatial models of the acute inflammatory response, investigating the biological interactions occurring at tissue level between leukocytes and inflammatory mediators. To this end, we extended the model of Dunster *et al.* (2014) into a PDE system comprising of cell populations (active neutrophils, apoptotic neutrophils and macrophages) and two groups of chemicals (pro- and anti-inflammatory mediators), including the description of both diffusion and cellular chemotaxis. We observed that the addition of the anti-inflammatory response and cellular feedback into the release of pro-inflammatory mediators are key for the system to permit sustained inhomogeneous oscillations, corresponding to chronic non-resolving outcomes. We further developed a novel ABM inflammatory model, improving on the previous model by including a differentiated phagocytosing mechanism for macrophages and prescribing their preferential chemotactic motion toward apoptotic neutrophils. We identified possible therapeutic strategies for the resolution of inflammation in the targeting of the initial damage size and severity and in cells' recruitment mechanisms. We then proceeded to develop a ABM of leukocyte's chemotaxis, modelling cells' motion in terms of bias toward a prescribed chemical and memory of past moves, calibrating the novel model against experimental data from Sapey *et al.* (2011), thus providing a proof of principle for modelling specific pathologies arising from poor chemotaxis. We finally included our improved description of chemotaxis into the ABM inflammatory model, investigating the impact of physiologic chemotaxis into resolving critical inflammatory states.

The highly interdisciplinary nature of this work and the prominence of inflammation in research topics provides interesting results that can be further extended and

investigated in future works. In particular, parametrisation remains a highly challenging issue for our modelling. To better tackle this, we suggest to identify parameters of interest (including those regulating diffusion and chemotaxis) through experiments tailored on specific conditions. In this regard, some parameters remain difficult to capture with traditional laboratory techniques, increasing the need to consider a fitted experimental design. Overall, to effectively investigate this, we suggest to focus on those parameters that models are sensitive to. Another key point of interest that prompts further studies is the more accurate modelling of the macrophage response and the relevant cell signalling it involves. In particular, macrophage action does not depend on a binary active/inactive state of the cells, rather operating on a spectrum of behaviours. This feature is only partially covered in the implementation of our ABM inflammatory model and can be further extended to better reflect the complex behaviour of macrophages. Moreover, an important step into further integrating this research with biology will be to consider software development aimed at providing simulations in the biological domain. This is particularly suited for models implemented through the ABM framework, for which the system's simulation settings can be easily designed, controlled and manipulated through a tailored Graphical User Interface (GUI), a feature where ABMs emerge as preferable to PDE ones. In the most recent literature, other researchers' work investigating mathematical models of inflammation have been mainly focused on targeting specific inflammatory conditions (such as psoriasis (Ringham *et al.*, 2019) and atherosclerosis (Thon *et al.*, 2019)) or pathologies closely linked to it, with the vast and growing research on in the field mathematical oncology on one hand (Karolak *et al.*, 2018) and agent-based modelling applied to biology on the other hand (Vodovotz & An, 2019). As such, this work can be conveniently extended and adapted to better describe and investigate specific inflammatory mechanisms and diseases that arising from the inflammation's spread and persistence. We note that, while our models pay close attention to leuko-

cyte movement within the tissue of interest, the description of how leukocytes arrive from the vasculature was kept deliberately simple throughout the inflammatory models of Chapters 2–5. In reality, cell transmigration from blood vessels depends on a complex set of events that reduce the velocity of cells flowing in blood and enable cell adhesion to the endothelial lining, resulting in the endothelial lining itself activating to allow cells to migrate through the vessel wall into the tissue (Nourshargh & Alon, 2014). While including all of these events would be unnecessarily complex in a model of generic inflammatory damage, the models presented here could easily be adapted to include feedbacks from mediators that enhance or restrict transmigration. We note that doing so within our ABM framework may involve replacing existing rules governing maximum global cell numbers with more localised analogues that account for spatial variations in endothelial lining activation. Such modifications constitute a valuable target for future work, but would be best addressed when suitable experimental data are available to focus the application of the models toward answering questions related to specific tissues or inflammatory conditions.

Furthermore, there is currently significant and growing interest in multimorbidity, *i.e.* the concurrent presence of two or more chronic conditions such as COPD and cardiovascular disease, which is more common with increasing age and is thought to be associated with inflammation and cellular dysfunction (Hughes *et al.*, 2020). Understanding how the inflammatory process is modified by disease, healthy ageing and drugs, both alone and in combination, is difficult but necessary if therapeutic targets are to be identified and their effects fully understood. The models presented in the previous chapters are generic but can act as a framework within which future modifications in line with specific tissue and/or disease can be easily incorporated. An example would be modelling the effects of Rheumatoid arthritis on the synovium where macrophage numbers have been shown to correlate with disease activity and their depletion has a therapeutic effect (Udalova *et al.*, 2016; Ouboussad *et al.*, 2019). Such

adaptation would require, among others, changes to our description of macrophage heterogeneity but could allow clinical investigations into the effects of drugs that target circulating monocytes and thereby reduce macrophage transmigration into tissue (Udalova *et al.*, 2016). In particular, with respect to the models of Chapters 4–5, the advantage of hybrid models, which integrate constituent underlying processes across multiple scales, is that they are easily comparable to experimental data (such as histological studies) and offer easily interpreted tools that could be used in progressing our understanding of such complex, multifaceted inflammatory scenarios. Finally, among other key open issues that this work prompts for further investigation, there is scope for better addressing the emerging links between ageing and inflammation and, more in detail, the impact of ageing neutrophils on inflammatory diseases (Lord *et al.*, 2001).

Bibliography

S. Abar, G. K. Theodoropoulos and P. Lemarinier. Agent based modeling and simulation tools: a review of the state-of-art software. *Computer Science Review*, 24: 13–33, 2017.

A. Adamatzky and G. J. Martinez. *Designing Beauty: The Art of Cellular Automata*, volume 20 of *Emergence, Complexity and Computation*. Springer, 2016.

A. Agusti, L. D. Edwards, S. I. Rennard, W. MacNee, R. Tal-Singer, B. E. Miller, J. Vestno, D. A. Lomas, P. M. A. Calverley, E. Wouters, C. Crim, J. C. Yates, E. K. Silverman, H. O. Coxson, P. Blake, R. J. Mayer and B. Celli. Persistent systemic inflammation is associated with poor clinical outcomes in copd: A novel phenotype. *PLoS One*, 7(5), May 2012.

M. Ahangaran and H. Beigy. Cellular learning and automata with external and input and its and applications in pattern and recognition. In IEEE, editor, *Computing with Words and Perceptions in System Analysis, Decision and Control*, pages 1–4. IEEE, 2009.

M. S. Alber, M. A. kiskowski, J. A. Glazier and Y. Jiang. On cellular automaton approaches to modeling biological cells. In Springer, editor, *Mathematical ystems Theory in Biology, Communications, Computationn and Finance*, volume 134, pages 1–39, 2003.

E. Albrecht and H. R. Petty. Cellular memory neutrophil orientation reverses during temporally decreasing chemoattractant concentrations. *Proceedings of the National Academy of Sciences*, 95:5039–5044, 1998.

L. J. S. Allen. *An Introduction to Mathematical Biology*. Pearson, 2006.

G. An. Agent-based computer simulation and sirs: Building a bridge between basic science and clinical trials. *Shock*, 16(4):266–273, 2001.

G. An. Introduction of an agent-based multi-scale modular architecture for dynamic knowledge representation of acute inflammation. *Theoretical Biology and Medical Modelling*, 5(11), 2008.

G. An, Q. Mi, J. Dutta-Moscato and Y. Vodovotz. Agent-based models in translational systems biology. *Wiley Interdisciplinary Reviews: Systems Biology and Medicine*, 1(2):159–171, 2009.

M. Ashino, R. Nagase and R. Vaillancourt. Behind and beyond the matlab ode suite. *Computers and Mathematics with Applications*, 40:491–512, September 2000.

M. Aziz, A. Jacob, W. Yang, A. Matsuda and P. Wang. Current trends in inflammatory and immunomodulatory mediators in sepsis. *Journal of Leukocyte Biology*, 93 (3):329–342, March 2013.

M. Back, A. Yurdagul, I. Tabas, K. rni and P. T. Kovanen. Inflammation and its resolution in atherosclerosis: mediators and therapeutic opportunities. *Nature Reviews Cardiology*, 16:389–406, 2019.

F. Balkwill, K. A. Charles and A. Mantovani. Smoldering and polarized inflammation in the initiation and promotion of malignant disease. *Cancer Cell*, 7, March 2005.

P. J. Barnes and B. R. Celli. Systemic manifestations and comorbidities of copd. *European Respiratory Journal*, 33(5):1165–1185, 2009.

C. Barnig, N. Frossard and B. D. Levy. Towards targeting resolution pathways of airway inflammation in asthma. *Pharmacology and Therapeutics*, 186:98–113, June 2018.

S. Barquera, A. Pedroza-Tobias, C. Medina, L. Hernandez-Barrera, K. Bibbins-Domingo, R. Lozano and A. E. Moran. Global overview of the epidemiology of atherosclerotic cardiovascular disease. *Archives of Medical Research*, 2015.

F. Barros-Becker, P. Lam, R. Fisher and A. Huttenlocher. Live imaging reveals distinct modes of neutrophil and macrophage migration within interstitial tissues. *Journal of Cell Science*, 130(22):3801–3808, September 2017.

S. Bekkering and R. Torensma. Another look at the life of a neutrophil. *World Journal of Hematology*, 2(2):44–58, May 2013.

R. Brady, D. O. F. Ito, H. T. Tran, S. Janum, K. Mller, S. Brix, J. T. Ottesen, J. Mehlsen and M. S. Olufsen. Personalized mathematical model predicting endotoxin-induced inflammatory responses in young men. 2016.

R. Brown. A brief account of microscopical observations made in the months of june, july and august, 1827, on the particles contained in the pollen of plants; and on the general existence of active molecules in organic and inorganic bodies. *Edinburgh New Philosophical Journal*, pages 358–371, 1828.

A. L. Brubaker, J. L. Rendon, L. Ramirez, M. A. Choudhry and J. Kovacs. Reduced neutrophil chemotaxis and infiltration contributes to delayed resolution of cutaneous wound infection with advanced age. *The Journal of Immunology*, 190 (4):1746–1757, February 2013.

J. L. Burton, H. L. Bank and P. Law. Kinematic analysis of chemotaxis of fresh and stored neutrophils. *Annals of Clinical and Laboratory Science*, 17(6), 1987.

D. Busse, De La Rosa M., K. Hobiger, K. Thurley, M. Flossdorf, A. Scheffold and T. Hofer. Competing feedback loops shape il-2 signaling between helper and regulatory t lymphocytes in cellular microenvironments. *Proceedings of the National Academy of Sciences*, 107(7):3058–3063, February 2010.

B. A. Camley and W. Rappel. Physical models of collective cell motility: from cell to tissue. *Journal of Physics D: Applied Physics*, 50, 2017.

S. Cassani and S. D. Olson. A hybrid cellular automaton model of cartilage regeneration capturing the interactions between cellular dynamics and scaffold porosity. In *Journal of Mathematical Biology*, 2018.

I. Cecchi, I. A. De La Rosa, E. Menegatti, D. Roccatello, E. Collantez-Estevez, C. Lopez-Pedrera and N. Barbarroja. Neutrophils: Novel key players in rheumatoid arthritis. current and future therapeutic targets. *Autoimmunity Reviews*, 17(11): 1138–1149, November 2018.

E. A. Celaya, J. J. A. Aguirrezabala and P. Chatzipantelidis. Implementation of an adaptive bdf2 formula and comparison with the matlab ode15s. *Procedia Computer Science*, 29:1014–1026, 2014.

M. A. J. Chaplain and A. M. Stuart. A model mechanism for the chemotactic response of endotheliai cells and to tumour angiogenesis factor. *Journal of Mathematics Applied in Medicine and Biology*, 10(149-168), 1993.

M. S. Chimenti, P. Triggianese, P. Conigliaro, E. Candi, G. Melino and R. Perricone. The interplay between inflammation and metabolism in rheumatoid arthritis. *Cell Death and Disease*, 6(9):1887–1887, September 2015.

M. R. Cho, H. S. Thatte, R. C. Lee and D. E. Golan. Integrin-dependent human

macrophage migration induced by oscillatory electrical stimulation. *Annals of Biomedical Engineering*, 28:234–243, 2000.

C. Chuong and M. K. Richardson. Pattern formation today. *The International Journal of Developmental Biology*, 53(5-6):653–658, 2009.

E. A. Codling, M. J. Plank and S. Benhamou. Random walk models in biology. *Journal of the Royal Society Interface*, 5:813–834, 2008.

L. M. Coussens and Z. Werb. Inflammation and cancer. *Nature*, 420(6917):860–867, December 2002.

A. Cross, R. J. Moots and S. W. Edwards. The dual effects of tnfalpha on neutrophl apoptosis are mediated via differential effects on expression of mcl-1 and bfl-1. *Blood Journal*, 111(2), January 2008.

C. V. Curry. Differential blood count. Medscape, January 2015.

J. Day, D. M. Metes and Y. Vodovotz. Mathematical modeling of early cellular innate and adaptive immune responses to ischemia/reperfusion injury and solid organ allotransplantation. *Frontiers in Immunology*, 6, September 2015.

J. Day, J. Rubin and G. Clermont. Using nonlinear model predictive control to find optimal therapeutic strategies to modulate inflammation. *Mathematical Biosciences and Engineering*, 7(4):739–763, October 2010.

J. A. De Sales, M. L. Martins and D. A. Stariolo. Cellular automata model for gene networks. *Physical Review E*, 55(3), 1997.

K. A. Deans and N. Sattar. Anti-inflammatory drugs and their effects on type 2 diabetes. *Diabetes Technology and Therapeutics*, 8(1), 2006.

P. Delves and I. Roitt, editors. *Encycolpedia of Immunology, Second Edition.* Academic Press, June 1998.

A. Deutsch and S. Dormann. *Cellular Automaton Modeling of Biological Pattern Formation.* Modeling and Simulation in Science, Engineering and Technology. Birkhauser, 2016.

F. Devillard and B. Heit. Architectural model of a biological retina using cellular automata. *Journal of Computer and Communications*, 2:78–97, 2014.

R. F. Diegelmann and C. E. Chalfant, editors. *Frontiers in Inflammation. Basic Biology and Clinical Aspects of Inflammation*, volume 1. Bentham Science Publishers, 2016.

R. Dilao. Turing instabilities and patterns near a hopf bifurcation. *Applied Mathematics and Computation*, 164(2):391–414, May 2005.

M. Y. Donath and S. E. Shoelson. Type 2 diabetes as an inflammatory disease. *Nature Reviews Immunology*, 11, February 2011.

E. Dumas, P. E. Neagoe, P. P. McDonald, M. White and M. G. Sirois. New insights into the pro-inflammatory and activities of ang1 on neutrophils: Induction of mip-1beta synthesis and release. *PLoS One*, 11(9), September 2016.

J. R. Dunkelberger and W. Song. Complement and its role in innate and adaptive immune responses. *Cell Research*, 20:34–50, 2010.

J. L. Dunster. *Mathematical models of soft tissue injury repair: towards understanding musculoskeletal disorders.* PhD thesis, University of Nottingham, 2012.

J. L. Dunster, H. M. Byrne and J. R. King. The resolution of inflammation: A mathematical model of neutrophil and macrophage interactions. *Bulletin of Mathematical Biology*, 76:1953–1980, 2014.

J. L. Dunster and I. Dransfield. Mathematical approaches to studying inflammation. *Encyclopedia of Cell Biology*, 4:95–101, 2016.

G. A. Duque and A. Descoteaux. Macrophage cytokines: involvement in immunity and infectious diseases. *Fro*, 5, October 2014.

J. S. Economou and H. S. Shin. Lymphocyte-activating factor: I. generation and physicochemical characterization. *The Journal of Immunology*, 121:1446–1452, 1978.

F. Entschladen and K. S. Zanker, editors. *Cell Migration: Signalling and Mechanisms*. 2010.

G. B. Ermentrout and L. Edelstein-Keshet. Cellular automata approaches to biological modeling. *Journal of Theoretical Biology*, 160:97–133, 1993.

G. S. Firestein. Evolving concepts of rheumatoid arthritis. *Nature*, 423(6937):356–361, May 2003.

S. Fox, A. E. Leitch, R. Duffin, C Haslett and A. G. Rossi. Neutrophil apoptosis: Relevance to the innate immune response and inflammatory disease. *Journal of Innate Immunity*, 2:216–227, February 2010.

E. F. Foxman, E. J. Kunkel and E. C. Butcher. Integrating conflicting chrmotactic signals: the role of memory in leukocyte navigation. *The Journal of Cell Biology*, 147(3):577–587, November 1999.

M. O. Freire and T. E. Van Dyke. Natural resolution of inflammation. *Periodontology 2000*, 63(1):149–164, May 2013.

Ralph Van Furth, editor. *Mononuclear Phagocytes Characteristics, Physiology and Function*. Martinus Nijhoff Publishers, 1985.

W. Q. Gan, S. F. P. Man, A. Senthilselvan and D. D. Sin. Association between chronic obstructive pulmonary disease and systemic inflammation: a systematic review and a meta-analysis. *Thoraxis*, 59:574–580, 2004.

H. M. Gao and J. S. Hong. Why neurodegenerative diseases are progressive: uncontrolled inflammation drives disease progression. *Cell*, 2008.

E. Gavagnin and C. A. Yates. *Stochastic and deterministic modelling of cell migration*, volume 39. Elsevier BV, 2018.

A. Gerisch, D. F. Griffiths, R. Weiner and M. A. J. Chaplain. A positive splitting method for mixed hyperbolic-parabolic systems. *Numerical Methods for Partial Differential Equations*, 17(2):152–168, 2001.

P. Gerlee and A. R. A. Anderson. An evolutionary hybrid cellular automaton model of solid tumour growth. *Journal of Theoretical Biology*, 246(4):583–603, June 2007.

D. W. Gilroy, T. Lawrence, M. Perretti and A. G. Ross. Inflammatory resolution: New opportunities for drug discovery. *Drug Discovery*, 3:401–416, May 2004.

T. E. Gorochowski. Agent-based modelling in synthetic biology. *Essays in Biochemistry*, 60:325–336, 2016.

T. E. Gorochowski, A. Matyjaszkiewicz, T. Todd, N. Oak, K. Kowalska, S. Reid, K. T. Tsaneva-Atanasova, N. J. Savery, C. S. Grierson and M. Di Bernardo. Bsim: An agent-based tool for modeling bacterial populations in systems and synthetic biology. *PLoS One*, 7(8), August 2012.

J. M. Graham, B.P. Ayati, L. Ding, P. S. Ramakrishnan and J. A. Martin. Reaction-diffusion-delay model for epo/tnf- interaction in articular cartilage lesion abatement. *Biology Direct*, 7(9), 2012.

M. C. Greenlee-Wacker. Clearance of apoptotic nneutrophil and resolution of inflammation. *Immunological Reviews*, 273(1):357–370, September 2016.

S. I. Grivennikov, F. R. Greten and M. Karin. Immunity, inflammation, and cancer. *Cell*, 140(6):883–899, March 2010.

H. Gruler. Chemokinesis and necrotaxis of human granulocytes: the important cellular organelles. *Zeitschrift fur Naturforschung C*, 42:1126–1134, 1987.

A. Hald and J. Lotharius. Oxidative stress and inflammation in parkinsons and disease: is there a causal link? *Experimental Neurology*, 193:279–290, 2005.

S. Hannah, I. Nadra, I. Dransfield, J. G. Pryde, A. G. Rossi and C. Haslett. Constitutive neutrophil apoptosis in culture is modulated by cell density and independently of beta2 and integrin-mediated adhesion. *Federation of European Biochemical Societes Letters*, 421:141–146, 1998.

G. K. Hansson. Inflammation, atherosclerosis, and coronary artery disease. *The New England Journal of Medicine*, 352(16), 2005.

G. Hasko and B. N. Cronstein. Adenosine: an endogenous regulator of innate immunity. *Trends in Immunology*, 25(1):33–39, January 2004.

Y. Hattory, A. Yokoya and R. Watanabe. Cellular automaton-based model for radiation-induced bystander effects. *BMC Systems Biology*, 9(90), 2015.

L. A. Hawkins and A. Devitt. Current understanding of the mechanisms for clearance of apoptotic cells - a fine balance. *Journal of Cell Death*, 6:57–68, 2013.

P. M. Henson. Dampening inflammation. *Nature Immunology*, 6:1179–1181, December 2005.

F. L. Heppner, R. M. Ransohoff and B. Becher. Immune attack: the role of inflammation in alzheimer disease. *Nature*, 16, June 2015.

M. Hesketh, K. B. Sahin, Z. E. West and R. Z. Murray. Macrophage phenotypes regulate scar formation and chronic wound healing. *International Journal of Molecular Sciences*, 18, 2017.

P. S. Hiemstra. Altered macrophage function in chronic obstructive pulmonary disease. *Annals of the American Thoracic Society*, 10(Supplement):S180–S185, dec 2013.

L. E. Hind, J. L. MacKay, D. Cox and D. A. Hammer. Two-dimensional motility of a macrophage cell line on microcontact-printed fibronectin. *Cytoskeleton*, 71(9): 542–554, September 2014.

N. H. Hoang, C. N. Jones, L. Dimisko, B. Hamza, J. Martel, N. Kojic and D. Irimia. Measuring neutrophil speed and directionality during chemotaxis, directly from a droplet of whole blood. *Technology World Scientific*, 1(1), October 2013.

A. Hochreiter-Hufford and K. S. Ravichandran. Clearing the dead: Apoptotic cell sensing and recognition and engulfment and digestion. *Cold Spring Harbor Perspectives in Biology*, 2013.

A. G. Hoekstra, J. Kroc and P. M. A. Sloot, editors. *Simulating Complex Systems by Cellular Automata*. Springer, 2010.

C. Holmes and J. Butchart. Systemic inammation and alzheimers disease. *Biochemical Society Transactions*, 39(4):898–901, 2011.

A. R. Horwitz and D. R. Webb. Cell migration. *Current Biology*, 13(19):756–759, September 2003.

Rebecca Hoyle. *Pattern Formation: An Introduction to Methods*. Cambridge University Press, 2006.

M. J. Hughes, H. M. McGettrick and E. Sapey. Shared mechanisms of multimorbidity in copd, atherosclerosis and type-2 diabetes: the neutrophil as a potential inflammatory target. *European Respiratory Review*, 29, 2020.

P. Hunter. The inflammation theory of disease. *Embo Reports*, 13(11):968–970, 2012.

A. Hurwitz. On the conditions under which an equation has only roots with negative real parts. *Mathematische Annalen*, 46:273–284, 1895.

T. Iba, N. Hashiguchi, I. Nagaoka, Y. Tabe and M. Murai. Neutrophil cell death in response to infection and its relation to coagulation. *Journal of Intensive Care*, 1 (13), 2013.

S. H. Itzkowitz and Y. Xianyang. Inflammation and cancer. colorectal and cancer in inflammatory bowel disease the role of inflammation. *American Journal of Physiology Gastrointestinal and Liver Physiology*, 287, 2004.

J. E. Jansen, E. A. Gaffney, J. Wagg and M. C. Coles. Combining mathematical models with experimentation to drive novel mechanistic insights into macrophage function. *Frontiers in Immunology*, 10, jun 2019.

A. E. Jasper, W. J. McIver, E. Sapey and G. M. Walton. Understanding the role of neutrophils in chronic inflammatory airway disease. *F1000Research*, 8, 2019.

Y. Jiao and S. Torquato. Emergent behaviors from a cellular automaton model for invasive tumor growth in heterogeneous microenvironments. *PLoS Computational Biology*, 7(12), 2011.

T. Jin, X. Xu and D. Hereld. Chemotaxis, chemokine and human disease. *Cytokine*, 44(1):1–8, October 2008.

P. J. M. Jones, A. Sim, H. B. Taylor, L. Bugeon, M. J. Dallman, B. Pereira, M. Stumpf and J. Liepe. Inference of random walk models to describe leukocyte migration. *Physical Biology*, 12, 2015.

U. Jung, D. C. Bullard, T. F. Tedder and K. Ley. Velocity differences between l- and p-selectin-dependent neutrophil rolling in venules of mouse cremaster muscle in vivo. *The American Journal of Physiology*, 271(6), December 1996.

M. J. Kaplan and M. Radic. Neutrophil extracellular traps (nets): Double-edged swords of innate immunity. *The Journal of Immunology*, 189(6):2689–2695, September 2012.

J. Kari. *Cellular Automata*. University of Turku, 2013.

A. Karolak, D. A. Markov, L. J. McCawley and K. A. Rejniak. Towards personalized computational oncology: from spatial models of tumour spheroids, to organoids, to tissues. *Journal of the Royal Society Interface*, 15, January 2018.

A. G. Khandoga, A. Khandoga, C. A. Reichel, P. Bihari, M. Rehberg and F. Krombach. In vivo imaging and quantitative analysis of leukocyte directional migration and polarization in inflamed tissue. *PLoS One*, 4(3), March 2009.

M. Kim, W. Liu, D. L. Borjesson, F. E. Curry, L. S. Miller, A. L. Cheung, F. Liu, R. R. Isseroff and S. I. Simon. Dynamics of neutrophil infiltration during cutaneous wound healing and infection using fluorescence imaging. *Journal of Investigative Dermatology*, 128(7):1812–1820, July 2008.

W. Koenig. Inflammation and coronary heart disease: An overview. *Cardiology in Review*, 9(1), 2001.

E. Kolaczkowska and P. Kubes. Neutrophil recruitment and function in health and inflammation. *Nature Reviews Immunology*, 13:159–175, March 2013.

S. Kondo and T. Miura. Reaction-diffusion model as a framework for understanding biological pattern formation. *Science*, 329:1616–1620, September 2010.

D. Korns, S. Courtney Frasch, R. Fernandez-Boyanapalli, P. M. Henson and D. L. Bratton. Modulation of macrophage efferocytosis in inflammation. *Frontiers in Immunology*, 2(57), November 2011.

R. Kumar, G. Clermont, Y. Vodovotz and C. C. Chow. The dynamics of acute inflammation. *Journal of Theoretical Biology*, 230:145–155, 2004.

D. Lauffenburger and A. F. Horwitz. Cell migration: Review a physically integrated molecular process. *Cell*, 84:359–369, February 1996.

D. Lauffenburger and K. H. Keller. Effects of leukocyte and random motility and chemotaxis in tissue and inflammatory response. *Journal of Theoretical Biology*, 81:475–503, 1979.

D. Lauffenburger and C. R. Kennedy. Analysis of a lumped model for tissue inflammation dynamics. *Mathematical Biosciences*, 53:189–221, 1981.

D. Lauffenburger and C. R. Kennedy. Localized bacterial infection in a distributed model for tissue inflammation. *Journal of Mathematical Biology*, 16:141–163, 1983.

T. Lawrence, D. A. Willoughby and D. W. Gilroy. Anti-inflammatory lipid mediators and insights into the resolution of inflammation. *Nature Reviews Immunology*, 2, November 2002.

P. E. Lazzerini, P. L. Capecchi and F. Laghi-Pasini. Systemic inflammation and arrhythmic risk: lessons from rheumatoid arthritis. *European Heart Journal*, 38: 1717–1727, 2017.

R. J. LeVeque. *Numerical Methods and for Conservation and Laws*. Lectures in Mathematics. Birkhauser, 1999.

R. J. LeVeque. *Finite Difference Methods for Ordinary and Partial Differential Equations*. Siam, 2007.

R. Li, J. D. Hebert, T. A. Lee, H. Xing, A. Boussommier-Calleja, R. O. Hynes, D. A. Lauffenburger and R. D. Kamm. Macrophage-secreted TNFα and TGFβ1 influence migration speed and persistence of cancer cells in 3d tissue culture via independent pathways. *Cancer Research*, 77(2):279–290, 2017.

P. Libby. Inflammation and cardiovascular disease mechanisms. *American Journal of Clinical Nutrition*, 83, 2006.

P. Libby. Inflammatory mechanisms: The molecular and basis of inflammation and disease. *Nutrition Reviews*, 65(12):140–146, 2007.

M. Lin, Y. Chai, X. Yang and Y. Wang. Spatiotemporal patterns induced by hopf bifurcations in a homogeneous diffusive predator-prey system. *Mathematical Problems in Engineering*, 2019.

Y. Liu, X. Zou, Y. Chai and Y. Yao. Macrophage polarization in inflammatory diseases. *International Journal of Biological Sciences*, 10(5):520–529, 2014.

H.F. Lodish, A. Berk, C. Kaiser, M. Krieger, M. P. Scott, A. Bretscher, H. L. Ploegh and P. T. Matsudaira. *Molecular Cell Biology*. 6 edition, 2008.

J. M. Lord, S. Butcher, V. Killampali, D. Lascelles and M. Salmon. Neutrophil ageing and immunesenescence. *Mechanisms of Ageing and Development*, 122:1521–1535, 2001.

S. Lucas, N. J. Rothwell and R. M. Gibson. The role of inflammation in cns injury and disease. *British Journal of Pharmacology*, 147:S232–S240, 2006.

P. K. Maini and R. E. Baker. Modeling collective cell motion in biology. In *Advances in Applied Mathematics*, volume 87 of *Springer Proceedings in Mathematics and Statistics*, 2014.

P. K. Maini and H. G. Othmer. *Mathematical Models for Biological Pattern Formation*. Springer, 2001.

D. M. Mannino and A. S. Buist. Global burden of copd: risk factors and prevalence and future and trends. *Lancet*, 370:765–773, September 2007.

A. F. M. Mare, M. Komba, C. Dyck, M. Labecki, D. T. Finegood and L. Edelstein-Keshet. Quantifying macrophage defects in type 1 diabetes. *Journal of Theoretical Biology*, 233:533–551, 2005.

W. Mazin, K. E. Rasmussen, E. Mosekilde, P. Borckmans and G. Dewel. Pattern formation in the bistable gray-scott model. *Mathematics and Computers in Simulation*, 40:371–396, 1996.

J. M. McCracken and L. H. Allen. Regulation of human neutrophil apoptosis and lifespan in health and disease. *Journal of Cell Death*, 7, 2014.

J. S. McGough and K. Riley. Pattern formation in the grayscott model. *Nonlinear Analysis: World Applications*, 5:105–121, 2004.

Gjerrit Meinsma. Elementary proof of the routh-hurwitz test. *Systems & Control Letters*, 25:237–242, 1995.

K. Miles, D. J. Clarke, W. Lu, Z. Sibinska, P. E. Beaumont, D. J. Davidson, T. A. Barr, D. J. Campopiano and M. Gray. Dying and necrotic neutrophils are anti-inflammatory secondary to the release of alpha-defensins. *The Journal of Immunology*, 183(3):21222132, August 2009.

G. H. B. Miranda, J. Machicao and O. M. Bruno. Exploring spatio-temporal dynamics of cellular automata for pattern recognition in networks. *Scientific Reports*, 6, 2016.

S. F. Moss and M. J. Blaser. Mechanisms of disease: inflammation and the origins of cancer. *Nature Clinical Practice. Oncology*, 2(2), February 2005.

D. M. Mosser and J. P. Edwards. Exploring the full spectrum of macrophage activation. *Nature Reviews Immunology*, 8(12):958–969, December 2008.

J. D. Murray. *Mathematical Biology: I. An Introduction*. Springer, 2001.

J.D. Murray. *Mathematical Biology II: Spatial Models and Biomedical Applications*. Springer, 2003.

J. M. Nava-Sedeno, H. Hatzikirou, R. Klages and A. Deutsch. Cellular automaton models for time-correlated random walks: derivation and analysis. *Scientific Reports*, 7, December 2017.

M. Neilson, J. A. Mackenzie, S. D. Webb and R.H. Insall. Modelling cell movement and chemotaxis using pseudopod-based feedback. *Computational Methods in Science and Engineering*, 33(3):1035–1057, 2011.

M. Nguyen-Chi, B. Laplace-Builhe, J. Travnickova, P. Luz-Crawford, G. Tejedor, Q. T. Phan, Duroux-Richard I., J. levraud, K. Kissa, G. Lutfalla, C. Jorgensen and F. Djouad. Identification of polarized macrophage subsets in zebrafish. *eLife*, 4, 2015.

M. J. North, N. T. Collier, J. Ozik, E. R. Tatara, C. M. Macal and M. Bragen. Complex adaptive systems modeling with repast simphony. *SpringerOpen Journal*, 1(3), 2013.

M. J. North, E. R. Tatara, N. T. Collier and J. Ozik. Visual agent-based model development with repast simphony. 2007.

S. Nourshargh and R. Alon. Leukocyte migration into inflamed tissues. *Immunity*, 41(5):694–707, nov 2014.

P. A. Nuzzi, M. A. Lokuta and A. Huttenlocher. Analysis of neutrophil chemotaxis. *Methods in Molecular Biology*, 370:23–35, 2007.

A. Ortega-Gomez, M. Perretti and O. Soehnlein. Resolution of inflammation: an integrated view almudena ortega. *Embo Molecular Medicine*, 5:661–674, March 2013.

L. Ouboussad, A. N. Burska, A. Melville and M. H. Buch. Synovial tissue heterogeneity in rheumatoid arthritis and changes with biologic and targeted synthetic therapies to inform stratified therapy. *Frontiers in Medicine*, 6, mar 2019.

M. R. Owen, H. M. Byrne and C. E. Lewis. Mathematical modelling of the use of macrophages as vehicles for drug delivery to hypoxic tumour sites. *Journal of Theoretical Biology*, 226:377–391, 2004.

M. R. Owen and J. A. Sherratt. Pattern formation and spatiotemporal irregularity and in a model and for macrophage-tumour and interactions. *Journal of Theoretical Biology*, 189:63–80, 1997.

A. Oyler-Yaniv, J. Oyler-Yaniv, B. M. Whitlock, Z. Liu, R. N. Germain, M. Huse, G. Altan-Bonnet and O. Krichevsky. A tunable diffusion-consumption mechanism of cytokine propagation enables plasticity in cell-to-cell communication in the immune system. *Immunity*, 46:609–620, April 2017.

E. Palsson. A three-dimensional model of cell movement in multicellular systems. *Future Generation Computer Systems*, 17:835–852, 2001.

E. Palsson and H. G. Othmer. A model for individual and collective cell movement

in dictyostelium discoideum. *Proceedings of the National Academy of Sciences*, 97 (19):10448–10453, September 2000.

A. Parihar, T. D. Eubank and A. I. Doseff. Monocytes and macrophages regulate immunity through dynamic networks of survival and cell death. *Journal of Innate Immunity*, 2:204–215, 2010.

A. A. Patel, Y. Zhang, J. N. Fullerton, L. Boelen, A. Rongvaux, A. A. Maini, V. Bigley, R. A. Flavell, D. W. Gilroy, B. Asquith, D. Macallan and S. Yona. The fate and lifespan of human monocyte subsets in steady state and systemic inflammation. *Journal of Experimental Medicine*, 214(7):1913–1923, July 2017.

K. Penner, G. B. Ermentrout and D. Swigon. Pattern formation in a model and of acute inflammation. *Siam Journal on Applied Dynamical Systems*, 11(2):629–660, 2012.

F. Perez-Cerda, M.V. Sanchez-Gomez and C. Matute. The link of inflammation and neurodegeneration in progressive multiple sclerosis. *Multiple Sclerosis and Demyelinating Disorders*, 1(9), 2016.

V. H. Perry. The influence of systemic inflammation on inflammation in the brain: implications for chronic neurodegenerative disease. *Brain, Behavior and Immunity*, 18:407–413, 2004.

Pfizer. *Burden of Disease - Chronic Inflammation and Inflammatory Disease*, October 2017.

J. Phillips, P. Murray, P. Kirk and J. Crocker, editors. *The Biology of Disease*. Blackwell Publishing, 2006.

A. B. Pigozzo, G. C. Macedo, R. W. Dos Santos and M. Lobosco. On the compu-

tational modeling of the innate immune system. *10th International Conference on Artificial Immune Systems (ICARIS)*, 14(6), 2013.

J. Pillay, I. Den Braber, N. Vrisekoop, L. Kwast, R. De Boer, J. A. M. Borghans, K. Tesselaar and L. Koenderman. In vivo labeling with 2h2o reveals a human neutrophil lifespan of 5.4 days. *Blood Journal*, 116(4):625–627, July 2010.

B. Plytycz and R. Seljelid. From inflammation to sickness: Historical perspective. *Archivum Immunologiae et Therapiae Experimentalis*, 51:105–109, 2003.

R. M. Pollack, M. Y. Donath, D. LeRoith and G. Leibowitz. Anti-inflammatory agents in the treatment of diabetes and its vascular complications. *Diabetes Care*, 39(2), August 2016.

M. Ponzoni, F. Pastorino, D. Di Paolo, P. Perri and C. Brignole. Targeting macrophages as a potential therapeutic intervention: Impact on inflammatory diseases and cancer. *International Journal of Molecular Sciences*, 19(1953), 2018.

F. Porcheray, S. Viaud, A. C. Rimaniol, C. Leone, B. Samah, N. Dereuddre-Bosquet, D. Dormont and G. Gras. Macrophage activation switching: an asset for the resolution of inflammation. *Clinical and Experimental Immunology*, 142:481–489, 2005.

A. Presbitero, E. Mancini, F. Castiglione, V. V. Krzhizhanovskaya and R. Quax. Game of neutrophils: modeling the balance between apoptosis and necrosis. *BMC Bioinformatics*, 20(S6), dec 2019.

M. A. Qasaimeh, M. Pyzik, M. Astolfi, S. M. Vidal and D. Juncker. Neutrophil chemotaxis in moving gradients. *Advanced Biosystems*, 2, 2018.

M. T. Quinn, F. R. DeLeo and G. M. Bokoch, editors. *Neutrophils Methods and Protocols*. Humana Press, 2007.

V. Radosavljevic, K. Ristovski and Z. Obradovic. A data-driven acute inflammation therapy. *BMC Medical Genomics*, 6(3), 2013.

G. E. Rainger, C. Buckley, D. L. Simmons and G. B. Nash. Cross-talk between cell adhesion molecules regulates the migration velocity of neutrophils. *Current Biology*, 7:316–325, 1997.

E. R. Rayburn, S. J. Ezell and R. Zhang. Anti-inflammatory agents for cancer therapy. *Molecular Cell Pharmacology*, 1(1129-43), 2009.

S. L. Raymond, B. J. Mathias, T. J. Murphy, J. C. Rincon, M. C. Lopez, R. Ungaro, F. Ellett, J. Jorgensen, J. L. Wynn, H. V. Baker, L. L. Moldawer, D. Irimia and S. D. Larson. Neutrophil chemotaxis and transcriptomics in term and preterm neonates. *Translational Research*, 190, 2017.

M. N. Read, J. Bailey and T. Timmis, J. Chtanova. Leukocyte motility models assessed through simuation and multi-objective optimization-based model selection. *PLoS Computational Biology*, 12(9), September 2016.

A. Reynolds, J. Rubin, G. Clermont, J. Day, Y. Vodovotz and G. B. Ermentrout. A reduced mathematical model of the acute inflammatory response: I. derivation of model and analysis of anti-inflammation. *Journal of Theoretical Biology*, 242(1): 220–236, September 2006.

B. Ribba, T. Alarcon, K. Marron, P. K. Maini and Z. Agur. The use of hybrid cellular automaton models for improving cancer therapy. In P. M. A. Sloot, B. Chopard and A. Hoekstra, editors, *Lecture Notes in Computer Sciences*, volume 3305 of *ACRI 2004*, pages 444–453. Springer, 2004.

A. J. Ridley, M. A. Schwartz, K. Burridge, R. A. Firtel, M. H. Ginsberg, G. Borisy,

J. T. Parsons and A. R. Horwitz. Cell migration: Integrating signals from front to back. *Science*, 302, December 2003.

S. F. Rinaldi, J. L. Hutchinson, A. G. Rossi and J. E. Norman. Anti-inflammatory mediators as physiological and pharmacological regulators of parturition. *Expert Review of Clinical Immunology*, 7(5):675–696, 2011.

L. Ringham, P. Prusinkiewicz and R. Gniadecki. Skin patterning in psoriasis by spatial interactions between pathogenic cytokines lee ringham. *iScience*, 20:546–553, October 2019.

N. P. Rocha, F. M. Ribeiro, E. Furr-Stimming and A. L. Teixeira. Neuroimmunology of huntingtons and disease: Revisiting evidence from human studies. *Mediators of Inammation*, 2016.

J. Roquer and A. Ois. *Handbook of Disease Burdens and Quality of Life Measures*. Springer, 2010.

A. E. Ross and R. R. Pompano. Diffusional analysis of cytokines in lymph node tissue on a microfluidic chip. *The Journal of Immunology*, 198(1), May 2017.

A. E. Ross and R. R. Pompano. Diffusion of cytokines in live lymph node tissue using microfluidic integrated optical imaging. *Analytica Chimica Acta 1000*, pages 205–213, 2018.

E. J. Routh. *A Treatise on the Stability of a Given State of Motion: Particularly Steady Motion*. Macmillan, 1877.

A. Roy, S. Daun, G. Clermont, J. Rubin, Y. Vodovotz, C. Lagoa and R. S. Parker. A mathematical model of acute inflammatory response to endotoxin challenge. In AIChE Annual Meeting, editor, *Mathematical Biosciences and Engineering*, 2007.

B. L. Rozhdestvenskii. Discontinuous solutions of hyoerbolic systems of quasilinear equations. *Russian Mathematical Surveys*, 15(53), 1960.

C. Di Russo, J. B. Lagaert, G. Chapuisat and M. A. Dronne. A mathematical model of inflammation during ischemic stroke. 30:15–33, 2010.

B. E. Sansbury and M. Spite. Resolution of acute inflammation and the role of resolvins in immunity, thrombosis and vascular biology. *Circulation Research*, 119 (1):113–130, June 2016.

E. Sapey, Stockley J. A., H. Greenwood, A. Ahmad, D. Bayley, Lord J. M., Insall R. H. and Stockley R. A. Behavioral and structural differences in migrating peripheral neutrophils from patients with chronic obstructive pulmonary disease. *American Journal of Respiratory and Critical Care Medicine*, 183(1176-1186), 2011.

E. Sapey, H. Greenwood, G. Walton, E. Mann, A. Love, N. Aaronson, R. H. Insall, R. A. Stockley and J. M. Lord. Phosphoinositide 3-kinase inhibition restores neutrophil accuracy in the elderly: toward targeted treatments for immunosenescence. *Blood*, 123(2), January 2014a.

E. Sapey, H. Greenwood, G. M. Walton, E. Mann, A. Love, N. Aaronson, R. H. Insall, J. A. Stockley and J. M. Lord. Phosphoinositide 3-kinase inhibition restores neutrophil accuracy in the elderly: toward targeted treatments for immunosenescence. *Blood Journal*, 123(2):239–248, January 2014b.

M. Sarris, J. Masson, D. Maurin, L. M. Van Der Aa, P. Boudinot, H. Lortat-Jacob and P. Herbomel. Inflammatory chemokines direct and restrict leukocyte migration within live tissues as glycan-bound gradients. *Current Biology*, 22:2375–2382, 2012.

Moselio Schaechter, editor. *Encyclopedia of Microbiology, Third Edition.* Elsevier Academic Press, 2009.

J. L. Schiff. *Cellular Automata A Discrete View of the World*. Wiley - Interscience, 2008.

J. Schnyder and M. Baggiolini. Role of phagocytosis in the activation of macrophages. *Journal of Experimental Medicine*, 148:1449–1457, December 1978.

L. J. Schumacher, P. M. Kulesa, R. McLennan, R. E. Baker and Maini. P. K. Multidisciplinary approaches to understanding collective cell migration in developmental biology. *Open Biology*, 6(6), 2016.

J. Seoka, H. S. Warrenb, A. G. Cuencac, M. N. Mindrinosa, H. V. Bakerc, W. Xua, D. R. Richardsd, G. P. McDonald-Smithe, H. Gaoa, L. Hennessyf, C.C. Finnertyg, C. M. Lpezc, S. Honarif, E. E. Mooreh, J. P. Mineii, J. Cuschierij, P. E. Bankeyk, J. L. Johnsonh, J. Sperryl, A. B. Nathensm, T. R. Billiarl, M. A. Westn, M. G. Jeschkeo, M. B. Kleinj, R. L. Gamellip, N. S. Gibranj, B. H. Brownsteinq, C. Miller-Grazianok, S. E. Calvanor, P. H. Masone, J. P. Cobbs, L. G. Rahmet, S. F. Lowryr, R. V. Maierj, L. L. Moldawerc, D. N. Herndong, R. W. Davisa, W. Xiaoa and R. G. Tompkinst. Genomic responses in mouse models poorly mimic human inammatory diseases. *Proceedings of the National Academy of Sciences*, 110 (9):3507–3512, February 2013.

C. N. Serhan. Treating inflammation and infection in the 21st century: new hints from decoding resolution mediators and mechanisms. *Faseb Journal*, 31(4):1273–1288, April 2017.

C. N. Serhan, S. D. Brain, C. D. Buckley, D. W. Gilroy, C Haslett, L. A. J. O'Neill, A. G. Rossi and J. L. Wallace. Resolution of inflammation: State of the art, definitions and terms. *Faseb Journal*, 21(2):325–332, February 2007.

C. N. Serhan, N. Chiang and T. E. Van Dyke. Resolving inflammation: dual anti-

inflammatory and pro-resolution lipid mediators. *Nature Reviews Immunology*, 8 (5):349361, May 2008.

C. N. Serhan, P. A. Ward and D. W. Gilroy, editors. *Fundamentals of Inflammation*. Cambridge University Press, 2010.

M. J. Sevenoaks and R. Stockley. Chronic obtructive pulmonary disease, inflammation and co-morbidity - a common inflammatory phenotype? *Respiratory Research*, 7 (70), May 2006.

M. C. Shanthini and F. R. Balkwill. Inflammation and cancer: Advances and new agents. *Nature Reviews. Clinical Oncology*, 2015.

J. A. Sherratt and J. D. Murray. Models of epidermal wound healing. *Biological Sciences*, 241(1300):29–36, July 1990.

Q. Shi, J. Shi and Y. Song. Hopf bifurcation and pattern formation in a delayed diffusive logistic model with spatial heterogeneity. *Discrete and Continuous Dynamical Systems Series B*, 24(2):467–486, February 2019.

R. Shi, W. Feng, C. Zhang, T. Yu, Z. Fan, Z. Liu, Z. Zhang and D. Zhu. In vivo imaging the motility of monocyte/macrophage during inflammation in diabetic mice. *Journal of Biophotonics*, 11, 2018.

M. J. Simpson and Y. Lo, K. Sun. Quantifying the roles of random motility and directed motility using advection-diffusion theory for a 3t3 fibroblast cell migration assay stimulated with an electric field. *BMC Systems Biology*, 11(39), 2017.

M. Skoge, E. Wong, B. Hamza, A. Bae, J. Martel, R. Kataria, I. Keizer-Gunnik, A. Kortholt, P. J. M. Van Haastert, G. Charras, C. Janetopoulos and D. Irimia. A worldwide competition to compare the speed and chemotactic accuracy of neutrophil-like cells. *PLoS One*, 11(6), 2016.

E. Smirnova, D. Shurland, S. Ryazantsev and A. M. Van Der Bliek. A human dynamin-related protein controls the distribution of mitochondria. *The Journal of Cell Biology*, 143(2):351–358, October 1998.

A. M. Smith, J. A. McCullers and F. R. Adler. Mathematical model of a three-stage innate immune response to a pneumococcal lung infection. *The Journal of Theoretical Biology*, 276(1):106–116, May 2011.

S. Sozzani, W. Luini, M. Molino, P. Jilek, B. Bottazzi, C. Cerletti, K. Matsushima and A. Mantovani. The signal transduction pathway involved in the migration induced by a monocyte chemotactic cytokine. *The Journal of Immunology*, 147(1): 2215–221, 1991.

R. Strohmeyer and J. Rogers. Molecular and cellular mediators of and alzheimers disease inflammation. *Journal of Alzheimer's Disease*, 3:131–157, 2001.

B. Su, W. Zhou, K. S. Dorman and D. E. Jones. Mathematical modelling of immune response in tissues. *Computational and Mathematical Methods in Medicine*, 10(1): 9–38, March 2009.

J. Sullivan and I. Yotov. Mathematical and numerical modeling of inflammation. volume 2, 2006.

C. Summers, S. M. Rankin, A. M. Condliffe, N. Singh, A. Michael, P. Edwin and R. Chilvers. Neutrophil kinetics in health and disease. *Trends in Immunology*, 31: 318–324, 2010.

P. K. Sweby. High resolution schemes using flux limiters for hyperbolic conservation laws. *Siam Journal on Numerical Analysis*, 21(5):995–1011, October 1984.

S. E. Sweeney and G. F. Firestein. Rheumatoid arthritis: regulation of synovial

inflammation. *The International Journal of Biochemistry and Cell Biology*, 36(3): 372–378, March 2004.

T. Tak, K. Tesselaar, J. Pillay, J. A. M. Borghans and L. Koenderman. Whats your age again? determination of human neutrophil half-lives revisited. *Journal of Leukocyte Biology*, 94:595–601, 2013.

K. Takahashi. Development and differentiation of macrophages and related cells: Historical review and current concepts. *Journal of Clinical and Experimental Hematopathology*, 41(1):1–31, January 2001.

K. Tani, F. Ogushi, T. Shimizu and S. Sone. Protease-induced leukocyte chemotaxis and activation and roles in host defense and inflammation. *The Journal of Medical Investigation*, 48, August 2001.

H. B. Taylor, J. Liepe, C. Barthen, L. Bugeon, M. Huvet, P. D. W. Kirk, S. B. Brown, J. R. Lamb, M. P. H. Stumpf and M. J. Dallman. P38 and jnk have opposing effects on persistence of in vivo leukocyte migration in zebrafish. *Immunology and Cell Biology*, 91:60–69, 2013.

M. Thon, M. R. Myerscough and M. W. Gee. A spatially resolved and quantitative model of early atherosclerosis. *Bulletin of Mathematical Biology*, 81:4022–4068, August 2019.

J. Tibble, K. Teahon, B. Thjodleifsson, A. Roseth, G. Sigthorsson, S. Bridger, R. Foster, R. Sherwood, M. Fagerhol and I. Bjarnason. A simple method for assessing intestinal inflammation in crohns disease. *Gut Journal*, 47:506–513, 2000.

M. Torres, J. Wang, P. J. Yannie, S. Ghosh, R. A. Segal and A. M. Reynolds. Identifying important parameters in the inflammatory process with a mathematical model

of immune cell influx and macrophage polarization. *PLoS Computational Biology*, July 2019.

R. Toth, A. toth, C. Papp, F. Jankovics, vagvolgyi C., M. F. Alonso, J. M. Bain, L. Erwig and A. Gacser. Kinetic studies of candida parapsilosis phagocytosis by macrophages and detection of intracellular survival mechanisms. *Frontiers in Microbiology*, 5, November 2014.

A. Tovar, N. Patel, A. K. Kaushik, G. A. Letona and J. E. Renaud. Hybrid cellular automata: a biologically-inspired structural optimization technique. In *Multidisciplinary Analysis and Optimization Conference*. American Institute of Aeronautics and Astronautics, 2004.

X. Trepat, Z. Chen and K. Jacobson. Cell migration. *Comprehensive Physiology*, 2 (4):2369–2392, October 2012.

A. M. Turing. The chemical basis of morphogenesis. 1:32–72, 1952.

M. D. Turner, B. Nedjai, T. Hurst and D. J. Pennington. Cytokines and chemokines: at the crossroads of cell signalling and inflammatory disease. *Biochimica et Biophysica Acta*, May 2014.

I. A. Udalova, A. Mantovani and M. Feldmann. Macrophage heterogeneity in the context of rheumatoid arthritis. *Nature Reviews Rheumatology*, 12(8):472–485, August 2016.

J. S. Upperman, V. Camerini, B. Lugo, I. Yotov, J. Sullivan, J. Rubin, G. Clermont, R. Zamora, G. B. Ermentrout, H. R. Ford and Y. Vodovotz. Mathematical modeling in necrotizing enterocolitis - a new look at an ongoing problem. *Journal of Pediatric Surgery*, 42:445–453, 2007.

H. A. S. Van Den Brenk. Studies in restorative growth processes in mammalian wound healing. *Experimental Surgery*, 43(181):525–550, 1956.

B. Van Leer. Towards the ultimate conservative difference scheme. ii. monotonicity and conservation combined in a second-order scheme. *Journal of Computational Physics*, 14:361–370, 1974.

T. Vanden Berghe, N. Vanlangenakker, E. Parthoens, W. Deckers, M. Devos, N. Festjens, C. J. Guerin, U. T. Brunk, W. Declercq and P. Vandenabeele. Necroptosis, necrosis and secondary necrosis converge on similar cellular disintegration features. *Cell Death and Differentiation*, 17:922–930, 2010.

Y. Vodovotz and G. An, editors. *Complex Systems and Computational Biology Approaches to Acute Inflammation*. Springer, 2013.

Y. Vodovotz and G. An. Agent-based models of inflammation in translational systems biology: A decade later. *Wires Systems Biology and Medicine*, 11(6), 2019.

J. G. Wagner and R. A. Roth. Neutrophil migration during endotoxemia. *Journal of Leukocyte Biology*, 66, July 1999.

C. Warrender, S. Forrest and K. Frederick. Modeling intercellular interactions in early mycobacterium infection. *Bulletin of Mathematical Biology*, 68:2233–2263, 2006.

H. V. Waugh and J. A. Sherratt. Modeling the effects of treating diabetic wounds with and engineered skin substitutes. *Wound Repair and Regeneration*, 15:556–565, March 2007.

H. Weavers, J. Liepe, A. Sim, W. Wood, P. Martin and M. Stumpf. Systems analysis of the dynamic inflammatory response to tissue damage reveals spatiotemporal properties of the wound attractant gradient. *Current Biology*, 26:1975–1989, August 2016.

D. R. Webb. Animal models of human disease: Inflammation. *Biochemical Pharmacology*, 87:121–130, 2014.

T. Weidemann, R. Worch, K. Kurgonaite, M. Hintersteiner, C. Bokel and P. Schwille. Single cell analysis of ligand binding and complex formation of interleukin-4 receptor subunits. *Biophysical Journal*, 101:2360–2369, November 2011.

K. E. Wellen and G. S. Hotamisligil. Inflammation, stress, and diabetes. *The Journal of Clinical Investigation*, 115(5):1111–1119, 2005.

WHO. The top 10 causes of death, May 2018. URL `https://www.who.int/news-room/fact-sheets/detail/the-top-10-causes-of-death`.

N. Woolf. *Cell, Tissue and Disease. The Basis of Pathology.* Bailliere Tindall, 1986.

T. A. Wynn, and K. M. Vannella. Macrophages in tissue repair, regeneration and fibrosis. *Immunity*, 44, March 2016.

T. Wyss-Coray and L. Mucke. Inflammation in neurodegenerative review disease - a double-edged sword. *Neuron*, 35:419–432, August 2002.

T. Wyss-Coray and J. Rogers. Inflammation in alzheimer and disease - a brief review of the basic science and clinical literature. *Cold Spring Harbor Perspectives in Medicine*, 2012.

P. Xia, S. Wang, B. Ye, Y. Du, G. Huang, P. Zhu and Z. Fan. Sox2 functions as a sequence-specific dna sensor in neutrophils to initiate innate immunity against microbial infection. *Nature Immunology*, 16(4):366–375, April 2015.

J. S. Yudkin, M. Kumari, S. E. Humphries and V. Mohamed-Ali. Inflammation, obesity, stress and coronary heart disease: is interleukin-6 the link? *Atherosclerosis*, 148:209–214, 2000.

M. Zawrotniak and M. Rapala-Kozik. Neutrophil extracellular traps (nets) - formation and implications. *Acta Biochimica Polonica*, 60(3):277–284, July 2013.

H. Zhu, Y. Sun, G. Rajagopal, A. Mondry and P. Dhar. Facilitating arrhythmia simulation: the method of quantitative cellular automata modeling and parallel running. *BioMedical Engineering OnLine*, 3(29), 2004.

Appendices

Appendix A

Turing instability

Reaction-diffusion systems are generally a quite mathematically convenient form of describing many biological processes and present possible patterned behaviours in terms of spatial instability. It is thus of great interest to precisely determine how, even from homogeneous equilibrium states, a system can develop specific patterns and structures (Turing, 1952). In this regard, there are different mechanisms that lead to spatial pattern formation that are relevant and recurring in a variety of developmental or morphogenic processes. The main focus here is on systems presenting *steady state spatially heterogeneous patterns* (Murray, 2003), with the main aim of this section being to define the conditions under which such an instability is found.

In order to derive these conditions, let us consider a generic PDE system in two variables u, v:

$$u_t = f(u, v) + D_u \nabla^2 u, \tag{A.1}$$

$$v_t = g(u, v) + D_v \nabla^2 v, \tag{A.2}$$

with equations (A.1) to (A.2) being already presented in their dimensionless form, f and g representing the nonlinear reaction kinetics and D_u and D_v the respective diffusion constants.

Turing's theory explicits the constraints that allow a system in the form of (A.1)-(A.2), given a stable steady state in the absence of diffusive terms, to develop spatial inhomogeneity due to diffusion (in contrast with the traditional approach of regarding diffusion as a stabilising process). To this purpose, to properly pose the mathematical problem, given initial conditions are considered and boundary conditions are fixed. For convenience, to be consistent with the modelling tasks that will be developed in the following chapters, let us consider periodic boundary conditions, that is:

$$
\begin{aligned}
&u, v \colon \Omega \subset \mathbb{R}^n \to \mathbb{R} \\
&\Omega = (a_1, b_1) \times \cdots \times (a_n, b_n) \subset \mathbb{R}^n \\
&\begin{cases} u(x_1, \ldots, x_{i-1}, a_i, x_{i+1}, \ldots, x_n) = u(x_1, \ldots, x_{i-1}, b_i, x_{i+1}, \ldots, x_n) \\ v(x_1, \ldots, x_{i-1}, a_i, x_{i+1}, \ldots, x_n) = v(x_1, \ldots, x_{i-1}, b_i, x_{i+1}, \ldots, x_n) \end{cases} \\
&\forall (x_1, \ldots, x_n) \in \Omega,\ i = 1, \ldots, n,
\end{aligned}
$$

and let (u_0, v_0) be the solution associated to the steady state, satisfying

$$f(u_0, v_0) = 0, \tag{A.3}$$

$$g(u_0, v_0) = 0. \tag{A.4}$$

Since the instability of interest is spatially dependent only, the system is analysed in function of its state variables, by determining the conditions for the linear stability of the associated homogeneous steady state, firstly when diffusion terms are switched off and subsequently by imposing instability of the extended system inclusive of diffusive behaviour.

A.1 Stability of the homogeneous steady state

In the absence of diffusion, system (A.1)–(A.2) can be rewritten as

$$u_t = f(u, v), \tag{A.5}$$

$$v_t = g(u, v). \tag{A.6}$$

In order to determine stability conditions for (A.5)-(A.6), the linearisation around the steady state (u_0, v_0) is considered by defining $\mathbf{w} = (u - u_0,\, v - v_0)^\top$ which, given $\|\mathbf{w}\| \ll$, leads to the expression

$$\underbrace{\begin{pmatrix} u_t \\ v_t \end{pmatrix}}_{\mathbf{w}_t} = \underbrace{\begin{pmatrix} f_u & f_v \\ g_u & g_v \end{pmatrix}\Big|_{u_0,v_0}}_{\mathcal{A}} \underbrace{\begin{pmatrix} u - u_0 \\ v - v_0 \end{pmatrix}}_{\mathbf{w}}, \tag{A.7}$$

that is

$$\mathbf{w}_t = \mathcal{A}\,\mathbf{w}, \tag{A.8}$$

with $\mathcal{A}$ being the stability matrix, that is the Jacobian evaluated at (u_0, v_0) and its elements conveniently renamed as f_{u_0}, f_{v_0}, g_{u_0}, g_{v_0}.

The stability constraint is then met when the steady state $\mathbf{w} = \mathbf{0}$ has $\Re(\lambda) < 0$, for every eigenvalue λ. Eigenvalues can easily be determined as solutions to the equation $|\mathcal{A} - \lambda I| = 0$, with I being the identity matrix, to provide

$$\lambda_{1,2} = \frac{f_{u_0} + g_{v_0} \pm \sqrt{(f_{u_0} + g_{v_0})^2 - 4(f_{u_0} g_{v_0} - f_{v_0} g_{u_0})}}{2} \tag{A.9}$$

that, referring to matrix $\mathcal{A}$ definition in (A.7), can be rewritten as

$$\frac{\mathrm{tr}(\mathcal{A}) \pm \sqrt{\mathrm{tr}(\mathcal{A})^2 - 4\mathrm{det}(\mathcal{A})}}{2}. \tag{A.10}$$

By exploiting well known algebraic properties relating eigenvalues to their associated matrix, namely $\mathrm{tr}(\mathcal{A}) = \sum_i \lambda_i$ and $\mathrm{det}(\mathcal{A}) = \prod_i \lambda_i$, conditions for stability (that is $\Re(\lambda) < 0$) can be conveniently reformulated as

$$\mathrm{tr}(\mathcal{A}) = \lambda_1 + \lambda_2 < 0 \tag{A.11}$$

$$\mathrm{det}(\mathcal{A}) = \lambda_1\,\lambda_2 > 0 \tag{A.12}$$

that, applied to matrix $\mathcal{A}$ yield respectively to

$$f_{u_0} + g_{v_0} < 0 \tag{A.13}$$

$$f_{u_0} g_{v_0} - f_{v_0} g_{u_0} > 0. \tag{A.14}$$

The expressions in (A.13)-(A.14) specify the stability conditions with no spatial variations, holding for (A.5)-(A.6).

A.2 Adding diffusion

By re-introducing the diffusive terms in (A.5)-(A.6), equation (A.7) is updated accordingly:

$$\underbrace{\begin{pmatrix} u_t \\ v_t \end{pmatrix}}_{\mathbf{w}_t} = \underbrace{\begin{pmatrix} f_u & f_v \\ g_u & g_v \end{pmatrix}\Big|_{u_0,v_0}}_{\mathcal{A}} \underbrace{\begin{pmatrix} u - u_0 \\ v - v_0 \end{pmatrix}}_{\mathbf{w}} + \underbrace{\begin{pmatrix} D_u & 0 \\ 0 & D_v \end{pmatrix}}_{\mathcal{D}} \nabla^2 \underbrace{\begin{pmatrix} u - u_0 \\ v - v_0 \end{pmatrix}}_{\mathbf{w}}, \tag{A.15}$$

that is

$$\mathbf{w}_t = \mathcal{A}\mathbf{w} + \mathcal{D}\nabla^2\mathbf{w}. \tag{A.16}$$

A particular solution of (A.16) is in the form of

$$\mathbf{w} = \mathbf{w}_p e^{\lambda t} e^{ikx} = \underbrace{\begin{pmatrix} u_p \\ v_p \end{pmatrix}}_{\mathbf{w}_p} e^{\lambda t} e^{jkx}, \tag{A.17}$$

with λ representing the growth rate in time and k the wave number. Substituting (A.17) in the general expression (A.16) and considering the steady state $\mathbf{w}_t = \mathbf{0}$ yields to

$$\mathcal{A}[\mathbf{w}_p e^{\lambda t} e^{ikx}] + \mathcal{D}\nabla^2[\mathbf{w}_p e^{\lambda t} e^{ikx}] = \mathbf{0}$$

$$\mathcal{A}\mathbf{w}_p e^{\lambda t} e^{ikx} + \mathcal{D}\mathbf{w}_p e^{\lambda t}(-k^2) e^{ikx} = \mathbf{0}$$

$$\mathcal{A}\mathbf{w}_p = k^2\mathcal{D}\mathbf{w_p}$$
$$\mathcal{A} - k^2\mathcal{D} = \mathbf{0},$$

or, in its matrix form

$$\begin{pmatrix} f_{u_0} & f_{v_0} \\ g_{u_0} & g_{v_0} \end{pmatrix} - k^2 \begin{pmatrix} D_u & 0 \\ 0 & D_v \end{pmatrix} = \mathbf{0}. \tag{A.18}$$

The matrix $\mathcal{A}_k$ can then be defined as

$$\mathcal{A}_k = \begin{pmatrix} f_{u_0} - k^2 D_u & f_{v_0} \\ g_{u_0} & g_{v_0} - k^2 D_v \end{pmatrix} \tag{A.19}$$

and, analogously to the stability analysis in Section A.1, the characteristic polynomial can be computed as $|\mathcal{A}_k - \lambda I| = 0$ as follows

$$\begin{vmatrix} f_{u_0} - k^2 D_u - \lambda & f_{v_0} \\ g_{u_0} & g_{v_0} - k^2 D_v - \lambda \end{vmatrix} = 0$$

which straightforwardly leads to

$$\lambda^2 + \lambda[k^2(D_u + D_v) - (f_{u_0} + g_{v_0})] + \underbrace{k^4 D_u D_v - k^2(f_{u_0} D_v + g_{v_0} D_u) + \overbrace{f_{u_0} g_{v_0} - f_{v_0} g_{u_0}}^{|\mathcal{A}|}}_{h(k^2)} = 0.$$

The corresponding characteristic polynomial is then

$$p_k(\lambda) = \lambda^2 + \lambda[k^2(D_u + D_v) - (f_{u_0} + g_{v_0})] + h(k^2) \tag{A.20}$$

having defined the function $h(k^2)$ as

$$h(k^2) = k^4 D_u D_v - k^2(f_{u_0} D_v + g_{v_0} D_u) + |\mathcal{A}|. \tag{A.21}$$

When $k^2 = 0$, the analysis falls within the previous case with stability guaranteed under conditions (A.13)-(A.14). At this point, though, for instability of a *spatially inhomogeneous* solution of (A.16) it is required that at least one eigenvalue λ of $p_k(\lambda)$ presents $\Re(\lambda) > 0$, thus at least one of the conditions given by either

$$k^2(D_u + D_v) - (f_{u_0} + g_{v_0}) < 0 \tag{A.22}$$

or

$$h(k^2) < 0 \tag{A.23}$$

is expected to hold.

By firstly analysing expression in (A.22), it is straightforward to notice that, from (A.13) we have $f_{u_0} + g_{v_0} < 0$, thus both group of terms $-(f_{u_0} + g_{v_0})$ and $k^2(D_u + D_v)$ are actually always positive, therefore $k^2(D_u + D_v) - (f_{u_0} + g_{v_0}) > 0$ $\forall\, k \neq 0$. Hence conditions to have spatial instability have to be imposed on $h(k^2)$ only.

Given the conditions in (A.14), for $h(k^2)$ to be negative it is necessary, but not sufficient, that $f_{u_0}D_v + g_{v_0}D_u > 0$. Furthermore, from (A.13) it is known that $f_{u_0} + g_{v_0} < 0$, thus for $f_{u_0} + g_{v_0}$ to be positive we require that $D_u \neq D_v$.

In order to meet the assumption in (A.23), a negative value for $h(k^2)$ can be explicitly found at its minimum:

$$h(k^2) < 0 \Rightarrow \exists\, h_{min} \mid h_{min}(k^2) < 0$$

that is easily computed by differentiating $h(k^2)$ with respect to k^2 as

$$h'(k^2) = 2k^2 D_u D_v - (f_{u_0}D_v + g_{v_0}D_u) = 0,$$

yielding the following expression for the corresponding value for k^2

$$k^2_{min} = \frac{f_{u_0}D_v + g_{v_0}D_u}{2D_uD_v}. \tag{A.24}$$

Finally, substituting (A.24) in (A.21) gives the expression for $h_{min}(k^2)$:

$$h_{min}(k^2) = \frac{(f_{u_0}D_v + g_{v_0}D_u)^2}{4D_uD_v} - \frac{(f_{u_0}D_v + g_{v_0}D_u)^2}{2D_uD_v} + |\mathcal{A}| = \tag{A.25}$$
$$= -\frac{(f_{u_0}D_v + g_{v_0}D_u)^2}{4D_uD_v} + f_{u_0}g_{v_0} - f_{v_0}g_{u_0}.$$

The imposition $h_{min}(k^2) < 0$ thus implies that

$$(f_{u_0}D_v + g_{v_0}D_u)^2 - 4D_uD_v(f_{u_0}g_{v_0} - f_{v_0}g_{u_0}) > 0.$$

The conditions for instability due to space can hence be summarised as

$$f_{u_0}D_v + g_{v_0}D_u > 0 \tag{A.26}$$

$$(f_{u_0}D_v + g_{v_0}D_u)^2 - 4D_uD_v(f_{u_0}g_{v_0} - f_{v_0}g_{u_0}) > 0, \tag{A.27}$$

particularly with (A.26) implying $D_u \neq D_v$.

A.3 Critical points

A change in stability in the system behaviour occurs when at least one of the roots of the characteristic polynomial (A.20) is equal to zero. Thus, by conveniently reformulating it as

$$p_k(\lambda) = \lambda^2 + b\lambda + h(k^2), \tag{A.28}$$

the conditions that characterise such bifurcation are determined by

$$\frac{-b \pm \sqrt{b^2 - 4h(k^2)}}{2} = 0 \tag{A.29}$$

which straightforwardly leads to

$$h(k^2) = 0 \tag{A.30}$$

In this regard, for critical values of k^2 such that $h_{min}(k^2) = 0$, a bifurcation from stability to spatially driven instability can be observed. To fully characterise the stability in terms of wavenumber k let us consider $h_{min}(k^2) = 0$, that is, from (A.25):

$$f_{u_0}D_v + g_{v_0}D_u = 2\sqrt{D_uD_v(f_{u_0}g_{v_0} - f_{v_0}g_{u_0})} = \sqrt{2D_uD_v|\mathcal{A}|}. \tag{A.31}$$

Combining and substituting the expression from (A.31) in (A.24) gives

$$k_c^2 = \frac{2\sqrt{D_u D_v |\mathcal{A}|}}{2D_u D_v} = \sqrt{\frac{|\mathcal{A}|}{D_u D_v}},$$

finally yielding to the critical value of wavenumber k_c:

$$k_c = \sqrt{\frac{f_{u_0} g_{v_0} - f_{v_0} g_{u_0}}{D_u D_v}}. \tag{A.32}$$

By computing the roots of $h(k^2)$, as defined in (A.21), the interval $[k_1, k_2]$ of spatial instability can be found:

$$\begin{aligned} h(k^2): \quad & k^4 D_u D_v - k^2(f_{u_0} D_v + g_{v_0} D_u) + |\mathcal{A}| = 0 \\ k_{1,2}^2 = & \frac{f_{u_0} D_v + g_{v_0} D_u \pm \sqrt{(f_{u_0} D_v + g_{v_0} D_u)^2 - 4 D_u D_v |\mathcal{A}|}}{2 D_u D_v}. \end{aligned}$$

Accordingly, the interval of spatial instability can be expressed in function of the wavenumber k, or analogously of its squared value k^2 such that:

$$h(k^2) < 0 \quad \text{for } k_1^2 < k^2 < k_2^2, \quad k_c^2 \in [k_1^2, k_2^2] \mid h(k_c^2) = 0.$$

Appendix B

Routh-Hurwitz criterion

The Routh-Hurwitz criterion, originally independently proposed by both mathematicians E. J. Routh and A. Hurwitz ((Routh, 1877), (Hurwitz, 1895)) providing necessary and sufficient condition for the roots of a polynomial to present, respectively, all positive and all negative real parts, determines the number of positive and negative real part roots of a given polynomial by its coefficients ((Allen, 2006)). This result derives from the more general Routh-Hurwitz theorem ((Meinsma, 1995), (Murray, 2001)).

Theorem 1. *A polynomial* $p(x) = a_n x^n + a_{n-1}x^{n-1} + \cdots + a_0$*, with* $a_i \in \mathbb{R}$*,* $i = 0, 1, \ldots, n$ *and* $a_0 \neq 0$*, is stable if and only if all elements of the first column of the associated Routh matrix* $\mathcal{R}(p)$ *are nonzero and have the same sign.*

Given the polynomial

$$p(x) = a_n x^n + a_{n-1}x^{n-1} + \cdots + a_0 = 0 \tag{B.1}$$

where $a_n > 0$ and $a_0 \neq 0$, the corresponding Routh matrix is defined as:

$$\mathcal{R}(p) = \begin{pmatrix} a_n & a_{n-2} & a_{n-4} & a_{n-6} & \cdots \\ a_{n-1} & a_{n-3} & a_{n-5} & \cdots & \\ b_{n-1} & b_{n-2} & \cdots & & \\ c_{n-2} & c_{n-3} & & & \end{pmatrix}, \tag{B.2}$$

where elements b_i, c_i and followings directly depend on the polynomial coefficients and are computed as determinants of the minor matrix taking elements of column I and the column to the right of the current position and the two rows above, divided by the negative of the element of column I and row above the one that is being computed, that is

$$k_{i,j} = \frac{\begin{vmatrix} k_{i-2,1} & k_{i-2,j+1} \\ k_{i-1,1} & k_{i-1,j+1} \end{vmatrix}}{-k_{i-1,1}}. \tag{B.3}$$

The matrix construction ends as soon the computing procedure leads to a single null determinant matrix, while, where not present, all other matrix elements are to be considered zero. The sign permutations of the elements of the first column of the Routh matrix $\mathcal{R}(p)$ determine the stability of the associated polynomial, with each sign variation corresponding to a positive real part root and conversely each permanence to a negative real part root.

The information on the sign of the real part of polynomial roots provided by this criterion, straightforwardly leads to important implications in systems control and stability, particularly by studying the corresponding eigenvalues real part signs by analysing the first column of the Routh matrix (B.2) associated to the characteristic polynomial.

Appendix C

Table of parameters

Parameter	Definition
Chapters 2, 3, 4, 5	
γ_c	rate of mediator decay
γ_g	rate of anti-inflammatory mediators' decay
D_c	pro-inflammatory mediator diffusion constant
D_g	anti-inflammatory mediators diffusion constant
Chapters 2, 3	
χ_n	maximal rate of neutrophil's influx
ν	neutrophil's apoptosis rate
γ_a	rate of necrosis of apoptotic neutrophils
ϕ	rate of apoptotic neutrophil's removal by macrophages (secondary necrosis)
χ_m	maximal rate of macrophages' influx
α	mediator's production rate

Continued on next page

Table C.1 – continued from previous page

Parameter	Definition
β_a	apoptotic neutrophils' saturation constant (concentration of apoptotic neutrophils required for half maximal release of $c(t)$)
γ_m	rate at which macrophages leave the tissue
β_n	active neutrophils' saturation constant (concentration of active neutrophils required for half maximal release of $c(t)$)
β_{gc}	inflammatory mediators' saturation constant (concentration scale over which neutrophils influx rate decreases)
β_g	anti-inflammatory mediators' saturation constant (concentration of anti-inflammatory mediators over which apoptosis rate increases)
β_c	pro-inflammatory mediators' saturation constant (concentration of pro-inflammatory mediators over which apoptosis rate decreases)
γ_g	rate of anti-inflammatory mediators' decay
θ_n	active neutrophils' chemotaxis constant
θ_m	active macrophages' chemotaxis constant
D_n	active neutrophil's diffusion constant
D_m	macrophage's diffusion constant
k_a	mediator's concentration produced by apoptotic neutrophils
k_g	anti-inflammatory mediators' production from macrophages (concentration of $g(t)$ produced in response macrophages presence)
k_n	pro-inflammatory mediators' production from active neutrophils (rate of $c(t)$ concentration produced in response active neutrophils presence)

Continued on next page

Table C.1 – continued from previous page

Parameter	Definition
Chapters 4, 5	
c_0	initial pro-inflammatory mediators' concentration (damage severity)
r	initial damage's radius (damage size)
δ_{ac}	increment of pro-inflammatory mediators upon apoptotic neutrophils undergoing necrosis
δ_{nc}	increment of pro-inflammatory mediators upon active neutrophils activity
δ_{mg}	increment of anti-inflammatory mediators upon macrophagic activity
p_{nr}	probability of recruitment of new neutrophils
p_{nc}	probability conditioning release of pro-inflammatory mediators upon neutrophils activity
p_{mr}	probability of recruitment of new macrophages
p_{mg}	probability upon which macrophages initiate the anti-inflammatory response
p_{ml}	probability at which macrophages leave the tissue
p_{ma}	probability at which macrophages phagocytose apoptotic neutrophils
α_{ncr}	threshold of pro-inflammatory mediators above which new neutrophils are recruited
α_{ngr}	threshold of anti-inflammatory mediators below which new neutrophils are recruited
α_{mr}	threshold of pro-inflammatory mediators above which new macrophages are recruited

Continued on next page

Table C.1 – continued from previous page

Parameter	Definition
α_{ml}	threshold of pro-inflammatory mediators below which macrophages leave the tissue
n_{cell}	number of neutrophils
A_{chem}	maximum concentration of chemoattractant
n_{run}	number of moves per tick
β_{rand}	threshold minimum concentration of chemoattractant for chemotactic motion
σ_{mem}	standard deviation associated with the likelihood of cells changing their direction of motion
k_{grad}	scaling parameter appearing in the weighting function of (5.2)

Table C.1: Parameters appearing in the models of Chapters 2–5.